Novel methodologies and technologies for the multiscale and multimodal study of Autism Spectrum Disorders (ASDs)

PhD Thesis

PhD course on Automatic, Robotics and Bioengineering

XXIII (2008-2010)

SSD: ING-INF/06

Student: Lucia Billeci

Supervisors: Prof. Arti Ahluwalia, Dr. Giovanni Pioggia,
Dr. Michela Tosetti

University of Pisa

Interdepartmental Research Center "E.Piaggio"

Pisa April 9, 2011

Abstract

Autism Spectrum Disorders (ASDs) are a class of heterogenic neurodevelopmental pathologies. At present their diagnosis is based only on behavioral tests and interviews and no effective cure is available. Researchers argue that new approaches are required to overcome the standard clinical diagnostic methods and it is necessary to tailor the therapy for each child.
In the last decade the convergence between clinical science and bioengineering is providing new ways to investigate the nature of ASDs, such as highly precise measurement of brain structure and connectivity, behavior and physiology, not otherwise measurable, or highly precise control over experimental stimuli. The goal of these studies is to develop novel bioengineering tools such as imaging methodologies, informatics tools, experimental models and algorithms, for the analysis of the neurological basis of ASDs.
Analysis of the information processing units in the autistic brain indicates that abnormalities of neural connectivity are present at global or local levels. Based on this hypothesis, a multiscale and multimodal approach for the study of ASDs was followed.
At a microscale level neuronal growth and connectivity were ana-

lyzed to demonstrate how neurodevelopmental alterations in cerebral circuitry confer vulnerability to ASDs, an area of investigation which is still largely unexplored. To this end a non-invasive procedure of imaging neurons in-vitro following their growth was set up and a software for neuronal morphology analysis called NEMO (NEuron MOrphological analysis tool) was developed. The focus of the analysis was on Purkinje neurons as their morphology is completely altered in ASDs. Purkinje neurons extracted from GFP (Green Fluorescent Protein) expressed wild-type mice and animal models of ASDs were analyzed and compared. This software allows automatic and quantitative extraction of features related to the morphology and organization of neurons. Moreover it is efficient in characterizing the effect of the genetic background and the environment on neuronal morphology.

At a higher level, brain structure in ASDs was analyzed using the Diffusion Tensor Imaging (DTI) technique. DTI is a recent noninvasive magnetic-resonance-based method sensitive to the presence of subtle white matter abnormalities in the absence of volumetric changes detectable by conventional MRI. DTI studies in ASDs are based on the hypothesis that the disorder involves aberrant brain connectivity and disruption of white matter which tracts between regions are implicated in social functioning. Therefore a case-control study was performed in order to analyze white matter abnormalities in children with ASDs. The influence of echolalia on white matter structure in ASD children was also analyzed. This is one of the very few studies in very young ASD children and the first DTI investigation on echolalia.

Additionally, the functionality of the brain areas was analyzed through

fMRI experiments. A novel task that included presentation of human and robotic faces was developed to analyze dynamics in face processing both in ASD children and normal matched controls. The state-of-the-art confirms the usefulness of robots in ASD therapy to act as social mediators to increase the social interaction skills of ASD children. Thus, fMRI was used to analyze the cortical response during facial processing of robotic faces with different levels of anthropomorphism (mechanical robots and androids). This study helped to understand how the face processing network is altered in ASDs and how robots are differently processed in ASDs and control groups.

Finally global features characterizing behavioral and physiological condition of the child were also collected. These measurements can be correlated with structural and functional abnormalities of the autistic brain.

An integrated system consisting of a specially equipped room in which the child, wearing unobtrusive devices for recording physiological and behavioral data as well as gaze information, can interact with an android (FACE, Facial Automaton for Conveying Emotions) and a therapist was set up. Experimental sessions in which the reactions of ASDs subjects and controls were monitored were compared. In particular the focus of this work was the collection of behavioral measurements and the analysis of ECG signals. Scores relative to specific aspects of behavior and time and frequency domain features of ECG signals were extracted and analyzed.

These studies provide new insights on the study of ASDs using new multimodal and multiscale methodologies. The study of neural circuitry in animal models of autism leads to insights on autistic brain

connectivity at a local level, and how this influences abnormal early brain development. DTI and fMRI protocols allow the analysis of specific anatomical and social deficits not yet addressed in ASDs. Finally the investigation of the interaction of ASDs and controls with an android provides new ways to characterize behavioral and physiological parameters that will yield new knowledge on brain-behavior/physiology relationships.

Acknowledgments

I think that one of the most beautiful aspect of research is that you can know a lot of people. Maybe with the most of them you have only a brief interaction, maybe with other you spent more time working together allowing you to reinforce yourself from a research point of view, maybe with other you can also argue about research topics, but also this exchange of ideas let you grow, and finally some of them can also became your friends. I think I am very lucky because during my PhD I have known a lot of people and traveling a lot I have met also people from different countries. Everyone of them gave me something that helped me in increasing my love for research and to complete my PhD. Of course I cannot forget my family and all the friends that I know out of my work field who have been always present and supported me in every good or bad moment of these three intense years. It is not just a way of saying that it is impossible to thank here all the people I know and I met but I will try to remember the most of them.

First of all I want to thank my tutor, Prof. Arti Ahluwalia, who followed me from my Master thesis to the end of my PhD. I think she is a very good professor not only because she is professional and

she likes her job but also because she speaks with the students and she is always careful in understanding their needs and their interest. Maybe without her help I would never understood my passion for neuroengineering and neuroscience.
Another important person for my research activity is Dr. Giovanni Pioggia. I have known Giovanni for four years and now I can say that is almost a friend for me. I have a great admiration for his research capability and for his wonderful way of approaching working and personal life: he his always positive, smiling and determined. He has always transmitted me his optimism and his love for work and life and this was fundamental for my growth in research.
I want also to thank the leader of the Bioengineering group at the Center "E. Piaggio", Prof. Danilo De Rossi for giving me the opportunity of working in his team and for his great knowledge that always fascinate me.
During my PhD I had also the opportunity to work at IRCSS Stella Maris where I have known a lot of people. First of all Dr. Michela Tosetti who is the one who brought me in the world of MR. She loves this world and after a lot of suggestion, indications and sometimes discussions, she made me love it too. I want to really thank her for the great support she gave me in my MR-work. Another person I want to thank is Prof. Filippo Muratori for his interest in bioingeneering and imaging approach in the study of ASDs. Thanks to his open-minded approach in medicine he gave us the wonderful opportunity to test our methodologies in a clinical contest. Then I would like to thank my co-workers at Stella Maris, Dr. Laura Biagi, who is a very great physicist and helped me in the analysis of data, Dr. Danilo Scelfo, with which I spent nice moments working and travel-

ing together (although he forgot me in Tel Aviv...). Thank also to Dr. Roberta Igliozzi for her bravery in comparing with FACE and for her liking. A special thanks goes to Dr. Sara Calderoni "our neuropsychiatrist" who shared with me imaging study in ASDs. She assisted to my crisis and my euphoric moments at the Stella Maris and she has always listened to me and laughed with me.
Another group with which I collaborated during all my PhD is the one of the Department of Neuroscience at the University of Pisa. I'd like to thank Prof. Francesca Vaglini for her support in the in-vitro part of my work and also for believing in my abilities, which gave me always a big strength. I also want to really thank Dr. Claudio Gerace for the great help he gave me making the dissections and preparing the cultures. When a cultures went well or wrong I had always someone who shared my feeling with.
The person who made me start to be interested in MR and let me travel for the first time during my PhD, is Prof. Francesco Di Salle. I'd like to thank him for having guided me in the discover of this new field first in Naples with Dr. Adriana Aragri and Dr. Fabrizio Esposito, and then in Maastricht. I also want to thank him for always demonstrating a great interest for my activities and my work and for his suggestions. I take the opportunity to thank all the guys I met in Maastricht with which I spent very nice moments: Tommaso, Fabio, Rosamaria, Antonella, Matteo and Barbara.
A special thank goes also to Prof. Marco Catani who gave me the opportunity to work for five months in his laboratory at the King's College of London. His experience and his teaching were fundamental for me to increase my knowledge in DTI analysis and to complete my work. I want also to thank all the guys I met in London for their

suggestions and their friendship: thank to Flavio, Patrizia, Sanja, Stephanie, Michel and Stefania.
I want also to thank two researchers that helped me during my PhD: Dr. Nicola Vanello, for his support in fMRI studies, and Dr. Marcello Ferro, for is help in programming in which he is a magician.
I' m not forgetting my co-worker and friends in Pisa of course. Thanks to them the work at the "Centro Piaggio" and at the CNR has been much more pleasant and funny. I want to thank Tita, Daniele, Carmelo, Giovanni, Federico, Bruna, Francesca, Antonino, Yudan, Maria Angela, Serena and Nadia (the last but not least...she is the one who animates the lunches at CNR and the one with which I have a lot of common interests). I promise all of them that I will offer them a coffee as soon as I get my PhD! A great thank goes also to the Giovanni Pioggia's group at the CNR, Gennaro, Giovanni, Rossella, Daniele and Alessandro, which are very nice guys and which keep company with me during the long days at CNR.
Another thank goes to the students I followed during their thesis: Martina, Chiara, Andrea, Monica and Margherita. They helped me in completing my work and they gave me the opportunity to deepen and transmit my knowledge about the topics of my research.
Now it is the moment to thank all my friends who supported me during my PhD and let me relax during the weekend and the evening spending wonderful moments. Having a great time out of work is important to be a good worker!
A special thank goes to my greatest friends Silvia, Giada and Benedetta who have been always willing to listen to my problems, my successes and my delusions. I'd like to thank also all the friends closer to me: Sara, Laura, Giulio, Elisa, Sara, Gina, Cristina, Chiara, Francesca

and Liuba. With all these friends I spent and I spend a lot of wonderful moments, with them I shared laughs, travels, joys and difficulties and their presence is fundamental in my life.
I want to thank also Marco with which I spent my second half of my PhD and my last two years of life. He has been always present in all the moments I needed him for talking, crying, laughing or simply stay in silence with me. One of the most important and beautiful thing of our relationship is that we feel free to behave exactly how we are and this makes our relation special. Despite some discussions due to the moments of nervous for the job, his presence is necessary for me to be happy, to enjoy the life and to feel loved.
The last but most important thank goes to my family for they support and their love for me. With discretion my parents and my brother have been always closed to me to give me suggestions, help and to listen to me. Thank to my family I had the possibility to study and to reach this important goal of my life.

Contents

List of Figures

List of Tables

Introduction

Autism Spectrum Disorders (ASDs) are a set represented by a continuum of early-onset neurodevelopmental disorders that disrupt the development of intersubjectivity and have several cascading effects on neurocognitive functions. Despite the currently accumulating knowledge on brain structure and brain function in ASDs, current findings on links between behavioral or neuropsychological measures and neurofunctional findings are still limited.
Investigations of structural or functional brain abnormalities, within what has been termed "the social brain", have described a set of putative underlying frontal, limbic, and temporal lobe circuitry [23]. New procedures for studying brain connectivity include diffusion tensor imaging (DTI), a recently developed, non-invasive magnetic-resonance-based method that can detect the presence of subtle white matter abnormalities in the absence of volumetric changes detectable by conventional MRI [24]. DTI studies in ASDs are based on the hypothesis that the disorder involves aberrant brain connectivity. Disruption of white matter tracts between regions implicated in social functioning, i.e., ventromedial prefrontal cortices, anterior cingulate gyri, and temporoparietal junctions have been described [25]. Others

findings have emphasized anomalies in the superior temporal gyrus and temporal stem [26]. All these brain abnormalities can have important effects on social and intersubjective behaviors. Researchers have traditionally focused on deficits in imitation, emotional recognition, gaze processing, and joint attention by using a model incorporating the identification of disrupted processing dynamics and abnormal neural connectivity, proposing a distorted information transfer model characterized by local over-connectivity and long-range underconnectivity [27]. This research is typically conducted on adolescents or adults with ASDs, but it is important to explore brain-behavior connections in younger children with ASDs, that is, at earlier stages of the neurodevelopmental disorder. Evidence that signs of ASDs are apparent within the first 2 years of life has emerged from several studies [28], such that one of the chief goals of ASD research is to identify and validate screening instruments for infants and to develop early intervention programs. Indeed, early diagnosis and treatment are considered crucial steps for improving the outcomes of children with ASDs: intensive and specialized early treatment can have a beneficial impact by enhancing these children's language abilities, cognitive skills, and peer relations and by lightening the overall burden on their families.

At present ASDs are usually defined on the basis of behavioral symptoms through gold-standard instruments; nevertheless, numerous researchers have argued that new approaches, which go beyond the standard methods and focus on social, cognitive and linguistic aspects of the phenotype, will be needed for identifying subtypes, within ASDs, which may be useful for new knowledge on brain-behavior relationships and for genetic studies.

In the past decade, novel engineering technologies have opened up new opportunities in ASD research.
These new methodologies investigate ASDs at different scales using different modalities. Indeed to study this complex disorder it is necessary to combine our knowledge at the single cell level with knowledge on human physiology and behavior. The interaction between biologists, clinicians and engineers is essential not just to find structure in the vast quantities of data flowing from experiments but also to integrate this information into models that explain at multiple scales of time and space how this disease works.
This PhD contributed to ASD research in three correlated fields at three different scales. First, given that "connectivity" is defective in autism and is the basis of the behavioral symptoms manifested in patients, through the development and testing a software tool dedicated to the analysis of neuron connectivity in animal models of ASDs at a microscopic level. The second aspect is highly correlated to the first because it is the analysis of brain anatomical and functional connectivity but at a higher scale as it considered the whole brain in-vivo. Finally the physiological response and behavior of ASD subjects was investigated using new technologies for exploring emotions and imitation. The aim was to develop and test a novel instrument, called FACET (Facial Automation for Conveying Emotions Therapy), that consists of: a) FACE, an interactive and biomimetic android consisting of an anthropomorphic body equipped with a believable face based on biomimetic principles and a facial tracking and expression recognition device; b) a specially equipped room, provided with two remotely orientable video cameras. In addition, children were requested to wear a biomimetic wearable suit

(BWS) for the unobtrusive acquisition of physiological and behavioral signals and a hat able to record the gaze of the child on the scene.

In order to study and model brain anatomy and function in ASDs it is important to start from the analysis of single neurons and neural networks. Connectivity can be defined in terms of network structure evaluating the dendrite connections and/or bifurcations, the neuritic segments, the orientation and the spatial extent of the arborizations and density of possible synaptic pathways. Courchesene [29] relates connectivity to both an excess or a lack of neurons. The density of the neuron population affects the geometry of the synaptic connections of the network both in terms of number of arborization processes emerging from single soma and in terms of the number of synapses formed. Both pertain to a wider framework where connectivity of a network results from the synergic interplay between structure (structural connectivity) and function (functional connectivity). Geometrical constraints may affect network activity (functionality) and vice-versa: the network dynamics (activity) by plasticity of neurons/synapses, modifies the topology [30]. This bilateral relation between activity and topology gives rise to networks whose function follows form and whose form drives dynamics [31]. The study of the morphology and topology of network connectivity can thus provide fundamental cues on functionality. 2D-cultured neural networks have been studied by Ben-Jacobs group [32, 33, 34, 35]. 2D cultured neural networks develop organotypic synaptic connections similar to those observed in-vivo [34].

The use of animal model of ASDs can be very useful to study in-vitro morphology and connectivity. One of the candidates gene of interest

is the Engrailed 2 gene (En2). Both an En2 knockout (loss of function) as well as a transgenic mouse that causes the misexpression of the gene have been generated. Both mutants display a phenotype reminiscent of the cerebellar anatomical abnormalities reported in autism.

Part of the activity of this PhD was the development and comparison of imaging analysis methods for quantitative measurements of single cell neuronal morphology, neuronal clustering and connectivity, in cerebellar tissue derived from knock-out transgenic mice (Engrailed 2 and Reeler) models for autism. In particular a software for the semi-automatic quantitative assessment of cell number, density, and morphology (NEMO - Neuron Morphological Analysis Tool) was developed. Using this tool it is possible to model neuron morphology and connectivity and identify alterations at a microscale level [36, 37]. Although is evident that connectivity is defective in ASDs, besides the very recent paper by Lewis and Elman [38], in which local neural network models have been modulated to show that functional modifications of connectivity during development leads to a reduction in global anatomical (structural) connectivity, specific studies on the evolution of microscale neurostructural abnormalities during development of the autistic brain have not been undertaken. So this study is the first attempt at addressing this critical question and can hopefully also help in performing an early diagnosis, and in designing new strategies for circuitry remodeling before the establishment of permanent networks.

To study in-vivo brain anatomy a powerful tool is Diffusion Tensor Imaging (DTI). DTI is a recent non-invasive magnetic resonance-based method (first clinical application in 1996) sensitive to the

presence of subtle white matter abnormalities in the absence of volumetric changes detectable by conventional MRI. DTI provides information about white matter tracts and their organization based on water diffusion.
This technique was used in this work to study white matter structures in ASD children together with its relation to a a specific language disorder, that is echolalia (the automatic repetition of vocalization made by another person).
This study is the first DTI study that analyze this kind of disturb related to ASDs, moreover it is one of the few Italian studies and one of the very few on very young children.

At the same scale it's possible to analyze also brain function using Functional Magnetic Resonance Imaging (fMRI). Various studies have been performed that relate autism with functional activation in the brain while the patient performs certain cognitive processes. This non-invasive, in-vivo method allows changes in the organization of these processes to be documented. Functional MRI provides a way of investigating the neuropsychological basis of the deficits in social cognition (e.g. the processing of emotional cues or facial expressions) [39] and executive functioning (e.g. flexibility in generating situation-appropriate actions, rather than exhibiting stereotyped behavior) [40] that constitute the principal characteristic of autism. This study focused on one of the functions that has been found to be altered in ASDs: face processing. In this work an fRMI study on ASD children was performed. This study is the first one in which not only human faces are presented to ASD subjects but also robotic faces. In fact there is quite recent evidence in the literature of how robots elicit some functions (such as emotional process or imitation)

in ASDs that are not activated in interactions with humans.
Finally to correlate anatomical and functional connectivity with behavior and physiology of ASD children, it is necessary to use technological tools that allow to investigate the autistic phenotype more precisely. Humanoid robots are currently being used in research on imitation, learning and social responsiveness. The employment of robotic systems to engage proactive interactive responses in children with ASDs has been suggested in order to allow the experimenter to correlate responses observed in subjects to precise and measurable stimulus-events. This approach could also lead to the understanding and subsequent teaching of the processing of socio-emotional abilities. Several reports underline the usefulness of the interaction of a robot in ASDs within a highly structured environment where it is possible to recreate social and emotive scenarios which can be used to enhance and anticipate actions of a subject and provide important insights for the comprehension of human-robot interaction in ASDs [41]. At the Interdepartmental Research Center "E. Piaggio" and at the Scientific Institute Stella Maris, an integrated system was set up to assess the use of a humanoid robot on social and emotional training in ASDs and validate an evaluation and treatment protocol based on robotic and advanced engineering technology [42]. The integrated sensing, monitoring, processing and emotionally responsive android-based therapeutic platform is termed FACE-T (FACE Therapy). Firstly, the impact of human-like robots in assessment and treatment in ASDs is evaluated using a methodological approach, in which psychological, physiological and behavioral data are analyzed in parallel. Secondly, given the naturalistic therapeutic setting, emotional and social variables which may confuse and stress subjects

with ASDs, can be limited and controlled; the platform enables the efficacy of the socio-emotional-cognitive training approach to be assessed.

In Chapter 1 an overview of ASDs is given highlighting the neurological deficits underlining this disorder. Moreover it presents a panorama of the novel methodologies for diagnosis and treatment of ASDs. These methodologies cover many critical aspects of ASDs and range from biological methods to high level technologies. Biological methods explore genetic and microsctructural abnormalities in ASDs especially through the use of animal models. Several imaging techniques have been successfully used to investigate structural and functional abnormalities in disorders with neurological bases like ASDs. Moreover a number of assistive technologies with different degrees of complexity have been developed and used in the attempt to improve the diagnosis and the social dysfunction of ASDs.

In Chapter 2 NEMO, the morphological analysis tool for the study of neuronal circuitry in cultures and histological sections developed in this work, is presented. First a non-invasive procedure to photograph the evolution of cultures or organotypic slices in-vitro was set up. Then the application of NEMO to the pictures obtained allows automated and quantitative extraction of all the metrical features of interest. In this work this tool was applied: i) to the study of the differences in morphology of Purkinje neurons cultured in the absence and in presence of glia, ii) to the study of branching of L7GFP Purkinje neurons from wild-type mice, iii) to the analysis of topological organization of L7GFP organotypic slices of cerebellum of Reeler mice and iv) to the study of the differences in morphology of L7GFP Purkinje neurons extracted from wild-type mice and animal

models of ASDs (Engrailed 2).
In Chapter 3 the basic principles of DTI and the applications developed in this work to the study of ASDs are described. First this technique was applied in a multicenter study in order to compare data acquired in different centers with different MR scanners. Then a methodological approach was set up to perform a DTI case-control study in order to analyze the differences in the global white matter and in specific tracts in ASD children and controls. ASD subjects were then subdivided according to the presence or absence of echolalia. The two subgroups were compared using the same DTI methodological approach as in the case-control study. Moreover a phantom with different fiber crossing configurations, PIVOH (Phantom with Intra-Voxel Orientation Heterogeneity), was developed in collaboration with a physics researcher. This phantom allows to test sophisticated algorithms that overcome the limits of DTI such us the reconstruction of crossing fibers.
Chapter 4 describes the application of fMRI to the analysis of the cortical response in ASDs. First a brief explanation of fMRI principles and an overview of the state of the art of fMRI in studying face processing in ASDs are given. Then the case-control study performed in this work is described. A face processing task in which human, android and robotic faces were presented to ASDs and controls was developed. Data acquired were then analyzed with standard fMRI analysis methods.
In Chapter 5 the platform FACE-T is described and the first tests performed on ASDs and controls are reported. The FACE-T platform consists of a robot and an ensemble of signal and video acquisition equipment. In the first application of this tool, sessions

of interaction with ASD children and controls were performed and behavioral and physiological signals were acquired and analyzed. In particular this work was focused on the behavioral performance of the children and on the analysis of ECG signals. Dedicated tools were used for ECG pre-processing, temporal and frequency analyses.

Chapter 1

Overview on Autism Spectrum Disorders (ASDs) and methodologies for their diagnosis and treatment

Dustin Hoffman's portrayal in the movie Rain Man may have turned public focus to autism but scientists have been scrutinizing it for years. Following decades of research, significant advances have confirmed that biology is behind this brain disorder, which is marked by deficits in the higher order cognitive abilities involved in social, communication and problem-solving. New findings on the genetic and anatomical roots of autism are helping researchers piece together how the disorder evolves, which could lead to new treatments.
The present chapter describes the most important aspects of autism, or Autism Spectrum Disorders (ASDs), in order to give a general idea of this disease and to report the state of the art of the novel methodologies for its diagnosis and treatment.

1.1 What are ASDs?

According to the Autism Society of America the prevalence of autism is of 1-2 per 1,000 and close to 6 per 1,000 for ASDs [43].
Leo Kanner first gave a name to this disorder in 1943 after a study on eleven children: early infantile autism. In the same period Hans Asperger, described the milder form of the disorder, named Asperger syndrome. Nowadays these disorders are cataloged in the Diagnostic and Statistical Manual of Mental Disorders (DSM) as the five Pervasive Developmental Disorder (PDD). The other two disturbs belonging to this group are Rett syndrome and the Childhood disintegrative disorder (CDD). All this disturbs are characterized by disabilities of different degrees in the development of multiple basic functions including socialization and communication as well as by repetitive, restricted and stereotyped behaviors. The number of reported cases of autism increased dramatically in recent years. This increase is largely attributable to changes in diagnostic practices, referral patterns, availability of services, age at diagnosis, and public awareness, though unidentified environmental risk factors cannot be ruled out [44].
The first symptoms of autism start in early childhood and evolve during development [45]. It is a very heterogeneous disease as no two children or adults with the same profile can be found so it is very difficult to extract some general characteristics [46]. To consider this diversity and to underline the absence of clearly detectable symptoms, the proper term to indicate this disease is Autism Spectrum Disorders (ASDs) rather than autism.

1.2 Symptoms

All ASDs have deficits in the following areas, known as "core symptoms":

- Social interaction;
- Verbal and non verbal communication;
- Repetitive behaviors and interests.

Most of children with ASDs have a difficulties in learning social interaction in everyday life [47]. Some evident aspects of these social interaction problems are difficulties in non verbal communication such as eye contact, facial mimics, posture and communicative gestures, difficulties in developing relations with other children, lack of spontaneous sharing of experiences with others and lack of social and emotional reciprocity. These features are always present within ASDs but can change during life and in different situations and also have different level of intensity in different subjects in accordance with the degree of disability.
Another characteristic is language retardation or even its absence [48]. In subjects able to speak there are often difficulties in starting a conversation or a stereotyped, repetitive and eccentric use of language. Tone, volume, speed, rhythm and emphasis of language are often abnormal (for example interrogative tones in affirmative sentences).
The presence of stereotyped behaviors that often recur during the day is also characteristic of ASD subjects [49]. They are apparently not targeted and sometimes become the only activity of the day.

Moreover ASD subjects have a narrow range of interests and are concentrated on single aspects or details. The resistance to change sometimes can have the characteristics of a phobic terror so that the subject can explode in fit of crying or laughter or become self-mutilating and aggressive towards others and objects. On the contrary, other ASD subjects show an excessive passivity and hypotonia so that they seem to be impassive to every stimulus.
In addiction to the symptoms described above, other less specific symptoms are often present such as abnormal postures, coordination and motor organization deficits, perceptive alteration (for example hyper acusia) that brings to abnormal response to sensorial stimuli of normal intensity, eating mannerisms, disturbed sleep, anxiety, odd emotional relationships and moodiness [50].

1.3 The causes

The causes of ASDs are only hypothesized and the concatenation of events that generate such complex and variegated disease is still a topic of intense study. Due to the high number of structures involved both from an anatomical and functional point of view, the hypothesis is that there is multisystemic impairment.
Almost all the researchers agree on the presence of a biological cause of the disease, such as the dysfunction or a lesion of a system, and the hypothesis of a psychosocial or psychodynamic origin has almost been abandoned. Indeed there is a clear evidence of genetic, neuronal, sensorial, biochemical and immunological cause. There are a lot of cues that suggest the importance of genetics in ASDs. For ex-

ample the higher incidence in men than in women can be explained as an alteration of sexual chromosomes; indeed in women symptoms are more serious [51]. Moreover studies on couples of twins show that an identical twin of a subject with autism has a higher probability to be affected than a heterozygous twin [52]. Studies on twins show how ASDs should be considered as a strongly genetic disorder while linkage studies and chromosomic abnormalities seems to imply specific chromosome regions.

Genetics of autism are complex due to interactions among multiple genes, the environment and epigenetic factors. Numerous candidate genes have been located, with only small effects attributable to any particular gene.

In addition to genetic alterations, neuronal and sensorial abnormalities are also at the basis of ASDs. An abnormal development of the brain causes deficits in the most important areas of the central nervous system.

Several lines of evidence point to synaptic dysfunction as a cause of autism [53]. Some rare mutations may lead to autism by disrupting some synaptic pathways, such as those involved with cell adhesion [54]. Gene replacement studies in mice suggest that autistic symptoms are closely related to later developmental steps that depend on activity in synapses and on activity-dependent changes [55]. All known teratogens (agents that cause birth defects) related to the risk of autism appear to act during the first eight weeks from conception, and though this does not exclude the possibility that autism can be initiated or affected later, it is strong evidence that autism arises very early in development [56].

1.4 Methodologies for diagnosis and treatment of ASDs

Due to the complexity and herogenity of ASDs the diagnosis and treatment are very complicate. So far no effective cure for ASDs is available and the diagnosis is often confused. This is especially because the deeply social aspect of the disease does not lend itself to simple treatment using physical apparatus or trivial clinical methods. Therefore is easy to understand how important novel tools can be useful to increase the power of diagnosis and treatment. In the past decade considerable effort has gone into the exploration of technology to aid in the diagnosis and treatment of the disease, resulting in innovative tools and methods that can improve the everyday life of an autistic person and also answer some of the open questions about the nature of the disease [57]. The principal methods of diagnosis and of treatment of ASDs are described in the following sections and summarized in Table 1.1.

1.4.1 Traditional methods

At present, there is no a medical test for autism; a diagnosis is based on observed behavior and educational and psychological testing [58]. To make an ASDs diagnosis it is necessary that problems in at least one of the following areas appears in the first three years of life appear: communication, socialization and limited behaviors.
Diagnosis requires a two step procedure: in the first step a screening of the development during regular pediatric control is performed, in the second step a comprehensive evaluation is realized by a multi-

Methods	Description	Examples
Traditional methods	Psychological testing (d) Behavior/communication methods (t) Dietary (t) Medications (t)	Parents interview, Play with child Treatment of repetitive behaviors Elimination of gluten and casein Risperidone
Biological and genetic methods	Animal models (d) Treatment with neuromodulators (t)	Engrailed 2 and Reeleer mice Oxytocin/vasopressin, Serotonin
Neuroimaging techniques	Neuropathological and structural imaging, DTI and fMRI (d)	Post-mortem and in studies Tractography, Face-processing tasks
"Low-tech" assistive technologies	Focus on: comprehension skills, communication skills, social skills (t)	Visual schedules and rules PECS Social stories
"Mid-tech" assistive technologies	Based on VOCAs systems (t)	VoicePod
"High-tech" assistive technologies	Virtual reality (t) Robotics (t) Affective computing (t) Wearable computer (t)	Immersion, VRH Robota, Infanoid, Mobile robots Galvactivator, PalmPilot Hearing aid, Eye-tracking

Table 1.1: *The most common methods that are currently used or that could be used for diagnosis (d) and treatment (t) of ASDs.*

disciplinary team.

During the first step developmental screening tools are used. They consist in short tests to tell if children are learning basic skills when they should, or if they might have delays. During developmental screening the doctor might ask the parent some questions or talk and play with the child during an examination to see how it learns, speaks, behaves and moves. A delay in any of these areas could be a sign of a problem.

The second step allows experts to confirm or exclude autism by the analysis performed by a a multidisciplinary team. This thorough review may include looking at the child's behavior and development and interviewing the parents. It may also include a hearing and vision screening, genetic testing, neurological testing, and other medical testing. In some cases, the primary care doctor might choose to refer the child and family to a specialist for further assessment and diagnosis. Specialists who can do this type of evaluation include developmental pediatricians, child neurologists, child psychologists or psychiatrists.

There is no single best treatment for all children with ASDs. However, well-planned, structured teaching of specific skills is very important. Some children respond well to one type of treatment while others have a negative response or no response at all to the same treatment. Before deciding on a treatment program, it is important to talk with the child's healthcare providers to understand all the risks and benefits. Research shows that early intervention treatment services can greatly improve a child's development [59, 60].

Common methods of treatment include behavior and communication approaches. According to reports by the American Academy of

Pediatrics and the National Research Council, the treatments that help children with ASDs are those that provide structure, direction, and organization for the child in addition to family participation. There are several methods of behavior modification that are used to treat inappropriate, repetitive, and aggressive behavior and to provide autistic patients with skills necessary to function in their environment.

Other treatments include dietary modifications and medication. Researchers have found elevated levels of proteins in wheat, oats and rye (gluten) and casein (protein in dairy products) in patients with ASDs, suggesting that the incomplete breakdown or excessive absorption of these substances may affect brain function. Eliminating foods that contain gluten and casein from the diet may cause side effects and should not be done without the advice of a health care practitioner [61].

There are no medications that can cure ASDs or even treat the main symptoms. But there are medications that can help some people with related symptoms. For example, medication might help manage high energy levels, inability to focus, depression, or seizures. Also, the U.S. Food and Drug Administration approved the use of risperidone (an antipsychotic drug) to treat 5- to 16-year-old children with ASDs who have severe tantrums, aggression, and cause self-injury [62].

1.4.2 Biological and genetic methods

The importance of finding early indicators of ASDs, makes the research in biology and genetics very important. The hope is that

the human body exhibits some biological features very early on in development (perhaps prenatally or at birth) that predicts autism. An earlier diagnosis allows earlier intervention, which is crucial in developmental disorders.

Szatmari and Jones, in [63], argue that autism is a strongly genetic disorder. There are many efforts currently under way to map autism genes using the gene analysis technology made available over the last years. The fact that a large number of genes may be involved in autism and the mystery of autism's exact mode of transmission makes genetic research in autism a challenging endeavor.

In light of these ambiguities, hope is held that an animal model of autism may help elucidate matters. The fundamental neurobiology approach posits that basic mechanisms are conserved among organisms and are expanded on or modified through evolution. By defining molecular and cellular mechanisms that regulate brain region development or mediate cognitive functions, we can identify molecular targets whose disruption may contribute to an ASDs-related abnormality.

Other current research takes a different approach. Instead of trying to identify the genetic expression indicative of autism, researchers have found that certain peptides are elevated in children with autism from birth [64]. Mass spectrometry in proteins is used to detect certain characteristics in samples and compare them to find differences specific to autism [65]. The aim is to find a biomarker for autism. The technology being employed is in the early stages of development, but might be quick and accurate enough for biomarkers to hold some promise as a method for early autism diagnosis.

1.4.2.1 Animal models of ASDs

Given the multifactorial etiology of ASDs there is no single animal model that captures all of the molecular, cellular, or organismic features of ASDs. Many mouse mutants show Purkinje cell deficits, although Engrailed 2 (En2) has been of particular interest for several reasons. Specifically, En2 deletion or overexpression produces Purkinje cell deficits; the diminished posterior cerebellar vermis and lobules in mice are also seen in some human autism neuropathology, and human EN2 localizes close to the chromosomal 7 region identified by several ASDs genome linkage scans. Studies of En2 gene overexpression [66, 67] as well as gene deletion have been performed in-vivo and in-vitro [68, 69]. Overexpression of En2 in neural precursors in culture maintains precursor proliferation and reduces neuronal differentiation, mechanisms that could conceivably contribute to ASDs cerebellar neuropathology. Both En2 knockouts (loss of function) as well as a transgenic mouse that causes the misexpression of the gene have been generated. Deficits in social behavior were reported in En2-/- mice across maturation that included decreased play, reduced social sniffing and allogrooming, and less aggressive behavior. Deficits in two spatial learning and memory tasks were also observed [70]. Adult mice for both mutants are non-ataxic, but their cerebella are hypoplastic, with a reduction in the number of PNs and other cortical neurons [68, 71].
One of the molecules that are under examination as a risk factor in autism is Reelin, a protein of the extracellular matrix, with a key role in migration and positioning of neurons [72, 73]. Reelin mRNA and protein are down-regulated in cortical GABAergic neurons of

patients with ASDs [74, 75]. The gene coding for reelin is highly conserved between mice (Reln) and humans (RELN) [76]. Because of reelin (haplo) insufficiency, the heterozygous reeler mouse is of wide interest. The reeler mutation arose spontaneously, showing autosomic recessive transmission. The homozygous reeler mouse completely lacks the protein, presenting an impaired phenotype characterized by striking neurological signs (dystonia, ataxia, tremor) and severe alterations in the architecture of laminar structures like the cerebral cortex, the cerebellum and the hippocampus [77, 78]. Levels of Reelin are reduced by 50% in heterozygous mutants which, compared to wild-type animals, do not show lamination defects in the SNC nor the classical reeler phenotype. It has been documented that, in the first weeks of life, heterozygous mice show progressive loss of PNs [79]. The phenotype also shows subtle neuro-anatomical and behavioral abnormalities [80, 81, 82, 83, 84] that are similar to those found in post-mortem brain tissue from autistic patients.

1.4.2.2 Treatment with neuromodulators

Genetic discoveries allow scientists to focus attention on a number of developmental regulators and processes, neurotransmitter and synaptic components and, potentially, novel genetic mechanisms that contribute to ASDs susceptibility in the context of specific environmental factors. Hopefully, animal models studies will allow additional definition of the molecular pathways in human ASDs populations. For example, the oxytocinvasopressin receptor studies have led to new human genetic studies, and the association of EN2 with

ASDs raises questions about the relationships of genotype to brain morphology, on the one hand, and the range of clinical symptoms, on the other.

Among all neurochemical investigations in autism, serotonin (5-hydroxytrypamine or 5-HT) has stimulated the most research and investigation. Early studies of blood serotonin in autism consistently found hyperserotonemia in one third of people with autism; this has been replicated in more than 25 published studies [85]. The magnitude of this elevation is usually expressed as 5-HT in whole blood, and has typically been about 50% above normal levels [86]. Subsequent research has established that more than 99% of whole blood serotonin is contained in the platelets [87] and that platelet serotonin accounts for the hyperserotonemia in autism [88]. However, the cause and significance of these elevated levels of blood serotonin in autism remain unclear.

1.4.3 Imaging neurobiological aspects of ASDs

Neuroimaging techniques such as magnetic resonance imaging (MRI) or positron emission tomography (PET) are one of the most prominent examples of recently developed technology that allows some analysis of the structure and functioning of the brain. MRI and PET studies have been carried out in a variety of contexts, including post-stroke damage assessment and recovery or the study of brain activity during linguistic, numerical or social task learning, among many others.

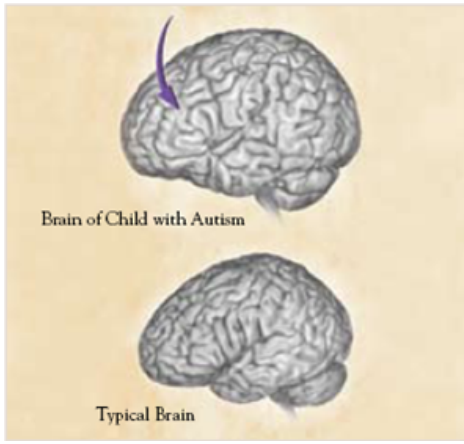

Figure 1.1: *Increase of brain volume in ASD subjects [1].*

1.4.3.1 Neuropathological and structural imaging

These studies are based both on postmortem tissue analysis and on non-invasive imaging technique in order to establish which brain areas are involved in ASDs.
Many studies show an increase of brain volume in ASD subjects with respect to controls (Figure 1.1).

For example Chiu et al. [89] concluded that head circumference was normal at 1 year of age, but at 30 months the size was 27% above the norm and then returned to normal again at 5 years of age. Courchesne indicated that ASDs are linked to two phases of head growth abnormality: a lightly reduced head circumference at birth and a sudden and excessive increase in head circumference in later development (Figure 1.2). This growth pattern may be one biological indication that, together with other behavioral signs, may lead to early detection of risk for autism [2].

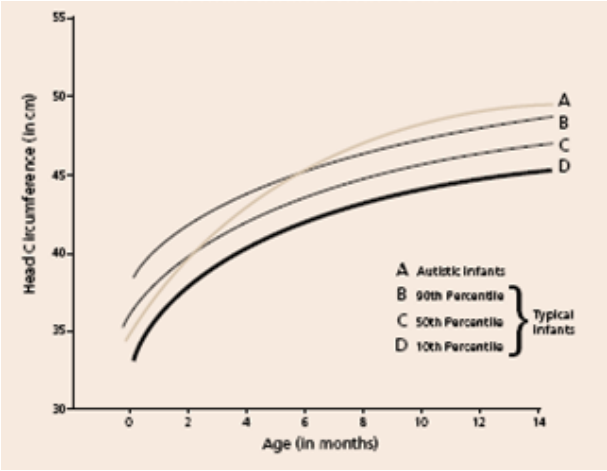

Figure 1.2: *Average growth of head circumference in male infants with autism [2].*

Neuropathological studies showed alterations in encephalic trunk, cerebellum and in limbic structures such as hippocampus, amygdala or anterior cingulate cortex [90].
Kemper and Barman examined postmortem brain tissues of almost 30 ASD subjects and showed that limbic neurons are small, packed and immature, in fact they have a lower complexity of the dendritic tree then cells of normal subjects [91].
Aylward et al. [92], using MR imaging, showed a reduction of amygdala volume while Dager et al. [93] reported, in some patients with autism, an alteration of the hippocampal shape with an inward deformation of the subiculum and Haznedar et al. observed a reduction of volume of anterior cingulate cortex [94].
Bauman and Kemper showed also abnormalities in cerebellum of children and adults with ASDs: a significant decrease in the number

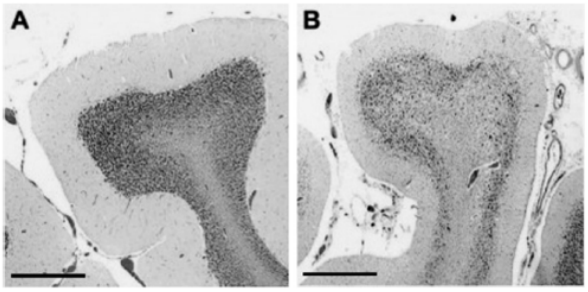

Figure 1.3: *a) Purkinje cells of a normal cerebellum b) Reduction of Purkinje cells number in an ASD subject [3].*

of Purkinje cells, primarily effecting the posterolateral neocerebellar cortex and adjacent archicerebellar cortex of the cerebellar hemispheres (Figure 1.3) [91].

Fatemi and colleagues showed that in addiction to a reduction of Purkinje cells number there is also a reduction of their dimensions while density is the same [75]. Purkinje neurons inhibit excitatory stimuli from the deep cerebellar nucleus so that a reduction of their number and dimension cause an abnormal over-connectivity along the cerebellum-thalamus-cortex circuitry (Figure 1.4).

This abnormal connectivity may contribute to a variety of functional and anatomic abnormalities, including variable functional topography in the cerebral cortex; excessive growth of cerebro-cortical areas, impaired modulation of frontal event-related potentials, and over excitation of thalamocortical projections, increasing central nervous system "noise" and decreasing efficient information processing [3].
Although abnormalities of cerebellar Purkinje cells are the most evi-

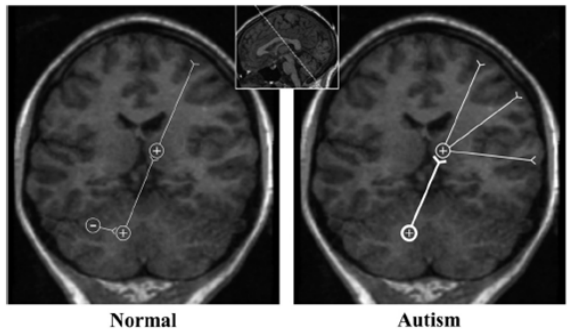

Figure 1.4: *Increase of connectivity along the cerebellum-thalamus-cortex circuitry shown in a MR study [3].*

dent, neuropathological studies show other abnormalities within the cerebellum. For example Bauman and Kemper reported a reduction of granular cells and an increase of dimension of deep cerebellar nuclei neurons [91]. In terms of cerebellar sub-regions, reduced size of one or more regions in the cerebellar vermis, which is predominantly gray matter, is frequently reported in autism MRI studies (Figure 1.5). Courchesne observed a localized reduction in the size of cerebellar vermis lobules VI-VII, sometimes associated with a reduced size of the cerebellar hemispheres, apparently proportionally correlated to the seriousness of the disease. Since ASD subjects need longer times than controls to move their attention, he concluded that lobules VI-VII could have had a role in this function, causing an information loss on contest and content.

Cerebellar pathology in the context of a developing brain may influence the behaviors and symptoms of autism via at least two paths. Through a direct route, the pathology will lead to cerebellar

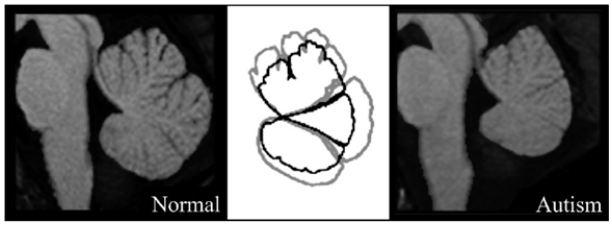

Figure 1.5: *Midsagittal T1-weighted MR images from a representative normal control subject and an individual with autism. Superimposed tracings highlight the difference in midsagittal vermis area between these two individuals [3].*

dysfunction, which, due to the cerebellar role in diverse cognitive, social, and emotional functions, is a likely contributor to some of the hallmark symptoms of autism. Additionally, through an indirect route, cerebellar pathology is hypothesized to influence the abnormal development of anatomic and functional connections between the cerebellum and other brain regions and thereby impact functioning in diverse brain systems.

Other abnormalities are present at the level of minicoloumns of the neocortex. Minicolumns are the fundamental processing units and are made of pyramidal cells and interneurons vertically assembled. Casanova [95] and Courchesne [96] showed a reduction in dimensions and an increase in number of minicoloumns in ASD subjects. The reason why minicoloumns are underdeveloped could be a defect in migration of neurons so that they distribute unequally in the different levels.

1.4.3.2 Diffusion tensor imaging

Diffusion tensor imaging (DTI) is a non-invasive method for mapping the diffusion properties of tissue water [97]. DTI is extremely sensitive to subtle differences in the architecture of white matter (WM) at the microstructural level. The white matter contains pathways known as fiber tracts that connect functional areas of the brain. It is also possible to realize a diffusion tensor tractography (DTT) that allows estimation of the trajectories of the white matter fiber tracts. Several indices can be used to characterize WM structure like the fractional anisotropy (FA) that is a measurement of the integrity of the tracts. Details on this imaging technique will be given in Chapter 3.
There are some studies in which diffusion tensor imaging indices have been analyzed in ASD subjects. These studies have found lower FA in individuals with autism, compared with controls, in the corpus callosum [98, 25], [99], the anterior cingulate, ventromedial and subgenual prefrontal areas, temporoparietal junction, and in the superior temporal gyrus (STG) white matter and temporal stem [25, 26].

Studies that have employed Diffusion Tensor Tractogaphy (DTT) to examine the integrity of specific WM tracts in individuals with autism relative to typically developing individuals have focused primarily on intra-hemispheric tracts. For example, one study reported alterations in the structural integrity of long-range fibers in the frontal cortex in children within the autism spectrum [100], while another reported significant reductions in the micro-structural integrity of the right superior cerebellar peduncle and short intra-cerebellar fibers in adults with Asperger syndrome (Figure 1.6) [4].

A more recent study revealed a significant increase in the number of streamlines (i.e., the lines that depict the fibers in a tract) in bilateral inferior longitudinal fasciculus (ILF) and the cingulum bundle, as well as a reduction in streamlines in the right uncinate fasciculus (UF) [101]. Importantly, these tracts are associated with behavioral functions that are known to be impaired in autism. For example, the ILF and the inferior fronto-occipital fasciculus (IFOF) are critical for higher-level visual and emotion processing [102], [103], domains shown to be atypical in individuals with autism [104], [105], [106], [107].
All these results are from studies on late childhood subjects or on adults. More recent studies investigated children under 3 years old. For example in 2008 Ben-Bashet and colleagues realized a DTI study on young children and found an FA increase in a lot of brain areas (in particular in the left hemisphere and frontal lobe) [5] (Figure 1.7). These results are in agreement with the finding of abnormal brain growth and connections in the first years of life.

1.4.3.3 Functional neuroimaging

Various studies have been performed that relate ASDs with functional activation in the brain while the patient performs certain cognitive processes [108, 109]. This noninvasive, in-vivo method allows changes in the organization of these processes to be documented.
Functional MRI provides a way of investigating the neuropsychological basis of the deficits in social cognition (e.g. the processing of emotional cues or facial expressions) and executive functioning (e.g. flexibility in generating situation-appropriate actions, rather than

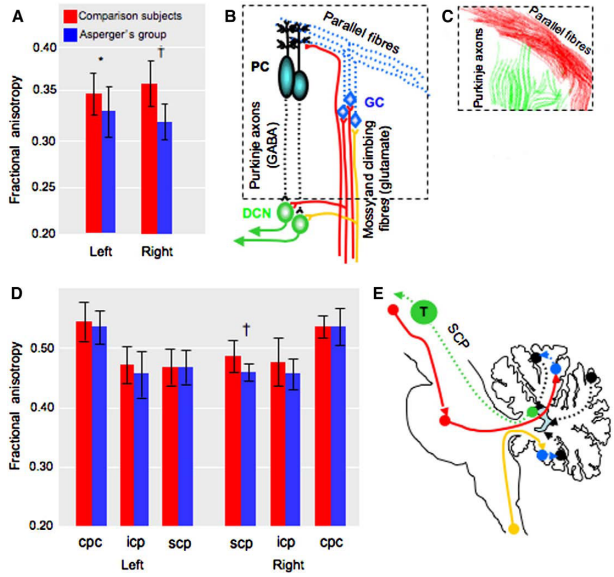

Figure 1.6: *Tract-specific measurements of fractional anisotropy for short and long cerebellar pathways. A) Compared to controls the Asperger syndrome group shows lower fractional anisotropy values in the right short intracerebellar connections, with a trend towards significant difference in the left short intracerebellar connections. B) Reduced fractional anisotropy values in the short intracerebellar connections are likely to reflect changes in the parallel fibers (dotted cyan fibers) and Purkinje (PC) axons (dotted dark cyan lines). C) Detail of the tractography reconstruction of the parallel and Purkinje fibers. D) Overall the Asperger syndrome group shows reduced fractional anisotropy values in the long cerebellar pathways with significant differences in the right superior cerebellar peduncle (scp) compared to controls. E) Overall these results suggest a specific involvement of the main cerebellar outflow tract within the cerebello-thalamic network and intracerebellar connections (dotted lines indicate affected pathways) (cpc, red lines; scp, green lines; icp, yellow lines; short intracerebellar connections, black lines) [4].*

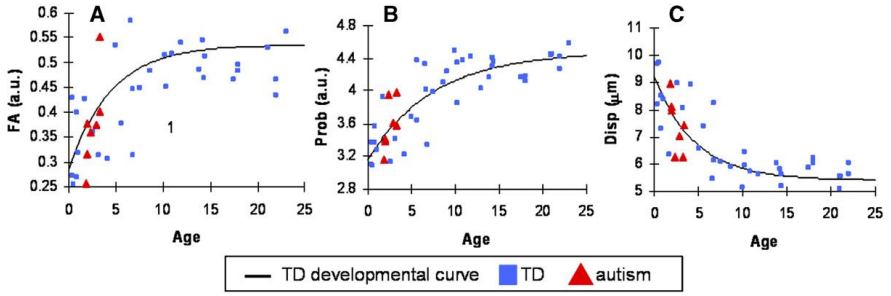

Figure 1.7: *DTI data obtained studying brain development of left brain hemispheres of ASD subjects under 3 years old. Development curves obtained through minimum squares regression analysis: fractional anisotropy (FA) value, probability and regions displacement in ASDs and control subjects [5].*

exhibiting stereotyped behavior) that constitute the prime characteristic of autism. For example attention deficits are related to an activity reduction within the posterior superior temporal sulcus [110], deficits in face processing, social perception or in emotions are related with an activity reduction within the amygdala [111, 112, 29, 113, 114].

Functional Magnetic Resonance Imaging (fMRI) studies also allow brain connectivity to be studied and show how it is altered in ASD subjects. Many studies, amongst which that of Courchensne and Pierce [27], show that ASDs are associated with a reduction of connectivity between different local neural networks specialized for different functions in the brain, this means a low long-range connectivity, on the other hand, there is a high connectivity inside single local networks, meaning a high degree of local connectivity. Anatomi-

cal evidences of this theory are first of all the increase in brain size during the first steps of development in which synaptogenesis, apoptosis and myelinization are at the top of their level and this infer on normal development of connection at a cortical level. Moreover abnormal cellular growth and differentiation or altered synaptogenesis, compromise many neuropsychological or behavioral functions, in particular abnormalities in information integration.
The increase of local connectivity and the of global connectivity compromise discrimination of signal from noise. Such evidence can be confirmed by fMRI studies. In a low-connected network sensorial input should evoke an abnormal over-connectivity both for expected stimuli and for unexpected stimuli, generating an abnormal increase of activation but a reduction of sensitivity in the sensorial regions. On the contrary, regions dedicated to functional integration, should show a reduction of activation and in functional correlation with sensorial regions. Belmonte' studies, during a visuo-spatial attention task, show exactly this pattern (Figure 1.8) [6].

1.4.4 Assistive technology

According to the Technology-Related Assistance for Individuals with Disabilities Act of 1988 (Public Law 100-407), an assistive technology means any item, piece of equipment, or product system, whether acquired commercially, off-the-shelf, modified or customized, that is used to increase, maintain, or improve functional capabilities of individuals with disabilities. Various types of technology from "low" tech to "high" tech, have been used to try to improve social dysfunction of ASD subjects [57], [115]. The following sections are meant to

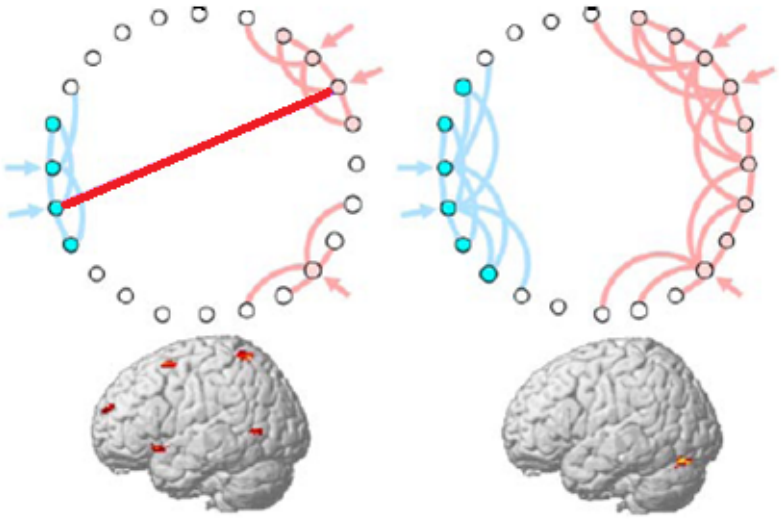

Figure 1.8: *Potential effects of network connectivity patterns on brain activation. Top: In the network on the left, a combination of strong local connectivity within delimited groups of neural units and selective long-range connectivity between local groups allows easy discrimination of signal (double arrows) from noise (single arrow). In the network on the right, strongly connected subregions are not appropriately delimited and differentiated, and computationally meaningful long-range connections fail to develop. Bottom: The brain images from a visual attention task, display distributed patterns of functional activation in the normal brain (left) and abnormally intense and regionally localized activation in the autistic brain (right) [6].*

give an overview of the different approaches that have been taken towards building useful assistive technology that can be used in coping with autism.

1.4.4.1 Low technology

Low technology approaches do not involve any type of electronic or battery operated device and are easy to use equipment. They treat ASD disabilities focusing on comprehension skills [116], communication skills [117] or social skills [118].
A variety of low tech strategies can be used to increase an individual's understanding of his or her environment and the expectations surrounding that environment. These technology are mainly based on visual systems. Other low-tech approaches focus on expanding a child's expressive communication skills, especially crucial for nonverbal patients [119]. One of the more famous and successful approaches is the Picture Exchange Communication System (PECS) (Figure 1.9), described in [117]. The child can communicate the desire to obtain particular objects by giving the partner a card depicting that object.
Yet other low-tech measures focus on social skills, helping to teach children appropriate behavior in social settings and generalizing the behavior.

1.4.4.2 Mid technology

Mid technology approaches are battery operated devices or "simple" electronic devices requiring limited advancements in technology and mostly, this concerns Voice Output Communication Aids (VOCAs)

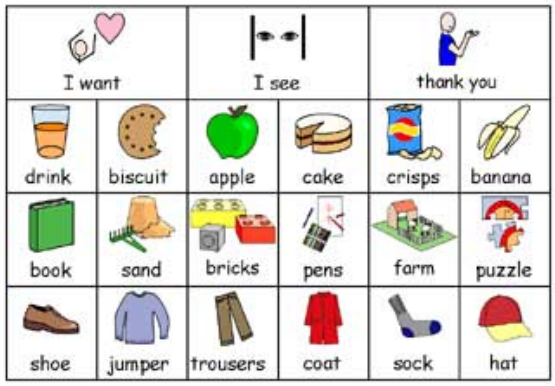

Figure 1.9: *The Picture Exchange Communication System.*

[120]. These devices produce synthetic or digitized speech when a symbol is selected from the VOCAs display and have been found to be easily adopted by autistic children. Their main benefit lies in their ability to facilitate natural interpersonal interactions and socialization due to the speech output they generate. VOCAS also constitute a crucial component in aiding language development.
An example of this kind of technology is the the VoicePod [121] (Figure 1.10). It is a digital recording and playback system ideal for photos, language cards and communication symbols. It features thirty-six reusable, two-sided sleeves with an ID strip to access recordings. The VoicePod provides a motivating and novel alternative for focusing on sequence stories, which are typically difficult for the student with ASDs. The student listens to the sentence on the card, which describes a picture that is part of a story sequence. The student can then put the appropriate picture in sequential order for the story,

Figure 1.10: *The VoicePod.*

according to the message given on the VoicePod. It can also be used to practice spelling words, math facts, history dates, and any key concepts from subject area classes.

1.4.4.3 High technology

More recently several computer technology tools used in teaching and therapy of ASDs have been developed. There is a lot of evidence that the use of computers with autistic children led to increases in focused attention, attention span, in-seat behavior, fine motor skills, generalization skills, etc. probably due to their predictability and consistency, their controllability by the child and their lack of confusing social messages [122]. Various computer-based solutions have been developed for example for language, talking word processing [123] or mind reading [124].
There are hundreds of software programs that can assist ASD subjects with receptive language skills. Talking word processing software [123] has also been developed to support spelling and general communication in disabled children. Such software, together with similarly

functioning speech generating devices [125] have been shown to be helpful in supporting the learning of spelling by providing children with instantaneous text and speech feedback.
Mind Reading [124] helps children learn about emotions and their expression, especially in human faces. It provides an interactive guide and a library of videos of people expressing emotions, together with quizzes and games to check the child's progress.
Most of these computer-based solutions aim at a teaching environment. Although they make use of some of the benefits afforded by computer technology, they are often based on exactly the same concepts as lower-tech solutions. Most recently innovative technological tools based on new key concept have been developed and are described in the following paragraphs.

Virtual reality Virtual Environment (VE) is a computer generated, 3D environment that aims to surround, or immerse the user so that he or she becomes part of the experience in a simulated environment, and potentially allowing the transfer of skills from the virtual to the real world. There are several levels of VE, the most sophisticated of which is called immersion. In this version the user wears sensorized systems that tracks the person's movement and uses that to reposition the user's location in the scene.
The application of virtual environments to ASDs has several advantages. It can be used to rehearse problematic real-life situations and simulate different scenarios in a safe learning environment in which the individual may make mistakes which might be physically or socially hazardous in the real world. In addition, the environment can be altered gradually to teach generalization and cross-recognition.

Figure 1.11: *The Virtual Reality Hypnosis System [7].*

Strickland [126] presents several games that teach children diagnosed with autism about a range of social situations. In a study of two children with mild to moderate degrees of autism, Strickland et al. [127] found that they accepted the VR equipment (headset), and responded to the computer-generated world by verbally labeling the names and colors of objects.
More recently Austin et al. [7] experienced the use of virtual reality hypnotherapeutic (VRH) procedure for feasibility as a possible treatment modality for autism with two teenage boys. The VRH method uses a head mounted display (Figure 1.11) to create a non-threatening, virtual reality environment, where the hypnotherapeutic process can be implemented.

Robotics In recent years, in treatment and rehabilitation of people with cognitive disorders, traditional instruments have been supported by a variety of robotic technologies. The merging between

Figure 1.12: *The PETS robot prototype [8].*

psychology and robotics, epigenetic, is an emerging discipline of particular importance. The basis of this discipline is the development of epigenetic processes by which the cognitive system grows as a result of interaction with social and physical environment.
Recent studies show that subjects with this kind of disorders perceive and treat the robots not as machines, but as their artificial partners [128], [129]. Based on this theory several robotic artifacts have been used to engage proactive interactive responses in children with ASDs. This approach could also lead to the understanding and teaching the processing of socio-emotional abilities.
Interesting studies are carried out by Plaisant, who introduces the Pet Robot [8] (Figure 1.12), a storytelling robot technology for therapeutic play with the hope that it will provide a richer environment useful for children with a variety of challenges.

Franois Michaud and his team are investigating the use of mobile robots (Figure 1.13) and characters with an engineering approach as their research is focused on testing several robots with different

Figure 1.13: *Michaud's mobile robotic platform (left) and its application in a playing setting with an ASD child (right) [9].*

Figure 1.14: *Three Robota robots [10].*

shape, color and behavior [9].

Dautenhahn's group [130], [131], [132] in the Project AURORA (Autonomous mobile Robot as a Remedial tool for Autistic children; [133]), use robotic dolls as therapeutic or educational toys specifically for children with autism. Robota [10], developed within this project, is a doll-shaped robot toy that allows researchers to systematically assess the child's social skills (Figure 1.14).

Kozima et al. built a child-like humanoid, Infanoid, and a small creature-like robot, Keepon, (Figure 1.15) by which they investigate

Figure 1.15: *Keepon (left) and Infanoid (right) robot [11].*

human social development, especially of interpersonal communication [11], [134]. The objective is to help children with ASDs establish a mapping between the feelings and actions of the robot, and their own feelings and actions. Similar to the AURORA project, they propose engaging the child in imitation play, gradually increasing the complexity of the interaction.

Affective Computing Picard's group [135] is working on a new discipline called affective computing with the aim of realizing new technologies that people with communication challenges, like ASD subjects, can use to improve their abilities to communicate emotion. The technology-mediated interaction created by this group is capable of recording actions, timing and various expressive parameters. The field draws its inspiration from the increasing literature that emphasizes the interplay of emotion and reason: brain is no longer considered as a purely cognitive information processing system but is seen instead as a system in which affective and cognitive functions are inextricably integrated with one another [136]. Accordingly, researchers in affective computing argue that an accurate model of the

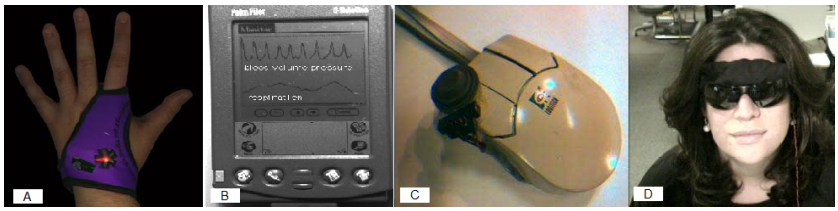

Figure 1.16: *a)The Galvactivator: a skin-conductance sensing glove that converts level of skin conductance to the brightness of a glowing LED [12], b)The PalmPilot: a PDA that can be used without obscuring the user's vision [13], c) The pressure mouse: the physical pressure applied is associated with frustration, caused by poor usability in a computer interface [14], d) The Expression glasses: discriminate facial expressions of interest or surprise from those of confusion or dissatisfaction [15].*

user would have to incorporate the affective as well as the cognitive processes that drive the user's reasoning and actions.
Since the inception of this field, a number of researchers have charged ahead with building machines that have affective abilities. The Expression-Glasses [15], the Galvactivator [12], the PalmPilot [13] and the pressure mouse [14] (Figure 1.16) are just a few examples of the different approaches that have been implemented to detect emotion from nonverbal cues.
Open research problems include making these affect-sensing systems more robust to variations in interaction contexts, applying them to spontaneous human-computer and human-human interaction contexts, and building more intelligence in the systems with regards to the range of mental states that are sensed.

Wearable computers There has been an increasing surge of interest in developing wearable devices with the goal of applying them in applications of augmented reality and perceptual interfaces, especially vision-based interfaces.

For example the emotional hearing aid, which was first introduced in el Kaliouby and Robinson [137], is a portable assistive computer-based technology designed to help children with Asperger Syndrome read and react to the facial expressions of people they interact with in real-life situations. The emotional hearing aid is made up of two components: an automated mind-reading system that infers the mental states of people by analyzing their facial expressions [138], [139] and a reaction advisor, which suggests appropriate reactions for the child to take based on the inferences made by the mind-reading system. The system's software goes beyond tracking simple emotions like sadness and anger to estimate complex mental states like agreeing, disagreeing, thinking, confused, concentrating and interested.

It is possible to extend the function of the emotional hearing aid to incorporate information about the context in which an interaction occurs since many people diagnosed with ASDs have problems integrating mental state concepts from facial expression into wider contexts [140].

An innovative technology used in ASD research, the eye tracking technology, which has mostly found applications in the military domain, for example in visually guided targeting systems, enabled the researchers to give a quantitative meaning to the degree of social competence an autistic person exhibits.

Eye-tracking studies have been performed monitoring the eye movements of ASDs and controls whilst they performed a test of emo-

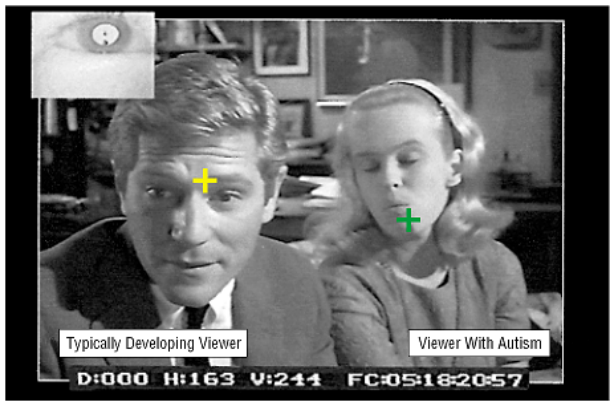

Figure 1.17: *Typical still frame used during coding of visual fixation patterns. Points of regard for an autistic viewer as well as a control are superimposed on the image, as is coordinate data of a control [16].*

tion recognition from photographs of facial expressions. The subjects with autism spend a smaller percentage of time examining the core features of the face (eyes, nose and mouth; subsequent analysis showed this effect to be driven by less gaze time to the eyes and nose [141, 142]).
Eye-tracking can also be used with video clips, as exemplified in a study by Klin et al. [16] (Figure 1.17).

Chapter 2

Development of a morphological analysis tool for the study of neuronal circuit in cultures and in slices: NEMO

2.1 Introduction

The cerebellum is one of the most common sites of anatomic abnormality in ASDs as described in section 1.4.3.1. Moreover genetic and MRI behaviour correlation studies [143] suggest that cerebellar abnormality plays a central role in ASDs, and the related motor, cognitive and social deficits [6].
The cerebellum is a large structure located at the roof of the hindbrain that helps control the coordination of movement by making connections to the pons, medulla, spinal cord, and thalamus. It may also be involved in aspects of motor learning. Like the cerebral cortex, the cerebellum is comprised of white matter and a thin, outer layer of densely folded grey matter. The folded outer layer of the cerebellum (cerebellar cortex) has smaller and more compact folds

than those of the cerebral cortex. The cerebellum contains hundreds of millions of neurons for processing data.
The cerebellar cortex is histologically homogeneous and divided into three distinct cellular layers (Figure 2.1a). These layers overly an inner core composed of white matter and three pairs of symmetrical clusters of deep cerebellar nuclei (DCN). Bordering the white matter core and lying immediately above it is the granule cell (GC) layer. The small GCs (the most numerous neuronal cell type in the brain) comprise the great majority of this layer. The somata of the Golgi cell and Lugaro cell interneurons as well as the unipolar brush cells (UBCs), recognized only recently as a distinct neuronal type, also reside in the granular layer. The next layer is called the Purkinje cell (PC) layer because it is primarily a monolayer of PC somata; it also contains the somata of Bergmann glia and candelabrum cells, which are both wedged between the much larger PC soma. The molecular layer is most superficial and is made up primarily of PC dendrites and GC axons (parallel fibers) but also contains stellate and basket cell interneurons in addition to palisades of Bergmann glia fibers.
Three classes of afferents project to the cerebellum and provide a multitude of signals to all lobules (Figure 2.1b). The first class, mossy fibers, originates from many locations in the brain and spinal cord, and the terminals of each axon are located within the granular cell layer. The second class of afferents, climbing fibers, originates solely from the various nuclei of the inferior olive, located within the medulla oblongata of the brainstem. Climbing fibers terminate only in the molecular layer of the mature cerebellar cortex, where each climbing fiber interacts with the dendritic tree of one PC. In addition to climbing fibers and mossy fibers, a third class of afferents

projects to the cerebellum. This last class consists of a diffuse set of afferents, including noradrenergic afferents from the locus coeruleus, cholinergic afferents from the pedunculopontine nucleus, and serotonergic afferents from the raphe nucleus. The terminals of the third class of afferents are mapped within all layers of the cerebellar cortex and do not appear to be localized to particular lobules.
In the adult cerebellum, mossy and climbing fiber afferents terminate in stripes that are similar to the patterns set up by ZebrinII (brain-specific respiratory isoenzyme strongly expressed in Purkinje cell parasagittal domains) PC stripes (Figure 2.1b).

Maybe the most interesting neurons of the cerebellum, both for their elaborate dendritic structure as well as for their role in cerebellar development and function, are the PCs. PCs represent the only output of the cerebellar cortex. Moreover, they are involved in the first stage of cerebellar development and it has been suggested that PC electrophysiological and morphological properties may influence the growth and connections of cells which develop successively [144]. The study of the evolution of morphology of PC is very important to understand how it influences the connectivity of the cerebellum.
The morphology of a neuronal tree is characteristic of the neuronal cell type. Morphometric analysis of tree structures is demanded in studies of, for instance, lifespan alterations in the dendritic/axonal field of neurons and time points of major changes; of neuronal morphological correlates of diseases; of the morphological implications of neurons under experimental conditions; and of structure-function relationships in dendritic trees. The size of neuronal trees depends upon their maturational state. Many conditions can induce changes

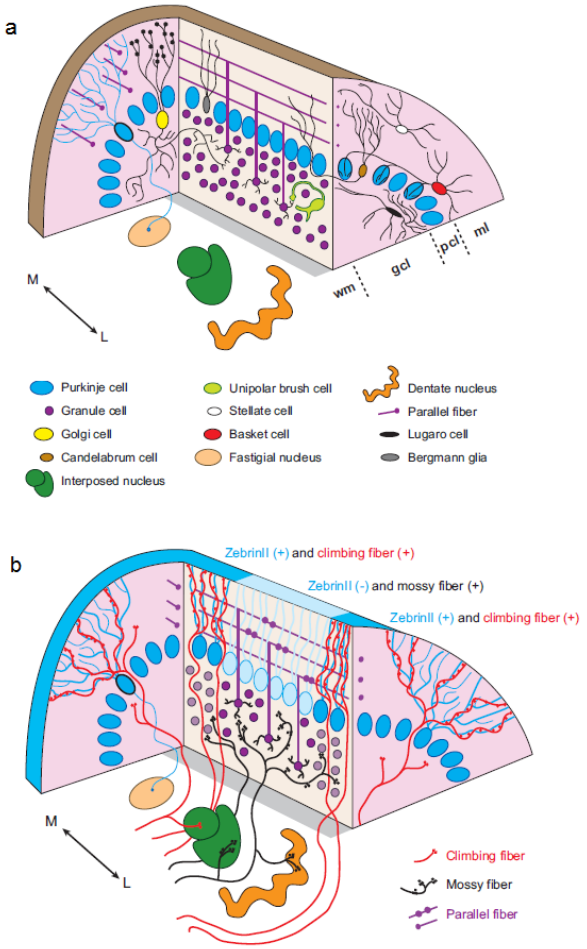

Figure 2.1: *a) Cytology in the cerebellum. Abbreviations: ml, molecular layer; pcl, Purkinje cell layer; gcl, granule cell layer; wm, white matter; M, medial; L, lateral; V, vermis; H, hemisphere, PC, Purkinje cell, b) Mossy (black) and climbing (red) fibers. Their terminal fields are organized into parasagittal domains that align with ZebrinII Purkinje cell (PC) parasagittal domains. M, medial; L, lateral. [17]*

in neuronal tree structures, such as learning, 'enriched' environment, hormonal fluctuations and levels of neuronal bioelectric activity. To answer these kinds of questions, well-defined metrics are needed for assessing quantitatively the morphological characteristics of neuronal branching patterns.

Several studies describe Purkinje cell microstructural morphology in great detail [145], [146], [147], [148]. The most common methods employed for the analysis of microscale neuronal structure in-vitro are based on optical imaging [149]. In fact, optical images can be analyzed with computational methods to quantitatively measure and assess morphological characteristics of neuronal branching patterns [150]. A powerful imaging technique is that of fluorescence microscopy and several reports describe neural growth dynamics and network organization using fluorophores [35], [151], [152].
In order to discriminate PCs from the other cells of the culture, it is necessary to use specific dyes. However, most of these specific dyes are cytotoxic, which makes it impossible to evaluate the dynamics of a network.
Moreover most of these have been conducted on tissue fixed slices. On the other hand only a limited number of studies report on the quantification of PC morphology in dissociated cultures. Since the PC is essentially a planar cell, dissociated cultures allow single cell architecture to be studied free from interactions with other cells, in a topological context which is similar to that in-vivo. Moreover, many morphometric features are easier to quantify and extract, because the cells are easier to distinguish from their neighbours.

The first aim of this work was to tune a non-invasive method that allows to follow the evolution of the PCs in dissociated culture. A further aim was to develop a method for the extraction of morphological characteristics of PCs. An automated quantitative tool for microstructural analysis called NEMO (NEuron MOrphological analysis tool) was developed.
In this work the principal application of this tool was the evaluation the morphological differences in PCs associated to ASDs.
In the first step of the work the tool was tested on PCs extracted from wild-type mice [37] and L7GFP wild-type mice in order to verify its efficiency. The use of GFP (Green Fluorescent protein) in such a way that is expressed only by PCs increase the ability to recognize these cells and improve the pre-processing of the images.
In the second step PCs were analyzed in presence and in absence of glial cells in order to evaluate the effect of glia on PC morphological growth.

The role of of glial cells is still unclear. Recent discoveries indicate that astrocytes are an active in neuronal signaling, suggesting that information processing is based on multiple cells rather than only neurons [153], [154], [155], [156]. In fact, one of the roles of astrocytes is to sense and modulate synaptic activity. So, the network of information processing is not made up only by neurons but it is the result of a dialogue between two parallel networks: one consisting of neurons and one consisting in astrocytes. Moreover, there is wide ranging evidence that a bilateral relation between activity and topological or geometrical constraints may affect network activity and vice versa: networks dynamics due to plasticity of neu-

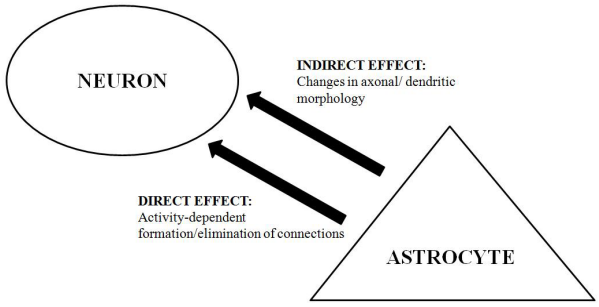

Figure 2.2: *Effects of astrocytes on neuronal morphology.*

rons/synapses modifies this topology [30]. Astrocytes in particular can modify neuronal morphology in order to influence the functional processing of neural networks. For example, it has been shown that astrocytes change the number of synaptic connections of neurons. This change can occur in two ways 2.2. First, astrocytes change the number of synaptic connections directly via synaptogenic signals: they release factors that enhance or inhibit synaptic transmission. Zhang et al. demonstrate that ATP released by glial cells act as activity-dependent signaling molecules in neuron-glia communication, resulting in astrocyte Ca^{2+} wave and synaptic modulation in hippocampal slices [157].

Astrocytes also act indirectly by modifying the morphology of axons and dendrites and thus the potential for synapse formation. These modifications are due to the secretion of factors such as laminins [158], neurotrophins [159], S100B [160], [161] and activity-dependent neurotrophic factors [162] that act on neuronal morphology. From this prospective, investigations on neuronglia interactions as the basis of human brain information processing are currently taking off. So

far, there are no extensive mathematical studies on the effect of neuronglia interactions on neuronal morphology. Morphometric analyses are relevant for the study of alterations in the dendritic/axonal field of neurons or neuronal morphological correlates of diseases that can be due to inappropriate functionality of glial cells [150]. Experiments on organotypic cultures show a crucial role of astrocytes in the structural maturation of cerebellar cells [163] and in their process of migration [164]. It can be supposed that if the function of the glia is compromised, the maturation and migration of PCs is abnormal. Indeed, there is wide-ranging evidence to show that loss and abnormalities in both PCs and their associated glia compromise cerebellar development and outputs in autism spectrum disorder [165], [91], [75]. For example, the absence of gliosis (the proliferation of neuroglial tissue that can follow neural damage) has been observed in postautopsy tissue from autistic subjects [166].
The analysis of PC morphology in absence and in presence of glial can help to clarify the role of this cells in PC development.

The following step was the application of NEMO to the evaluation of morphological differences between PCs extracted from GFP wild-type mice and Engrailed 2 mice. As described in section 1.4.2.1 these mice have abnormalities at the cerebellar level similar to that found in ASD human subjects.

Moreover in this work algorithms for the analysis of organotyipic slices of cerebellum were developed. These slices keep alive in culture so it is possible to follow their evolution in time. The analysis of slices allows to extract other features with respect to dissociated

cultures that are important for this study. For example the number of neurons that is an indicator of cell loss and topological features characterizing the organization of PCs in the cerebella cortex. In this study the algorithms developed for slice analysis were tested on organotypic slices from the cerebellum of L7GFP wild-type mice and L7GFP Reeler mice.

In this chapter first NEMO features are described in details, then the applications of the tool performed in this work are presented.

2.2 NEMO implementation and Usage

NEMO is a tool implemented in Matlab® code (The MathWorksTM, Inc., USA). The Matlab GUIDE tool was used to create a graphical user interface (GUI) environment (Figure 2.3). The GUI was provided with the following capabilities:

- Image pre-processing;
- Morphological Analysis;
- Topological Analysis;
- Neuron count;
- PCA or 3way-PCA;
- Plot variables.

Images of neurons or slices must be loaded in the Software before starting the analysis. In order to organize images it is convenient to

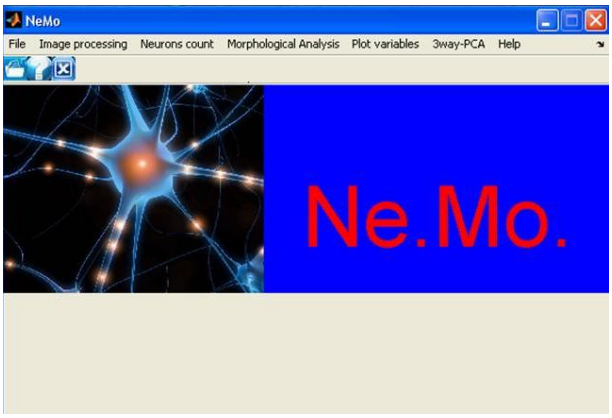

Figure 2.3: *NEMO GUI.*

rename them in a proper way. Image type is indicated by the first letter of the name: letter "p" stands for photograph, letter "b" for binary image and letter "s" for skeleton. The following part of the name is made up of four numbers: the number indicated the culture, the number of the neuron or slice belonging to the culture, the day in which the photograph was made (numeration starts from the first day in which the first photograph was made) and finally the number of cell divisions. Both the last two numbers are needed because usually cells are not photographed from the first day of culture as they are too vulnerable.
In the following sections all these features will be explained in detail.

2.2.1 Image pre-processing

The aim of the image pre-processing is to obtain a suitable image for the subsequent analyses. If the analyses are performed on a single

neuron to study morphology, the aim is to obtain the skeleton of the cell, that is a binary image reduced to one pixel thick lines. In the case of the analysis of topology of neurons in a slice or of the count of neurons, the purpose of the pre-processing is to obtain a binary image in which neurons are white and the background is black.
Neuron images can be processed using an editor, which allows the user to perform a semi-automatic procedure to obtain the skeleton, or a more complicated GUI, that gives more freedom in the choice of parameters but is less automatic. The choice is a compromise between automation and integration of some parameters: there is no a single best approach, it depends on the quality of the image.
There are some differences between the editor and the GUI. First, there are some s implemented only in the GUI: in fact, they are used only for poorly contrasted images. Then, there are some differences in the way of inserting parameters. In fact, in the editor, if it's necessary, the execution of the program stops and first a message box is displayed, that gives the user information about parameters to be included, and then a message box is opened, that allows the user to insert them. Instead, in the GUI there are fields, naming edits, that enable users to enter some parameters. If the user does not enter anything, default parameters are automatically used. Dwelling with the mouse cursor on the edits that make up the GUI, a label appears, that describes parameter function, and any default value.
As shown in Figure 2.4, there are some panels in the GUI, and each of them is related to one or more algorithms. There are also two panels for displaying photographs: the panel above represents the image before applying the algorithm while the panel below shows the modified image. In this way the user, by comparing the two pictures,

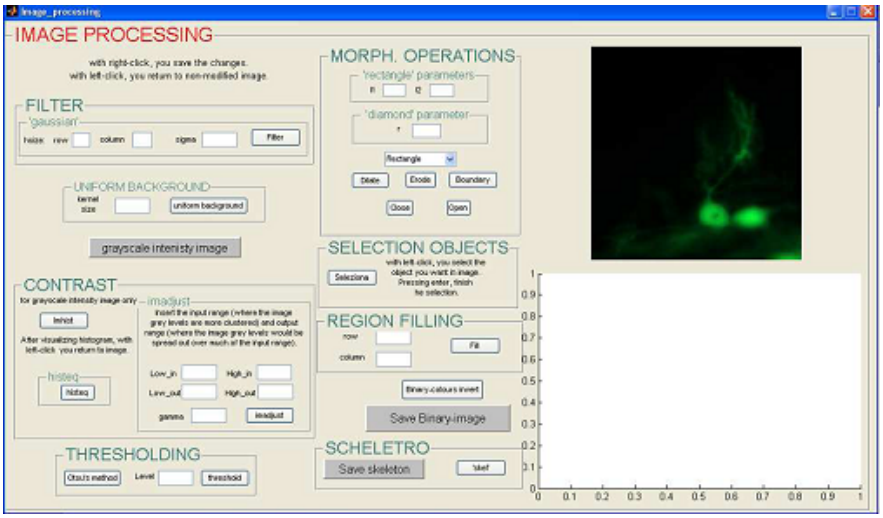

Figure 2.4: *GUI for manual image pre-processing.*

can decide whether the performed operation has led to an optimal image for further processing. For saving the changed image, the user must press the right mouse button; otherwise the user presses the left mouse button so that he/she can go back to the previous image.

The editor on the other hand, displays a window, where the user can see the original image and the modified one. At the end of the processing, one single box is shown representing the original image, the histogram after enhancing the contrast, the binary image and the skeleton (Figure 2.5). Besides, in the editor, the intermediate images are automatically saved, so there is no possibility to change the sequence of execution of the algorithms, or of conducting them several times with different parameters, during the processing.

Finally, while in the GUI the user can save the binary image and the skeleton clicking on "Save Binary image" and "Save skeleton"

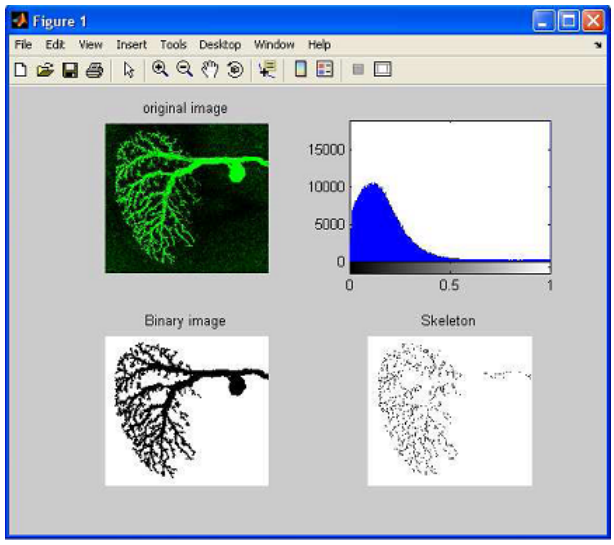

Figure 2.5: *GUI for semi-automatic image pre-processing.*

buttons; in the editor, at the end of processing, first different boxes display the binary image and the skeleton, then another box is displayed asking the user whether to save or not. In both the GUI and the editor, the binary image and the skeleton are automatically saved in the same folder of the original image. Both GUI and editor supply information on the pixel (pixel value and coordinates) where the cursor is placed. The following subsections describe in details each algorthim implemented specifying if the belong only to the GUI or to both the editor and the GUI.

2.2.1.1 Filter

It may be convenient to apply a slight gradient to the image, in fact, it is desiderable to minimize small variations in colors and to

prevent the detection of non-existent and unwanted contours. Hence a Gaussian filter, that is a low pass filter was implemented. This algorithm is implemented in both the editor and the GUI. In the GUI there are two edits in which the user needs to insert the mask size and the standard deviation, that model transfer function and define the filter's area of influence, then it has to click on the "Filter" button to apply the operation. In the editor, default parameters are used. First the algorithm converts the image from RGB to YCbCr space, in order to isolate the luminance component, that is the first matrix plane. Then, it applies a low pass filter only on this component, and reconstructs the image by combining the new luminance value with the second and third matrix component, that are unchanged. Finally, it reports all in RGB space.

2.2.1.2 Uniform background

Sometimes it can be useful to remove impurities in the image that are due to the culture itself or to the acquisition, so an algorithm to make the background uniform,was implemented. This algorithm is present only in the GUI. The operation consists of two phases:

1. Estimation of background brightness: the algorithm performs an opening operation, with a very large structuring element; the result is a matrix, called background, that represents the background color;

2. Creation of a more uniform background: the algorithm calculates the difference between the starting image and the background.

In this way it is possible to obtain a more uniform background with a color clearly different from the objects in the image.

2.2.1.3 Grayscale image

After running algorithms on truecolor image, it is possible to convert an RGB image to a greyscale intensity image. This image can be more efficient in term of storage: in fact, matrix size is reduced as the image is changed from three to two dimensions. Besides, greyscale image can be improved in term of contrast, spreading out its histogram. Obviously, this function is implemented both in the GUI and in the editor.

2.2.1.4 Contrast enhancement

Clicking on the "Imhist" button in the GUI panel "CONTRAST", the user can display the histogram of the image; that is a graph indicating the number of times each grey level occurs in the image. In the editor, at an appropriate point, the program execution stops and the histogram it is displayed . There are two ways of enhancing contrast:

1. Histogram stretching: the user can stretch out the grey levels in the center of the range by applying a piecewise function. A Matlab function is used, that maps the intensity values in the image to new values, so that these values goes from an in range map to an out range. These ranges are inserted by the user, in addition to a parameter which describes the shape of the function. This function is also implemented in the editor;

2. Histogram equalization: it is an automatic procedure that changes the histogram to another one which is uniform. This algorithm is implemented only in the GUI.

In the GUI, it can be useful to use both the algorithms, so that it is possible to take advantage of the single operations.

2.2.1.5 Thresholding

After enhancing image contrast, it is necessary to perform a segmentation of the image, which refers to the operation of partitioning an image into component parts, or into separate objects. The core of image segmentation is thresholding, that allows a binary image to be obtained. It is very efficient in terms of storage, because there are only two possible values for each pixel, 0 and 1, that are logical values. So, value of each pixel is described with a single bit.
There are two ways of finding the threshold:

1. A greyscale image is turned into a binary (black or white) one first by choosing a grey level T in the original image, and then turning every pixel black or white according to whether its grey value is greater than or less than T. T value is visually sought rolling the mouse over the image. This is very useful for a poorly contrasted image;

2. If it is not possible to obtain a single threshold value which will isolate objects completely, the user can click on the "Otsu method" button starting an algorithm that automatically find the threshold with Otsu Method [167]. This is implemented both in the GUI and in the editor.

In both the operations, the result is an image with white objects and black background in the case of a photograph which represents neurons expressing GFP, so with objects brighter than background. Otherwise, for images representing neurons from wild-type mice, the user has inverted colors, because objects are darker than the background.

2.2.1.6 Morphological operations

This branch of image processing is particularly useful for analyzing shapes in images. Four morphological operations have been implemented in the GUI:

- Dilate: adds pixels to the boundaries of objects in an image. This functions is based on Minkowsky addition. Morphologically dilating an image is very useful to connect parts of the same object, which are separated by thresholding;
- Erode: removes pixels on object boundaries. This functions in based on Minkowsky subtraction. Morphologically eroding image is useful to remove unwanted items, produced by thresholding;
- Open: erodes an image and then dilates the eroded image using the same structuring element for both operations. It removes small objects in an image while preserving the shape and size of larger object in the image;
- Close: dilates an image and then erodes the dilated image using the same structuring element for both operations. It

tends to smooth an image, fuses narrow breaks and thin gulfs, and eliminates small holes.

The number of pixel added or removed from the objects in an image depends on the size and the shape of the structuring element used to process the image. In the GUI, the user can choose between two structuring element shapes, listed in the pop-up menu:

- Rectangle: creates a rectangle-shape structuring element. The user can specify the mask size in the appropriate editor;
- Diamond: creates a diamond-shape structuring element. The user can specify distance from the structuring element origin to the points of the diamond in the appropriate editor.

In the GUI, the user can choose the sequence of operations, and the same operation can be performed several times. In the editor, only dilatation has been implemented, using a rectangle structuring element, and the user can only decide its size.

2.2.1.7 Boundary detection and region filling

If the image is poor in contrast, in the GUI there is the possibility to use a boundary detection algorithm. It has been implemented using morphological operations. After inserting mask shape and size, the user need to click on the "Boundary" button. The algorithm erodes binary images, and the result is subtracted from the original image. Every pixel in a binary image is represented with a logical value: so it can be helpful to use the logical operator AND.
To detect the boundary image, A&∼B operation is defined, where

B is the result of eroding the image A with the selected structural element. This logical operation always results in 0, unless both elements (A and B) are 1. Using a diamond shape, the user can get the best result. Working on an image bounded by an 8-connected boundary, the user can perform this function to fill up the entire region. With the mouse cursor, the user identifies a pixel p inside the object to be filled up, and inserts its coordinates in the appropriate edits. The logical operation is always A&∼B, but this time A is p-dilatation, with a structuring element, constituted by a matrix 3×3 of all ones, and B is the bounded image. Iterating this operation, A continues to expand until it fills the whole object.

2.2.1.8 Object selection

Images can contain multiple objects, which can be neurons, or in-vitro impurities. So it can be useful to select only some objects in the binary image, isolating these from others.
When the user clicks on the "Select" button, first a preliminary operation has been implemented, called "Labeling". This function labels connects objects in the binary image. It returns a label matrix, in which the pixels in the same connected objects are assigned the same integer. An 8-adjacency has been chosen, so two objects connected only by a pixel are considered as one.
After this operation, the labeled image is displayed, and lets the user select objects he/she wants using the mouse. Using the left button, he/she clicks on a pixel belonging to the object and on so doing adds all the pixels with the same label, that means the whole object. Backspace or Delete removes the previously selected object,

while pressing Return the selection ends . Not-selected objects become automatically black. This is a very useful technique because it allows visual identification of the object to be skeletonized and it is implemented both in the GUI and in the editor.

2.2.1.9 Skeletonization

As mentioned before, the skeleton reproduces the structure of the cell, reduced to one pixel thick. The skeleton must have some important characteristics: it must faithfully reproduce the structure of the cell and it must reduce neuron's soma to a single pixel, positioned in its center.
Mainly two algorithms that carry out skeletonization are present in literature: the Lantejoul's method and the thinning algorithm.
Both the algorithms present some problems. The first one is powerful in recognizing the soma, with a reduction of the whole area to a single pixel, but it is not very efficient in reconstructing neuron structure. However, the second one is very accurate in the reconstruction of the dendrites, but it doesn't work well with the soma. So a synergic combination of the two algorithms was developed.
In the GUI, clicking on the "Skel" button, the input image is displayed then the program execution waits for the user to specify a crop rectangle, with the mouse which must contain the soma. In the editor, a message box is opened, which prompts user to select the soma, and automatically opens a window with the input image. After making the selection, the Lantuejoul's method runs. Then the program automatically executes the thinning algorithm, which allow the skeleton to be obtained from this intermediate image. Figure 2.6

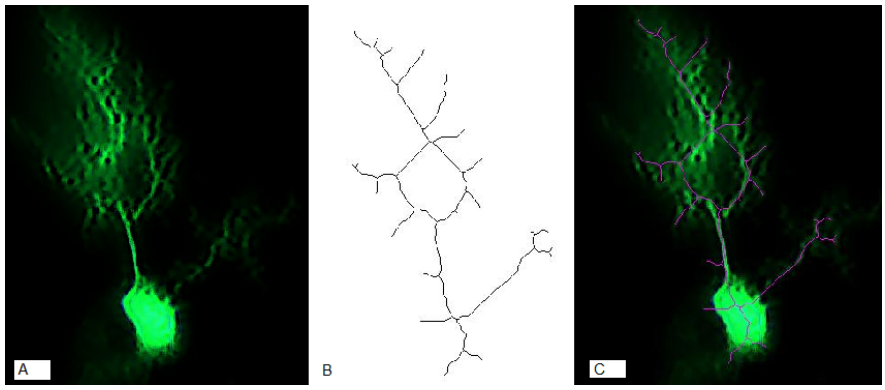

Figure 2.6: *a)The original image, b)the skeleton and c)the overlap between the two.*

represents the result of the synergy between the two algorithms. It is clear that the skeleton meets the specifications given so it is suitable for the extraction of morphological variables.

2.2.2 Morphological analysis

The morphological analysis allows the contribution of metrical features and their evolution to be studied quantitatively. Using the GUI, the metrical features relevant to the cell's structure and morphology were directly extracted (Figure 2.7). This subsection is focused on the methods used for the morphological analysis and on the variables extracted; a more detailed description of the GUI panels and commands and of the algorithms implemented in the GUI can be found in my M.S. thesis [168]. The morphological variables were chosen from those generally reported in the literature [150], [169] and divided into two groups, local and global variables. The former

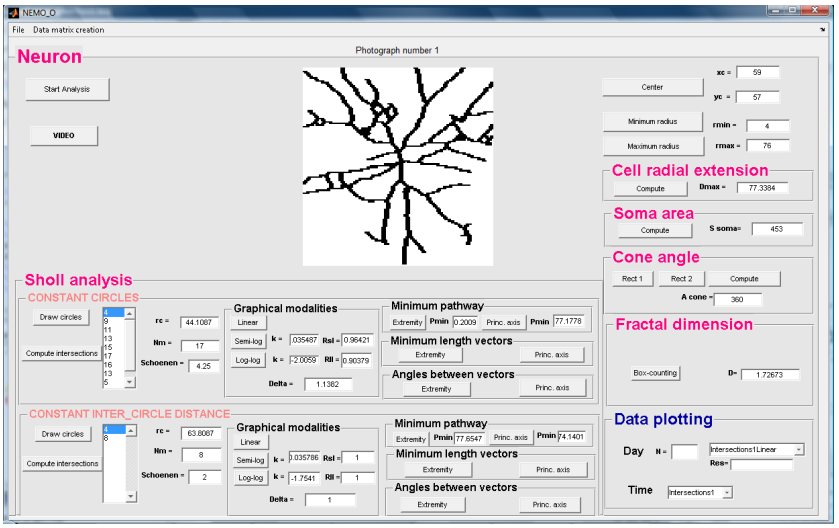

Figure 2.7: *GUI for morphological analysis of single Purkinje neurons.*

variables are referred to the dendritic tree, while the latter variables, such as radial extension, soma area, cone angle, and fractal dimension, relate to the whole cell structure. Following the Sholl method [170], each cell skeleton circumscribed a coordinate system consisting of a series of concentric circles centered on the soma. Local variables were extracted by counting the number of intersections between each circle and the cell's dendrites. A list of variables assessed is given in Table 2.1, those selected for the PCA analysis are checked. In order to generalize the data processing algorithms and GUI, all the lateral dimensions are represented in terms of pixels. All the values in the figures and tables are therefore expressed in pixels. At the magnification used, one pixel corresponds to 0.182 μm.

Variables	PCA
Intersections	
Critical radius (R_c)	X
Maximum number of intersections (N_m)	X
Schoenen ramification index	
Regression coefficient for log-log method (k_{LL})	
Regression coefficient for semi-log method (k_{SL})	X
Correlation coefficient for log-log method (R_{LL})	
Correlation coefficient for semi-log method (R_{SL})	
Determination ratio (Δ)	
Minimum length vectors	
Angles between minimum length vectors	
Minimum pathway (P_m)	X
Radial extension (E)	X
Cone angle (C_a)	X
Soma area (S_a)	X
Fractal dimension (F_d)	X

Table 2.1: *List of variables and variables selected for three-way PCA analysis. X: variables selected for the PCA analysis.*

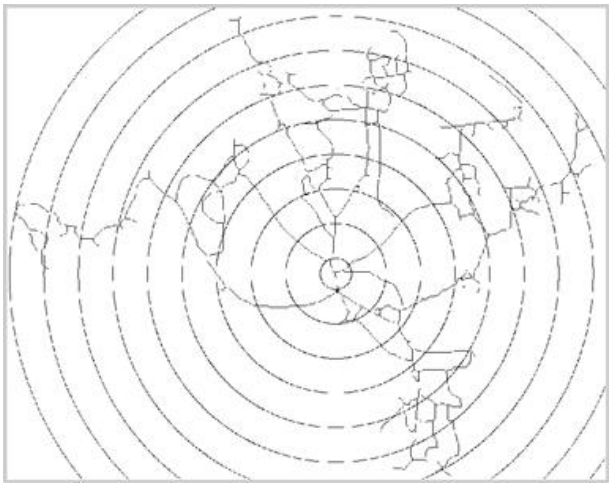

Figure 2.8: *Sholl reference system.*

2.2.2.1 Sholl analysis

The Sholl analysis is a method for the quantitative study of the radial distribution of the neuronal dendritic arborization pattern around the cell's soma (Figure 2.8). It allows dendritic geometry, ramification density and dendritic branching patterns to be evaluated and is applied to binary images representing the cell skeleton.

The Sholl analysis can be applied in three different graphical modalities as demonstrated by Milośević and Ristanović [171].

1. *Linear method*: The plot of the number of dendritic intersections calculated per intersecting circle area, versus the circle radius;

2. *Semi-log method*: The plot of the logarithm of the number of dendritic intersections per intersecting circle area, versus the

circle radius;

3. *Log-log method*: The plot of the logarithm of the number of dendritic intersections per intersecting circle area, versus the logarithm of the circle radius.

As demonstrated by Sholl [170], at least in the semi-log or loglog methods, a linear behavior is apparent. The method which better approximates a straight line provides relevant cues about the dendritic tree structure. The linear method is characterized by:

- R_L *(critical radius)*: The radius of the circle with the maximum number of intersections;
- N_m: Maximum number of intersections;
- *Schoenen ramification index*: Quotient of the maximum number of intersections and the number of primary dendrites of the cell (the branches directly arising from the soma).

The semi-log and the loglog methods are characterized by:

- k_{SL}*(Sholl regression coefficient)*: Slope of the fitted straight line in the semi-log plot. It measures the decay rate of intersection numbers versus the distance from the soma;
- k_{LL} *(Sholl regression coefficient)*: Slope of the fitted straight line in the loglog plot. It measures the decay rate of intersection numbers versus the distance from the soma;
- R_{SL} *(correlation coefficient)*: Degree of data correlation in semi-log method;

- R_{LL} *(correlation coefficient)*: Degree of data correlation in loglog method;

- Δ *(determination ratio)*: $\Delta = R_{SL}^2/R_{LL}^2$. It allows the more appropriate graphical method to be determined. If $\Delta < 1$ the loglog method is preferred, while if $\Delta > 1$ the semi-log method is better.

2.2.2.2 Morphometric parameters

Besides the Sholl analysis, other morphometric variables relative to the cells were calculated. If the cell is not uniformly extended in all directions, it is also possible to extract the principal axis of each cell, which corresponds to the thickest dendrites which determines the direction of extension of the cell. From the intersections obtained from the Sholl analysis and the principal axis, other variables such as the minimum length vectors, the angles between minimum length vectors and the minimum pathway (P_m) can be evaluated. The minimum length vector between two adjacent circles can be extracted by evaluating the minimum Euclidean distance between the cell intersections on the two circles and the corresponding angle with the radial axis. The minimum pathway is the sum of the magnitudes of the minimum length vectors. Other parameters were:

- *Radial extension (E)*: In order to evaluate the cell dimensions, the radial extension of the cells can be assessed as the Euclidean distance from the cells center to the furthest pixel of the cell skeleton (Figure 2.9);

Figure 2.9: *Radial extention of a Purkinje cell.*

- *Cone angle (C_a)*: In order to characterize the cells orientation, the angle of the cone in which the cell is contained can be extracted. Once the direction of extension is assessed, cones can be drawn on the cell image using a semi-automated procedure (Figure 2.10), and the cone angle subtended by the cell is computed using Carnot's theorem. If the cell is uniformly extended in all directions the cone angle is fixed at 360 °;

- *Soma area (S_a)*: The soma area can be calculated by approximating each soma to an ellipse. After manually marking the major and minor axes of the ellipse, the algorithm determines their lengths and the area of the ellipse (Figure 2.11).

- *Fractal dimension (F_d)*: Fractal dimension is a measure of a feature common to several biological systems, their fractal nature or complexity. An object is fractal if it expresses the

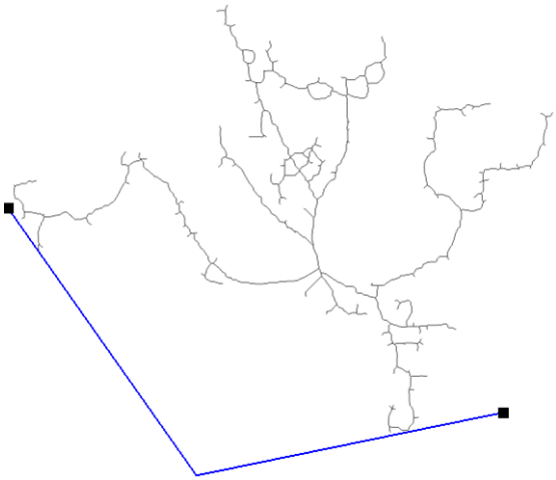

Figure 2.10: *Cone lateral projections.*

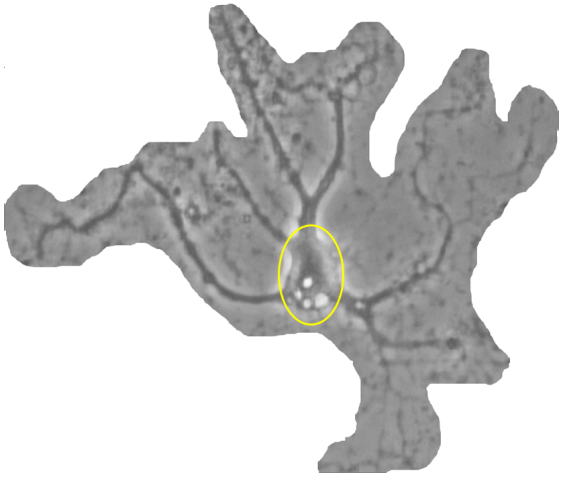

Figure 2.11: *Approximation of the soma to an ellipse for soma size estimation.*

property of self-similarity: it is made up of copies of itself at different scales. As argued in several studies neurons can be represented as fractal or space-filling objects and the fractal dimension represents an important parameter for the characterization of the dendritic structure [172], [173], [174], [175]. There are several methods to evaluate the fractal dimension; in this study the box-counting method was used as described by Jelinek and Fernandez [174], implemented in a specific Matlab Library (Matlab Database, Universität Stuttgart). In this method the cell image is inscribed in a squared grid of sides r. The size r of each square or box in the grid is initially equal to the image size and is progressively decreased, while the number of non-empty boxes, N(r), is counted. After this calculation a plot of log(n) versus n is obtained. This plot can be fitted with a straight line, of slope S, where S is an estimation of the fractal dimension (F_d).

$$F_d = S$$

While a mathematical fractal requires infinite orders of magnitude of power-law scaling and therefore is fractal over all scales, physical, biological and other structures in nature are fractal over relatively small scaling range [176].

2.2.3 Topological analysis

The topological analysis allows the contribution of metrical features and their evolution to be studied quantitatively. Segments of cere-

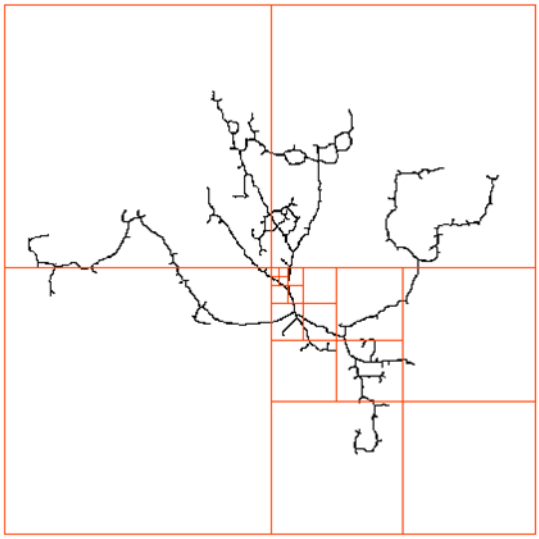

Figure 2.12: *Box-counting method for fractal dimension computation.*

bellar folia must be selected for the analysis (Figure 2.13) and photographed each day of culture. Using the GUI, the metrical features relevant to the slice topology were directly extracted (Figure 2.14). The variables chose in this analysis are relevant to study the migration of the cells during the days of culture in a quantitative way. This kind of analysis is important in the study of Purkinje cells from animal models of ASD as some studies show that all migration is defective in ASD [177], [178].
In the GUI, after a pre-processing step in which images of slices were converted to binary images, some quantitative topological features where computed automatically:

- *Mean fluorescence intensity (F)*: The fluorescence intensity is a

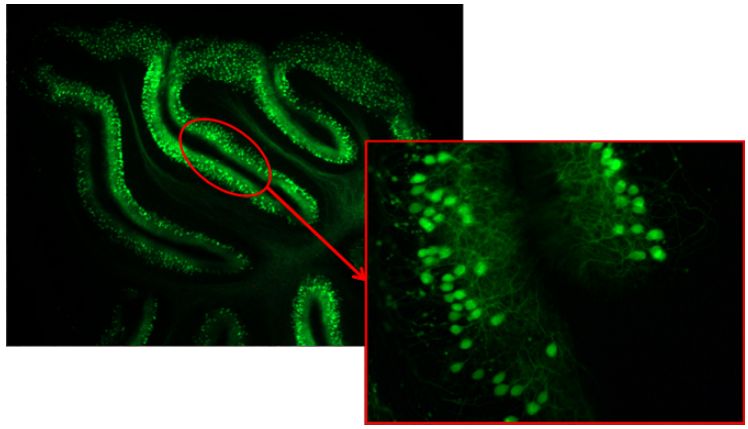

Figure 2.13: *Cerebellar folia in an organotypic slice, magnification 10X (left) and segment selected for th anlaysis, magnification 20X (right).*

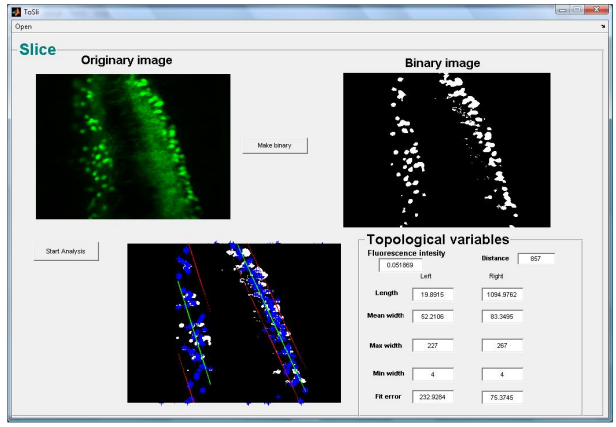

Figure 2.14: *GUI for topological analysis of cerebellar slices.*

measure of the ability of the Purkinje neurons to express GFP in time. It is compute as the mean pixel value of the image converted in greyscale levels.

- *Distance (D)*: The distance between two opposite layers of cells within a segment. The maximum external distance between the two layers was considered.

- *Length (L)*: Two measurements related to the lengths of the two layers of the segment. In order to compute this and the following measures, it was necessary to separate pixels belonging to the two layers. To do that two pixel between the layers must be selected and a line through the two point is computed.;

- *Average width (W_{av})*: Two measurements related to the mean width of the two layers of the segment;

- *Min width (W_{min})*: Two measurements related to the minimum width of the two layers of the segment;

- *Max width (W_{max})*: Two measurements related to the maximum width of the two layers of the segment;

- *Linear fit error (E)*: For each layer the width the layer for each raw of the image was computed. For each of the measurements of width found the mean point was then considered. In order to evaluate the degree of the alignment all the mean points were then approximated with a line and the least square error of the fit was computed.

2.2.4 Neuron count

Sometimes it can be interesting to calculate the number of objects in an image. In case of the analysis of neurons extracted from animal models of autism, it may be useful to know the number of Purkinje cells displayed in the photograph of cerebellum slices. In fact, several studies show that Purkinje cell number in the cerebellum is reduce in autistic individuals compared to normal [91] and the same occurs in the Engrailed2 mouse [68], [71]. The basic idea of the algorithm is to obtain a binary image, and then to count the white objects, which represent the cells. It is clear that it is not necessary to reconstruct all the shape of the neurons in the image, because it is enough to count the somas. Furthermore, it may be useful to have only somas in the image, so that it is not possible to count the different parts of the cell several times, which may can be separated during thresholding.
There are two editors to perform the neuron count: one is for fluorescent (GFP) neurons and the other is for wild-type neurons. It is necessary to make a distinction because while fluorescent cells are brighter than the background, and so, after thresholding, the result is white objects against black background, non-fluorescent cells, are darker than the background, so the contrary happens and it is necessary to invert the color of the binary image after thresholding. The neuron count algorithm is similar to the image processing algorithm, so the first steps are filtering, generation of a uniform background and greyscale conversion.
Above all for fluorescent cells, the soma is brighter than the other parts of the cell, so the contrast enhancement is not implemented.

In this way, dendrites are not emphasized: for this type of operation, dendrites are not relevant. After thresholding, it is necessary to perform some morphological operations on the binary image in order to remove dendrites and axons and to isolate somas:

- Erosion, with a structuring element of appropriate shape and size;
- Opening, performed with a specific Matlab command, that allows removal of small objects;
- Removal of spurious pixels, performed with an other specific Matlab command.

Using these algorithms a label operation is performed. The higher number used to label objects corresponds to the number of these objects in the image.

2.2.5 Database construction

The data extracted with the above described analyses are then saved in a three-dimensional matrix structure which is nominated "datamatrix" and are organized into cells or slices, variables and time. Variables extracted from different neurons or slices can be collected in the same datamatrix so that they can be easly extracted and compared. Indicating with n the number of cells or slices, with m the variables extracted and with t the days in which the images were obtained, the final structure of the datamatrix results as follows:

$$n \times m \times t$$

When the statistical analysis is performed using the three-way PCA (described in the following subsection) it is necessary to reorganize the database in order to obtain a suitable structure for this kind of the analysis. After the reorganization the datamatrix has the following structure:

$$(m \cdot t) \times n$$

2.2.6 Statistical analysis

The statistical analysis was performed by the three-way Principal Component Analysis (PCA) multivariate technique [179] operating on the datamatrix. Three-way PCA technique is a generalization of PCA, a popular technique that is often used for the exploratory analysis of a set of variables. While PCA analyzes data varying in two dimensions, three-way PCA permits the analysis of sets of variables associated with three-way data sets, the so-called modes: the variables, the objects and the conditions (time intervals). This technique is aimed at transforming data so as to summarize the associated information in a small number of novel variables or principal components able to express as much information as possible. Several models and algorithms implement the three-way PCA methodology [180]. In this work, the Tucker 3 model was adopted as described by Leardi et al. [179]. Briefly, data are firstly pre-processed in order to remove scaling and standardization offsets, then the number of components can be chosen. To obtain principal components the covariance matrix of data is decomposed in a eigenvectors matrix and a eigenvalues matrix. Eigenvectors are the columns of the rotational matrix that is transposed and multiplied for the datamatrix. The

multiplication result is the principal components matrix (mathematically it corresponds to performing a series of orthogonal rotations on a cubic core array, G, expressing the correlations between the data from the "datamatrix" denoted by objects, variables and conditions planes. The orthogonal rotations are iterated until a body-diagonal common orientation is reached). The minimum number of components is selected on the basis of an optimized data fitting and stability and interpretability criteria such that data variance is maximized. In fact, only a small number of principal components are chosen and they constitutes the axes of the plots in which data are reported. The final transformation is given by the following equation:

$$x_{ijx} \cong \sum_{P}^{p=1} \sum_{Q}^{q=1} \sum_{R}^{r=1} a_{ip} b_{jq} c_{kr} g_{pqr}$$

where x_{ijx} are the elements of the original datamatrix, while a_{ip}, b_{jq}, c_{kr} and g_{pqr} are the elements of the matrices A, B, C and G. G is the core efficiency describing the main relations in the data.
The component matrices A, B, and C describe how the particular subjects, variables and conditions are related to their associated components. The three data modes are plotted in three different graphs whose axes represent the principal components. The meaning of the principal components requires careful interpretation and analysis. Typically after the PCA analysis, objects, variables and conditions are represented in a two-axes plot and correlations between the two axes and the parameters can be deduced by an analysis of the plots. Each parameter has a specific coordinate according to the weight it bears with respect to the axis. If the coordinate is near 0, then the weight is small, if it is greater or less than 0, the weight is high.

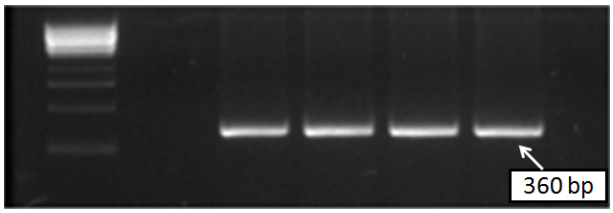

Figure 2.15: *Photograph of an agarose gel after electrophoresis of L7GFP mice DNA. A band at 360bp (base pairs) must appear.*

2.3 Materials and methods

2.3.1 Development of the L7GFP mouse and of EN2$^{-/-}$/L7GFP hybrid

Among the genes contributing to the molecular identity of PCs is Purkinje cell protein 2 (Pcp-2) [181]. This gene was identified via the cDNA clones PCD5 [182] and L7 [183], [184] and is noteworthy because Pcp-2 mRNA and the 99-amino-acid cytoplasmic protein it encodes have been found only within cerebellar Purkinje and retinal bipolar neurons [182], [183]. L7GFP mice have been developed where expression of GFP in PCs is specifically driven by the Pcp-2 promoter . Fluorescence in PCs is retained for weeks in cultures and thus these cells can be directly monitored in long term confocal and/or fluorescence studies [185].
Homozygous L7GFP males were crossed with EN2$^{-/-}$ females and hybrids were genotyped with standard PCR procedures after extracting genomic DNA from tails (Figure 2.15).

F1 mice from different litters were crossed to obtain founders homozygous EN2$^{-/-}$/L7GFP. Founders were crossed to establish a

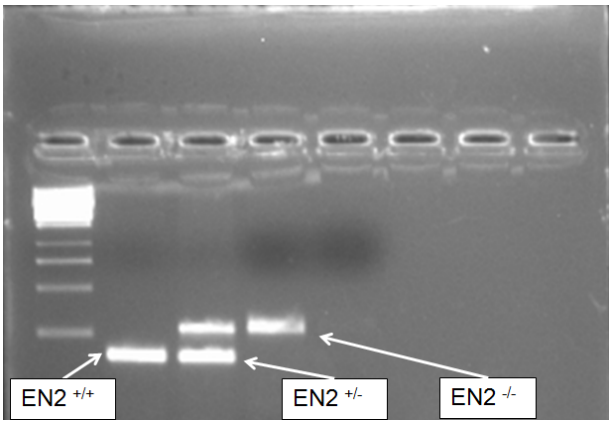

Figure 2.16: *Photograph of an agarose gel after electrophoresis of EN2/L7GFP mice DNA. Three different configuration of bands can appear according to the three different genotypes:* $EN2^{+/+}$, $EN2^{+/-}$ *and* $EN2^{-/-}$.

new hybrid line. Each animal subjected to subsequent analysis has been genotyped (Figure 2.16).

2.3.2 Culture preparation

Unless stated, all the culture reagents were from Sigma (Sigma, Italy) and materials from Falcon (Falcon, Italy). Purkinje cells were prepared from P1 CD1 mice pups (wild-type, L7GFP or EN2/L7GFP) and maintained according to previously described procedures [186], [187]. Timed pregnant CD1 mice were purchased from Harlan, Italy. P1 mice cerebella were dissected in $Ca^{2+}Mg^{2+}$ free phosphate buffered saline (PBS) containing gentamicin (10 μg/mL) and placed in a 15 mL plastic tube (Falcon 2096). The tube was centrifuged at 1000

rpm, 4°C for 1-3 min. After the supernatant was aspirated, fresh PBS was poured into the tube. Tissue dissociation was realized both enzymatically and mechanically. The enzymatic dissociation was obtained by the addition of trypsin (0.1% w/v in PBS), maintained at 33°C for 13-15 min, and, after two rinses in PBS, DNAse (5 U/mL in PBS) was added. The mechanical dissociation was obtained using a borosilicate-coated fire-polished Pasteur pipette, after which the cell suspension was centrifuged at 1200 rpm, 4°C for 5 min. After removing the supernatant, cells were counted and the density was adjusted to 5×10^6 cells/ml using the seeding medium consisting of 100 mL of Dulbecco's modified Eagle medium (DMEM)F-12 in a 1:1 mixture containing 10% fetal calf serum. A 100µL drop of the medium containing the cells was placed on 15μg/mL polylysine-coated culture plates (radius 360 mm). After 3 h incubation, 1 mL of culture medium was added to each plate. Culture medium consisted of DMEM/F-12 in a 1:1 mixture containing 20 μg/mL of transferrin, 40 nmolof progesterone, 20 μg/mL of insulin, and 0.5 ng/mL of tri-iodothyronine. Cells were maintained in a humidified cell culture incubator (37°C, 5% CO_2). In the culture without glia, every 3 days, half of the medium was replaced with a fresh one enriched with 100 μg/mL of bovine serum albumin (BSA) and 4 mmolof Ara-C (cytosine arabinoside-Upjohn, USA), a glial proliferation inhibitor. In the culture with glia, after 2 h of incubation with the medium with serum, it was replaced with a serum-free medium without Ara-C. Every 3 days, half of the medium was replaced with fresh medium. Purkinje cells survived in culture for about 20 to 25 days.

2.3.3 Organotypic slice preparation

Organotypic cultures were prepared from P7-10 mice (Reln/L7GFP). Unless stated, all the culture reagents were from Sigma (Sigma, Italy). After euthanasia the brain was quickly removed from the skull and placed in 500 mL ice-cooled Geys (GIBCO^{TM}, Invitrogen)solution supplemented with 4.8 mL glucose 50%, 0.05 g ascorbic acid and 0.1 g sodium pyruvate. The cerebellum is then isolated under a stereomicroscope and immediately sectioned in 400 μm parasagittal slices with a McIlwain (Brinkmann Instrument, westbury, NY, USA) tissue chopper. During the entire procedure tissues stayed immersed in the cooled Geys solution. Groups of 3-5 slices were plated onto Millicell-CM inserts Millipore (Millipore). Each insert was placed inside a 35 mm Petri dish containing 1.1 mL of culture medium, and incubated at 34°C in 5% CO_2 for up to 30 days in-vitro (DIV). Culture medium is as follows: Eagle Basal Medium 50%, horse serum 25%, Hanks balanced salt solution 25%, glucose 0.5%, 200 mmol L-glutamine 0.5%, antibiotic/antimycotic solution.

2.3.4 Optical and fluorescence imaging

Cells were observed daily and photographed using a microscope (Olympus PR54, Italy) with a X20 objective interfaced to a digital camera (Alkeria, Pisa) 2.17. The digital camera was connected to a PC where a dedicated Software was installed. Using the interface of the Software it was possible to see in real time what the objective of the microscope was framing and to adjust the acquisition parameters in order to improve the quality of the images. In order to observe the same area of the culture dish, a grid was posi-

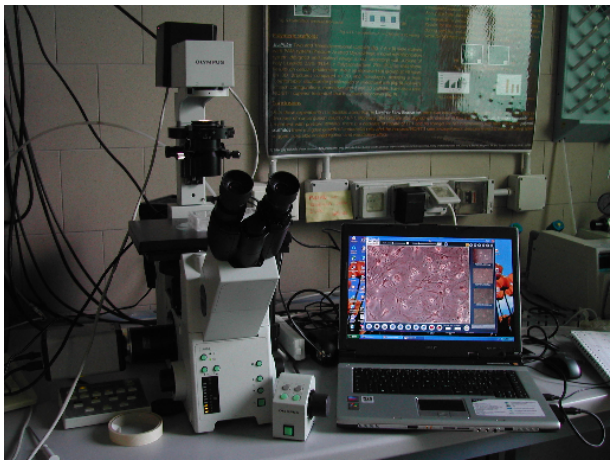

Figure 2.17: *Optical microscope interfaced to a digital camera and a PC.*

tioned on the bottom of each well. The unit length of the grid was 100 μm. Images of neurons from wild-type mice were obtained using the white light of the microscope while to photograph neurons from GFP mice blue fluorescent light was used.
In the first phase of this work non fluorescent cells were analyzed. A total of 25 cells in the presence of Ara-C and a total of ten cells with glia were analyzed and a comparison between the two groups of cells was performed. In the second phase fluorescent cultures and organotypic slices were considered.

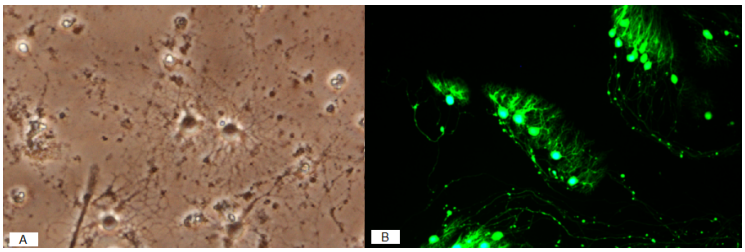

Figure 2.18: *a) Photograph of wild-type Purkinje neurons, b)Photograph of GFP Purkinje neurons.*

2.4 Testing and results

2.4.1 Pre-processing of GFP Purkinje neurons images

The use of GFP is a great advantage from a pre-processing point of view as it makes the process easier and faster. In an image of wild-type cells the contrast is very low (Figure 2.18a) while in GFP images the contrast between the neurons and the background is clear (Figure 2.18b).

In order to evaluate the efficiency of the pre-processing algorithms implemented in NEMO, a comparison was made using of a combination of two freeware software largely used in biomedical image processing: Mipav [188] and Image J [189]. Some images of GFP Purkinje neurons from cultures and slices were analyzed with the different methods in order to obtain the skeleton of the cell and then the skeletons were overlapped with the original photograph of the neurons.

Figure 2.19 show the results obtained applying the two methods to

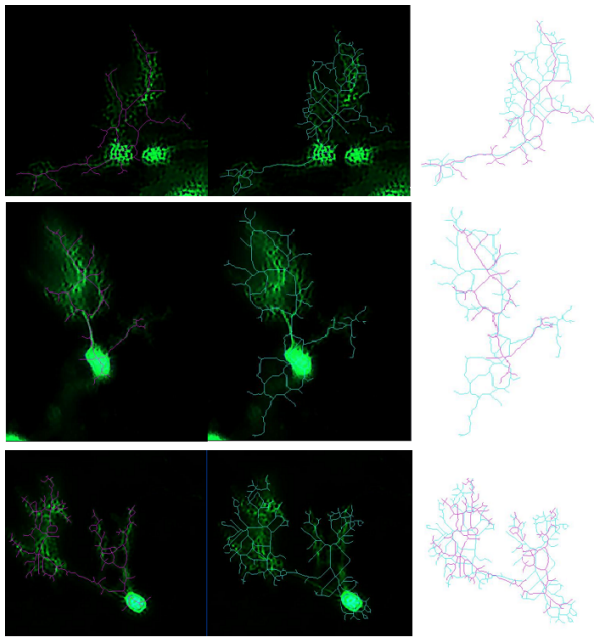

Figure 2.19: *Skeletons of Purkinje neurons obtined with NEMO (pink) and Mipav and Image J (cyan) and their overlap.*

the preprocessing of some images of Purkinje neurons and the overlapping of the two skeletons. The figure shows how usually in both cases the structure of the neuron is faithfully reproduced but in some cases the application of NEMO gives better results in comparison to the other software. Moreover there is a great improvement in the processing time as the algorithms implemented in NEMO are automatic or semi-automatic and this is a great advantage when the number of images to be processed is huge. Other advantages due to the automation of the process are the decrease of computational costs and of the burden on the user.

2.4.2 Assessment and comparison of neural morphology in neuron and neuronglia cultures

Purkinje cells with glia were imaged and analyzed at the mature stage of their growth, about the 18th day. The presence of glial cells within the cultures alter the development of dendrites and the directionality of cells to favor their connection with other neurons (Figure 2.20). The survival and the dendrogenesis of the Purkinje cells are favored by supplying cell culture medium and by the presence of other cells able to provide signals necessary for their growth.

Purkinje cells without glia were imaged starting from the first day of dendritic development, generally the 7th-12th day (Figure 2.20). During the growth period, observed three major changes were observed:

- Increase of size and dimensions;
- Development of dendrites;
- Orientation of the cells in a specific direction.

During the last few days of culture, a decrease in the cell size and in the number of dendrites was observed, indicative of suffering and cell initiation of death. After the image preprocessing to obtain the cell skeleton (Figure 2.20c), all the images obtained were submitted to the GUI. In the GUI morphological data analysis, the linear, semilog, and loglog methods of the Sholl techniques were implemented . Two coordinate of systems were considered: one with a constant number of circles and the other with a constant intercircle distance. The results obtained with the two systems were similar, the

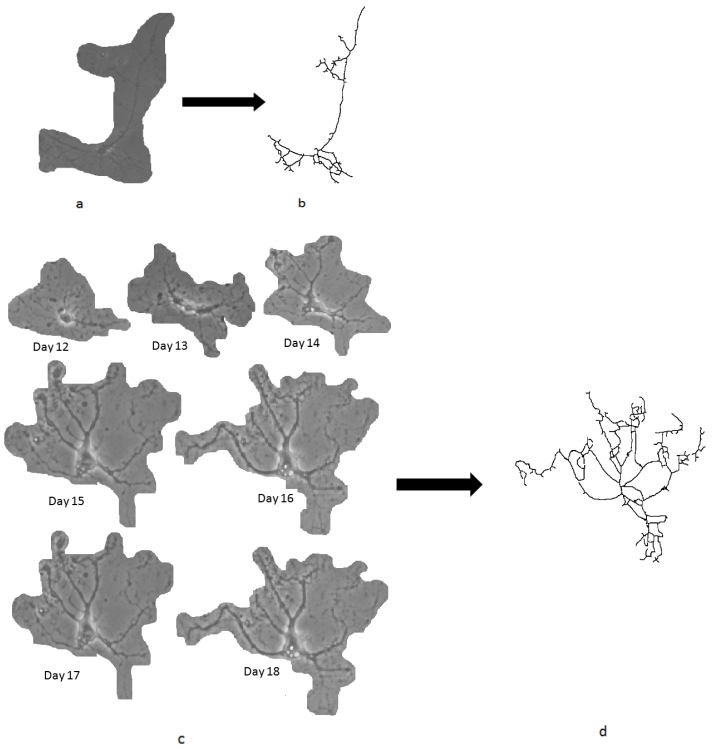

Figure 2.20: *a)Purkinje cell cultured in the presence of glia. c) Growth of a Purkinje cell cultured in the absence of glia. b),d) Skeletons of Purkinje cells.*

constant number of circles was used for its graphical simplicity. Figure 2.21b,d shows that the variation of number of intersections with radius for the cells in the presence of glia has a peak near the soma of the cell (Figure 2.21). The distribution of the value of number of intersections can be approximated to a Poisson distribution. The number of intersection versus radius for the cells without glia follows a unimodal distribution, i.e., low near the soma, high in the middle, and low far from the soma as shown in Figure 2.21a. In both cases, the number of intersections/area decreases logarithmically with the distance from the soma (Figure 2.21).

The semi-log and log-log methods are reported in Figure 2.22. The results obtained for the cells with glia are not general; in fact, for some cells the semi-log method is better (Figure 2.22a) while for some other cells, the log-log fits the data better (Figure 2.22c). In agreement with this result, for some cells, Δ is higher than 1, and for some others is lower, although Δ remains close to 1 in both cases (Figure 2.22e). For all the cells without glia, the semi-log method (Figure 2.22b) approximates a straight line while the regression error is worse in the log-log method (Figure 2.22d) indicating the former one as the most suitable for modeling dendritic organization in the cells. This is also confirmed in Figure 2.22f, where the determination ratio Δ for all the cells is higher than 1. The values of Δ are consistently higher than the values obtained for the cells with glia (Figure 2.22e,f).

The dynamic behavior of the cells without glia was assessed by plotting the number of intersections and the maximum number of intersections versus time. Figure 2.23a shows a typical plot of intersections versus time for a sample cell. For all cells, peaks coinciding

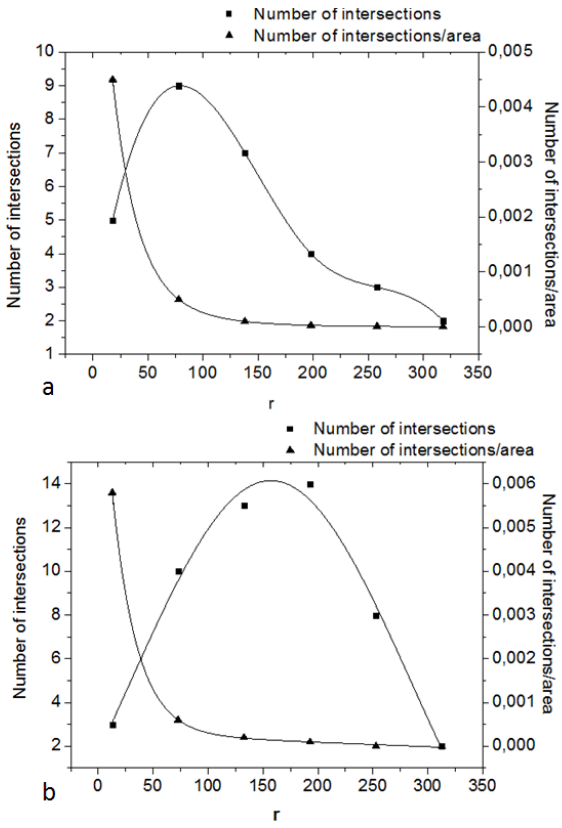

Figure 2.21: *a) Interpolation of the number of intersections as a function of radius (given in units of pixels) and logarithmic fit of the number of intersections per circle area as a function of radius for a typical cell cultured in the presence of glia. b) Unimodal distribution of the number of intersections as a function of radius and logarithmic fit of the number of intersections per circle area as a function of radius for a typical cell cultured in the absence of glia.*

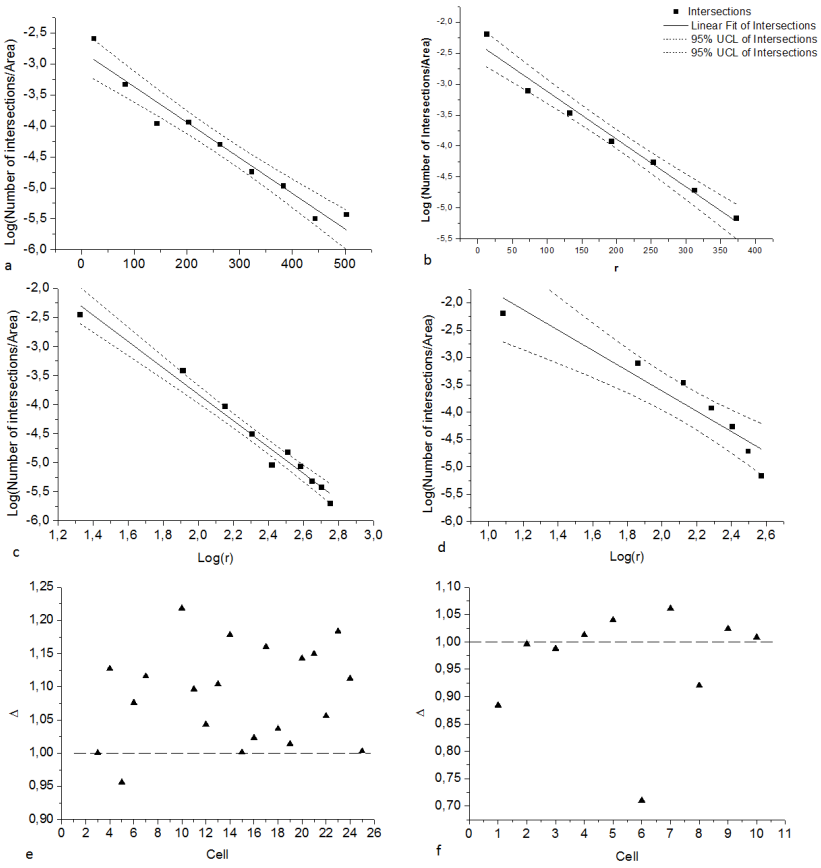

Figure 2.22: *a) Sem-log method for a cell in the presence of glia. b) Sem-log method for a cell in the absence of glia. c) Log-log method for a cell in the presence of glia. d) Log-log method for a cell in the absence of glia. e) Value of Δ for all the cells cultured in the presence of glia. f) Value of Δ for all the cells cultured in the absence of glia. The radius r is given in units of pixels.*

with the days after the culture medium was changed were observed (days 11, 13, 16, and 18). This indicates that the cells reacted to nutrient supply by developing new dendrites.
and can be seen clearly in the plot of the maximum number of intersections versus time (Figure 2.23b). Toward the end of culture period, the cells began to suffer and did not react to the nutrient supply, as shown by the low rate of dendrite growth (Figure 2.23a) and the downward trend of (Figure 2.23b).

Figure 2.24a,b shows the cell vectors of minimum length and angles, respectively, for a typical cell in the presence of glia. The plot of the minimum length vectors is quite linear (Figure 2.24a) while the plot of angles has a high number of peaks (Figure 2.24b). This means that the axis is tortuous but with a regular structure. On the other hand, the analysis of the evolution of the principal axis during the development of cells without glia shows that on the first few days, the minimum length vectors do not change in magnitude (Figure 2.24c), while the angles are small and maintain a narrow range (Figure 2.24d). This implies that the principal axis starts developing perpendicular to the cell soma. During active cell growth (days 15-20), there is an increased number of peaks in both plots (Figure 2.24c,d) and as time goes on and the cell begins to die, the behavior is once again linear and the range of angles is small.

In the cells of the culture with glia, the principal axis always corresponds to the radial extension. The mean radial extension of these cells is 92 μm (Figure 2.25a) In cells without glia, the principal axis is not always the longest dendrite. Figure 2.25b shows that the mean minimum pathway varies logarithmically with time. The minimum value is around 40 μm, while the maximum 90 μm

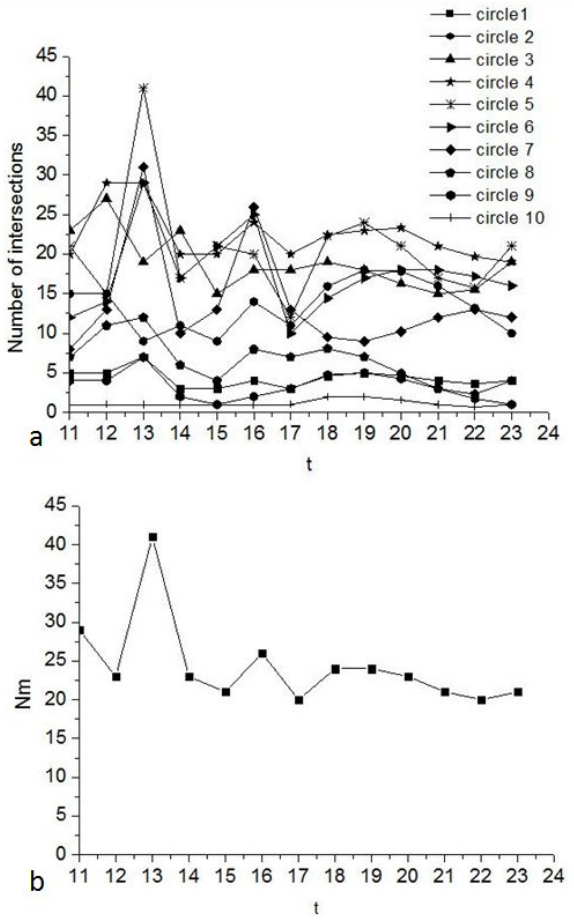

Figure 2.23: *a) Number of intersections for all the circles as a function of time for a typical cell cultured in the absence of glia. b) Maximum number of intersections as a function of time for all the cells.*

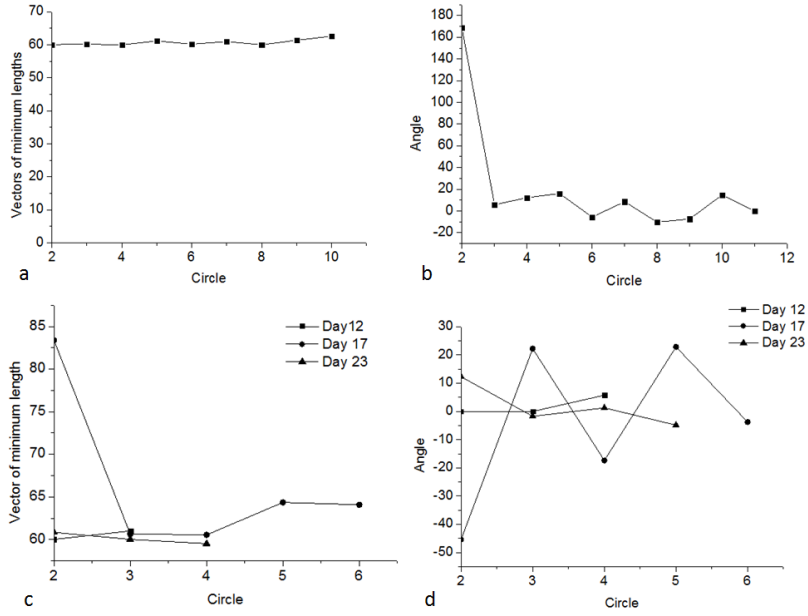

Figure 2.24: *a) Vectors of minimum length as a function of circles for a typical cell cultured in the presence of glia. b) Angles between vectors of minimum length as a function of circles for a typical cell cultured in the presence of glia. c) Vectors of minimum length as a function of circles on three different days of growth for a typical cell cultured in the absence of glia. d) Angles between vectors of minimum length as a function of circles in three different days of growth for a typical cell cultured in the absence of glia.*

and the principal axis grows at 4.5 μm per day. In agreement with the dynamic cellular growth theory [190], the mean radial extension for all the cells shows a logarithmic increase as reported in (Figure 2.25c) The minimum extension is around 45 μm and the maximum extension around 100 μm, so the cells grow at an average of 4.5 μm per day. Both groups of cells, with and without glia, have similar mean values of radial extension.

A plot of the cone angle for all the cells with glia, shown in Figure 2.26a, shows that these cells are very oriented. The cone angle is always narrow and is about 50 μm. The dynamic analysis of cells without glia shows that, for many cells, the angle subtended decreased to about $100 - 150\,^{\circ}$, indicating a preferential direction of extension, although they are less oriented than cells with glia (Figure 2.26c). Moreover, a few cells maintain an isotropic radial extension throughout the culture period, since the cone angle is always $360\,^{\circ}$ throughout the culture period (Figure 2.26c).

The soma size of the cells cultured with glia is quite small (Figure 2.26b). The variation in soma size fell into two main categories (Figure 2.26d). Cells with isotropic extension increased their soma area, while the soma of cells with a preferential direction of extension increased during the first few days of culture and then suddenly decreased. This is probably because the cells extended along a particular direction, and the soma becomes thinner in comparison with the cells having isotropic extension, in which somas maintain a more rounded shape. It can be noticed that the soma size of cells with glia was similar to that obtained for the group of cells cultured in Ara-C with a preferential direction of extension. This is a confirmation of the fact that cells with glia are very oriented.

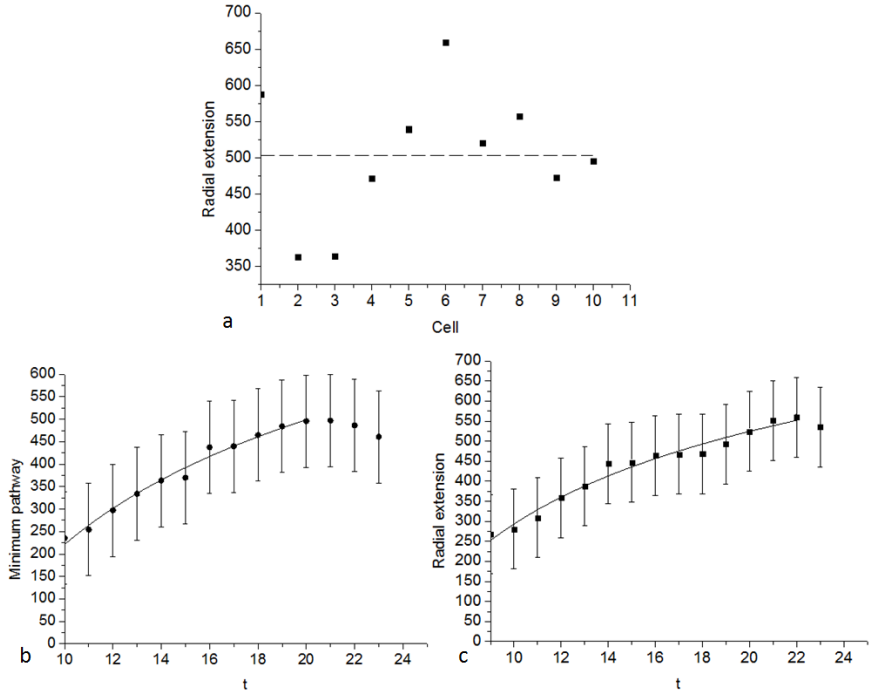

Figure 2.25: *a) Radial extension (given in units of pixels) for all the cells cultured in the presence of glia and mean value (dashed line). b) Mean minimum pathway as a function of time and logarithmic fit. c) Mean radial extension as a function of time and logarithmic fit.*

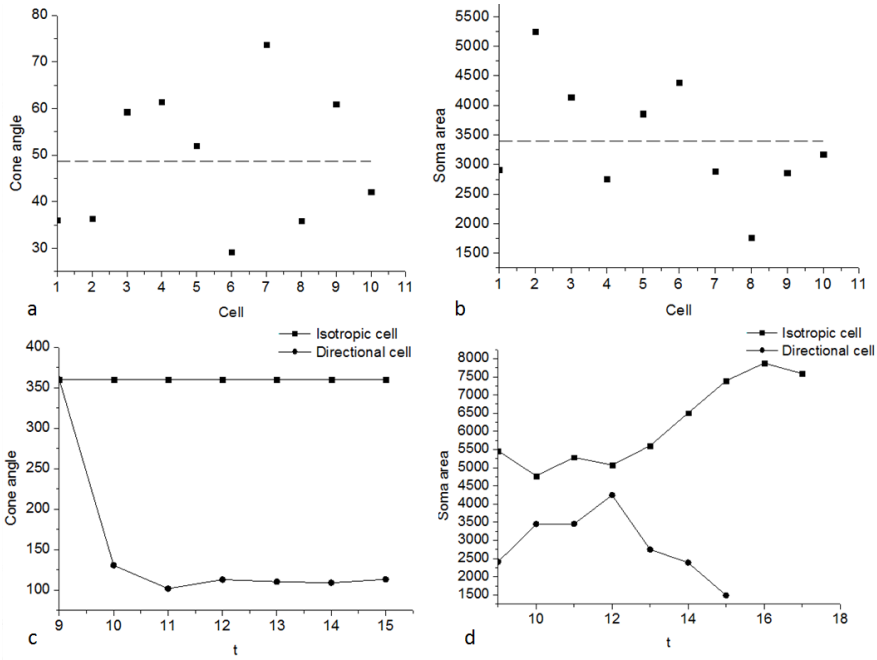

Figure 2.26: *a) Cone angle for all the cells cultured in the presence of glia and mean value (dashed line). b) Soma size for all the cells cultured in the presence of glia and mean value (dashed line). c) Cone angle as a function of time for an isotropic cell and for a directional one, both cultured in the absence of glia. d) Soma size as a function of time for an isotropic cell and for a directional one, both cultured in the absence of glia*

For the fractal analysis, both the box-counting and the box-counting-slope method were applied, comparing our results with ones obtained with a space-filling 2D image of the same dimensions (Figure 2.27a,c). The n(r) versus r plot for Purkinje cells in both groups follows a power law. The discrepancy between the two curves indicates that the structures are not completely space-filling. Plotting the local slope of the curve versus r, confirmed the presence of fractal properties in a particular range of r was confirmed and the fractal dimension was evaluated in this range. The range of r in which the slope of curve is constant is smaller for cells in presence of glia (Figure 2.27b,d).
The fractal dimension of both cells with and without glia is about 1.97 (Figure 2.27e,f). This value is very close to 2; our results indicate that Purkinje cells are neither fractal nor pure space-filling objects but fall somewhere in between. The fractal properties of biological systems and, in particular, of neurons are widely debated particularly because most measurements of fractal dimension cover only relatively few decades of radii, so that some authors have suggested that most biological patterns are not fractals but space-filling objects [191] while others demonstrates that they are fractal [192]. In order to analyze the evolution of fractality over time, the mean fractal dimension versus time was plotted (Figure 2.27f). The figure shows that the fractal dimension is almost constant, indicating how cells grow regularly while maintaining the initial fractal dimension.

Table 2.2 summarizes the differences found between the two cell populations.

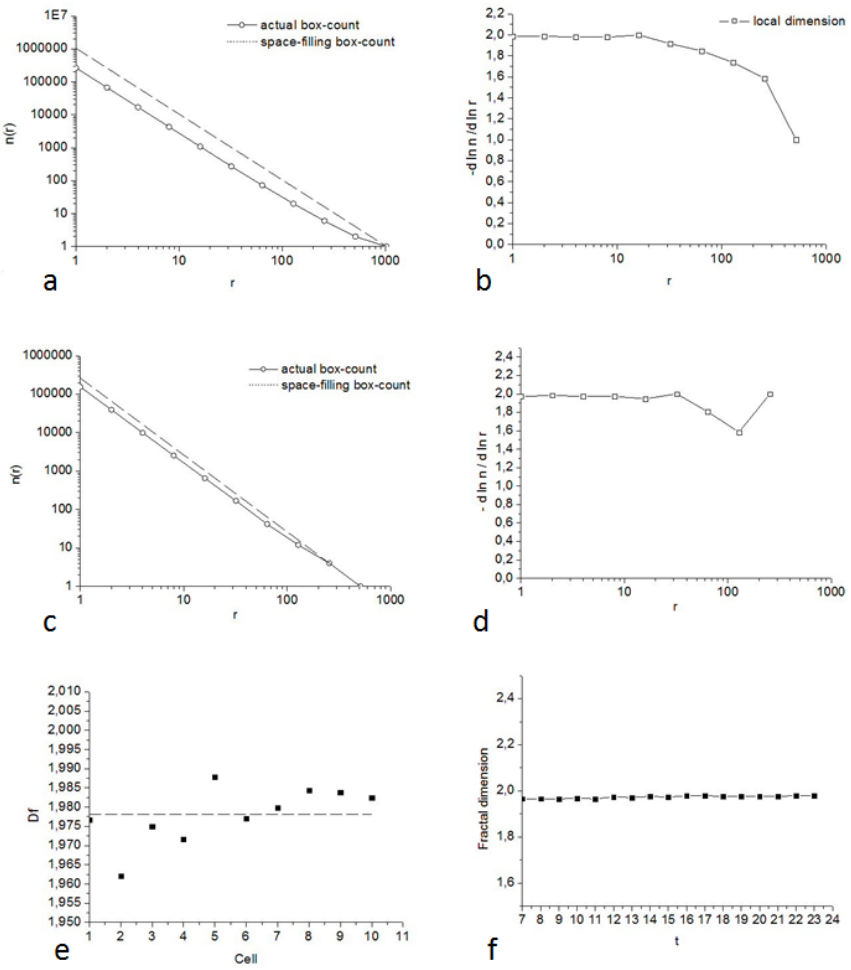

Figure 2.27: *a) Cone angle for all the cells cultured in the presence of glia and mean value (dashed line). b) Soma size for all the cells cultured in the presence of glia and mean value (dashed line). c) Cone angle as a function of time for an isotropic cell and for a directional one, both cultured in the absence of glia. d) Soma size as a function of time for an isotropic cell and for a directional one, both cultured in the absence of glia*

Variable	**PCs with glia**	**PCs without glia**	**Comments**
Plot of the number of intersections versus r	Maximum at r small and smaller at r large	Gaussian	Dendrites localized near the soma in the presence of glia
Plot of log-log semi-log method	Both, depends on cell	Semi-log is better	Without glia all neurons are clearly more branched and disorganized
Value of Δ	≈ 1	>1	Dendrites are longer and less branched in cells supported by glia
Plot of minimum length vectors	Same	Same	
Plot of angles between minimum length vectors	A lot of high peaks	Small peaks	The principal axis is more tortuous in cells with glia
Radial extension	Same	Same	
Cone angle	About 50 °	Variable	Cells with glia are highly oriented
Soma size	Small	Variable	Cells with glia are smaller
Fractality	High only at small r	High for a wide range of r	Linearity in a small range of r

Table 2.2: *Comparison of features extracted from image, Sholl and fractal analysis for Purkinje cells with and without glia.*

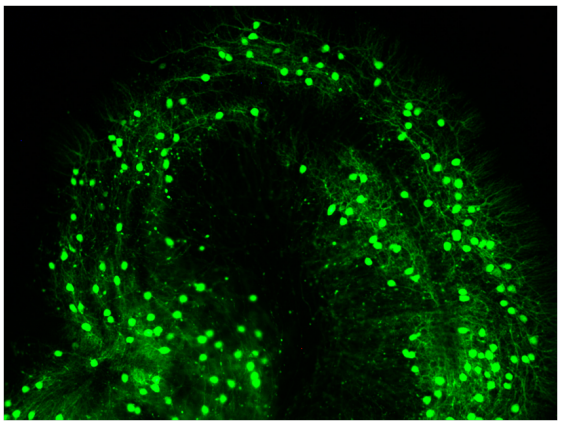

Figure 2.28: *Organotypic slice from a L7GFP mouse.*

2.4.3 Counting of neurons in organotypic slices

Photographs of organotypic slices were submitted to the counting algorithm to evaluate the ability of this algorithm to estimate precisely the number of neurons in the image. Thanks to the fact that Purkinje cells expose GFP and so the contrast with the background is high, the counting procedure is quite easy. Figure 2.28 shows an example of organotypic slice used to test the counting algorithm.

Photographs of slices from different cultures have been selected and the number of Pukinje cells within each image was calculated both automatically and manually. A histogram was then realized to compare the results obtained with the two methods. Figure 2.29 shows the results obtained for some comparisons for different slices.

Histogram analysis shows that the percentage mean error is 5%: this meens that the algorithm implemented for automatic count is effective. It is important to notice that Purkinje cells in the cerebel-

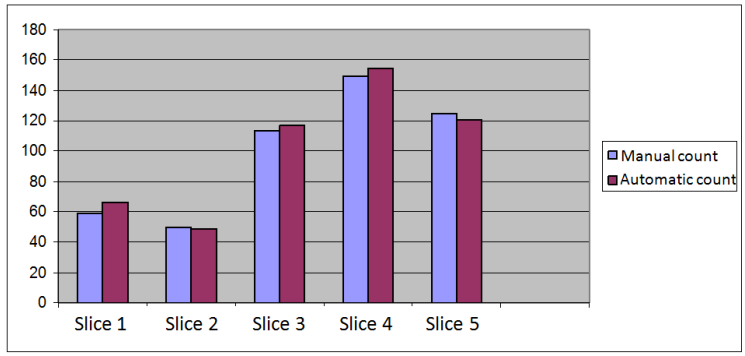

Figure 2.29: *Histogram in which results obtained with manual and automatic count are compared.*

lar cortex slices are located in different layers so that is impossible to focus all of them in the same time. This is means that the cells counted are only those in the higher layer. A possible solution could be to photograph the same area of the cerebellum adjusting different layers and counting neurons for the different layers.

2.4.4 Assessment and comparison of morphology in cultures extracted from L7GFP wild-type and L7GFP/EN2+/- mice.

The comparison of Purkinje cells extracted for L7GFP wild-type mice and L7GFP/EN2+/- was realized on cultures fixed at different cell division (8, 10, 14 and 15 div for wild-type; 10 and 15 div for EN2+/-). All the cells considered in this analysis were cultured without glia.
First the analysis of the different variables extracted for all the cells

at the different times of fixation was executed, then the analysis of the evolution of the variables in time was realized. In the second kind of analysis the mean values of all the cells analyzed for the two different types of mice were considered.
The analysis of intersections showed that the trend of intersections vs. radius is Gaussian only in wild-type mice, with a peak corresponding to intermediate values of the radius. In En2+/- the peak of intersections is instead more shift towards lower values of the radius.
The plot of log-log and semi-log methods revealed that both in wild-type and En2+/- the log-log is more appropriate as approximates better the values of intersections. This result was confirmed by the value of delta that is in both cases less than 1 for the great part of cells although the difference between the number of cells for which delta is less than 1 and greater than 1 in the case of En2+/- is less significant.
The observation of the plots of mean vector lengths on the principal axis and of angles between these vectors revealed that plots of En2+/- cells have very smaller peaks with respect to wild-type cells.
The plot of the values of fractal dimension for all the cells of the two cultured showed that although in both cases values are included in an interval from 1.4 to 1.7, the mean value of the cells extracted form En2+/- is lower than the mean value of the cells extracted from wild-type mice (1.45 vs. 1.55).
Table 2.3 summarizes the significant differences found between the two cell populations at the single time points analysis.

As regards the temporal analysis it was possible to notice that the maximum number of intersection, the extension and the length

Variable	**PCs from L7GFP wild-type**	**PCs from L7GFP/ En2+/-**	**Comments**
Plot of the number of intersections versus r	Gaussian	Maximum at r small and smaller at r large	Dendrites localized in the center in wild-type and near the soma in En2+/-
Plot of log-log semi-log method	Log-log is better	Log-Log is better	
Value of Δ	<1	<1	
Plot of minimum length vectors	A lot of high peaks and higher value	Very small peaks	The principal axis is less tortuous and smaller in cells of En2+/-
Plot of angles between minimum length vectors	A lot of high peaks	Very small peaks	Confirms that the principal axis is less tortuous in cells of En2+/-
Fractal dimension	About 1.55	About 1.45	The fractality is lower in cells of En2+/-

Table 2.3: *Comparison of features extracted from image, Sholl and fractal analysis for Purkinje cells extracted from L7GFP wild-type and L7GFP/EN2+/-.*

of the principal axis increase from the 8th to the 15th day of division in the case of wild-type mice while the values decrease from the 10th to the 15th day in EN2+/-. Moreover values reached by the cells form wild-type mice are higher with respect to the cells from En2+/-: the maximum radial extension is 127 μm in wild-type and 73 μm in En2+/-, while the maximum principal axis length is 150 μm and 89 μm for En2+/-.
The soma area value has a different trend in the two cultures; in fact while in wild-type cells it increases up to the 10th day and then decreases, in cells from En2+/- the value keeps constant. Moreover the size is smaller in En2+/- being 69 μm^2 in comparison to 116 μm^2 of wild-type cells.
Finally the fractal dimension remains constant in both cases although in En2+/- the value is lower.
Table 2.4 summarizes the significant differences found in the evolution in time of the mean values of the two cell populations.

2.5 Discussion and conclusions

It is well known that even at the microstructural level, neuronal morphology is important for higher level brain function [193], [194]. Therefore morphological features such as neuron shape, size, branching and asymmetry can elucidate the functional role of different neurons. Moreover, morphometric analyses are relevant for the study of alterations in the dendritic/axonal field of neurons or neuronal morphological correlates of diseases [195].
Classically neuron morphology is investigated using stained and fixed

Variable	**PCs from L7GFP wild-type**	**PCs from L7GFP/ En2+/-**	**Comments**
Maximum number of intersections	Higher value, peak at div 15	Lower value peak at div 10	Less arborized dendrites in En2+/-
Radial extension	Higher value peak at div 15	Lower value peak at div 10	Cells of En2+/- grow less and die earlier
Principal axis length	Higher value peak at div 15	Lower value peak at div 10	Cells of En2+/- grow less and die earlier
Cone angle	Same	Same	
Soma size	Decreases in time	Constant, smaller	Cells of En2+/- are smaller and less directional
Fractal dimension	Constant	Constant	

Table 2.4: *Comparison of the evolution in time of mean features extracted from image, Sholl and fractal analysis for Purkinje cells extracted from L7GFP wild-type and L7GFP/EN2+/-.*

dissociated cultures or slices [148]. Most investigators now use fluorescent confocal microscopy, and several reports describe neural growth dynamics using fluorophores such as tracker dyes or calcium sensitive dyes [152], [151], [31]. In several instances these dyes can be phototoxic over long periods [196], or may require repeated probe injections.

Genetically encoded probes are now becoming commonplace, and are an extremely useful tool for analyzing neural cell morphology, although most efforts are dedicated towards cell signaling particularly at the synaptic level [197].

More recent reports use techniques such as 2-photon or confocal microscopy on organotypic slices, which enable short term (10 min) recordings of calcium dynamics through the use of Ca^{2+} specific dyes or very high magnification static analysis of dendritic spine distribution [198]. At the most the dynamic studies are of the order of a few hours [199].

PC morphology in cerebellar slices has been described in detail in classical reports such as [200], [201]. More recent reports use software tools, for example Bosman et al. [202] obtained information on global features, dendritic structure and statistical properties of PCs in fixed slices using different programs: a custom written Labview Vis software for the measure of somatodendritic area, Neuron- Morpho for dendritic reconstruction, a custom-written software for Sholl analysis and the PAST software for cluster analysis.

The only investigation which uses long-term analysis of living cells is based on a GAD67-GFP mouse in which PCs were studied over a period of 25 days, and 4 time points and is performed by Tanaka et al. [203]. The authors quantified dendritic length, density and

branching using a manual technique.

In the present study a non-invasive method for the analysis of dissociated cultures was developed. In order to follow the evolution in-vitro: the position of each cell was labeled using a grid and the evolution of its dendritic tree was recorded using time-lapse optical microscopy. It should be noted that cells in-vivo are organized into a three-dimensional architecture while the morphometric analysis presented here has been conducted in two-dimensional cultures and slices. However, Purkinje neurons are essentially two-dimensional cells, so the basic topology of the cells is conserved in in-vitro dissociated cultures.
The cells were photographed at different times of the growth and analyzed using automated feature extraction and statistical models. An important aspect of this study is in fact the automation of the method through the software NEMO. NEMO consists of a set of computation algorithms in Matlab implemented in a GUI framework, in which it is easy to access the data and have a global view of the results. These algorithms permit the extraction and classification of metrical variables which characterize cell morphology.
Using NEMO photograph of single cells or of organotypic slices can be pre-processed in order to obtain a suitable image for the following analysis. Multiple images representing the skeleton of a single cell can be opened automatically for the extraction of the metrical features of interest. Dedicated algorithms were then implemented in order to extract relevant features, such as morphometric variables, fractal dimension, and directionality, from the acquired images of the cultures. Sholl and fractal analyses were performed to unravel

correlations between morphometric variables and allow classification of cells according to their morphology.
Topological features as well as the number of neurons present in the image, can be obtained from organotypic slice.
All the data are collected in a single file and statistical analysis is performed.

Commercial software for morphometric analysis of neurons such as NEUROLUCIDA (MBF Bioscience) or IPLab (BD IPLab) are available and used successfully by several investigators [204], [205]. Although these software are able to extract some of the morphological parameters of interest, many routine operations require significant manual intervention and interpretation, such as the tracing of each branch with a pencil tool or mouse. The principal disadvantages of NEUROLUCIDA and other commercial software tool are the considerable costs and the impossibility of customizing the software for ones own purpose. Some freeware such as Neuron-Morpho [206], provide a possible alternative to these commercial packages.
An important novel aspect of NEMO in comparison for example with Neuron-Morpho or NEUROLUCIDA, is the organization of the analysis algorithms and of the results. In both Neuron-Morpho and NEUROLUCIDA, images need to be opened one at a time, traced, and then data are collected and saved for single images. When dealing with multiple images of the same cell tracked over time, the procedure takes a considerable amount of effort. On the other hand, NEMO allows all the morphological features of interest and their variation in time to be obtained in a single operation. NEMO offers two possibilities: the user can select a specific function and obtain

the associated measurement or parameter for a single cell at a specific time, or can start a global flow of operations to obtain all the parameters for the cell at different times. This second option is very useful because all the information relative to a single cell is saved in a single matrix (the datamatrix) from which selected parameters can be plotted. The concatenation of matrices from different cells then allows graphical analyses and comparisons between different groups and parameters. Finally, as far as data analysis is concerned, most studies and software based methods which describe neuron morphometrics use very simple statistical tests such as the t- or f-tests. The analyses method described here is based on the use of the three-way PCA [179], [180] in which multivariate data are represented in three dimensions. This kind of analysis has already been used for statistical investigations on other biological systems [207], [208], [209] but has not been used specifically for the classification of cells. The three-way PCA was used to unravel correlations between significant morphometric variables in PCs and for the classification of cells according to their morphology [37].

In this study primary Purkinje cells derived from the cerebellum of P1 mice, cultured in-vitro and organotypic slices of the cerebellum of P7 mice, were analyzed using the tools developed within NEMO. Non-fluorescent cells and cells from L7GFP mice were considered. Moreover wild-type Purkinje cells dissociated from the cerebellum of P1 mice in-vitro in the absence and presence of glia were analyzed. Finally the L7GFP/En2 hybrid was developed as a new ASD model to study microscopic alterations in cerebellar neurons. Purkinje cells were extracted from L7GFP/En2+/- and compared with

wild-type mice.

The use of GFP allowed an easy recognition of PCs and increased the image contrast so that image pre-processing was faster. The pre-processing algorithms were quite fast and semi-automatic and allowed a precise reconstruction of the cell skeleton.
Morphological and statistical analysis on PCs extracted from L7GFP wild-type mice is not reported in this work as it confirmed the results obtained from the analysis on not-marked Purkinje cells [37].
Moreover in this study, a quantitative microstructural analysis of branching organization of Purkinje cells isolated from mice in the absence and in the presence of glia was performed. A time dependent analysis was made on cells cultured in a medium without glial cells and then the results of this analysis were compared to that obtained analyzing cells cultured in the presence of glia at their maturation stage. The evaluation of the quantitative changes of Purkinje cell morphology due to their interaction with astrocytes can be useful to understand in what way alterations or the absence of glia can affect Purkinje cell functionality.
The glia has recently come into the limelight for its role in regulating and coordinating synaptic transmission. That astrocytes and glial cells, in general, are involved in regeneration or rather the failure of neurons to generate following injury is well established. Furthermore, several publications show that glial contact provides guidance to axonal and dendritic growth both in-vivo and in-vitro [210]. This interaction is two-way, since glial development is also influenced by the axonal microenvironment [211].
Despite the great interest in glialneuronal communication, there is

surprisingly little quantitative information on the structural and morphological interactions between the two. This work therefore represents a important step in the establishment of a systematic and automated method for assessing quantitative differences in neuron morphology in a variety of experimental conditions. Using this method, the role of the glia and the way in which its composition, density, and characterization modulate neuronal morphology can be easily identified and quantified.

The method developed in this work was used to analyze primary Purkinje cells dissociated from the cerebellum of P1 mice in-vitro in the absence and presence of glia, respectively, in order to quantify morphological differences between the two cultures. Furthermore, the morphological evolution of a Purkinje cell culture in the absence of glia was studied over a period of 23 days using the optical microscopy.

As is evident from table 2.2, as well as the results, there is a clear distinction between the two cultures. In the presence of glia, the Purkinje cells are more oriented, and smaller dendritic branching is concentrated close to the soma and close to the principal axis. In this sense, the glia provide the Purkinje cells with a framework which maintains compactness and orientation, as well as a greater level of structural organization and consequently a less random branching. On the other hand, cells cultured with Ara-C are larger and have a more casual organization: for example, some are oriented and others have an isotropic structure. In fact, the most interesting structural difference due to the presence of glia was the increase of directionality of the cells. The cone angle was very narrow and the soma was small and oriented in the direction of cellular extension. This

increase in directionality was probably due to the chemical stimuli secreted by the glial cells that orient the cells in order to favor the formation of synapses with other cells.

Successively NEMO was applied to the extraction and comparison of morphological features extracted from L7GFP wild-type mice and L7GFP/En2+/- in order to evaluate possible morphological abnormalities in animal models of ASDs. Although the En2-/- is the most studied and has stronger behavioral deficits, also the En2+/- was found to be an animal model of ASDs. In this first study the En2+/- was selected in order to see if at a microscopic level morphological abnormalities in the structure of neurons are present also in this animal.
As tables 2.3 and 2.4, as well as the results, show, there is a clear distinction between the two cultures. The first evidence is that cells from En2 survive in culture less than wild-type mice and start to suffer earlier. It was possible to notice in fact that while cells from wild-type mice continue their growth at the 15th day of culture, as indicated by the increase in parameters like the maximum number of intersections, the radial extension and the length of the principal axis, cells from En2+/- start to suffer after the 10th day of cultures, the same parameters in fact start decreasing. This premature death in culture may reflect the reduced number of Purkinje cells that was found in postmortem studies.
Another observation was that the dimensions of the cells from En2+/- are reduced with respect to cells extracted from wild-type mice. This can be inferred by the fact that the maximum value of radial extension, length of the principal axis and soma reached lower values in

En2+/-.
There is a reduction also in the arborization of the dendritic tree as shown by the reduced number of intersections and maximum number of intersections in En2+/- with respect to wild-type. Moreover the principal axis is less tortuous in fact the plot of the minimum length vectors and of the angles between these vectors have very small peaks. The reduced complexity of the dendritic tree is also demonstrated by the fact that the fractal dimension is lower in En2+/- with respect to wild-type mice.
Finally while cells from wild-type increase their directionality during the days of culture as shown by the decrease of the soma area and the cone angle, in cells from En2+/- there is not this trend but the values remain constant. This could be explained with a reduced presence of chemical stimuli secreted by other cells in the culture medium of cells extracted from En2+/- maybe because cells are reduced in number.
The method implemented in this work is shown to be highly efficient for the classification and analysis of cells and cell variables pertaining to neural morphology and to their evolution in time.
The comparison between Purkinje cells extracted from wild-type mice and from En2+/-, confirms some of the results found in literature in postmortem studies, such as the reduced dimensions and arborization of En2 cells, although with the present analysis is possible to quantify these differences and to follow the evolution of abnormalities during the growth of the cells, at an early stage of development.

Algorithms for the analysis of organotypic slices were also developed and tested.

As regards the neuron count, the result obtained with the algorithm was similar to that obtained with manual count. As the automatic method is faster than the manual count, it should be preferred. Counting of neurons in a slice in the several days of culture is very important in a study on ASDs because, as reported in section 1.4.3.1, the number of PCs is reduced in cerebellum of ASDs. A dynamic study of the number of neurons allows to understand at which point of the neuronal evolution the loss of cells occurred.
The topological features extraction algorithms were tested on organotypic slices of Reeler/L7GFP mice. Results obtained from this analysis are not reported in this work as the number of samples was consistently low and is not possible to extract general characteristics. Anyway the analysis showed that the algorithms were efficient in extracting dynamic topological features. These algorithms could be useful to quantitatively characterize PC migration and observe how is defective in ASDs.

The originality of this study lies in the analysis technique which allows automatic processing of a large amount of quantitative information on cell morphology and slice topology. The tools, methods and associated software developed provide a starting point to insights on the influence of the different genes in abnormal early brain development in ASDs. It will also enable early diagnosis, and lead to the design of new strategies for circuitry remodeling before establishment of permanent networks.

Chapter 3

Diffusion Tensor Imaging methodologies (DTI) and applications to Autism Spectrum Disorders (ASDs)

3.1 Background on Diffusion Tensor Imaging

The success of diffusion MRI lies in the fact that during their random, diffusion driven displacements molecules probe tissue structure at a microscopic scale well beyond the usual image resolution. This is an exquisite example of a multiscale integrated process by which fluctuations in molecular random motion at microscopic scale can be inferred from observations at a much larger scale using statistical physical models, although the individual molecular structure and pathway is completely ignored.
Diffusion MRI is the only method that presently allows measurement of white matter fiber orientation in the human brain in-vivo. The

white matter fiber tracts are actually large bundles of axons that interconnect the gray matter processing areas both within and across hemispheres (the brain consists of two main parts: the white matter, containing axons that transmit information; and the gray matter, containing cell bodies of neurons that integrate information). DTI is different from standard structural MR imaging which measures quantities related to tissue composition (the T1 and T2 relaxation times depend on water and fat content). In diffusion MRI, the quantity measured also relates to the three-dimensional organization of the tissue. Consequently, it is not always possible to transfer image visualization or analysis methods directly from standard structural imaging to diffusion imaging.

All diffusion-tensor magnetic resonance imaging (DTI) studies of nerve, spinal cord white matter and brain white matter rely on the underlying phenomenon that water diffusion is highly anisotropic in these tissues of the nervous system. A basic understanding of the influence of various structural components on anisotropic water diffusion is a prerequisite for interpreting alterations in diffusion and anisotropy as a result of various disease processes or abnormal development.

Diffusion is a physical process that involves the translational movement of molecules via thermally driven random motions called Brownian motion. At a macroscopic scale, this phenomenon yields a diffusion process. In an isotropic medium, the diffusion coefficient D was related by Einstein [212] to the root mean square (RMS) of the diffusion distance as:

$$RMS = \sqrt{2Dt_{dif}} \tag{3.1}$$

As the diffusion coefficient of water in brain tissue at body temperature is about 1×10^{-3} mm^2 s^{-1}, the Einstein diffusion equation indicates that about two thirds of diffusion-driven molecular displacements are within a range not exceeding 10 μm during diffusion times currently used with MRI (around 50 ms), well beyond typical image resolution. Indeed, water molecules move in the brain while interacting with many tissue components, such as cell membranes, fibers or macromolecules, etc, and the indirect observation of these displacements embedded into the diffusion coefficient provides valuable information on the microscopic obstacles encountered by diffusing molecules, and in turn, on the structure and the geometric organization of cells in tissues, such as cell size or cell orientation in space.

However, the overall signal observed in a "diffusion" MRI image volume element (voxel), at a millimetric resolution, results from the integration, on a statistical basis, of all the microscopic displacement distributions of the water molecules present in this voxel, and some modeling is necessary to make inferences between those two scales.

The scalar constant D, known as the diffusion coefficient, measures the molecule's mobility. In the isotropic case, it depends on the molecule type and the medium properties but not on the direction. The macroscopic process of diffusion can also be described by Fick's first law, derived by Adolf Fick in 1855 [213]. It relates the concentration difference of the diffusion substance C to a flux. The flux, J, is proportional to the gradient of the concentration, ∇C. The proportionality constant D is the diffusion coefficient and the governing equation is given by:

$$J = -D\nabla C \tag{3.2}$$

The general diffusion displacement probability density function (PDF), is written as P(R, t). It represents the probability that a water molecule located at r_0 will have moved by amount R = r - r_0 in time τ. In the diffusion tensor model, if we take the Taylors expansion of P about R and τ and ignore the higher order terms, we can use Einsteins relation of Eq. 3.1 to obtain:

$$\frac{\partial P(R,t)}{\partial t} = D\nabla^2 P(R,\tau) \tag{3.3}$$

The solution to Eq. 3.3 is P, the Gaussian diffusion PDF of water molecules:

$$P(R,t) = \frac{1}{\sqrt{4D\pi t}} exp\left(-\frac{R^2}{4Dt}\right) \tag{3.4}$$

If we use Fick's law and the law of conservation of mass, $\partial C/\partial t = -\nabla \cdot J$, we get:

$$\frac{\partial C}{\partial t} = D\nabla^2 C \tag{3.5}$$

which is the same as Eq. 3.3 with the diffusion PDF P replaced by the concentration of the medium C. Both the Einstein's Eq. 3.3 and Ficks Eq. 3.5 describe the classical diffusion equation. In the case D is the identity matrix (isotropic medium), it is called the heat equation and in the anisotropic case, it is called the geometric heat equation.

Isotropic diffusion occures when in the means the diffusion has not a privileged direction of movement. In fibrous tissues, including white

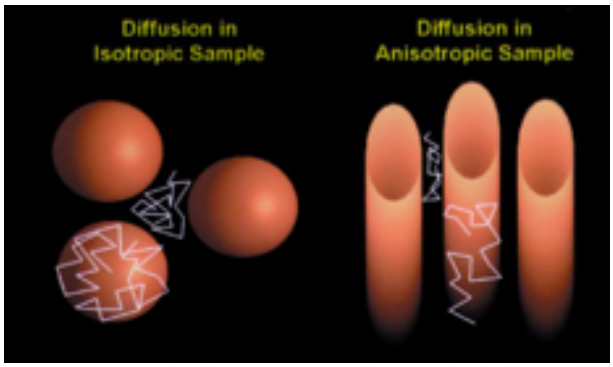

Figure 3.1: *Isotropic and anisotropic diffusion. Molecules with equal diffusion in all directions experience isotropic diffusion. Molecules that prefer diffusion in one direction to others experience anisotropic diffusion [18].*

matter, the diffusion is not the same in all directions so it is called anisotropic [214] (Figure 3.1). The measured macroscopic anisotropy is due to microscopic tissue heterogeneity [215]. In the white matter of the brain, diffusion anisotropy is primarily caused by cellular membranes, with some contribution from myelination and the packing of the axons [18], [216]. The myelin sheath around the axons, the axonal membrane, and the neurofibrils are all longitudinally oriented microstructures that are barriers to diffusion and reduce diffusion in the perpendicular direction with respect to parallel diffusion. DTI takes advantage of this directional dependence on diffusion and can map the orientation in space of white matter tracts assuming the direction of the fastest water diffusion indicates the overall orientation of the fibers [215], [217].

In the original diffusion MRI method, diffusion is fully described

using the diffusion coefficient, D [218]. Note that the diffusion coefficient measured in diffusion MRI is not the true diffusion coefficient of water unless the imaging object is pure water. The diffusion is restricted by the structure of the tissue and this is normally called the apparent diffusion coefficient (ADC). In the presence of anisotropy, diffusion cannot be characterized by a scalar coefficient, but requires a tensor matrix, D, to describe fully molecular mobility along each direction as well as the correlations between directions [219].
The tensor is a 3×3 covariance symmetric matrix with six degrees of freedom, such that a minimum of six diffusion-encoded measurements is required to accurately describe the tensor. The diffusion tensor is obtained from diffusion-weighted measurements in at least six non-collinear directions. Using more than six directions will improve the accuracy of the tensor measurement for any orientation [220], [221]. The tensor can be written in matrix form as:

$$\mathbf{D} = \begin{bmatrix} D_x x & D_x y & D_x z \\ D_y x & D_y y & D_y z \\ D_z x & D_z y & D_z z \end{bmatrix} \tag{3.6}$$

Diagonalizing the matrix, the diffusion tensor can be written in this form:

$$\mathbf{D} = E^T \begin{bmatrix} \lambda_1 & 0 & 0 \\ 0 & \lambda_2 & 0 \\ 0 & 0 & \lambda_3 \end{bmatrix} E \tag{3.7}$$

where E is a matrix of the eigenvectors describing the major, medium

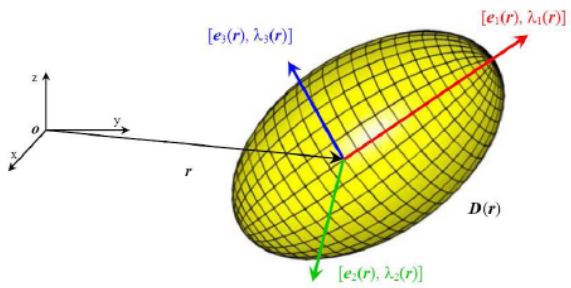

Figure 3.2: *Diffusion tensor ellipsoid characterized by the eigenvectors (λ_1,λ_2,λ_3), and eigenvalues (ϵ_1,ϵ_2,ϵ_3).*

and minor principle axes of the ellipsoid (Figure 3.2) fitted to the data, and λ_i are the eigenvalues for each eigenvector, which represent the diffusivity along each axis.

The Stejskal-Tanner imaging sequence [19] is used to measure the diffusion of water molecules in a given direction g_i, i = 1, ...,N. This pulse sequence is illustrated in Figure 3.3. This sequence uses two gradient pulses g(t) in the direction g, of duration time δ, to control the diffusion-weighting. They are placed before and after a 180 ° refocusing pulse. More specifically, a first 90 ° RF is applied to flip the magnetization in the transverse plane. The first gradient pulse causes a phase shift of the spins whose position are now a function of time. Spin position is in fact assumed to stay constant during time δ. Finally, the 180 ° pulse combined with the second gradient pulse induces another phase shift. It is applied after a time Δ separating the two gradient pulses. This pulse cancels the first phase shift only for static spins. On the other hand, spins under Brownian motion during the time period Δ separating the two pulses undergo

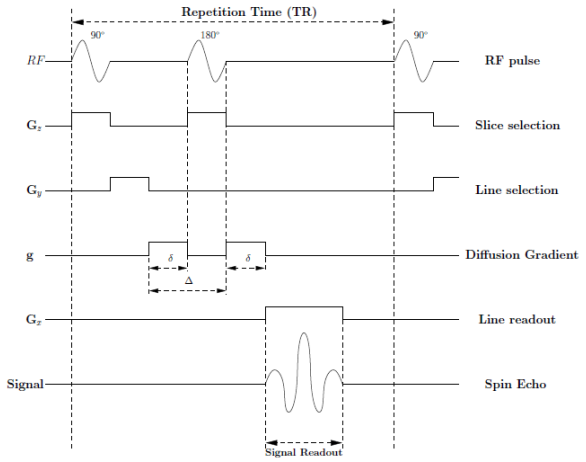

Figure 3.3: *Schematic Stejskal-Tanner imaging PGSE sequence [19].*

different phase shifts by the two gradient pulses, resulting in a T2 signal attenuation.

By assuming the pulses to be infinitely narrow (narrow pulse approximation), i.e. if the gradient pulse duration δ is short enough for the diffusion of the water molecule to be negligible during that time, [19] showed that the signal attenuation is expressed as the 3-dimensional (3D) Fourier transform F of the ensemble average of the diffusion PDF or diffusion propagator of water molecules introduced earlier.

$$\frac{S(q,\tau)}{S_0} = \int_{\Re^3} P(r|r_0,\tau) exp(-2\pi i q^T \Re) dr = F[P(r|r_0,\tau)] \qquad (3.8)$$

where the value of q is given by $q = \gamma\delta G/2\pi$ with γ the nuclear gyromagnetic ratio for water protons, G the applied diffusion gradient vector, S_0 is the baseline image acquired without any diffusion

gradients (also called b_0 image) and $P(r|r_0, \tau)$ is the diffusion PDF or diffusion propagator of water molecules introduced earlier. This P is ultimately the function we are looking to reconstruct in diffusion MRI. Intuitively, one has to sample the diffusion PDF along many q vectors to be able to reconstruct the diffusion PDF. The space of all possible 3D q vectors is called q-space. Under a Gaussian assumption, the signal attenuation can be expressed as:

$$S = S_0 e^{-bD} \tag{3.9}$$

where D is the apparent diffusion coefficient, and b is the diffusion-weighting described by the properties of the pulse pair:

$$b = \gamma^2 G^2 \delta^2 (\Delta - \frac{\delta}{3}). \tag{3.10}$$

DTI approximates the diffusion PDF by a 3-variate normal distribution with zero mean. Hence, D can be viewed as the covariance matrix describing the Brownian motion of water molecules at each imaging voxel.

Since D is symmetric, it has six unknown coefficients that we need to estimate. Therefore, DTI needs at least six DW images and one unweighted diffusion image (b = 0 s/mm^2) to solve the system of equations. With a 1.5 T scanner typically the b-value of 1000 s/mm^2 is used with 7 to 60 or more gradient directions.

DT is a rich mathematical tool with interesting properties that one can exploit for diffusion MRI visualization and analysis.

The DT is systematically decomposed into its three eigenvalues λ_1, λ_2, λ_3 where $\lambda_1 < \lambda_2 < \lambda_3$ and corresponding eigenvectors e_1, e_2, e_3. The diffusivity along the principal axis, λ_1 is also called the longitu-

dinal diffusivity or the axial diffusivity or even the parallel diffusivity. The diffusivities in the two minor axes are often averaged to produce a measure of radial diffusivity $\lambda_2 + \lambda_3/2$. This quantity is an assessment of the degree of restriction due to membranes and other effects and proves to be a sensitive measure of degenerative pathology in some neurological conditions. It can also be called the perpendicular diffusivity.

Several invariant scalar indices made of combinations of the eigenvalues are used to characterize diffusion anisotropy. A scalar invariant is a function of the tensor that outputs a scalar which is the same regardless of the coordinate frame of the tensor. It is invariant to rotation of the tissue in the MRI magnet because it can be expressed as a function of the eigenvalues of the tensor, which are invariant to rotation. The most widely used invariant measure of anisotropy is fractional anisotropy (FA) [217]:

$$FA = \sqrt{(\frac{3}{2})\frac{(\lambda_1 - \bar{\lambda})^2 + (\lambda_2 - \bar{\lambda})^2 + (\lambda_3 - \bar{\lambda})^2}{\lambda_1^2 + \lambda_2^2 + \lambda_3^2}} \tag{3.11}$$

FA is a scalar value that ranges between 0 and 1. Increasing FA values indicate a higher tensor ellipsoid anisotropy. FA, with no other information, is a highly sensitive but fairly non-specific biomarker of neuropathology and microstructural architecture. This combination produces challenges to the interpretation of DTI measurements for both diagnostic and therapeutic applications. However, most agree that FA is a marker of white matter integrity. The trace of the tensor (Tr), or sum of the diagonal elements of D, is a measure of the magnitude of diffusion and is rotationally invariant. Another simple and clinically useful scalar invariant is the average

of the eigenvalues, that is the trace divided by 3. This average is referred to as the mean diffusivity, or MD [214] or Apparent Diffusion Coefficient (ADC) [222] and it relates to the total amount of diffusion in a voxel, which is related to the amount of water in the extracellular space.

Unlike conventional scalar MRI images, DTI is fundamentally three-dimensional, in that the quantity measured at each voxel is diffusion information in 3D. This poses a visualization and analysis challenge. Various techniques for visualizing diffusion tensor data were reported so far and can be categorized in the two groups. One is the series of image-based methods in which each voxel value represents local anisotropy measure or principle direction of diffusion, and the 3D rendering of those images by volume rendering or surface rendering of the isosurface. The other is the group of symbolic (or geometric) display methods by using various types of glyph such as ellipsoid.

In the first category, the voxel values are determined on the basis of eigenvectors and eigenvalues of diffusion tensor at the location. The voxel value represents the value of maximum diffusion coefficient λ_1, anisotropy measure such as FA, orientation of the maximum diffusion coefficient e_1 and so on. For example, images may be displayed of any anisotropy measure, or of the trace. Another type of image can represent the major eigenvector field using a mapping to colors. The color scheme commonly used to represent the orientation of the major eigenvector works as follows: blue is superior-inferior, red is left-right, and green is anterior-posterior [223] (Figure 3.4). The brightness of the color is controlled by tensor anisotropy (FA).

Varieties of display methods based on the use of symbolic objects have been proposed. Those symbols are arrow, ellipsoid, and other

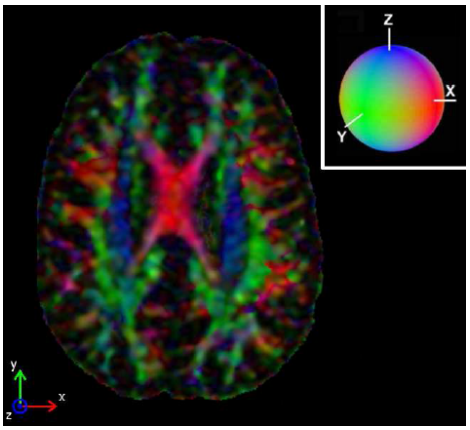

Figure 3.4: *Colormap showing major eigenvector direction indicated by color (red: right-left; green: anterior-posterior; blue: superior-inferior).*

combined objects and are aimed at displaying spatial distribution of the anisotropy and the principle directions of the diffusion tensor. The ellipsoid display is the most basic method for visualization of tensor including stress and strain tensors in materials mechanics. An ellipsoid of diffusion tensor represents distance covered in 3D space by molecules in a certain diffusion time. Another visualization method uses small three dimensional objects called glyphs to display information from each tensor eigensystem.

The dominant method for three-dimensional visualization of DTI is tractography, a very commonly employed method which estimates the trajectories of major fiber tracts in white matter [224]. It is closely related to an earlier method for visualization of tensor fields known as hyperstreamlines. The central theme of tractography is tracing paths by following probable tract orientations, in order to reconstruct an estimate of the underlying white matter fiber structure.

Many methods have been proposed in the literature for addressing this problem, and most produce output which corresponds well to known anatomy in regions.
The streamlines tractography is the most common approach and is generally what is meant by the word tractography (Figure 3.6).

Tractography is basically based on the line propagation technique, in which a tracking line is propagated from a start point called "seed". For a given seed point P_0, series of node coordinates P_i (i=1,2,...) in the trajectory are determined iteratively as follows:

$$P_{i+1} = P_i + \delta d_i(D(P_i)) \tag{3.12}$$

where δ is a scalar value of the propagation step distance, d_i is the unit vector of propagation direction depending diffusion tensor D at the location P_i. The simplest propagation is based on the principle eigenvector e_1 of the tensor.
The first step in performing streamline tractography is to associate the major eigenvector with the tangent to a curve (the putative fiber path). Then the curve may be estimated by stepping repeatedly in the direction of the tangent (Figure 3.5).

An important consideration is that an eigenvector has an orientation but not a direction so consistency of orientations must be checked on each step. This can be done simply by taking the dot product of the current and previous tangent, and switching the sign of the current tangent if the dot product was negative.
Another important consideration is calculation of the tangent at an arbitrary location, which may be done for example by interpolating the tensor there (component-wise) and then computing the major

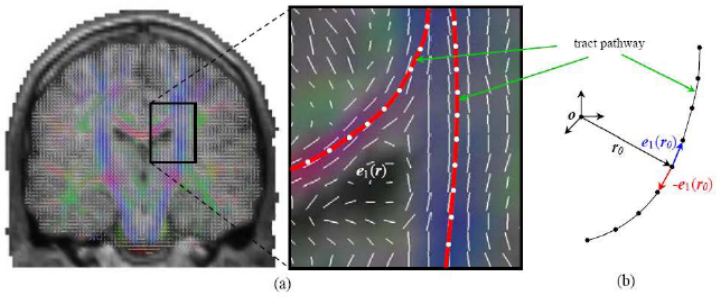

Figure 3.5: *Tractography algorithm. a) Particular of tractographic process (white tracts represent maximum diffusivity direction) and b) Particular of the reconstructed pathway.*

eigenvector. To estimate the path from its tangents, standard numerical solution methods for differential equations can be used.
For example FACT (Fiber Assignment by Continuous Tracking) [225], takes only one step per voxel, so the step size varies and each voxel's tensor is used directly without interpolation [226]. This is the approach followed for the reconstruction of the tracts in this work and it is one of the most common deterministic method. Deterministic refers to the propagation modality of the reconstructed tract that is determined by the direction of maximum diffusivity of the voxel that is considered. This class of methods contrasts with the class of probabilistic methods that instead of using either only the major eigenvector, or the full tensor, place a probability model on the fiber orientation at each voxel. Rather than producing one path from each seed point, a distribution of paths is produced by sampling.

The standard tractographic curve estimation approach has one

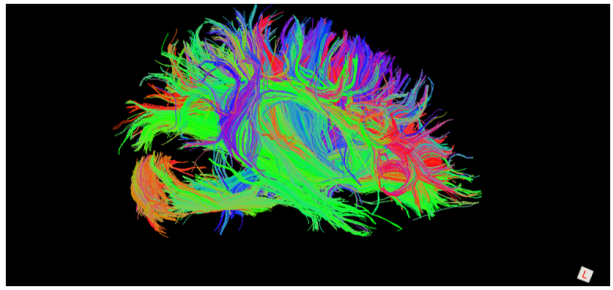

Figure 3.6: *Three-dimensional DTI visualization in TrackVis.*

main drawback, which is that all decisions are made locally.
An important limitation of the model is that it cannot represent voxels containing multiple fiber bundles with different orientations. In this case, the principal eigenvector is determined by an average over the fibers within the voxel. If two fibers are of comparable size then the combined vector may not represent either direction, causing the tracking algorithm to follow neither tract. Alternatively, if one track is much larger than the other then the tracking is likely to incorrectly jump from the minor to the major tract (Figure 3.7).
It may also difficult to differentiate between "kissing", "crossing" and "branching" fibers, as shown in Figure 3.8. In the case of kissing fibers, the two fibers merge into a single voxel before diverging without crossing over each other. The direction given by the diffusion tensor in each case may be the same, although the anisotropy should be lower for crossing fibers compared to kissing fibers. In both of these cases, the eigenvector does not correspond to the direction of either fiber.

One way to reduce these problems is to simply reduce the voxel size; with smaller voxels there is less chance that a single voxel will

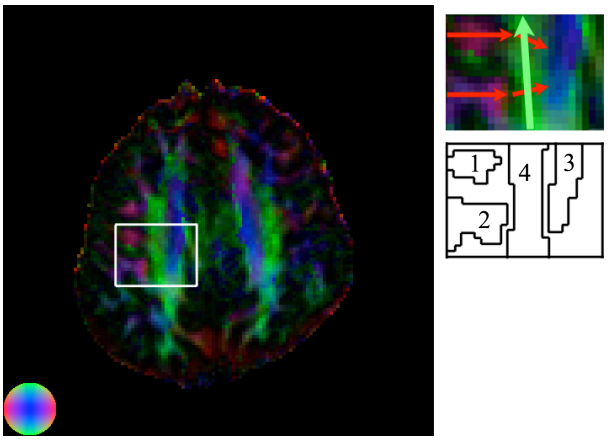

Figure 3.7: *Example of crossing fibers in a human brain. Inset: Enlargement showing motor fibers crossing right-left through the larger longitudinal fasciculus which runs in the anterior to posterior direction. The major axis of the diffusion ellipsoid in the crossing voxels is determined primarily by the longitudinal fasciculus such that the tracking algorithm is unable to connect the motor fibers to cortico-spinal tract. The crossing regions exhibit reduced anisotropy compared to the rest of the longitudinal fasciculus. The tracking algorithm is unable to connect fibers (1) and (2) to (3) due to the presence of (4).*

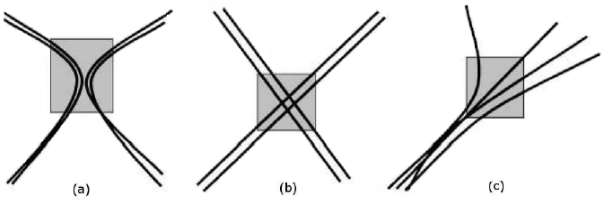

Figure 3.8: *Heterogeneous configurations inside a single voxel: a) kissing, b) crossing and c) branching.*

contain more than a single fiber tract, so the validity of the diffusion tensor model is increased. However, decreasing the voxel size comes at a cost of increased acquisition time and decreased signal-to-noise ratio, such that with current MR scanner hardware and clinically realistic acquisition times, it is difficult to reduce the voxel size to less than a few mm^3. Since this is still several orders of magnitude greater than the fiber dimensions, decreasing the voxel size will reduce but not eliminate these problems.
An alternative approach is to increase the number of directions in which the diffusion is measured and then fit this data to a different, higher order model than the tensor. This High Angular Resolution Diffusion Imaging (HARDI) [227] holds the promise to be able to determine the directions of multiple fibers within a single voxel.

The idea now is to sample q-space along as many directions and q-magnitudes as possible in order to reconstruct the true diffusion PDF. This true diffusion PDF is model-free and can recover the diffusion of water molecules in any underlying fiber population.
The visualization of 3D diffusion PDF at every voxel is computationally intensive. Hence, people either take an isosurface of the diffusion PDF for a certain radius r or the diffusion orientation distribution function (ODF) is computed. The diffusion ODF contains the full angular information of the diffusion PDF and is defined as:

$$\Psi(\theta, \phi) = \int_0^\infty P(r, \theta, \phi) dr \tag{3.13}$$

where $\theta \in [0, \pi]$ and $\phi \in [0, 2\pi]$.

Among HARDI techniques q-ball imaging (QBI) [228] is one of the most studied. It has the advantage of being model-independent.

QBI showed that it was possible to reconstruct a smoothed version of the diffusion ODF directly from single shell HARDI acquisition with the Funk-Radon transform (FRT). The FRT value at a given spherical point is the great circle integral of the signal on the sphere defined by the plane through the origin perpendicular to the point of evaluation. The ODF is intuitive because it has its maximum(a) aligned with the underlying population of fiber(s). Hence, it is a more interesting function for tractography than the ADC. The original QBI has a numerical solution and more recent methods have introduced an analytical spherical harmonic reconstruction solution that is faster and more robust to noise.

In any of the method chosen if it is necessary to visualize specific tract of interest, several seed points are generated within a region (or volume) of interest (ROI or VOI) set interactively for visualization of a tract. A tracking result, that is series of coordinates data of trajectory nodes, is displayed by using line or tubular object with supporting objects such as surface of brain, slice image in 3D space of computer graphics. As ellipsoidal display is aimed at visualization of local anisotropy, color mapping of trajectory line, tube, or surface, is effective for visualization of local property of the tract object. Once the tract of interest have been reconstructed is possible to extrat some measures that quantify its property: mean length of streamlines, number of streamlines, volume of the tract, FA, MD, parallel and perpendicular diffusivity.
It should be cautioned that the term "number of streamlines" does not denote exact fiber count but, rather, some measure of fiber number. This "number of fibers" depends on FA and angular deflection thresholds and ROI placement [229]. FA, MD, parallel and perpen-

dicular diffusivity are mean measures that results from the average of quantity calculated at different positions separated by a fix distance on the tract.

Despite the limitations above mentioned, DT-MRI tractography is a promising technique to explore the anatomical basis of human cognition and its disorders. Using the diffusion anisotropy and the principal diffusion directions an estimation of white matter connectivity patterns in the brain from white matter tractography may be obtained. Many developmental, aging, and pathologic processes of the central nervous system influence the microstructural composition and architecture of the affected tissues. The diffusion of water within tissues will be altered by changes in the tissue microstructure and organization; consequently, diffusion-weighted (DW) MRI methods, including DTI, are potentially powerful probes for characterizing the effects of disease and aging on microstructure.

In this work DTI analysis was used in a case-control study to analyze differences in white matter patterns between controls and ASDs. This study is innovative as there are very few DTI studies on young children in literature, and this is one of the few Italian study on children. Moreover the study was focused on echolalia that is a disturb of language that causes the repetition ad echo of a sentence, or part of a sentence, after hearing it and can be classified as delayed or immediate, depending on the elapsed time between utterance production and repetition [230, 231].

Before performing these studies on ASD subjects a multicentric analysis of images acquired on two healthy subjects was performed in order to understand if the differences between different MR scanners were significant or not. The possibility to collect data acquired in

different centers in the same database could allow the increase of the number of subjects so it is an important opportunity to investigate. Moreover a phantom for the testing of HARDI algorithms was realized. This is an experimental model with different fiber crossing configurations (PIVOH, Phantom with Intra-Voxel Orientation Heterogeneity), able to simulate the structural complexity of white matter, in correspondence of fiber intersection. This phantom was realized at the Interdepartemental Research Center "E. Piaggio", while images were acquired and analyzed at the IRCSS Stella Maris. This work was the Master thesis activity of Dr. Danilo Sclefo [232].

3.2 Multicentric study

3.2.1 Introduction

Clinical studies are often highly expensive and time-consuming; moreover it is not easy to find a high number of subjects, both controls and patients, necessary to have a strong statistic power. Multicentric studies exhibit a good alternative to get a representative set of data. However, the data of different clinical centers are generated with different MR scanners and under different conditions which is challenging to an algorithmic analysis.
The need to verify the possibility to perform a multicentric study was determined by the fact that the IRCCS Stella Maris is involved in a project denominated IDEA (Inquiry into Disruption of Intersubjective equipment in Autism spectrum disorders in childhood), in which three centers are involved in the acquisition of DTI images: the IRCCS Stella Maris, The University of Pavia (Modino Institute)

and the University of Udine. The objective of the workpackage of the project dedicated to the study of brain connections is to perform a case-control study using traditional volumetric MRI and DTI techniques. Young ASD subjects and controls must be submitted to MRI scanning and analyzed in order to evaluate differences in white matter structure between the two groups.
The three centers in Pisa, Pavia and Udine have three different MR scanners, a GE, a Siemens and a Phillips respectively, so the question was if images acquired on controls and ASD children by the three centers could be collected in the same database in order to increase the number of subjects in the same study.
To answer this question DTI images on two control adult subjects were acquired and image processing and statistical analyses were performed to evaluate analogies and differences in DTI indices and white matter tracts.

3.2.2 Materials and methods

3.2.2.1 Participants

Two healthy volunteers were recluted for this study. The subjects were both females, one was 33 years old and the other one was 30 years old. Control participants were screened for current and past psychiatric disorders and contraindications to MR imaging. The two subjects will be referred in the following sections as RM and FL respectively.

3.2.2.2 Image acquisition

Structural and diffusion tensor MRI of the brain were performed on three 1.5 T MR systems. In Table 3.1 the acquisition parameters of each center are reported.

3.2.2.3 Image processing

Images were processed using the FSL (FMRIB Software Library, FMRIB, Oxford, UK) [233] software package. For each subject, all images including diffusion weighted and b_0 images, were corrected for eddy current induced distortion and subject motion effect using FDT (FMRIBs Diffusion Toolbox) [234]. Brain mask was created from the first b_0 image using BET (Brain extraction Tool) [235] and FDT was used to fit the tensor model and to compute the FA, MD, axial diffusivity and radial diffusivity maps. FA maps were imported in Matlab program where specific algorithms were implemented in order to analyze these maps and extract measures that allowed a comparison of the results. The following analyses were applied to the maps for each subject and each center: histogram, mean, standard deviation and entropy. The entropy of an image is defined as:

$$H = -\sum_{i=1}^{n} p(x_i) log_2 p(x_i) \tag{3.14}$$

where p contains the histogram counts for each value x_i. The entropy is in inverse proportion to the quality of the image: the higher is entropy the lower is the quantity of information.
Finally a ROI analysis was performed. In particular four rectangular ROIs were selected in specific areas of the brain: peritrigonal white

Center	**Pavia**	**Udine**	**Pisa**
Brand of scanner	**Philips**	**Siemens**	**GE**
Model of scanner	**Intera (1.5 Tesla)**	**Avanto (1.5 Tesla)**	**SignaHorizon (1.5 Tesla)**
Orientation	axial	axial	axial
TR (ms)/TE (ms)	11871/81	7700/80	11000/106
Sequence	SE-EPI	SE-EPI	SE-EPI
Number of directions	32	12	25
b-value	0/800	0/1000	0/1000
Number of slices	60	64	31
Slice thickness (mm)/gap (mm)	2/0	1.8/0	3/0
FOV (mm)	224x224x120	240x240x115	190x190x93
Acquisition matrix	112x110	128x128	64x64
Reconstruction matrix	128x128	256x256	256x256
Acquisition voxel (mm)	2x2.036x2	1.875x1.875x1.8	2.969x2.969x3
Reconstruction voxel (mm)	1.75x1.75x2	0.9375x0.9375x1.8	0.7422x0.7422x3
Number of averages	2	3	2

Table 3.1: *Acquisition parameters used by the three centers involved in the multicentric study.*

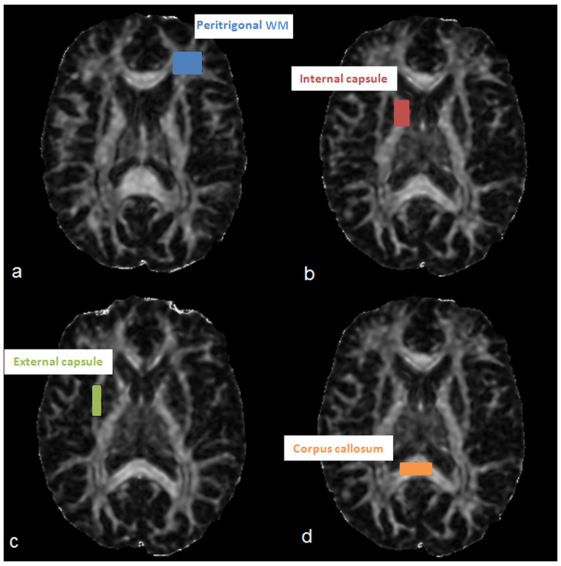

Figure 3.9: *ROIs selected for the analysis on several brain areas: peritrigonal WM, internal capsule, external capsule and corpus callosum.*

matter (WM), internal capsule, external capsule and corpus callosum (Figure 3.9). The same ROIs were transfered on the maps of the three centers and for the two subjects, scaling dimensions according to the size of the image. Then the mean FA value of each ROI was computed for the maps of each center and subject. Plots of each of these measures were realized in order to compare the results obtained for the same subject in the different center.

Diffusion tensor vectors were computed using TrackVis software (http://www.trackvis.org/). For each dataset the arcuate fasciculus was reconstructed following the procedure described in [236].

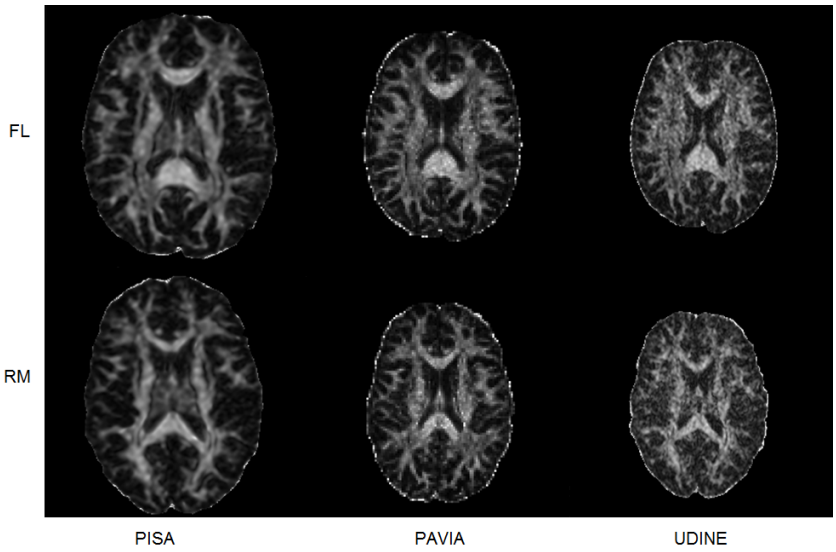

Figure 3.10: *FA maps of the two subjects (FL and RM) obtained with FSL Software.*

3.2.3 Results

The FSL processing of the images allowed to obtained the maps of the most important invariant idices used to characterize white matter structure. In particular we focused on FA maps.
In Figure 3.10 FA maps of the two subjects (FL and RM) obtained from the data acquired in the three centers are reported.

The histograms of the FA maps obtained from the dataset acquired in the three centers for the two subjects were realized. The three histograms for each subjects were plotted in the same graph in order to compare the results (Figure 3.11).

It should be noticed that the acquisition matrix of PAVIA center

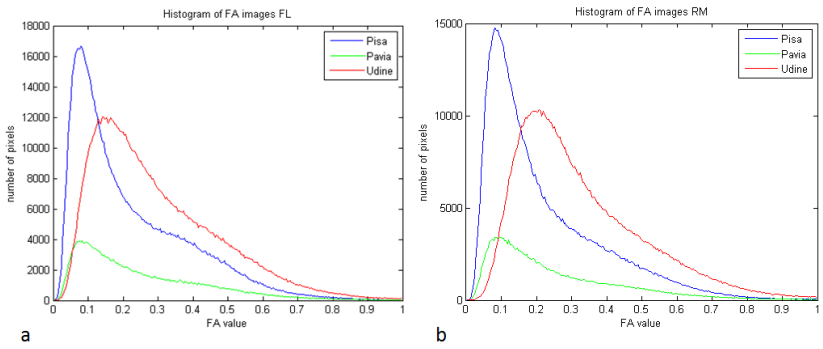

Figure 3.11: *Histograms of FA maps of the two subjects (a,FL and b,RM) obtained from the dataset of the three centers.*

is smaller than the other centers (128×128 vs. 256×256) this is why the peak of the histogram is lower than the others. Moreover, observing the histograms, we noticed that for both subjects the peak of the histograms of the maps of Pisa and Pavia centers were positioned in correspondence of the same value of FA while the histogram of the maps of Udine center was more shifted to higher FA values.
The mean value for each slice of the three dimensional FA maps were also plotted. In order to obtain a weighted measure, each number of slice was multiplied for the slice thickness. In this way FA is related to the portion of the brain covered at each slice point. Also in this case the plot obtained on the maps of the three centers for the two subjects were compared (Figure 3.12).

As regards FA values, it can be noticed that the values of mean FA are similar for Udine and Pavia centers, especially in the case of FL subject, while the mean values of FA for Pisa centers are higher. The global mean values of the three dimensional FA maps were also

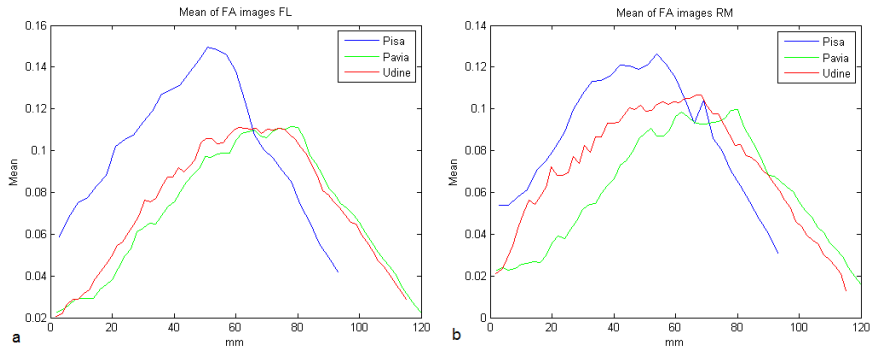

Figure 3.12: *Plot of mean FA vs. the length of the brain covered at each slice point in the maps of the two subjects (a,FL and b,RM) obtained from the dataset of the three centers.*

computed for the two subjects and compared for the three centers. Results are presented in Figure 3.13. Also in this plot it is possible to observe that the FA values of the maps of Pisa center are higher than the others. Although the values of the mean FA are different in the maps of the three center, it can be noticed that in all the cases the values of FL subject are higher than RM subject.

In order to the evaluate the quantity of information included in each map, the entropy was computed for each subject and center. In Figure 3.14 the results of this analysis are reported. Observing these plots it is possible to notice how in the middle slices, that are the ones in which the maps are larger, the quantity of information brought in the maps of Udine center is higher with respect to the maps of Pavia center. The values of entropy of the maps of Pisa center were higher than the others, so the information was lower. The entropy per size unit (pixel) was also computed as the size of the three maps

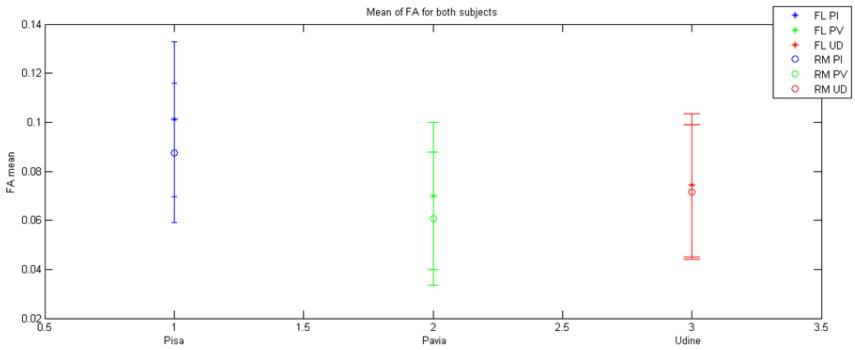

Figure 3.13: *Comparison of the global mean FA of the maps the two subjects (FL, stars and RM, circles) obtained from the dataset of the three centers.*

was not the same (in particular the map of Pavia center was smaller than the others). The plots of these measures are reported in Figure 3.15. The analysis of these plots showed that there is an inversion between Pisa maps and Pavia maps: the entropy per pixel of the maps of Pisa center was lower than the maps of Pavia center that means that the quantity of information per pixel was higher.

The results obtained through the ROI analysis are reported in Figures 3.16 and 3.17. Figure 3.16 shows how the mean FA values obtained in the different ROIs on the maps of the same subjects for the three centers were different. Figure 3.17 shows that, although the mean FA values of the different centers were different, differences between the two subjects were maintained.

The tractographic analysis allowed to reconstruct for each subject the arcuate fasciculus. Results are reported in Figure 3.18. It can be noticed that the tracts of the same subject obtained from the dataset

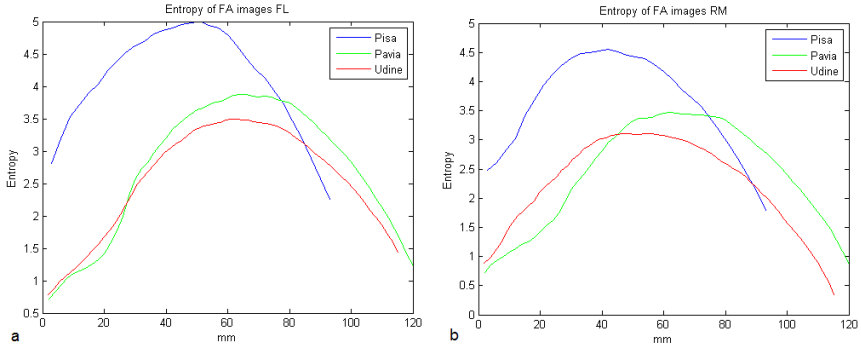

Figure 3.14: *Plot of entropy vs. the length of the brain covers at each slice point in the maps of the two subjects (a,FL and b,RM) obtained from the dataset of the three centers.*

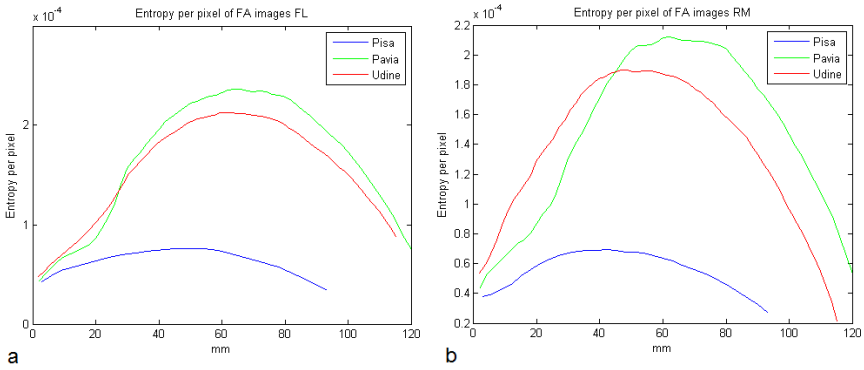

Figure 3.15: *Plot of entropy per size unit (pixel) for each slice of the maps of the two subjects (a,FL and b,RM) obtained from the dataset of the three centers.*

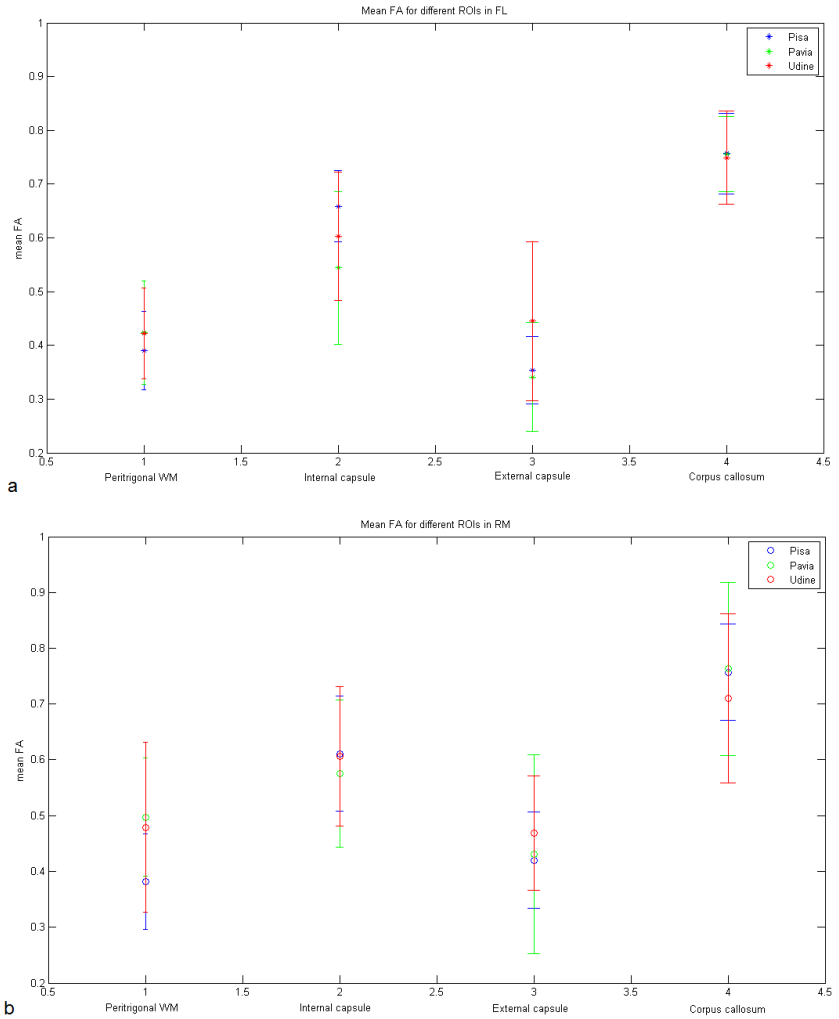

Figure 3.16: *Comparison of the mean FA in four different ROIs (peritrigonal WM, internal capsule, external capsule and corpus callosum) realized on the maps the two subjects (a,FL and b,RM) obtained from the dataset of the three centers.*

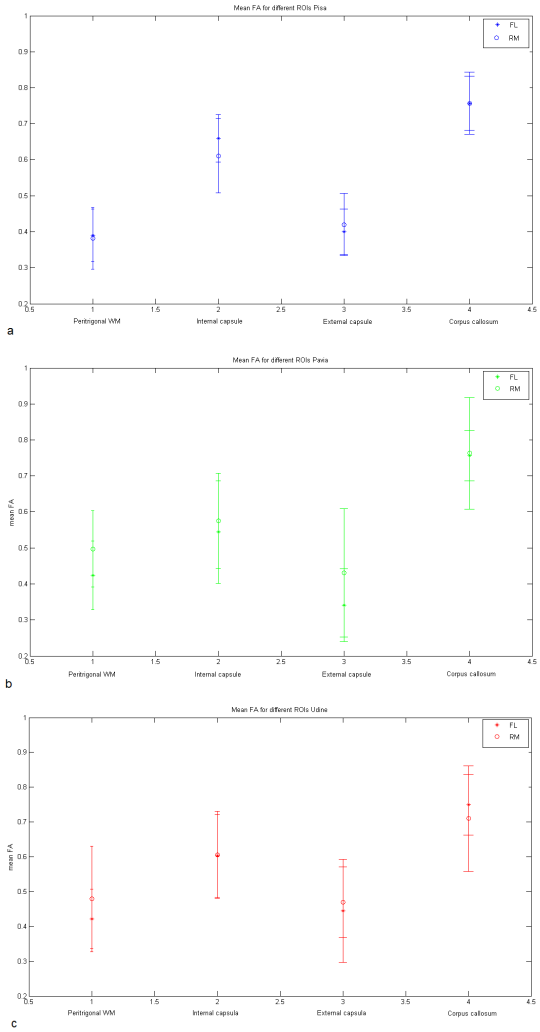

Figure 3.17: *Plots of the mean FA values for four different ROIs for the two subjects (FL and RM) realized on the maps of the three centers (a, Pisa; b, Pavia and c, Udine).*

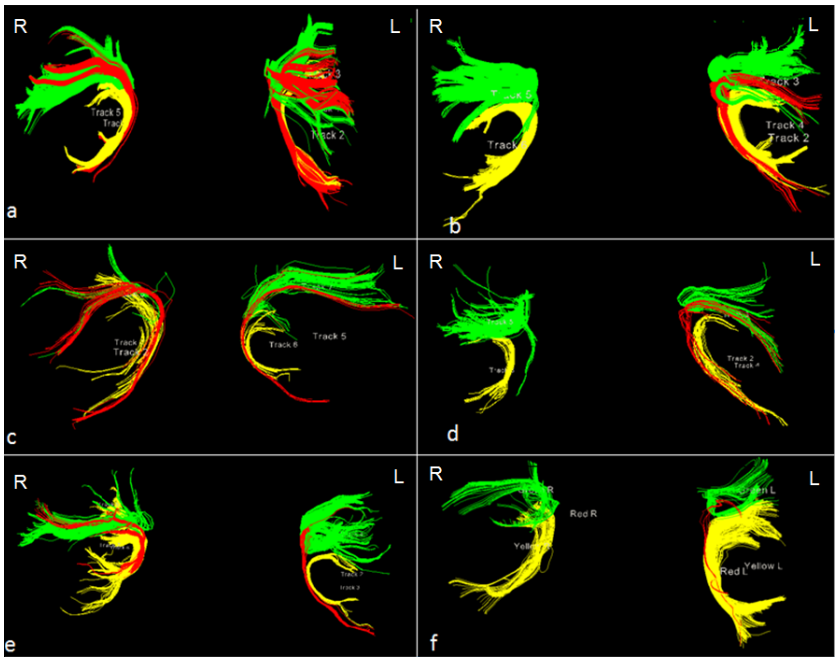

Figure 3.18: *Reconstructions of the arcuate fasciculus for each center and subject: a) FL, Pisa, b) RM, Pisa, c) FL, Pavia, d) RM, Pavia, e) FL, Udine and f) RM, Udine. Tracts are displayed in radiological convention.*

of the three centers were different in length and thickness. However in all the three cases RM subject appear to be highly lateralized as the direct segment (the red one) of the right arcuate fasciculus could not be reconstructed.

3.2.4 Discussion and conclusions

This study was a preliminary step before the preparation of the database of ASDs and control subjects that needed to be analyzed. The aim was to see if the data acquired by the three centers involved in the study gave the same information about the diffusion process occurring in the brain and so about the integrity of white matter tracts.

A qualitative observation of FA maps obtained with FSL showed how the maps of the different centers were different in terms of quality and resolution. In order to quantify this differences some algorithms in Matlab were implemented. They allowed to extract quantitative measures that were then compared through graphs. The result was that the three maps were different in mean FA and entropy for each subject. Despite the differences in the values obtained from the three centers the difference between the subjects was maintained.

As usually it is desirable to have information on specific white matter areas rather than on the entire brain, a ROI analysis was also performed. Also in this case different values of mean FA were obtained for the selected ROIs but the difference between the subjects was maintained.

The tractographic analysis allowed to compare the tract reconstruction achievable from the diffusion data of the three centers. The arcuate fasciculus was selected because it was the tract the DTI analysis on ASD children intended to concentrate on. The reconstructions obtained were different for the three centers in thickness and length. This means that some fibers of the arcuate could not be reconstructed maybe due to the low FA values along them. The

differences in the reconstruction could also be due to the differences in evaluating the directions of the fibers inside each voxel.
Although these differences, in all the three cases the tractography was not able to reconstruct the direct segment of RM subject. This means that this subject was highly lateralized and its direct segment was so thin and characterized by a low FA that with DTI technique it was not possible to reconstruct a continuous trajectory between equivalents of Broca's and Wernicke's territories in the right hemisphere. As Catani et al. revealed in their study [237] in 60% of the normal population there is an extreme degree of leftward lateralization.
After this study the decision was to not construct an unique database of data acquired in the different centers but to maintain separate databases. The aim of the analysis was in fact not only to identify the differences between groups of subjects but also to quantify these differences. The inclusion in the analysis of data that brought to different FA maps and tractographic reconstruction could have altered the results.
The solution that could be adopted in the future in order to increase the number of subjects is to realize an analysis in which the center is used as covariate. In this case however the acquisition parameters of data in each center need to be adjusted so that the quality of the images obtained in each center would be optimized. In Table 3.2 an hypothesis of the parameters that could be used in each center is reported in which the parameters that should be modify are shown in bold.

Center	**Pavia**	**Udine**	**Pisa**
Brand of scanner	**Philips**	**Siemens**	**GE**
Model of scanner	**Intera (1.5 Tesla)**	**Avanto (1.5 Tesla)**	**SignaHorizon (1.5 Tesla)**
Orientation	axial	axial	axial
TR (ms)/TE (ms)	11871/81	7700/80	11000/106
Sequence	SE-EPI	SE-EPI	SE-EPI
Number of directions	32	12	25
b-value	0/800	0/1000	0/1000
Number of slices	**35**	**35**	**35**
Slice thickness (mm)/gap (mm)	**3/0**	**3/0**	3/0
FOV (mm)	**200x200x105**	**200x200x105**	**200x200x105**
Acquisition matrix	**68x66**	**64x64**	64x64
Reconstruction matrix	**256x256**	256x256	256x256
Acquisition voxel (mm)	**2.941x3.036x3**	**3x3x3**	2.969x2.969x3
Reconstruction voxel (mm)	**0.7813x0.7813x3**	**0.8x0.8x3**	0.7422x0.7422x3
Number of averages	2	5	2

Table 3.2: *Optimization of the acquisition parameters that could be used by the three centers involved in the multicentric study. In bold are shown the parameters that should be changed.*

3.3 DTI study in Autism Spectrum Disorders (ASDs)

3.3.1 Introduction

Despite the accumulating knowledge on brain structure and brain function in ASDs, current findings on links between behavioral or neuropsychological measures and neurofunctional findings are still limited and controversial. Generally though, the evidence resulting from structural MRI studies is somewhat inconclusive. However, new image processing methods currently being developed provide dramatically more information about the morphological characteristics of brain structures than previously available. At present, there is almost generalized thinking that brain alterations in ASDs are not limited to a single brain area, but involve different structures within a globally affected neuronal network. Diffusion tensor imaging (DTI) approach [238, 239] is a powerful tool for non-invasive investigation of microstructure and of neuronal network and it seems to be extremely efficient in study of developmental brain.

3.3.2 Materials and methods

3.3.2.1 Participants

Twenty-three children (age range 2-11) with autism spectrum disorder were recruited from the clinical autism research program at the IRCSS Stella Maris Institute and ten healthy control children (age range 2-11) participated in the study. Control subjects were retrospectively selected from the database of clinical DTI. As for ASDs,

the control subjects patients underwent DTI in absence of a specific clinical indication, as a completion of the diagnostic pathway with the aim of excluding brain alterations. Controls had an IQ within the normal range (Table 3.3).

	Control group (n=10)	**ASD group (n=23)**
Age, months: mean (s.d) range	5.25 (2.46) 2-11.22	5.54 (2.03) 2.88-11.33
IQ (non verbal): mean (s.d) range	5.8 (0.42) 5-6	4.09 (1.38) 2-6

Table 3.3: *Participants characteristics.*

3.3.2.2 Image acquisition

Structural and diffusion tensor MRI of the brain were performed on a 1.5 T MR system (Signa Horizon LX, GE Medical System). The subjects were anesthetized for the acquisition. A sagittal three-dimensional fast spoiled gradient (SPGR) dataset covering the whole head was acquired. The parameters were: TR=12.3 ms, TE=2.4 ms, voxel resolution 256 x 256, field of view 280 mm, 124 slices, 1.1 mm slice thickness. For the DTI analysis, a multislice echo-planar imaging (EPI) acquisition sequence, using 25 directions of diffusion gradients, was used. After an interpolation automatically applied by the MR system the resolution is 0.7422mm x 0.7422mm x 3mm with a field of view 190mm x 190mm and coverage of the whole brain (TE= 107 ms, TR=11000 ms, b-value= 1000 s/mm).

3.3.2.3 DTI processing

Maps reconstruction Images were processed using the FSL (FMRIB Software Library, FMRIB, Oxford, UK) [233] software package. For each subject, all images including diffusion weighted and b_0 images, were corrected for eddy current induced distortion and subject motion effect using FDT (FMRIBs Diffusion Toolbox) [234]. Brain mask was created from the first b_0 image using BET (Brain extraction Tool) [235] and FDT was used to fit the tensor model and to compute the FA, MD, axial diffusivity and radial diffusivity maps.

TBSS analysis Voxelwise analysis was performed using TBSS [240]. First the most representative FA image was identified and all subjects' FA data were aligned to this target image using the non-linear registration tool FNIRT, which uses a b-spline representation of the registration warp field [241]. Next, the mean FA image was created and thinned to create a mean FA skeleton which represents the centers of all tracts common to the group. A threshold of $FA > 0.25$ was applied to the skeleton to include only major fiber bundles. Each subject's aligned FA data was then projected onto this skeleton and the resulting data fed into voxelwise cross-subject statistics.

Statistical analysis Statistical analysis was performed voxel by voxel to detect regions of significant differences of FA among the two groups of subject. The correlations of FA with age and with IQ were also investigated introducing these parameters as covariates in the contrast matrix. Individual FA maps were included in a

non-parametric permutation-based group model using "randomize" in FSL [242]. The TFCE (Threshold-Free Cluster Enhancement) option in randomize was used in order to avoid the need for the arbitrary initial cluster-forming threshold. Both contrasts were computed using 5000 permutations. Results are reported at corrected threshold $p < 0.05$.

3.3.2.4 Tractography

Tract reconstruction Diffusion tensor vectors were computed using ExploreDTI software (http://www.exploredti.com/). After the application of motion and distortion correction, a deterministic tracking algorithm was applied. Tract data were then transformed in NifTi format using a homemade MATLAB program including also information on length, FA and MD of each tract.
NifTi files were finally imported in TrackVis software for the reconstruction of the tracks of interest. White matter areas that TBSS analysis showed to be significantly different in the groups were selected for the analysis: the cingulum and the arcuate fasciculus [236] (Figure 3.19). These tracts were selected because this study and in particular the following one, were focus on language problem and both the cingulum and the arcuate are related to language and cognitive task.
The cingulum is a medial associative bundle that runs within the cingulate gyrus all around the corpus callosum. It contains fibers of different length, the longest of which run from the anterior temporal gyrus to the orbitofrontal cortex. The short U-shaped fibers connect the medial frontal, parietal, occipital, and temporal lobes and dif-

ferent portions of the cingulate cortex. The cingulum was dissected using a one-ROI approach. A single region was defined on the top three slices. When the cingulum separated into two branches an anterior and posterior region were defined on each slice. Artifactual (callosal) fibers were removed using an exclusion ROI defined around the corpus callosum.
The arcuate fasciculus is a lateral associative bundle composed of long and short fibers connecting the perisylvian cortex of the frontal, parietal, and temporal lobes. A three ROIs approach was used to reconstruct the three segments of the arcuate fasciculus. The first ROI was defined on the Broca's area, in the frontal lobe selecting three coronal slices of brain. The second ROI was identified on three axial slices catching the Wernicke's territory in the temporal lobe. The last ROIs was identified in the Geschwind area of the parietal lob selecting three appropriate slices in the sagittal view of the brain. Following this approach the three segments of the arcuate fasciculus were reconstructed: the long direct segment connecting Wernicke's area with Broca's area, the anterior indirect segment linking Broca's territory with the inferior parietal lobule and the posterior indirect segment linking the inferior parietal lobule with Wernicke's territory. The reconstruction of the tracts was performed with an FA threshold of 0.2 to avoid false positive due to artifacts.

Tractography outcome measures For each tract selected for the analysis the following measures were extracted: number of streamlines, mean length of streamlines, volume of the tract, fractional anisotropy (FA), mean diffusivity (MD), parallel diffusivity and perpendicular diffusivity.

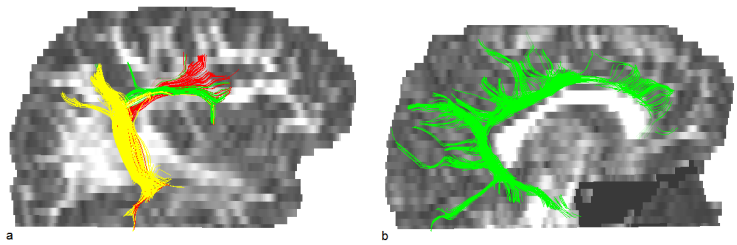

Figure 3.19: *Selected tracts reconstruction: a) arcuate fasciculus and b) cingulum.*

Statistical analysis Statistical comparisons of the tractography outcome measures were performed using SPSS software (SPSS Inc, Chicago, Ill). General linear model (GLM) analysis for repeated measures was used with side (left and right hemisphere) and tracts (cingulum and the three segments of the arcuate fasciculus) as the within-subject factors and group as between-subjects factor. Then, univariate ANOVA was performed on all the tractography measures.

3.3.3 Results

3.3.3.1 Group characteristics

There were no significant between-group differences in age (control group mean age 5.25±2.46 years; ASD group mean age 5.54±2.03; p=.73) while the non verbal IQ was found significantly different between the two groups (control group mean IQ 5.8±0.42; ASD group mean IQ 4.09±1.38; p=.0006).

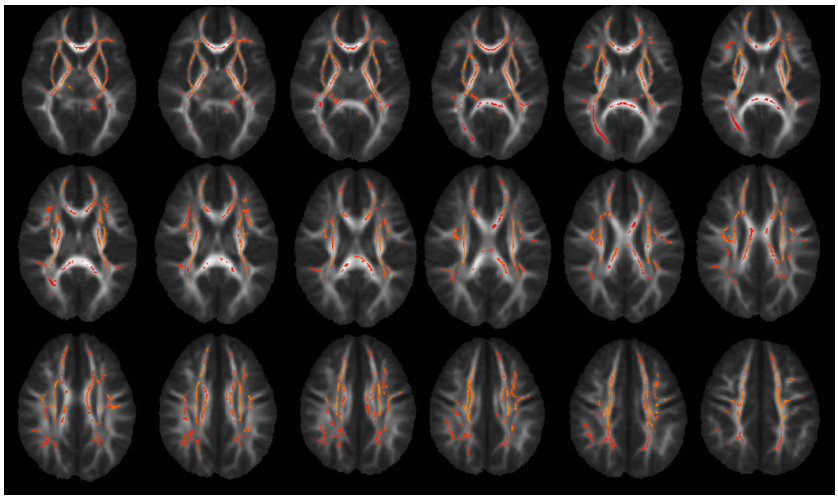

Figure 3.20: *Regions of significantly increased FA in ASDs than in controls (in red), superimposed on the mean FA image ($p<0.05$, non parametric permutation test, corrected for multiple comparisons). All images are in radiological convention, i.e. the right side of the subjects is on the left side of the images.*

3.3.3.2 FA differences between groups

Young children with autism spectrum disorder had a significant increase of FA in a lot of white matter areas. In particular increase in corpus callosum, cingulum, external and internal capsula, arcuate fasciculus was found (p=.05) (Figure 3.20).

3.3.3.3 FA correlation with age

No correlation with age was found for any of the two groups.

3.3.3.4 Tract-specific measurements

Number, length and volume of streamlines The GLM showed a significant group-by-side-by-tract interaction (p=.01) and tract-by-side-by-age (p=.03) interaction in the arcuate fasciculus. Comparison of the individual tracts revealed a significant increase in the length of streamlines bilaterally within the cingulum in ASD group (left cingulum: mean=88.7±14.2, right cingulum: mean=77.7±10.4) than in controls (left cingulum: mean =69.2±17.6; p=.002, right cingulum: mean=58.2±11.8; p=.0001). There was also a significant reduction in the number of streamlines within the posterior indirect segment of the left arcuate fasciculus in ASDs (mean=129.5±77.3) than in controls (mean=190.8±98.5; p=.06). No significant difference in the volume of the analyzed tracts was found.

FA, MD, parallel and perpendicular diffusivity FA in ASD group was significantly increased bilaterally in the cingulum (left cingulum: p=.002, right cingulum: p=.003) and in the fornix (p=.004). There was also an increase of MD in ASD group in comparison to controls in the following areas: within the left cingulum (p=.05), within the right indirect posterior (p=.02) and the right indirect anterior (p=.04) segments of the fasciculus arcuate. Finally a significant increase in parallel diffusivity in the ASD group was found in the right cingulum (p=.02).

3.4 DTI study in Autism Spectrum Disorders (ASDs): focus on echolalia

3.4.1 Introduction

Since first description of autistic patients [243], echolalia was indicated as a primary and common feature of their deviant productive language. According to its definition [244], echolalia is the repetition ad echo of a sentence, or part of a sentence, after hearing it and can be classified as delayed or immediate, depending on the elapsed time between utterance production and repetition [230]. Seminal studies on this topic have been reported mainly in 60's, 70's and 80's ASD research, where echolalia is described as a common (it concerns up to 75% of verbal ASD children in [245]) but aspecific symptom of ASDs [246]. Indeed, it can occur in a wide range of developmental disabilities (e.g. mental retardation), psychiatric disorders (e.g. schizophrenia, Tourette syndrome, Ganser syndrome), neurological conditions (mixed transcortical aphasia, Alzheimer's disease, frontotemporal dementia, Huntington's disease, Parkinson's disease, progressive supranuclear palsy, amyotrophic lateral schlerosis, left frontal lobe epilepsy, nonconvulsive status epilepticus), internistical diseases (a history of liver transplant, cerebral malaria, systemic lupus erythematosus), besides being a feature of typical language acquisition process in many children. However, other authors have underlined some echolalia patterns peculiar of ASDs, as its automatic and indiscriminate nature, often associated to a monotonous vocal delivery [247], and its mechanical, birdlike quality [248].
Speculations about the ASD echolalia meaning propose a variety of

functions (see the echolalia categories in [249] and [250]), besides its classical interpretation of "meaningless repetition" [251] of another speaker's utterances or "repetition in absence of comprehension" [252]. On the other hand, the neuroanatomic correlates of echolalia are still unclear. Early reports focalized on 'isolation' [253] or 'deactivation' [254] of the speech areas from the rest of the brain, while subsequent studies indicate the involvement of supplementary motor area (SMA) [255, 256], left thalamic lesions [257, 258] or disruption of connection between Broca's area and SMA [259].

Notwithstanding the first information on anatomical basis of language and its dysfunctions were achieved from postmortem examination or computed tomography (CT), only the advent of structural MR imaging methodologies has allowed for a deep, non-invasive in-vivo characterization of brain structures. Diffusion tensor imaging (DTI) is one of such techniques and it was employed in the investigation of fasciculus arcuate, revealing new and more complex features of its anatomy [260]. In particular, besides the well-known arcuate pathway connecting Broca's and Wernicke's areas (i.e. direct or long segment) and involved in automatic word repetition, it was reported the existence of an indirect pathway connecting Broca's and Wernicke's territories via the inferior parietal cortex (Geschwind's territory). The latter pathway is in turn composed of an anterior segment, which joins Broca's and Geschwind's areas and regards semantic production, and of a posterior segment, connecting Geschwind's and Wernicke's areas and concerning semantic comprehension.

These findings have shed light on the neuroanatomical basis of several types of language disorders having reference to lesion or hyperfunction of different fasciculus arcuate segments. In this picture

abnormalities in the arcuate pathways could therefore be associated with symptom of enhanced repetition of others speech, i.e. immediate echolalia [261].

3.4.2 Materials and methods

3.4.2.1 Participants

Ten ASD children with echolalia (age range 3-11) and ten without echolalia (age range 3-10) were recruited from our clinical autism research program at the IRCSS Stella Maris Institute and ten healthy control children (age range 2-11) participated in the study. Control subjects were retrospectively selected from the database of clinical DTI. As for ASDs, the control subjects patients underwent DTI in absence of a specific clinical indication, as a completion of the diagnostic pathway with the aim of excluding brain alterations. Controls had an IQ within the normal range (Table 3.4).

		Autism Spectrum Disorder	
	Control group (n=10)	**With echolalia (n=12)**	**Without echolalia (n=8)**
Age, months: mean (s.d),range	5.26 (2.61) 2-11.22	5.72 (2.35) 2.83-11.33	4.87 (1.35) 3-9.83
IQ (non verbal): mean (s.d), range	5.89 (0.33) 5-6	4.4 (2.37) 2-6	3.3 (1.25) 2-5

Table 3.4: *Participants characteristics.*

3.4.2.2 DTI processing

The methods used for DTI processing were exactly the same described in the precedent study (see section 3.3.2.3).

3.4.2.3 Tractography

The same procedure for the computation of diffusion tensor vectors and of tracts reconstruction as the one described in section 3.3.2.4 was used.
In addition to the arcuate fasciculus and the cingulum, the fornix was also reconstructed following the procedure described in [236] (Figure 3.21).
The fornix is a C-shape bundle that connects the medial temporal lobe to the mammillary bodies and hypothalamus. A single ROI was defined around the body of the fornix. To visualize the entire course of the fornix (including its temporal portion), additional regions around the fimbriae of each side were included in the ROI.
In the first step of the analysis a seed FA threshold of 0.2 was chosen for the computation of diffusion tensor vectors. The tracts of interest reconstruction, showed that lot of streamlines of the fornix were missed. This happened because the fornix is a small tract and has, especially in young children, a low value of FA, below 0.2. So tractography vectors were computed also with a threshold of 0.1 and these tensors were used for the reconstruction of the fornix. The reconstruction of the other tracts (the cingulum and the arcuate fasciculus) was performed with an FA threshold of 0.2 to avoid false positive due to artifacts.
Once the tracts have been reconstructed, the same measures com-

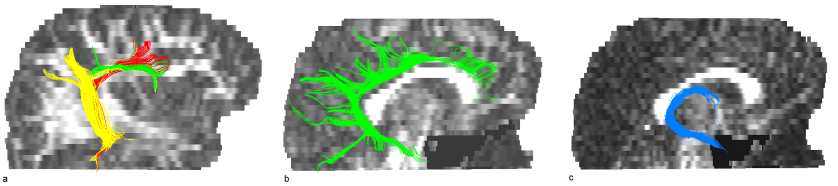

Figure 3.21: *Selected tracts reconstruction: a) arcuate fasciculus, b) cingulum and c) fornix.*

puted in the case-control study and the same statistical analyses were performed (see section 3.3.2.4 and section 3.3.2.4).

3.4.3 Results

3.4.3.1 Group characteristics

There were no significant differences in age between the two groups of ASDs (echolalic group mean age 5.72±2.35 years; non-echolalic group mean age 4.87±5.542.03; p=.43) or between the control group (mean age 5.26±2.61 years) and the echolalic (p=.67) or the non-echolalic (p=.72) ASD group. The non verbal IQ was not significantly different between the two groups of ASDs (echolalic group mean IQ 4.4±2.37; non-echolalic group mean IQ 3.3±1.25; p=.43) while it was found significantly different between the control group (mean IQ 5.89±0.33) and the echolalic (p=.04) or the non echolalic (p=.0002) ASD group.

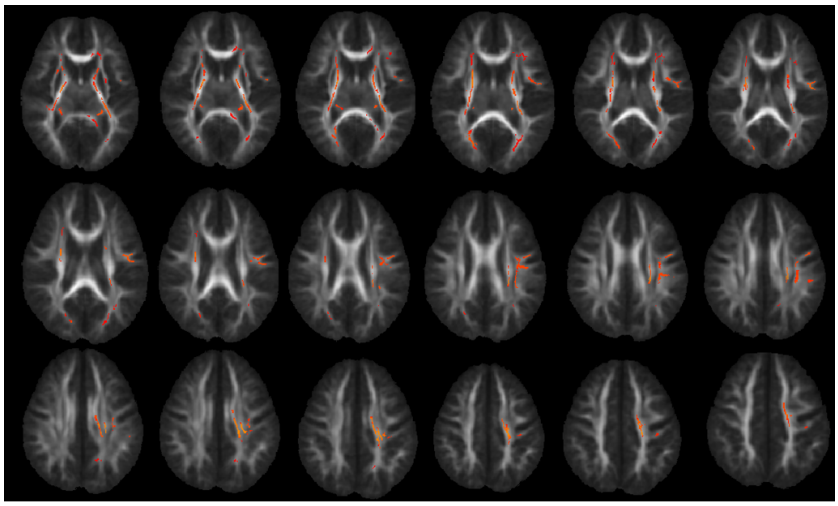

Figure 3.22: *Regions of significantly increased FA in echolalic ASDs than in non echolalic ASDs (in red), superimposed on the mean FA image ($p<0.05$, non parametric permutation test, corrected for multiple comparisons). All images are in radiological convention, i.e. the right side of the subjects is on the left side of the images.*

3.4.3.2 FA differences between groups

Significant differences between the echoloalic and not-echolalic autistic groups were found. In particular FA was increased in the group of subjects with echolalia in the corpus callosum, the fornix, the arcuate fasciculus and the cingulum (p=.05) (Figure 3.22). No significant increase of FA was found in the group of subjects without echolalia in comparison to the other one.

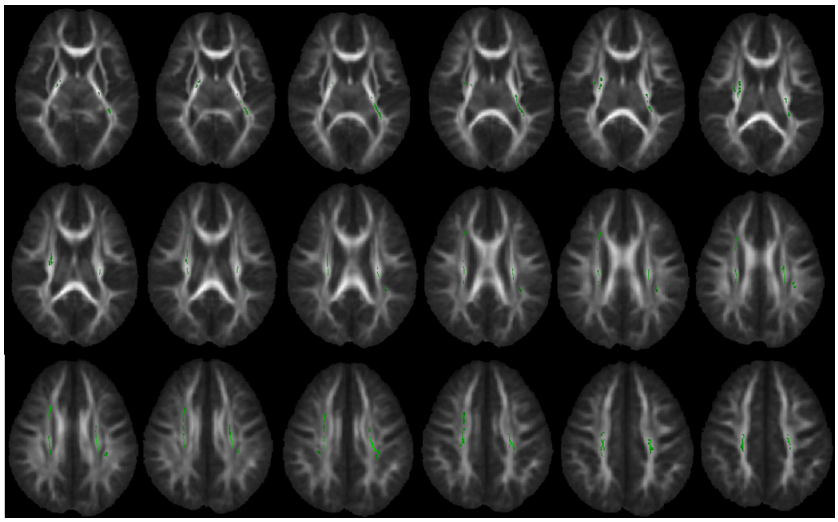

Figure 3.23: *Regions of significantly increased FA with increasing age (in blue) in echolalic group, superimposed on the mean FA image ($p<0.05$, non parametric permutation test, corrected for multiple comparisons). All images are in radiological convention, i.e. the right side of the subjects is on the left side of the images.*

3.4.3.3 FA correlation with age

Positive correlation of FA with age have been found for the two ASD groups (p=.05).

3.4.3.4 Tract-specific measurements

Autism-spectrum disorder without echolalia v. controls

Number, length and volume of streamlines The GLM showed no significant interactions in the arcuate fasciculus or in the

cingulum. Comparison of the single tracts revealed a significant increase in the length of streamlines bilaterally within the cingulum in ASDs without echolalia (left cingulum: mean=92.7±11.5, right cingulum: mean=79.1±8.5) than in controls (left cingulum: mean=69.2±17.6; p=.002, right cingulum: mean=58.1±11.8; p=.0001). There was also a significant reduction in the number of streamlines within the posterior indirect segment of the left arcuate fasciculus in ASD group without echolalia (mean=115.7±66.4) than in controls (mean=190.8±98.5; p=.05). No significant difference in the volume of the analyzed tracts was found.

FA, MD, parallel and perpendicular diffusivity FA was significantly increased in ASD group without echolalia bilaterally in the cingulum (left cingulum: p=.004, right cingulum: p=.01). There was also an increase of MD in ASD group without echolalia in comparison to controls in the following areas: the right indirect posterior segment (p=.01) and bilaterally within the indirect anterior segments of the arcuate fasciculus (left segment: p=.04, right segment: p=.06). Finally a significant increase in perpendicular diffusivity in the left indirect posterior segment of the arcuate fasciculus (p=.05) was found in the ASD group without echolalia.

Autism-spectrum disorder with echolalia v. controls

Number, length and volume of streamlines The GLM showed a significant group-by-side-by-tract (p=.01) interaction in the arcuate fasciculus. No significant interactions were found in the cingulum. Comparison of the individual tracts revealed a significant

increase in the length of streamlines bilaterally within the cingulum in ASD group with echolalia (left cingulum: mean=85.5±15.9, right cingulum: mean=76.8±12.1) than in controls (left cingulum: mean =69.2±17.6; p=.03, right cingulum: mean=58.1±11.8; p=.002). There was also a significant increase in the number of streamlines within the anterior indirect segment of the right arcuate fasciculus in ASDs (mean=46.5±33.8) than in controls (mean=99±65.7; p=.03) and also in its volume (ASD mean=2.7±1.1, controls mean=1.4±0.8; p=.01). Finally there was a significant increase in the length of the fornix in ASD group with echolalia (mean=97.1±19.6) with respect to the control group (mean=82.3±15, p=.06).

FA, MD, parallel and perpendicular diffusivity FA was significantly increased in ASD group with echolalia bilaterally in the cingulum (left cingulum: p=.02, right cingulum: p=.01). Moreover FA was increased in the fornix in ASD group with echolalia with respect to controls (p=.006). There was also an increase of MD in ASD group with echolalia in comparison to controls in the bilaterally within the cingulum (left cingulum: p=.06, right cingulum: p=.06). Finally a significant increase in parallel diffusivity in the ASD group with echolalia was found bilaterally within the cingulum (left cingulum: p=.03, right cingulum: p=.03).

Autism-spectrum disorder with echolalia v. autism-spectrum disorder without echolalia

Number, length and volume of streamlines The GLM showed no significant interactions between side, group, tract and

age in the cingulum. A significant tract-by-age (p=.04) and tract-by-side-by age (p=.05) interaction was found in the arcuate fasciculus. A significant increase of the number of streamlines of the right anterior indirect segment of the arcuate fasciculus was found in the echolalic group (mean= 99.0±65.7) with respect to the not echolalic one (mean=37.0±39.1, p=.03). A significant increase of the volume of this tract was found in the echolalic group (mean: 2.7±1.1) with respect to the not echolalic one (mean=1.1±1.0, p=.008).

FA, MD, parallel and perpendicular diffusivity FA was found significantly increased in the left posterior indirect segment of the arcuate fasciculus in the echolalic group with respect to the not echolalic one (p=.02).

3.5 Discussion and conclusions of DTI studies in ASDs

In the first study a systematic methodological procedure for DTI and tractographic analysis was set up. In order to optimize the analysis a combination of different software and of home-made Matlab algorithms was used.
The first step of the analysis was the TBSS, a tool that allows to investigate FA differences in whole brain without requiring prespecification of tracts of interest. This is achieved by estimating a "group mean FA skeleton", which represents the centers of all fiber bundles that are generally common to the subjects involved in a study. Each subject's FA data is then projected onto the mean FA skeleton in

such a way that each skeleton voxel takes the FA value from the local center of the nearest relevant tract resolving issues of alignment.
The TBSS analysis allowed to identify in which brain areas there were clusters of significant differences in FA between the two groups.
The second step of the analysis was to compute the diffusion vectors in order to perform tractography. This analysis was performed in ExploreDTI software. Among all the software available for the computation of diffusion vectors, this software was used because it offers a lot of options. First of all it is possible to perform a motion and distortion correction before performing the analysis. The motion correction is very important because it decreases the artifacts and it is necessary in cases like the one of this study, because ASD children have difficulties in staying still in the scanner. Moreover while performing tractography is possible to choose a set of parameters like seedpoint resolution, seed FA threshold, FA and MD tracking threshold range and fiber length range.
The problem with this software is that the drawing of ROIs for the selection of the tracts of interest is quite tricky. For this reason Trackvis software was used in order to perform the reconstruction of tracts. In this software in fact the selection of the ROIs is much easier and effective. Due to the fact that the format of data that ExploreDTI gives as an output and the format used in Trackvis are different, conversion algorithms were used. In addition to the diffusion tracts information relative to their length, FA and MD were also imported. Comparison of the individual tracts allowed to investigate in which specific segments of each tract the differences of FA and MD were present. Moreover it allowed to compare also information about tract length, volume and number of streamlines.

This optimized methodology was applied to all the subjects considered in this study and then statistical analyses on the tracts were performed in order to evaluate the significance of the differences between the two groups.

This study was one of the first studies on very young autistic children. The TBSS analysis showed a significant increase of FA in ASDs with respects to control in corpus callosum, cingulum, external and internal capsula, arcuate fasciculus. The increase of FA in young ASD children is in agreement with the study of Ben-Bashet et al. [5] who found increased restricted diffusion in white matter in overall analysis as well as in selected ROIs in young children with confirmed diagnosis of autism. This increase of FA might be a confirmation of accelerated brain growth in autism in the first 24 years of life.

The cingulum and the arcuate fasciculus were selected for the reconstruction and the tractographic analysis. Significant differences in this white matter tracts were found. The cingulum is the most prominent tract connecting limbic system and cerebral cortex and is involved in higher-level cognitive processes like error monitoring, attention, visuospatial and memory functions, abilities that are frequently compromised in ASD subjects. On the other hand, the arcuate fasciculus is a fiber bundle related to language, a function always impaired in ASDs, at least from the qualitative point of view.

In particular the most significant result was the increase in the length of streamlines of the cingulum in ASDs in comparison to controls. It is important to underline that the length measure is a mean of all the streamlines so that if the number of short streamlines is higher the mean is lower. This finding confirm the result found by Sundaram at al. [100] that is the only other study on very young autistic children.

These researchers found that the fiber length of the long association fibers was higher in the ASD group than in controls although they said that it was unclear from their study which specific long association tracts were involved. From the findings of the present study it seems that the predominant long association fibers belong to the cingulum. The hypothesis of Sundaram and colleagues was that one of the mechanisms related to increased long range fiber length could be altered serotonin. In fact, many previous studies have shown that serotonin acts as a neurotrophic factor involved in axonal outgrowth during development [87, 88]. In-vitro measures of serotonin synthesis in animal models of autism could help to clarify the role of altered serotonin in autism in white matter structural changes.

In the second study the same methodological procedure optimized in the previous study for analysis of FA maps and for the reconstruction of the tracts of interest was used. The aim of this study was to see if using the TBSS and tractography was possible not only to discriminate between cases and controls but also to distinguish between subtypes of pathological subjects. In particular the focus of this analysis was the echolalia. For the first time in this study DTI analyses were used to investigate white matter correlates of this kind of disturb.

Among the original database of subjects used for the previous study, four ASD subjects were excluded as they were preverbal.

The application of the TBSS analysis revealed an increase of FA in echolalic group with respect to the not echolalic one in the arcuate fasciculus, the cingulum and the fornix. The arcuate fasciculus is a white matter tract specific of language. The fornix and the cingulum are implied in memory tasks so an involvement of these tracts in

echolalic disturb could mean that there is a link between the obsessive repetition of words and the process of memorization for learning. The following analysis allowed a tractographic reconstruction of this tracts and a comparison of the metrical features characteristic of each tract. This analysis showed differences in the anterior and posterior indirect fasciculus of the arcuate fasciculus.
Further studies are needed in order to correlate these findings with behavioral measures so that it would be possible to clarify the meaning and the clinical implications of these results.

3.6 A new fiber crossing phantom for validation of diffusion function reconstruction techniques

3.6.1 Introduction

DTI-based fiber tracking gives insights into the complex architecture of the brain. However, it is well known that it presents a number of limitations, especially in presence of heterogeneous configurations inside one single voxel (Intra-Voxel Orientational Heterogeneity, IVOH), that means configurations in which fiber bundles have different orientations. This limit has suggested the development of new algorithms based on non-parametric reconstruction techniques. The validation of fiber reconstruction by these different approaches remains challenging and requires suitable test-phantoms. For isotropic diffusion, the ADC can be well verified on pure spherical water phantoms, whilst the use of simulated data is limited

by the fact that no real MRI data are considered, with particular regard to the presence of normal imaging artifacts, noise characteristics, and voxel size limitations. These aspects have suggested the realization of an experimental model with different fiber crossing configurations (PIVOH, Phantom with Intra-Voxel Orientation Heterogeneity), able to simulate the structural complexity of the white matter, in correspondence of fiber intersection. In particular in this work PIVOH was used to test the Q-ball imaging algorithm.

3.6.2 Materials & Methods

3.6.2.1 Experimental model realization

PIVOH was built in a modular way with several configurations, diversifying for geometry and material, in order to evaluate the reconstruction of fiber bundles at different levels of anisotropy and different types of crossing. It presented four different structures (abbreviation: *str.*), enclosed in a poliver box (diamagnetic material) with a airtight closure (Figure 3.24).

Figure 3.26 shows the four different structures and Table 3.5 lists their correspondent features. Fibers of structures I, II and IV were made in nylon (impermeable), whilst those of structure III were realized by hollow filaments (permeable) (Figure 3.25). The structures in nylon reproduced a situation of hindered diffusion, whilst the structure III replicated a restricted diffusion state [262]. Str. I and II were realized with 200 μm diameter fibers. To test the angular resolutions of the different reconstruction methods str. I and II presented two different angles at the fiber crossing zone, i.e. 90 ° and 77 °. Str. IV presented a 90 degrees crossing angle and was made up

Figure 3.24: *PIVOH.*

of 60 μm diameter fibers. This choice aimed to better recreate the white matter fibers environment where mean fiber diameter ranges from a few *microns* to some dozen of *microns*. Str. III was realized with polysulfone (permeable material) hollow fibers and aimed to recreate a restricted diffusion state. It presented a 90 ° fiber crossing zone. Inner and outer fiber diameters of str. III were 180 μm and 230 μm respectively.

A careful procedure for the disposition of the fibers was used in order to allow the maximum proximity of them (Figure 3.27). Structures were positioned on silicon rings that allowed a modular configuration of PIVOH.
The box in which the structures were enclosed was made up of six panels of poliver, attached one to the others using a dry procedure in

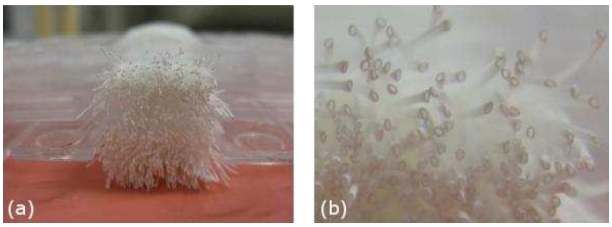

Figure 3.25: *a) Hollow fiber structure (III), b) Particular of the extremities.*

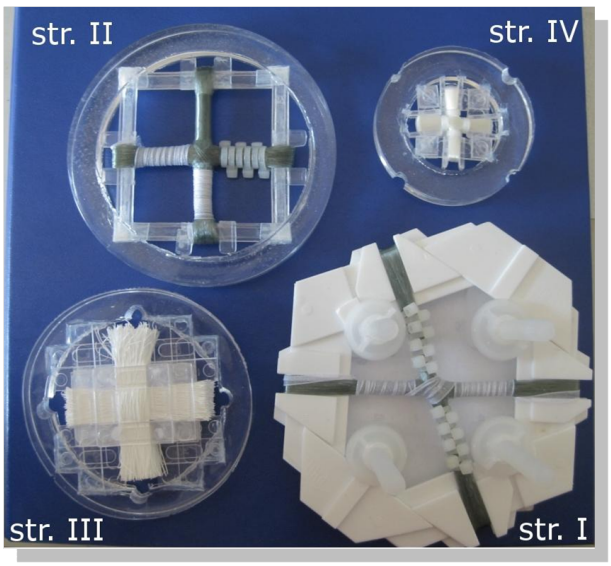

Figure 3.26: *Fiber crossing structures.*

Structure	Material of fibers	Diameter of fibers (μm)	Crossing (degrees)
I	nylon	200	77
II	nylon	200	90
III	polysulfone	180-230	90
IV	nylon	60	90

Table 3.5: *Characteristics of fiber crossing structures.*

Figure 3.27: *Construction procedure of the str. I, II and IV.*

order to obtain a high hermetic closure. On the upper panel of this box two hermetic valves were positioned for box emptying and refilling with different liquids as physiological or customized solutions. In order to reduce the susceptibility artifacts due to the presence of air bubbles between adjacent fibers the phantom was filled with distilled water using a vacuum process.
A simple instrumentation was included inside the box: a thermometer, a homemade manometer and two spirit levels.

3.6.2.2 Image acquisition and analysis

All diffusion weighted images were acquired using a 1.5 T MR system (Signa Horizon LX, GE Medical System) and an interleaved single-shot pulsed field gradient spin-echo sequence. Two datasets were collected with different MR parameters. The first was registered in order to evaluate the analysis based on the diffusion tensor imaging, using 25 directions of diffusion gradients (TR/TE=11000/106 ms, b-value=1000 s/mm^2, FOV=19cmx19cm, matrix=64x64, NEX=2, 28 slices, slice thickness=3mm), whilst the second dataset was collected applying 55 directions of diffusion gradients (TR/TE=4000/106 ms, b-value=1500 s/mm^2, FOV=19cmx19cm, matrix=64x64, NEX=2, 12 slices, slice thickness=3mm positioning three slices for each structure) in order to perform Q-Ball reconstruction of the fiber tracts. Data analysis was performed by a Matlab code for the calculations of diffusion invariants and the Trackvis software package for fiber tracking. Data acquired with a high number of encoding directions were analyzed through Q-ball technique. In order to perform tractography in both cases several ROIs in correspondence of the fiber branches were selected.

3.6.3 Results

The analysis of the FA maps for the four structures (Figure 3.28) revealed that the nylon structures (str. I, II and IV) showed a high detectable degree of anisotropy in correspondence of the fiber branches, meaning that these branches had an high degree of directionality, while they did not present any anisotropy in the areas in which fiber crossing occurred. The observation the FA maps obtained for the

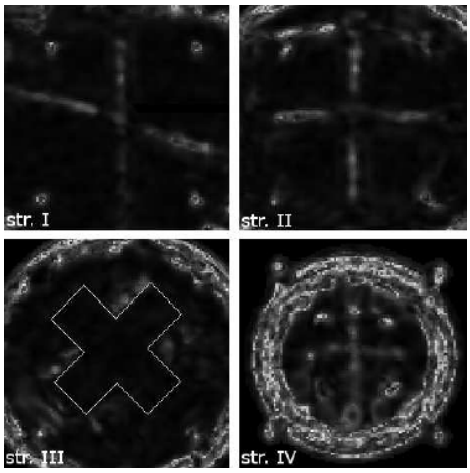

Figure 3.28: *FA maps of the structures of PIVOH (I, II, III and IV). Structures I, II and IV show a high degree of anisotropy in correspondence of the branches but a low anisotropy in the crossing area while str. III does not present any anisotropy.*

structure realized with the hollow fibers (str. III) revealed the lack of anisotropy in the diffusion of water molecules in every area of the structure. For this reason in the following elaborations this structure was excluded.

In order to increase the information on the anisotropy of water molecules diffusion for each structure, DEC maps were also realized. The observation of these maps revealed that str. IV was the one that assured the maximum directionality of the fibers especially in the areas of the branches next to the fiber crossing zone (Figure 3.29a). The ODF was computed and visualized through glyphs in the fiber crossing area of str. IV (Figure 3.29b). It is possible to notice how the two elongation directions of fiber bundles were correctly identify

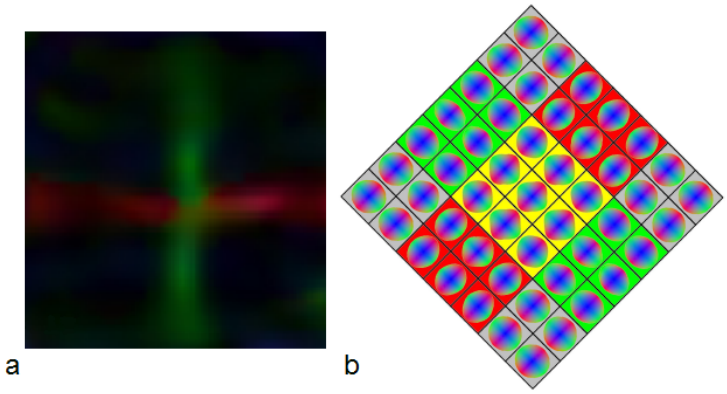

Figure 3.29: *a)DEC maps of str. IV, b) Representation of ODF in correspondence of fiber crossing area of str. IV. In the area external to the fibers (gray background) the glyphs are spherical (isotropic diffusion), in correspondence of the branches (red and green background) they have an ellipsoidal shape (linear diffusion), finally in the central area (yellow background) glyphs show two directions of local maximum in the directions of elongation of fiber bundles.*

by Q-ball technique through maximum directions presented by the multi-surfaces of the glyphs.

In order to evaluate the results obtained by the diffusion analysis, a Diffusion Tensor Tractography (DTT) was performed. The str. IV was selected for this analysis as it was shown to be the most directional. The tractography of this structure is shown in Figure 3.30a. It can be noticed that in correspondence of the fiber crossing area, tract reconstruction seems to block and in some cases even to deviate from the correct elongation direction of these tracts.
Using the same selection of the ROIs used for the DTI tractography

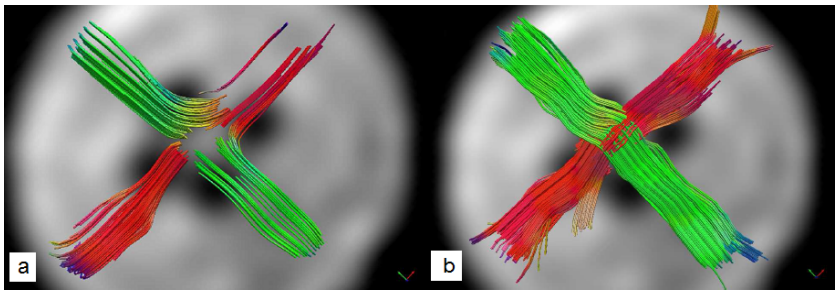

Figure 3.30: *a) Tractography of the str. IV. Due to the limitations of DTI the fiber crossing area can not be reconstructed, b) Q-ball tractography of str. IV. Unlike DTT this technique is able to reconstruct the fiber crossing area.*

the non-parametric method Q-ball was used for the reconstruction of fiber bundles of str. IV. Figure 3.30b shows how the fiber bundles were well reproduced also in the crossing zone, thanks to the ability of this method of resolving the Orientation Distribution Function, ODF, finding more local maxima.

3.6.4 Discussion and conclusions

In conclusion, the experimental model PIVOH seems to be a useful tool for the study of methods devoted to the resolution of the fiber-crossing problem.
The structures realized in nylon fibers (str. I, II e IV) showed detectable values of FA along the fibers tracts, whilst the structure III did not present significant values of FA even in correspondence of the bundles. Moreover, among all the structures, structure IV provided higher values of FA and thus, it appeared to assure a better direc-

tionality of the fiber bundles, especially in the areas closer to the crossing zone. This was due to the smaller diameter of the fibers of this structure since the dimensions of the realized compartments are comparable to the free quadratic random walk of water molecules. On the contrary, structure III produced the opposite result (low directionality and low FA values). This was due to the relative bigger inner diameter of hollow fibers and the lack of complete closeness of the fibers. The dimensions of the diameter did not allow to realize environments of dimension close to the free quadratic random walk of water molecules so, also if the presence of fiber bundles create an anisotropic means, in the times characteristic of the encoding gradients, diffusion occur in an almost isotropic way.

DTI technique showed to be able to identify diffusion characteristics of high directional fiber bundles. However this technique presented some limitations in the presence of fiber crossing configurations and was not able to reconstruct the fiber bundles. On the contrary Q-ball technique correctly identified the two principal elongation directions in correspondence of the fiber crossing area. In the tractography performed with this technique, in fact, the fiber structures were properly reconstructed.

Despite its limitation DTI is anyway a very powerful tool to identify brain areas with an altered diffusion process.

Results obtained from this study suggest that a close examination of non parametric techniques would be useful in order to reconstruct the tangled white matter fibers of the brain that are associated to important functional areas. In this way the spectrum of application of diffusion techniques in clinical-diagnostic field would be extended. Moreover, using experimental models like PIVOH, these techniques

could be tested with higher magnetic field (3 T and 7 T) to better characterize ODF and validate its application in the clinical-diagnostic field in the next future.

Chapter 4

Novel fMRI protocols to study cortical response in ASDs

4.1 Background on Functional Magnetic Resonance Imaging

Functional magnetic resonance imaging (fMRI) has rapidly become a popular tool for measuring brain function. fMRI reveals which parts of the brain are activated by behavioral tasks with a spatial resolution of 2-5 millimeters, which is superior to many of the other techniques in cognitive neuroscience. This means that places of activity in the brain that are as close as 2-5 millimeters apart in the brain can theoretically still be distinguished from each other. The temporal resolution (the minimal distance in time between two data points that can still be distinguished), however, is relatively poor (2-3 seconds) [263, 264].

The contrast technique most commonly used in fMRI is the so-called BOLD (Blood Oxygenation Level-Dependent contrast) technique. The BOLD technique is based on the fact that, under normal circumstances, neuronal activity and haemodynamics (regulation of blood

flow and oxygenation) are linked in the brain [265, 266].
The BOLD technique basically measures changes in the inhomogeneity of the magnetic field, which are a result of changes in the level of oxygen present in the blood (blood oxygenation) [265, 266, 267, 268]. Deoxyhaemoglobin (a haemoglobin protein contained within the red blood cells without an oxygen molecule attached to it) has magnetic properties and will cause an inhomogeneity in the magnetic field surrounding it. Oxyhaemoglobin (a haemoglobin protein contained within the red blood cells with an oxygen molecule attached to it) has hardly any magnetic properties and therefore has very little effect on the magnetic field surrounding it. Therefore, a high level of deoxyhaemoglobin in the blood will result in a greater field inhomogeneity and therefore in a decrease of the fMRI signal [265, 266, 267, 268].
The function of the BOLD signal against time in response to a temporary increase in neuronal activity is known as the haemodynamic response function (HRF) [265] (Figure 4.1). After a transient increase in neuronal activity the BOLD signal initially decreases because the active neurons use oxygen thereby increasing the relative level of deoxyhaemoglobin in the blood [265]. This decrease, however, is tiny and is not always found [269]. Following this initial decrease, there is a large increase in the BOLD signal which reaches its maximum after approximately 6 seconds [270, 265]. This increase is due to a massive oversupply of oxygen-rich blood. The result of this oversupply of oxygen is a large decrease in the relative level of deoxyhaemoglobin, which in turn causes the increase in the BOLD signal. Finally, the level of deoxyhaemoglobin slowly returns to normal and the BOLD signal decays until it has reached its original baseline level after an initial undershoot after approximately 24 sec-

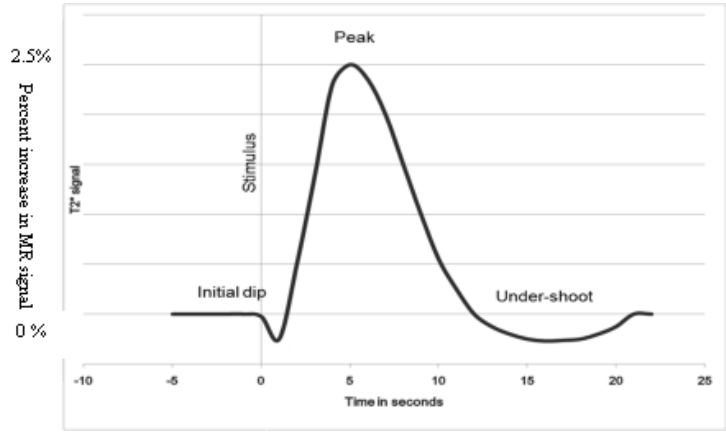

Figure 4.1: *Time course of the HRF in response to a short-lasting increase in neuronal activity at time = 0.*

onds [265]. This function of the BOLD signal against time is also known as the BOLD response. Data analysis of almost all fMRI studies is based on the signals coming from the much stronger positive BOLD response.

A major goal of fMRI measurements is the localization of the neural correlates of sensory, motor and cognitive processes. Another major goal of fMRI measurements is the characterization of the response profile in various Regions-Of-Interest (ROIs) by retrieving plots of averaged signal time courses for different experimental conditions. Inspection of the shape of (averaged) time courses may also help to separate signal fluctuations due to measurement artifacts from stimulus-related hemodynamic responses. In order to obtain fMRI data with relatively high temporal resolution, functional time series are acquired using fast MR sequences sensitive to BOLD contrast as for example the Gradient Recalled Echo sequence (GRE).

Over the course of an experiment, the brain is continuously active. This means that the level of oxygenation of the blood varies continuously. However, typically only 1 to 10 percent of this variation in oxygenation is actually related to the task at hand and constitutes the signal of interest. Therefore, great care must be taken when designing an fMRI experiment. The optimal experimental design maximizes the possibility of finding a reliable answer to the research question posed. In other words, the optimal design maximizes both statistical power and the power to draw inferences.
The first type of experimental design is the so-called block design, also known as the box-car [271] (Figure 4.2). In a block design, two or more conditions are alternated in blocks. Each block will have a duration of a certain number of fMRI scans and within each block only one condition is presented. By making the conditions differ in only the cognitive process of interest, the fMRI signal that differentiates the conditions should represent this cognitive process of interest. The contrast could be done between one condition and another one or between a condition and the baseline.
The second type of experimental design is the so-called event related design [271] (Figure 4.2). In an event related design the course of the HRF following each stimulus presentation is estimated. The multiple HRF's following a single type of stimulus can be averaged. An important aspect to be considered is the presentation of stimuli in a randomized order within the task in order to avoid cognitive adaptation strategies of the subjects.

In a typical fMRI experiment a measurement of the entire brain, known as a volume, is collected every 2 to 4 seconds, resulting in hundreds of collected brain volumes per experiment for each sub-

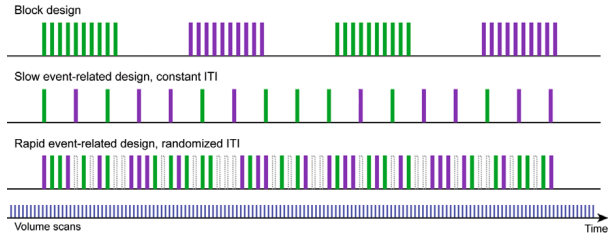

Figure 4.2: *In a block design (upper row), events belonging to the same condition are grouped together and are separated by a baseline block. In this example, two blocks of two main conditions (green, condition 1; violet, condition 2) are depicted. In slow event related designs, trials of different conditions appear in randomized order and are spaced sufficiently far apart to avoid largely overlapping BOLD responses. In rapid event related designs, stimuli are closely spaced leading to substantial overlap of evoked fMRI responses.*

ject. The ultimate goal is determining what areas of the brain show a significant increase in the BOLD response under certain task conditions. To achieve this goal, a number of steps must be performed on the fMRI dataset.

In order to reduce artifacts and noise-related signal components, a series of mathematical operations is typically performed prior to statistical data analysis. The most essential steps of these pre-processing operations include: head motion detection and correction, slice scan timing correction (necessary because the different slices are not acquired in the same time instant), removal of linear and non-linear trends in voxel time courses, spatial and temporal smoothing of the data and spatial normalization and co-registration.

After these pre-processing steps it is possible to perform the statis-

tical analysis of the data. The goal of the statistical analysis is to determine what areas of the brain are significantly activated under certain task conditions. Most commonly the General Linear Model (GLM) is used for this statistical analysis. The GLM is mathematically identical to a multiple regression analysis but stresses its suitability for both multiple qualitative and multiple quantitative variables.

The GLM is suited to implement any parametric statistical test with one dependent variable, including any factorial ANOVA design as well as designs with a mixture of qualitative and quantitative variables (covariance analysis, ANCOVA). Because of its flexibility to incorporate multiple quantitative and qualitative independent variables, the GLM has become the core tool for fMRI data analysis after its introduction into the neuroimaging community by Friston and colleagues [272, 273]. From the perspective of multiple regression analysis, the GLM aims to explain or predict the variation of a dependent variable in terms of a linear combination (weighted sum) of several reference functions. The dependent variable corresponds to the observed fMRI time course of a voxel and the reference functions correspond to time courses of expected (idealized) fMRI responses for different conditions of the experimental paradigm.

The reference functions are also called predictors, regressors, explanatory variables, covariates or basis functions. A set of predictors forms the design matrix, also called the model. Considering the block design, a predictor time course is typically obtained by convolution of a condition box-car time course with a standard hemodynamic response function. A condition box-car time course may be defined by setting values to 1 at time points at which the modeled condition

is defined (on) and 0 at all other time points.
After the design matrix and therefore the global shape of the BOLD response following a stimulus presentation has been modeled, this model has to be fit separately to the time course of each voxel. The t-test is used to determine if any linear combination of the predictor variables defined in the design matrix explain a significant amount of variance in the BOLD dataset. The result is a map of t-score for each voxel and for each linear combination of predictor variables reflecting how well the observed BOLD time course is explained.
In the cases where characterization and statistical assessment of general brain patterns is desired, multiple subjects have to be integrated in groups. Such group studies make it possible to generalize findings from a sample of subjects to the population from which the patients or healthy subjects have been drawn.
The integration of fMRI data from multiple subjects is challenging because of the spatial correspondence problem. In neuroimaging, the matching of brains is usually performed by a process called brain normalization, which involves warping each brain into a common space. The most commonly used target space for normalization is the Talairach space and the closely related MNI template space.
After brain normalization, the data from multiple subjects can be statistically analyzed simply by concatenating them over corresponding points. After concatenating the data, the statistical analysis described earlier can then be applied to the concatenated time courses. In the context of the GLM, the multi-subject voxel time courses as well as the multi-subject predictors may be obtained by concatenation and contrasts can be tested in the same way as described for single subject data. The obtained results can not be generalized to

the population level since the data is analyzed as if it stems from a single subject. Significant findings only indicate that the results are repeatable for the same subject (group of subjects). In order to test whether the obtained results are valid at the population level, the statistical procedure must assess the variability of observed effects across subjects (random effects analysis) as opposed to the variability across individual measurement time points as performed in the concatenation approach (fixed effects analysis).

A simple and elegant method is provided by multi-level summary statistics approach [274]. In a first level, mean effects (summary statistics) are estimated for each subject (level 1). The estimated effects at the first level per subject enter the second level as the dependent variable and are analyzed for significant effects. Since the summarized data at the second level explicitly models the variability of the estimated effects across subjects, the obtained results can be generalized to the population from which the subjects (sample) were drawn.

To summarize the data at the first level, a standard GLM may be used to estimate effects beta values separately for each subject. Instead of one set of beta values in fixed effects analysis, this step will provide a separate set of beta values for each subject. The obtained beta values can be analyzed at the second level using a standard ANOVA with one or more within-subject factors categorizing the beta values. If the data represent multiple groups of subjects, a between factor for group comparisons can be added.

These short explanations indicate that the statistical analysis at the second level does not differ from the usual statistical approach in medical studies. The only major difference to standard statistics

is that the analysis is performed separately for each voxel requiring methods to correct for a massive multiple comparison problem. Note that in addition to the estimated subject-specific effects of the fMRI design (beta values of first level analysis), additional external variables (e.g. an IQ value for each subject) may be incorporated as covariates at the second level.

4.2 Introduction

Autism Spectrum Disorders (ASDs) are a set represented by an early-onset neruodevelopmental disorders that disrupt the development of intersubjectivity and have several cascading effects on neurocognitive functions. A multiplicity of genetic and environmental factors play a role in ASDs. Recent studies on the neuroanatomic, neurofuntional and/or neurochemical features of autistic disorder suggest the hypothesis that different organic factors may lead to a disruption of cerebral development finally expressing with an autistic cognitive and behavior pattern.
In particular ASDs involve a basic impairment in social cognition and an abnormal brain connectivity and functional activation of cerebral areas that are the bases of their altered behavioral ability [275].
A lot of fMRI technique studies show a different pattern of brain activation during several tasks, such as language processing [276], working memory [277], executive functioning [278], visual imagery [279] but also in the resting state condition [280]. Experiments on facial processing show how in autistic subjects the activation of face-processing network is abnormal [281], [23], [282]. This network

is constituted by fusiform face area (FFA), inferior occipital gyrus (IOG), fusiform gyrus (FG), superior temporal sulcus (STS), amygdala, insula, limbic system, sensorimotor cortex and inferior frontal cortex (IFC). Autistic subjects present an atypical pattern of activation in particular in those areas that are involved in the "social brain" during the processing of facial expressions of emotion. The "social brain" includes areas such as of the occipital and temporal cortices, the amygdala, the orbito-frontal cortex (OFC) and the anterior cingulate cortex (ACC) that are important for processing social information.

The deficit in face processing network activity has been interpreted by some authors as the consequence of a poor gratification about this kind of stimuli [283] or as a difficulty in detecting and interpreting social interactions [284]. The neurofunctional correlate of the low interest for faces is expressed in a reduced BOLD activation of fusiform face area (FFA) in ASD patients [114], [285]. However several factors influence neurofunctional face response in ASD subjects such as age of participants and the kind of faces used in the experiment. For example in the study by Pierce et al. [286], the first one on only young autistic children, authors found an hypoactivation of FG in ASDs in comparison to normal controls while they observe an unknown face while the FG activated also in ASDs while watching their mother's or another child's face. This could mean that FG is not the principal site of a defect in face processing but there is instead a dysfunction in the systems that modulate FG activity.

Moreover some studies show that if patients are stimulated with specific tasks aimed to increase attention to social stimuli, neural response is similar to that of control subjects. For example FFA

activates in front of non-human stimuli such as cartoons [287]. This finding has a great relevance in the application of therapeutic and rehabilitative strategies directed towards the improvement of social abilities in ASDs. The state-of-the-art confirms the usefulness of robots in ASD therapy to act as social mediators to increase the social interaction skills of ASD children [288], [289].
Recently humanoid robots have been used in research on imitation, learning and social responsiveness. During the interaction with the androids important ability that deficit in ASD such as face identification, gaze perception and emotion evaluation of face expressions are elicited. This study investigated the neural correlates of face processing in autism by acquiring fMRI data during attentive viewing of human faces, android faces and robots.
Among the android faces we used also the face of a humanoid robot developed by the Hanson Robotics and the Interdepartmental Research Center "E. Piaggio" at the Scientific Institute Stella Maris called FACE (Facial Automation for Conveying Emotions) that is used for the therapy of autistic subjects and will be presented in the following chapter.
In this study a block design protocol was chosen as it increases statistical power and so it is more suitable for a study with children, especially autistic children, that usually move and cannot stay for a long time inside the scanner so that the time of experiment needs to be as short as possible.

4.3 Materials and Methods

4.3.1 Participants

In a pilot study three adults controls (one males and two females; mean age±standard deviation: 28.1±1.6) participated.
Data acquired on these subjects were used as a pilot study to tune the fMRI task for the following analyses and were not included in the final analysis or results.
In the following study six males with high functioning ASDs (mean age±standard deviation: 15.8±2.4; VIQ: 114.5±23.3; PIQ: 110.5±12.7) and six typically developing controls (four males and two females; mean age±standard deviation, 23.3±5.3) were recruited. Among the ASD subjects one did not want to enter the scanner and another one was excluded from the analysis because it was able to perform only one series of the task. The final group so was made up of four ASD subjects.
Diagnoses were confirmed with the Autism Diagnostic Interview-Revised (ADI-R, [290]), the Autism Diagnostic Observation Schedule (ADOS, [291]), and clinical judgment based on all available information from qualified professional clinicians. Intellectual functioning was estimated by means of an abbreviated version, that is, four subtests, of the Wechsler Intelligence Scale for ChildrenRevised (WISC-R, [292]). Control participants were screened for current and past psychiatric disorders, history of a developmental learning disability and contraindications to MR imaging. All participants gave informed consent to participate in the study.

4.3.2 fMRI task

For each subject, the experimental protocol, was presented back-to-back via LCD goggles (Resonance technology) in a passive viewing task. A block-design paradigm was used.
The stimuli consisted in 10 pictures of human faces (H), 10 pictures of android faces (A), 10 pictures of robotic faces (R) and 10 pictures of objects (O). Images were converted to gray-scale levels and a Matlab custom program was used to uniform size and luminance of all them. Images were downloaded from the website except for the photograph of the android FACE developed at the Interdepartemantal Research Center "E. Piaggio".
In the pilot study two kind of protocols were used: in the first one 10 blocks presented digital, greyscale pictures of 8 human faces (H), or 8 android faces (A) or 8 objects (O) (Figure 4.3.a), in the second one pictures of objects were replaced with pictures of robotic faces (R) (Figure 4.3.b). In both paradigms each image was presented for 2.5 s with 0.5 s inter-stimulus interval. The order of the images presented within each block was random and also the sequence of blocks was random. Each paradigm was repeated 2 times and the acquisition time for the whole fMRI session was about 20 minutes.

In the following study two kind of protocols were used: in the first one 12 blocks presented digital, greyscale pictures of 6 human faces (H), or 6 android faces (A) or 6 robotic faces (R), in the second study a mask constituted by 8 blocks of 6 robotic faces (R) or 6 objects was used. Also in this case in both paradigms each image was presented for 2.5 s with 0.5 s inter-stimulus interval, the order of the images presented within each block was random and also the

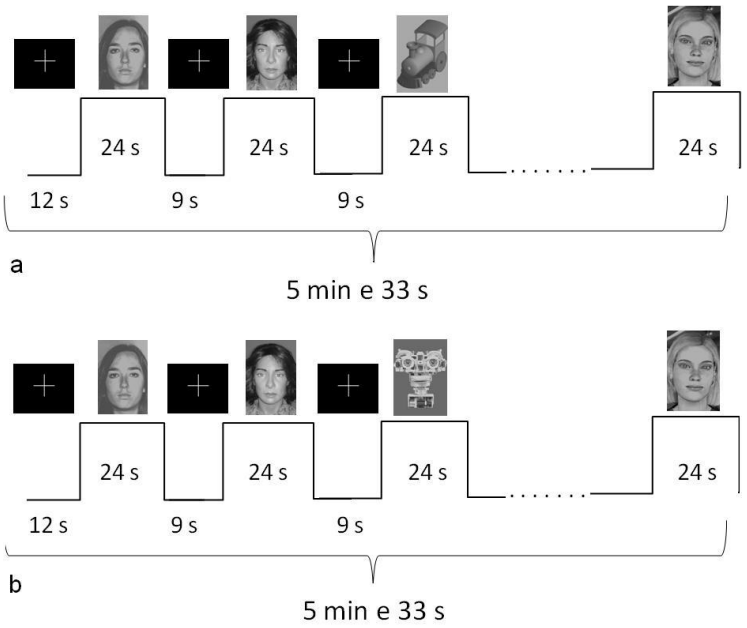

Figure 4.3: *Experimental paradigm in the pilot study with human faces, android faces and objects (a) and with human faces, android faces and robotic faces (b).*

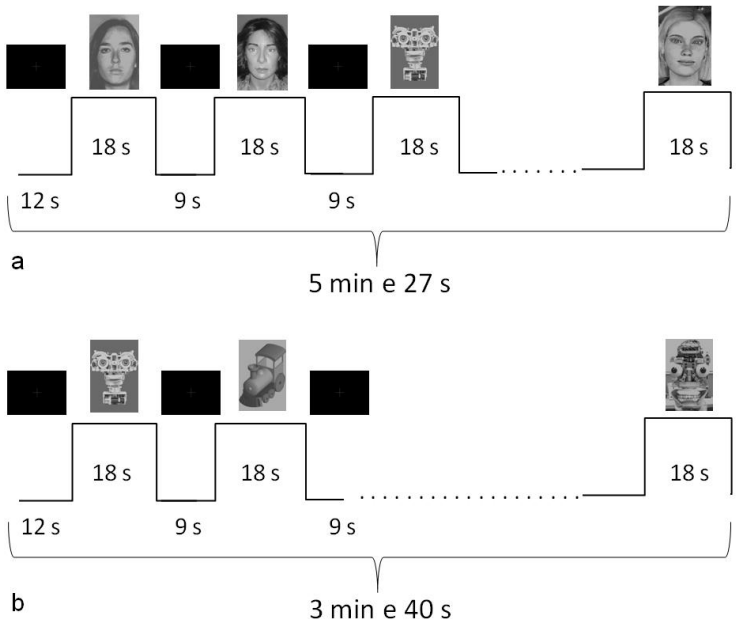

Figure 4.4: *Experimental paradigm in the second study with human faces, android faces and robotic faces (a) and mask with robotic faces and objects (b).*

sequence of blocks was random. The first paradigm was repeated 3 times while the second only once; the acquisition time for the whole fMRI session was about 20 minutes.

4.3.3 Image acquisition

Structural and functional MRI were performed on a 1.5 T MR system (Signa Horizon LX, GE Medical System). The MRI protocol provided a full-brain anatomical 3-D high-resolution T1-weighted structural images (TE= 11 ms, TR= 500 ms, 1 mm^3 voxel dimen-

sion, flip angle= 90 °) and BOLD functional data, collected using T2*-weighted echo-planar imaging (EPI) gradient-recalled echo sequence (TR= 3000 ms, TE= 23 ms, 21 slices; 5 mm thick, 64X64 matrix, flip angle= 80 °). The total acquisition time of all the MR session was about 45 minutes.

4.3.4 Data analysis

Data analysis was performed using the Brain Voyager QX software package (Brain Innovation, Maastricht, the Netherlands).
Before statistical analysis, raw data were corrected for head movements and high-temporal filtered in order to exclude temporal drifts. For each subject, all the two-dimensional functional data were co-registered, concatenated, aligned to the three-dimensional high resolution images and finally transformed into Talairach space [293].
A General Linear Model (GLM) approach was used to generate statistical parametric maps, using a hemodynamic response function modeled on the standard Boynton's function [294] and considering the four conditions: H, A, R, O.
For the multi-subject analysis, a random-effect model analysis was chosen. A ROI (Region-Of-Interest) analysis was conducted on the statistically significant clusters coming out from the application of the GLM analysis. In these ROIs, a single-subject analysis was performed measuring the average percent signal change of each individual subject. Then an average signal response for each ROI was obtained as the mean across the subjects.
The pilot study was used to test if stimuli activated the face-processing network and if the different conditions gave a different response.

In the second study four planned analysis were performed as follows: (i) to explore whether the used stimuli were able to activate the face-processing network the activity for all the observed faces versus the static conditions was contrasted (all stimuli > static conditions); (ii) to investigate the differences between ASD subjects and controls the activity related to observation of human faces, android faces, robotic faces and objects was compared for the two groups of subjects; (iii) to explore whether there were areas differentially responding to the kind of stimulus observed, the activity related to observation of human faces, android faces, robotic faces and objects was compared; and (iv) to assess the differential response to the different conditions, a ROI analysis on the regions activated by the contrast (iii) was performed.

4.4 Results

The pilot study revealed that the task developed in this work clearly yielded distinguishable activations in the areas of face-processing network in the control group. The group analysis showed that these areas activated in all control subjects as it can be can seen in Figure 4.5 where the activation of the sum of three stimuli with respect to the resting-state condition is reported. The protocol that used objects instead of robotic faces gave a similar activation so results are not reported. It should be noticed that although the gold standard method is reporting data for $p<0.05$ Bonferroni corrected, in this study, due to the low number of subjects, it was decided to visualize activation for $p< 0.001$ uncorrected.

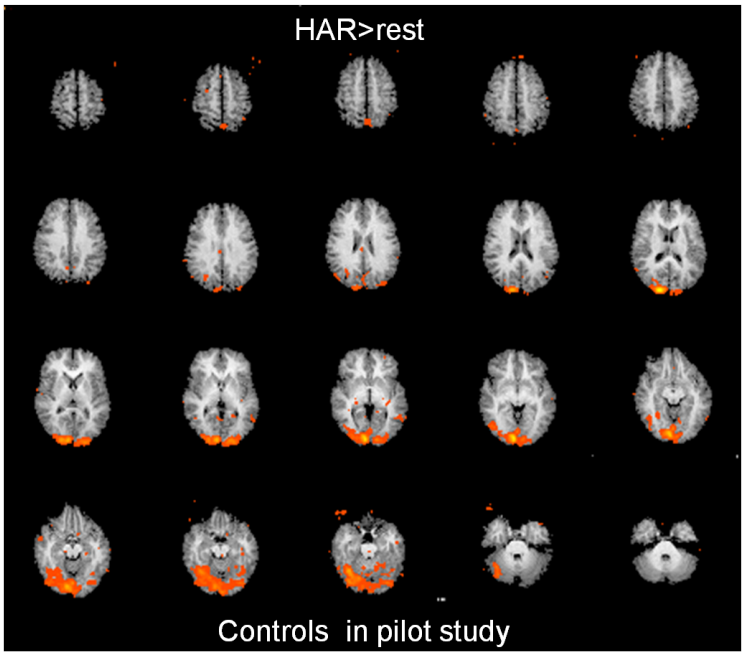

Figure 4.5: *Activation of face processing network in response to the three stimuli (H, A , R) vs. the rest condition in the three control subjects of the pilot study. All results are $p < 0.001$ uncorrected. The brain images are in radiological orientation.*

The second study confirmed the activation of the face-processing network both in controls and in ASDs. The pattern of activation of the two groups was quite similar as it can be observed in Figure 4.6. In this Figure the response to the three stimuli (humans, androids and robots) vs. the rest condition is shown.

Although the pattern of activation of the two groups was similar, some differences can be noticed. First of all it can be observed that in controls there is an activation of the frontal areas, especially in the right hemisphere, while this activation is missed in the ASD group. Moreover the activation of the ventral areas is reduced in ASDs with respect to controls. Single-subject analysis confirmed these finding for both ASDs and controls. Patterns of activation for each subject are not reported.
A comparison between the two groups in response to the three stimuli was also performed. Results are shown in Figure 4.7.

This result confirm the activation of frontal areas, in particular the right prefrontal gyrus, and in intraparietal areas in controls but not in the ASD group (areas in red). On the contrary there is an increased activation of the visual areas in ASDs with respect to controls (areas in blue).

The same analyses were realized for the other paradigm that was the objects-robots mask. Figure 4.8 shows the pattern of activation in response to these two stimuli vs. the rest condition both in controls and ASDs. It can be noticed that the activation of the frontal areas in controls is reduced with respect to the first paradigm. Moreover the the pattern of activation of controls and ASDs is more

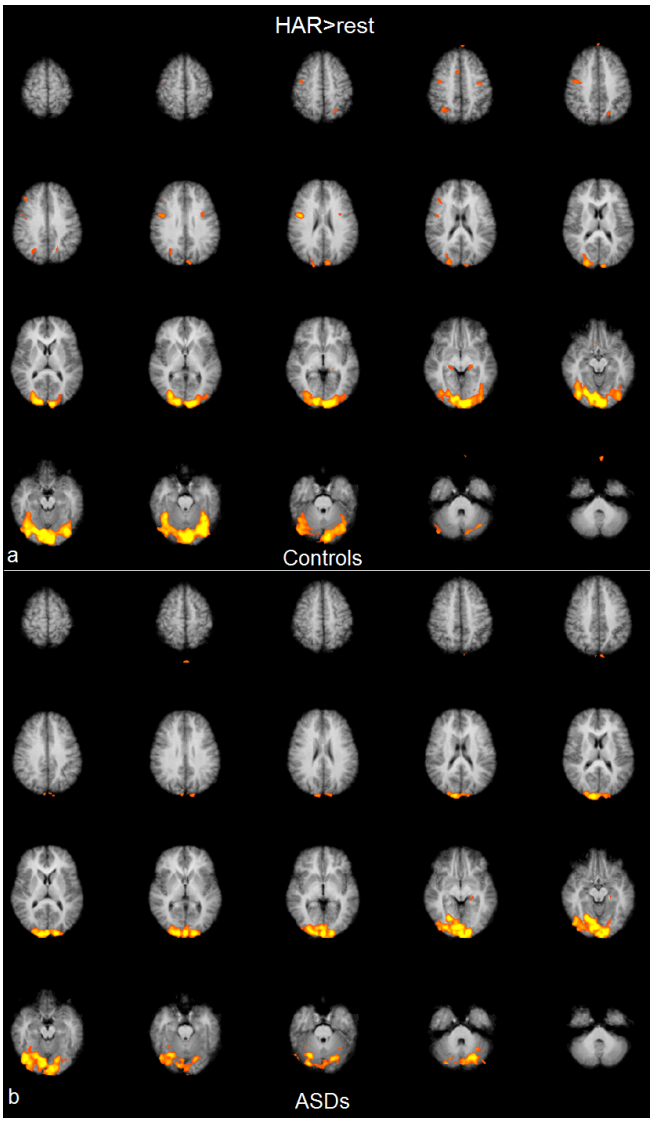

Figure 4.6: *Activation of face processing network in response to the three stimuli (H, A , R) vs. the rest condition in controls (a) and in ASDs (b). All results are $p < 0.001$ uncorrected. The brain images are in radiological orientation.*

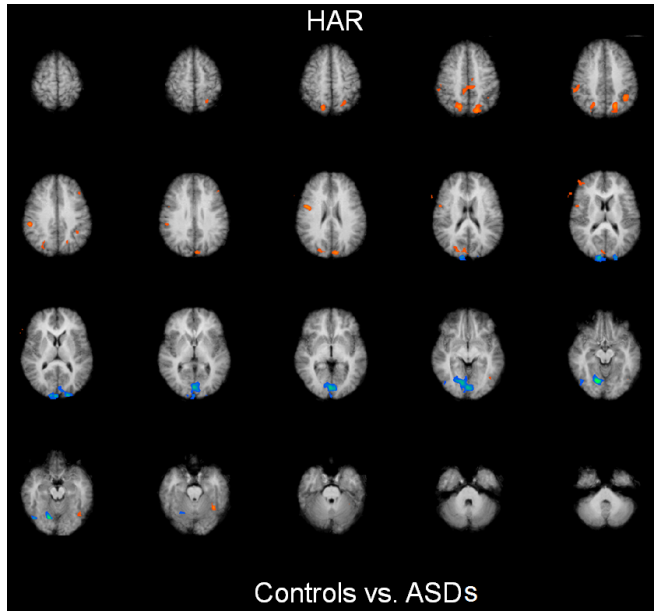

Figure 4.7: *Differential activation in response to the three stimuli (H, A , R) in controls vs. the same stimuli in ASDs. Areas in red activate more in controls than in ASDs, vice versa for the areas in blue. All results are $p < 0.001$ uncorrected. The brain images are in radiological orientation.*

similar one to the other.

Also in this case a comparison between the two groups was performed. As Figure 4.9 shows, there are very few areas in which the response of the two groups is different that are the blue regions in which the response in ASDs is higher with respect to controls while there are no areas in which the response is increased in controls.

In order to understand if there was some difference in the processing of human, android and robotic faces both in controls and in the ASD subject, patterns of activation across the three conditions were analyzed. The most interesting result was obtained in the comparison humans vs. androids. This contrast in the control group enhanced the activation of the precentral area as it can be observed in Figure 4.10. Regions Of Interests (ROIs) with a significant level of activation in the contrast human vs. android faces, are marked in Figure 4.10 and selected for a ROI analysis. The selected ROIs are indicated with 1, 2 and 3 numbers: ROIs 1 and 2 are part of the dorsolateral prefrontal circuit (they lay approximately on the right and left medial frontal gyrus respectively) while ROI 3 corresponds to the left precentral gyrus.

For each of the three ROIs selected, the time course of the BOLD signal in response to human, android and robotic faces was investigated. Results are reported in Figure 4.11. From the observation of the time courses it can be noticed that in each ROI the BOLD signal in response to human faces is higher with respect to the BOLD signals in response to the other two kind of stimuli.

The activation in response to humans in controls in comparison to the activation in response to humans in ASDs was also investigated. This contrast activated the right medial frontal gyrus in controls.

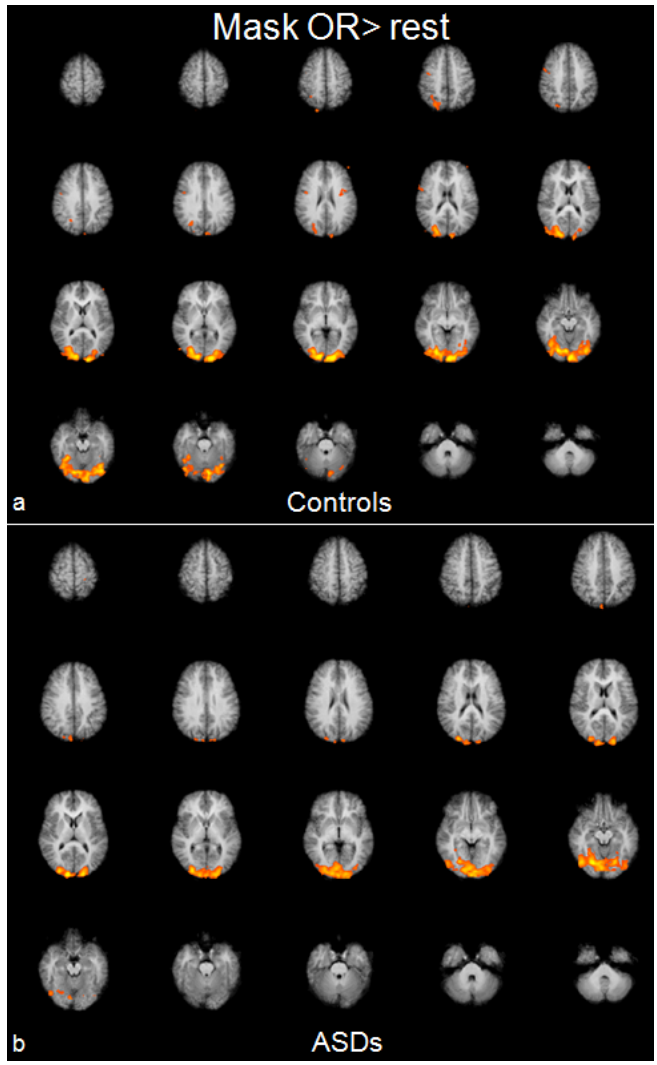

Figure 4.8: *Activation in response to the two stimuli (O, R) vs. the rest condition in controls (a) and in ASDs (b). All results are $p < 0.001$ uncorrected. The brain images are in radiological orientation.*

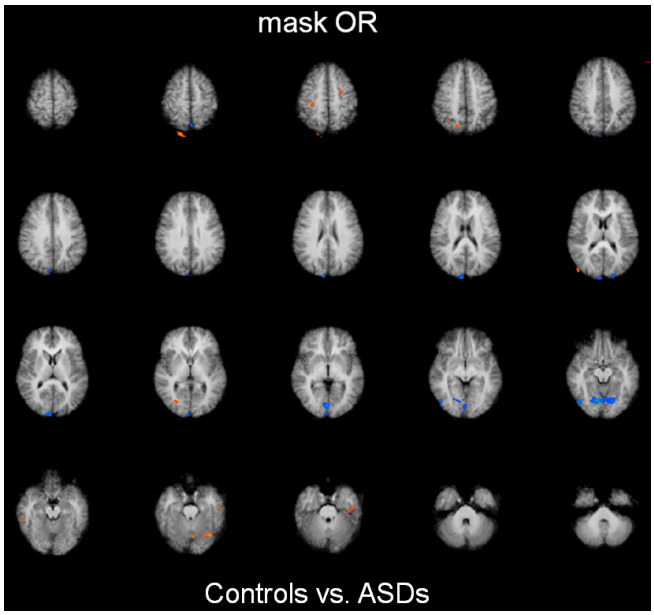

Figure 4.9: *Differential activation in response to the two stimuli (O, R) in controls vs. the same stimuli in ASDs. Areas in red activate more in controls than in ASDs, vice versa for the areas in blue. All results are p < 0.001 uncorrected. The brain images are in radiological orientation.*

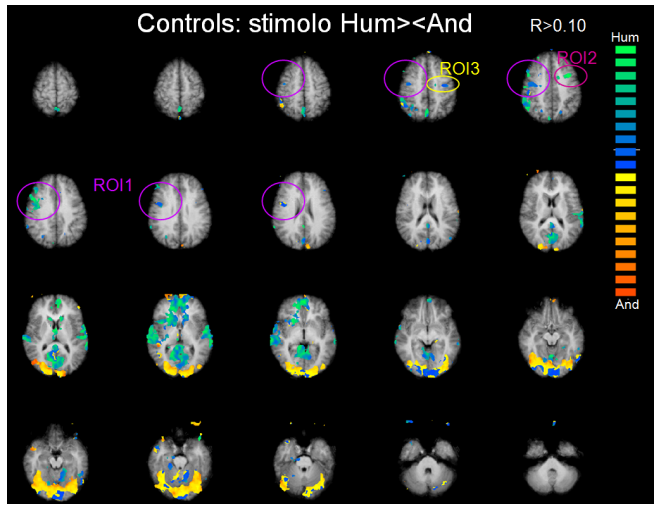

Figure 4.10: *Brain activation in response to the contrast humans vs. androids in control group. Areas in blue/green activate more in response to human faces while yellow/orange areas activate more in response to androids. ROIs in with the response to human faces is higher are marked. The brain images are in radiological orientation.*

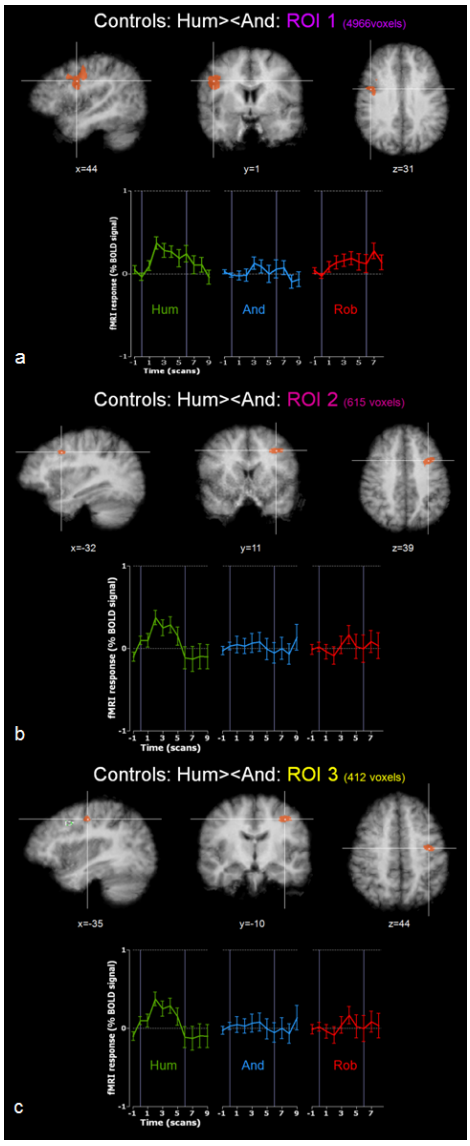

Figure 4.11: *a) Activation of ROI1 (a), ROI2 (b) and ROI3 (c) and relative BOLD signal time courses in response to human, android and robotic faces in controls. The brain images are in radiological orientation.*

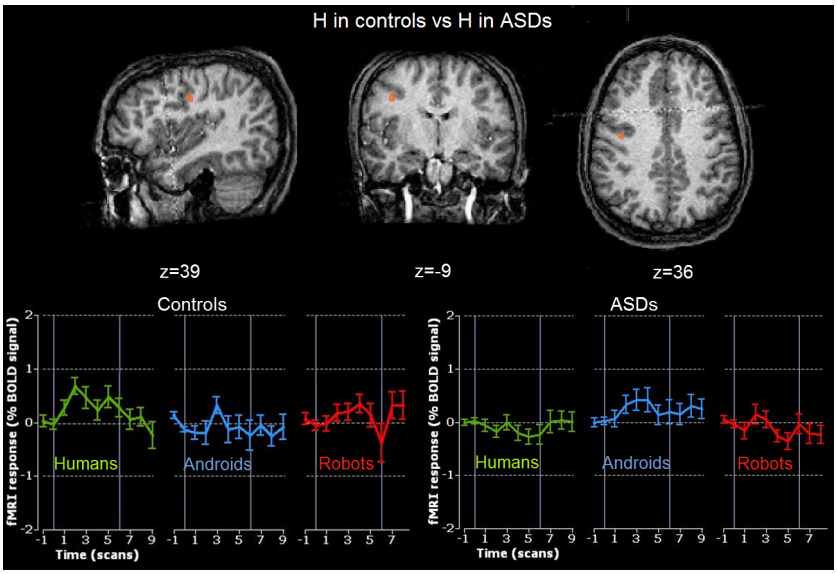

Figure 4.12: *Activation of the right medial frontal gyrus in response to the contrast humans in controls vs. humans in ASDs and relative BOLD signal time courses in response to human, android and robotic faces in controls and in ASDs. The brain images are in radiological orientation.*

The time course of the BOLD signal in response to human, android and robotic faces in both the two groups was analyzed. Results are shown in Figure 4.12. As it can be noticed in the figure in controls the BOLD signal was higher response to human faces with respect to the other two kinds of stimuli while in ASD group the BOLD signal was higher in response to android faces. The response to robotic faces was not significantly different between the two groups.

4.5 Discussion and Conclusion

In this study a novel protocol for the analysis of the response to human, android and robotic faces in ASDs and controls was developed. Despite the fact that this study is preliminary and the number of subjects is quite low, with an imbalance between the two groups, some important observations can be made.

First of all the task developed in this study was able to yield activations located in the areas of face-processing network in the control group, in agreement with other studies. This network is constituted by the fusiform face area (FFA), inferior occipital gyrus (IOG), gaze perception, superior temporal sulcus (STS) precentral gyrus (PG) and inferior frontal cortex (IFC).

Looking at the activation in response to the task presented in this study in ASDs it was possible to see that although the activation of the global network was similar to the one of controls, some differences were present. First of all in controls there was an activation of the frontal areas, especially in the right hemisphere, that was absent in ASDs, then in ASDs there was a reduced activation of ventral areas with respect to controls. However, the comparison between the response of the two groups revealed an increase of activation in ASDs in occipital areas.

The frontal areas of the right hemisphere are regions of the brain involved in planning, and spatial organization while the occipital areas are visual areas. A lack of activation in the frontal areas and an increased activation of the occipital areas in ASDs could be explained with the fact that ASD subjects are more focus on watching at the pictures than in understanding their content and also that they have

a reduced ability in integrating information.
The analysis of the BOLD signal within the frontal areas in controls revealed a higher response to human faces than the other three kind of stimuli. This result suggests that frontal areas are specific for human face processing recognition. In ASDs, in which frontal areas do not activate, there is in fact a deficit in the processing of human faces.
The most important novelty of this study was the investigation of the response in ASDs and controls not only to human faces but also to android ad robotic faces. While in controls the analysis of the response to the different kind of stimuli revealed a higher activation in response to humans with respect to the other stimuli, the same analysis showed that in the same areas that in controls activates for humans, in ASDs there was an increase in the response to android faces.
The response to robotic faces was similar to both the two groups. Moreover looking at the response to the robot-object mask it was possible to notice that neither of the two stimuli activate the frontal areas in controls or in ASDs. This means that both controls and ASDs process robotic faces similar to objects so they don't activate face processing areas.
From these preliminary results we can suppose that while ASD subjects have a reduced brain activation during processing of human faces, as reported in the literature, they seem to be more interested in looking at android or robotic faces. In particular while robotic faces elicited a response that is similar to objects, the response to android faces was similar to the response that controls had for human faces.

If this finding is confirmed in a larger sample of patients, it could have a great relevance in the application of androids as therapeutic and rehabilitative strategy directed towards the improvement of social abilities in ASDs. The interaction with the androids could activate areas of the brain that are important for social interaction and integration of information that usually do not activate in ASDs in the interaction with humans.

Chapter 5

Acquisition of behavioral and physiological signals through the FACE-T platform

5.1 Introduction

In recent years, robots have been proposed for the treatment and rehabilitation of people with cognitive disorders. Recent research has shown that certain subjects with cognitive deficits perceive and treat robots not as machines, but as their artificial partners [128, 129]. Based on these observations several robotic artifacts have been used to engage proactive interactive responses in children with Autism Spectrum Disorders (ASDs). A review of the robotic tools for autistic children was presented in Chapter 1 (1.4.4.3).
Human-like robots which emotional expressions, empathy and non-verbal communication have also been proposed for autism therapy [295]. They can be thought of as a sort of robot based on affective computing.
During the course of this thesis a life like android called FACE (Fa-

cial Android for Conveying Emotions), developed at the Interdepartmental Research Center "E.Piaggio", was employed to investigate its capability in elicit physiological and behavioral response. The importance of these experiments in the context of these thesis is the acquisition of behavioral and physiological parameters in an objective way that can be linked to brain structural and functional abnormalities in ASDs.

The FACE robot is capable, in its present embodiment, of mimicking a limited set of facial expressions, which are more easily accepted by autistic patients because of their simple and stereotypical nature.

FACE is used in a structured therapeutic environment in which the subject's behavior and responses are monitored using a multiplicity of sensors and then processed and fed back to the android to modulate and modify its expressions. The integrated sensing, monitoring, processing and emotionally responsive android-based therapeutic platform is termed FACE-T (FACE Therapy).

Physiological signals (electrocardiography (ECG), breath and electrodermal activity (EDA)) and eye gaze are acquired using a comfortable, unobtrusive sensorized shirt and a cap containing integrated cameras and mini gyroscopes.

Initial sessions confirmed the hypothesis that FACE can increase their emotional responsiveness in individual with ASDs. A further finding was that autistic children rarely showed fear of the robot, while control subjects were uncomfortable with some of the programmed expressions manifested by FACE [296]. Furthermore post-processing of acquired physiological data (heart rate) shows that they are correlated with the emotional participation of the patient and his/her interaction with FACE [297].

The acquisition of these parameters during the interaction with FACE allows to infer some information on emotional state of the child during specific tasks that are known to be compromised in ASDs like face processing, imitation and social interaction. Emotions are closely related to brain activity and so to its structure so that an anatomical abnormality in the brain reflects in dysfunction in the expression of emotions.

The Polyvagal Theory [20] links the evolution of the autonomic nervous system to affective experience, emotional expression, facial gestures, vocal communication and contingent social behavior. This theory provides a plausible explanation of several social, emotional and communication behaviors and disorders like ASDs.

According to this theory the mechanism of interaction between behavior and neural structures is explained by the Social Engagement System (Figure 5.1). This system has a control component in the cortex that regulates brainstem nuclei to control somatomotor components (e.g. looking and emotional expression) and visceromotor component. The vagus represents an integrated neural system that communicates in a bidirectional manner between the viscera and the brain.

Difficulties behaviors associated with the Social Engagement System (e.g., gaze, extraction of human voice, facial expression, head gesture and prosody) are common features of individuals with ASDs indicating an impairment of this system.

In this study FACE-T was first tested on healthy volunteers and then on ASD children and typical developing. Gaze and all physiological data have been acquired although in this study only ECG signals have been analyzed.

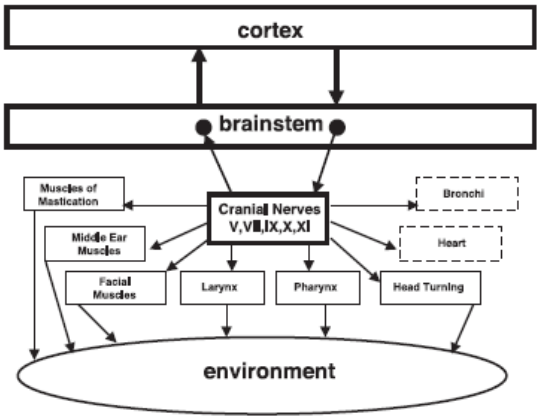

Figure 5.1: *The Social Engagement System consisting of a somatomotor component (solid blocks) and a visceromotor component (dashed blocks) [20].*

In fact heart activity is regulated by the vagal activity and so it is an indicator of the functionality of the Social Engagement System and of the neural structures that control it. Modulation of the vagal brake provides a neural mechanism to rapidly change visceral state by slowing (i.e., increasing vagal influences) or speeding (i.e., reducing vagal influences) heart rate. Functionally, the vagal brake, by modulating visceral state, enables the individual to rapidly engage and disengage with objects and other individuals and to promote self-soothing behaviors and calm behavioral states.

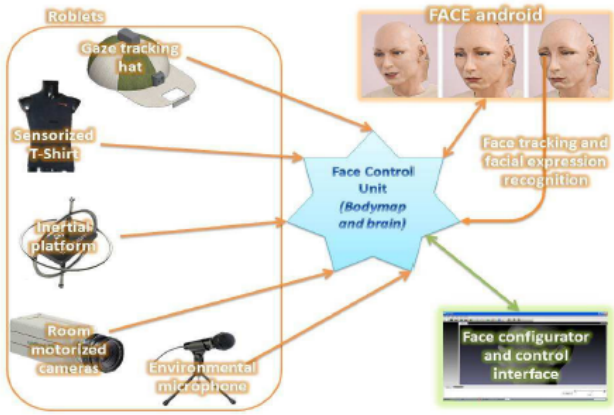

Figure 5.2: *Connection scheme of the FACE-T platform. The control unit is connected to the different roblets belonging to the platform and to the configurator roblet that allows therapist control and supervision.*

5.2 Materials and methods

The FACE-T set-up, in which the android guided therapy takes place, includes a room equipped with motorized cameras, directional microphones, and other acquisition systems as shown in Figure 5.2.

5.2.1 Face Robot Hardware

FACE is an android used as emotion conveying system. It consists of a female face made of FlubberTM, a skin-like silicone based rubber patented by HansonRobotics (Figure 5.3 a). Android faces produced by D. Hanson have been used in other robots, with their own software architectures, like the Ibn Sina Robot [298], the Javier Movellan's robot at UCSD [299],and the INDIGO project [300]. FACE is actu-

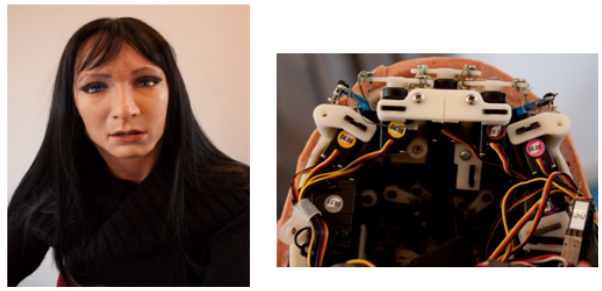

Figure 5.3: *a) The android FACE, b)Servo motors disposition inside FACE head.*

ated by 32 servo motors that move the artificial skin through cables inserted in the face according to the human anatomy. The motor cables act as tendons moving FACE skin and allowing human facial expressions to be re-created. FACE servo motors are all integrated in the android skull except for the 5 neck servos that allow pitch, roll and yaw movement of the head (Figure 5.3b).
The android has a CCD camera in the right eye used for face tracking of the subject through an OpenCV based face tracking algorithm [301].

5.2.2 Face Control

The entire FACE-T system behavior is controlled by custom made software responsible for monitoring the environment, the subject, and the robot. A number of subsystems control the different features of the system with the goal of combining reactive and deliberate behaviors. For example, the android should blink its eyes while performing other tasks. System modules are integrated using

a framework for programming robots called Robotics4.NET [302] whose purpose is to provide a robust communication infrastructure among software modules, called roblets, implementing autonomous behaviors. The underlying metaphor is the human nervous system: XML messages, corresponding to neural communications, are sent and received by roblets to and from the body map, where the state of the body is collected and used as a global perception by the program coordinating all the activities, a sort of brain.
The environment parameters are perceived through a number of different sensors (Figure 5.2), in part mounted on the android, in part on the surrounding environment. Nevertheless, from the software standpoint these are part of a single body even if they are connected to different computing systems. Roblets correspond to body organs, and embed autonomous reactive behaviors, possibly combining perception and actuation. This architecture guarantees signal synchronization.
A relevant aspect of the control software has been the development of a framework for controlling the 32 servo motors actuating FACE, responsible for defining facial expressions of the android (Figure 5.4. It is difficult to capture emotions in single expressions and combine them in an appropriate way. The subsystem was organized in layers implementing high level operations reduced into basic commands. At the very bottom motor values are normalized in the range 0-1 so that facial expressions can be reliably stored over time.

Motor configurations can be saved into XML files and later reloaded. In fact these files represent static facial expressions. Face movements are achieved by means of interpolation of known positions. This is a standard approach in the context of 3D animation that has

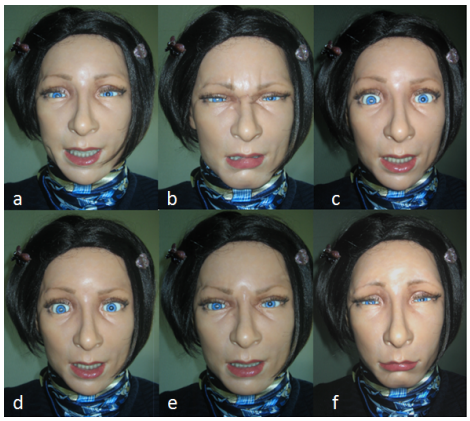

Figure 5.4: *The six basic expressions of FACE: happiness (a), digust (b), amazement (c), fear (d), anger (e) and sadness (f).*

greatly influenced the design of the control system, and it enables forward and backward compatibility with well-known graphic programs. This first abstraction layer, designed to decouple software from specific hardware, is used by another layer whose purpose is to receive requests for facial expression adaptation and combine them appropriately.

The control software is inherently concurrent and different behavioral modules are expected to send requests for facial expression adaptation without having to care for possible conflicts. This is the most important abstraction provided by the software layer since it is responsible for mixing reflexes such as eye blinking or head turning to follow the patient with more deliberate actions. Each created expression request has an associated priority, which is used to blend conflicting commands, and when it should be performed. The blending and animation process is necessary to resolve conflicting

Figure 5.5: *Sensorized shirt developed in collaboration with Smartex Srl, Prato, Italy.*

expressions that may be requested frequently.

5.2.3 Sensorized shirt

The sensorized shirt is based on e-textiles and was developed by Smartex Srl, Prato, Italy (Figure 5.5).

It gathers, computes and transmits ECG, skin conductance, skin temperature and respiratory rate, all of which are known to be bodily correlates of emotional states [122]. The shirt integrates textile sensors within a garment together with on-body signal conditioning and pre-elaboration, as well as the management of the energy consumption and the wireless communication systems.
Three key points make up the sensing shirt; these are the fabric electrodes based on interconnecting conductive fibers, a piezoresistive network and a wearable wireless communication unit [21] (Figure 5.6a).
Electrodes and connections are interwoven within the textile by means of natural and synthetic conductive yarns (Figure 5.6b). The

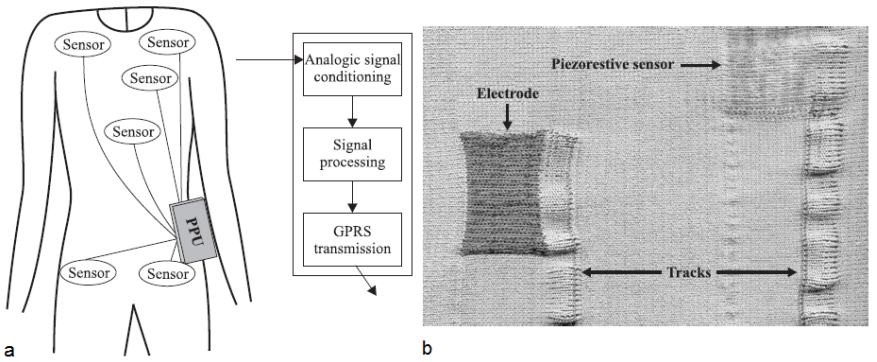

Figure 5.6: *a) Overall shirt function b) Part of the shirt interface [21].*

shirt allows physiological signal acquisition with a minimal subject discomfort and total unobtrusiveness which are of paramount importance when dealing with autistic children.

5.2.4 Eye-tracking

There is a growing body of research that makes use of eye-tracking technology to study attention disorders and visual processing in ASD. Atypical gaze patterns were already described for individuals with ASDs when presented with social scenes and faces [303, 304]. For instance, Klin et al. [305, 306] pointed out that, in social environments, individuals with autism show reduced eye-region fixation time in favor of an increased focus on mouths and objects.
Reduced attention to the face but not to the actions of a demonstrator to be imitated has been found by Vivanti et al. [303] in a group of children with autism. Gaze tracking is thus a critical and useful indicator of a subjects interest and emotional involvement dur-

ing a therapeutic session with FACE. To be acceptable to children, particularly those with social difficulties, the tracking technology should be unobtrusively and ecologically used in social experimental paradigms. To this end, a gaze tracking cap was developed, HATCAM which is a wearable device that was specifically designed to investigate early attention disorders in infants.

The HATCAM device (Figure 5.7) was designed to be wearable, comfortable and allow eye and head tracking. Basically HATCAM consists of a child-sized cap with a brim, on which a small rectangular mirror is fixed directed towards the wearer's eyes. An opening in the brim directs the reflection from the mirror to small video camera attached to the top of the cap. Thus the direction of the pupils with respect to the subjects head is constantly monitored and recorded. At the same time a 3 axis inertial platform maintains information on the orientation of the head, and together the 2 sets of data provide information on eye gaze within the framework of the therapeutic setting through a purposely developed algorithm [307].

Although more sophisticated instruments may be used to obtain accurate and repeatable data on pupillary motion, most of them require long lasting calibration procedures was developed which may completely spoil the child's collaboration. In accordance with this limitation a fast and easy calibration procedure which is intended to be the best trade off between accuracy and feasibility. In particular, the algorithm, use images of both subject eyes that allow calibrating the system using few calibration points than classic single eye algorithms [308, 309].

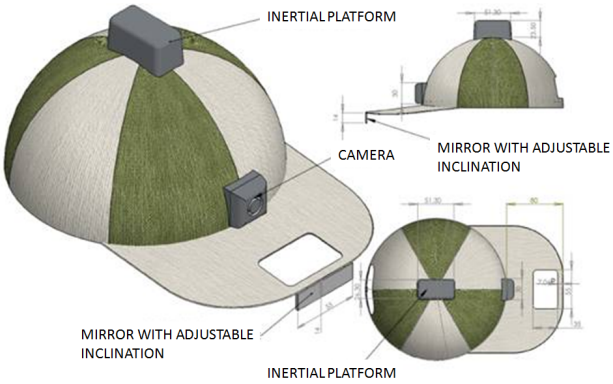

Figure 5.7: *HATCAM device.*

5.2.5 Data acquisition and analysis

5.2.5.1 Subjects

Preliminary data were acquired on a sample of 4 ASD subjects (all males) and 3 controls (2 males and 1 females). The age range of autistic group was 16-20 years old while the age range of controls was 6-18. One of the ASD children was diagnosed as Asperger while the others as high-functioning autistics. The diagnosis was formulated through gold standard instruments, such as ADOS-G and ADI-R or WISC-R and Leiter-R for intellectual functioning. All the ASD subjects were also evaluated by CARS (Childhood Autistic Rating Scale).

Figure 5.8: *A scene of the session of interaction with FACE.*

5.2.5.2 Session of interaction with FACE

The interaction with FACE is based on social-play and allows the child to familiarize with the robot (Figure 5.8). The child is not required to perform any specific task but play. The focus of the session is imitation, alternation of facial expressions and emotional display and recognition.
This experimental protocol allows to observe the spontaneous behavior of the child in response to the different configuration of the robot: when it is still (still face), when it orients the gaze and when it expresses some emotion. The session is divided in five different phases:

1. **Familiarization (A):** spontaneous interrogation without presses. The therapist remains in the background while FACE stays still. While the subject is involved in the observation of FACE

the therapist, positioned behind the subject, performs the name calling test.

2. **Interrogation and exploration (B):** the subject is requested to give a name to FACE which is then used in the entire session. During this phase FACE exhibits some facial expressions: sadness, fear, anger, disgust, amazement and happiness separated by neutral expression. For each of the mentioned expression the therapist asks the subject to assign it a label. Particular attention is given to the answers of the subject (verbal communication) and to spontaneous imitation. Then FACE moves the segments of the face one by one: the eyes (opening and closing), the mouth (movement towards the right or left direction) and the head (tilt and "yes" or "no" gesture).

3. **Conversation with the therapist on FACE (C):** the therapist asks the subject its impressions on FACE for example which are FACE's physical and relational characteristics and which could be its function and utility.

4. **Name calling (C1):** FACE calls the subject with its own name.

5. **Imitation at the request of the therapist (D):** the subject is requested to do "what FACE does". The ability of imitation of the subject once encouraged by the therapist is evaluated. Children with ASDs generally started spontaneous conversations with FACE. The therapist leave the subject free during this conversation.

6. **Shared attention (E):** during this phase the ability of the subject to follow the gaze of FACE is evaluated. In particular the android observes a specific object in the room and if the subject is capable of shared attention, he watches the same object.

The total duration of the session is about 30 minutes. After that the therapist watches the videos acquired during the session and performs a CARS evaluation.

5.2.5.3 Physiological data and gaze acquisition

Before the beginning of the therapeutic session, in a different room, the subject was asked to wear the sensorized shirt and the HATCAM 5.9.
HATCAM acquisition started with the beginning of the session and allowed following the gaze of the child during all the phases of interaction with FACE.
The sensorized shirt acquired ECG, skin conductance, skin temperature and respiratory rate. The acquisition of these parameters was synchronized with the beginning of the session with FACE. The signals acquired were visualized and monitored during the session from a separate room.

In this study the ECG was analyzed. The ECG consists of the electrical impulse generated by the heart. Each heartbeat generates a "complex" consisting of 3 parts (Figure 5.10):

- The **"P" wave** represents the electrical impulse traveling across the atria of the heart. Abnormalities of the P wave, therefore, reflect abnormalities of the right and/or left atrium.

Figure 5.9: *A subject wearing the sensorized shirt and the eye-tracking system HATCAM.*

- The **"QRS" complex** represents the electrical impulse as it travels across the ventricles. Abnormalities of the QRS are often seen when there has been prior damage to the ventricular muscle, such as in a prior myocardial infarction.

- **The "T" wave** represents the recovery period of the ventricular muscle after it has been stimulated.

The portion of the ECG between the QRS complex and the T wave is called the ST segment. Abnormalities of the ST segment and the T waves are often seen when the heart muscle is ischemic - that is, when it is not getting enough oxygen, usually because there is a blockage in a coronary artery.
The R peak corresponds to the systole and is the principal beat of the heart. The distance between two consecutive R peaks (R-R interval) is not constant. In order to quantify the variability in the

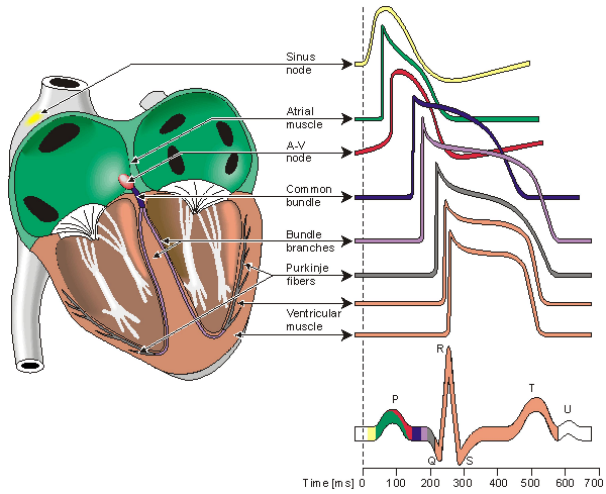

Figure 5.10: *Electrophysiology of the heart (redrawn from [22]). The different waveforms for each of the specialized cells found in the heart are shown.*

R-R series, several indices have been proposed.
Heart rate (HR) is determined by the number of heartbeats per unit of time, typically expressed as beats per minute (BPM), it can vary with the body's need for oxygen changes, such as during exercise or sleep. The measurement of heart rate is used by medical professionals to assist in the diagnosis and tracking of medical conditions.
Heart rate variability (HRV) measures the variability in the distance between one beat of the heart and the next. The interbeat interval (IBI) is the time between one R-wave (or heart beat) and the next, in milliseconds. The IBI is highly variable within any given time period. Multiple biological rhythms overlay one another to produce the resultant pattern of variability. In particular it is governed by the action of the body's autonomic nervous system (ANS) [310]. The continuous modulation of the sympathetic and parasympathetic innervations results in variations in heart rate. The most conspicuous periodic component of HRV is the so called respiratory sinus arrhythmia (RSA) which is considered to range from 0.15 to 0.4 Hz. In addition to the physiological influence of breathing on HRV, this high frequency (HF) component is generally believed to be of parasympathetic origin. Another widely studied component of HRV is the low frequency (LF) component usually ranging from 0.04 to 0.15 Hz including the component referred to as the 10-second rhythm or the Mayer wave. The rhythms within the LF band have been thought to be of both sympathetic and parasympathetic origin even though some researchers have suggested them to be mainly of sympathetic origin. The ratio LF/HF indicates the balance between sympathetic and parasympathetic systems [311]. The fluctuations below 0.04 Hz, on the other hand, have not been studied as much as the higher

frequencies. These frequencies are commonly divided into very low frequency (VLF, 0.003-0.04 Hz) and ultra low frequency (ULF, 0-0.003 Hz) bands, but in case of short-term recordings the ULF band is generally omitted. These lowest frequency rhythms are characteristic for HRV signals and have been related to, e.g., humoral factors such as the thermoregulatory processes and renin-angiotensin system.
Interbeat interval variations, or heart rate variability, have relevance for physical, emotional, and mental function. The variability in heart rate is an adaptive quality in a healthy body.

5.2.5.4 ECG data analysis

Time-domain analysis ECG data were synchronized with the videos recorded during the session with FACE and subdivided in different windows according to the different phases of the session. As the phase "name calling" was very short it was included in the previous phase "conversation with the therapist on FACE" so five phases were considered.
The ECG signals were then analyzed by Matlab algorithms. A preprocessing step allowed removal of artifacts and interferences from the ECG signal. First a pass-band filter between 2 and 50 Hz was applied. The high-pass cut-off frequency (2 Hz) allowed to remove the low frequency effects due to the patient respiration while the low-pass cut-off frequency (50 hz) allowed to remove the effect of muscle contractions that cause the generation of high frequency artefactual potentials and overlaps the frequency content of the QRS complex. Then a median filter was applied in order to remove salt and pepper

noise. The main idea of the median filter is to run through the signal entry by entry, replacing each entry with the median of neighboring entries. The median is the middle value after all the entries in the window are sorted numerically.
Finally the baseline wandering was removed using an wavelet approach based on the MODWT (Maximal Overlap Discrete Wavelet Transform) method [312].
The following step was the detection of R peaks within the ECG signals. This was done by using the "Peak detection" Matlab algorithm that finds local maxima of the signals. The values of the peaks were used to compute the tachogram that is the trend of RR intervals vs. the number of RR intervals present in the signal. From the tachogram several measures were computed:

- Maximum (RRmax), minimum (RRmin) and standard deviation (RRstd) of RR intervals;
- Time instants at which RRmax, RRmin and RRstd occurred;
- HR computed as the number of heartbeats per minute:

$$HR = \frac{60(sec)}{RR}$$

  where RR is the number of RR intervals in one minute.

Frequency-domain analysis The frequency analysis was realized using a dedicated Matlab tool called Kubios HRV. Kubios HRV is an advanced tool for studying the variability of heart beat intervals. Among the several features of this tool, the frequency-domain analysis was used in this work.

In the frequency-domain methods, a power spectrum density (PSD) estimate is calculated for the RR interval series. The regular PSD estimators implicitly assume equidistant sampling and, thus, the RR interval series is converted to equidistantly sampled series by interpolation methods prior to PSD estimation. In the software a cubic spline interpolation method is used. In HRV analysis, the PSD estimation is generally carried out using either FFT based methods or parametric autoregressive (AR) modeling based methods [313]. The advantage of FFT based methods is the simplicity of implementation, while the AR spectrum yields improved resolution especially for short samples. Another property of AR spectrum that has made it popular in HRV analysis is that it can be factorized into separate spectral components. The disadvantages of the AR spectrum are the complexity of model order selection and the contingency of negative components in the spectral factorization. Nevertheless, it may be advantageous to calculate the spectrum with both methods to have comparable results. In this software, the HRV spectrum is calculated with the FFT based Welchs periodogram method and with the AR method. Spectrum factorization in AR method is optional. In the Welchs periodogram method the HRV sample is divided into overlapping segments. The spectrum is then obtained by averaging the spectra of these segments. This method decreases the variance of the FFT spectrum.

The frequency-domain measures extracted from the PSD estimate for each frequency band include absolute and relative powers of VLF, LF, and HF bands, LF and HF band powers in normalized units, the LF/HF power ratio, and peak frequencies for each band.

Statistical analysis The parameters computed with the time and frequency-domain methods were statistically analyzed. In particular the time-domain measures considered were HR, RRmax, RRmin and RRstd while the frequency-domain parameters compared were VLF, HF, LF and LF/HF.
These parameters were analyzed for group differences (ASDs and controls) using Student's t-test for each autonomic index. Probability values (p) less than 0.05 were regarded as statistically significant.

5.3 Results

5.4 Behavioral performance

The evaluation of the treatment was performed by analyzing the recorded sessions through the CARS evaluation using 8 relevant items from the scale. The therapeutic trails are still in preliminary phases. Nevertheless, all the 4 ASD subjects as well as controls showed no fear in the presence of FACE, and all autistic subjects showed improvement in CARS scores, particularly as regards imitation, communication and emotional response. In particular, it was observed that the CARS score decreased or remained the same for all items after the therapy session. All the subjects demonstrated a decrease in the score of emotional response in the CARS scale between 1 and 0.5 points, while imitation improved in 3 out of 4 children, so implying a marked improvement in these areas after interacting with FACE.
With respect to controls ASD subjects are more interested in FACE:

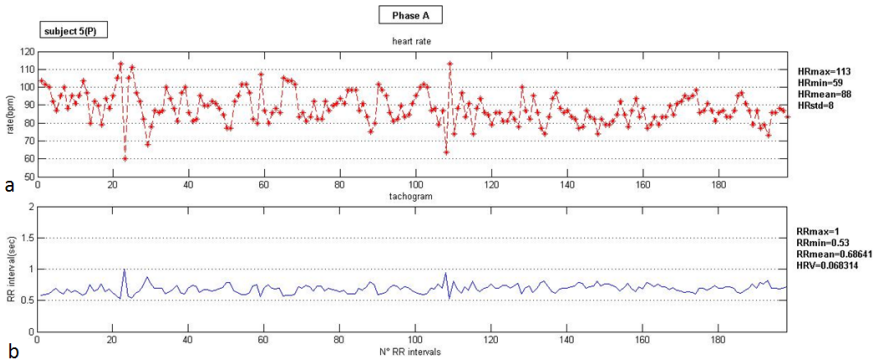

Figure 5.11: *Heart rate (a) and tachogram (b) of one ASD subjects during the phase of familiarization with FACE. For each plot minimum, maximum, medium values and standards deviation are reported.*

they fix their eyes on the android often, they converse with it and they imitate its expression both spontaneously and under the request of the therapist.

5.5 Autonomic response

With the time-domain analysis the HR and tachogram for each subject and each phase of the session with FACE were obtained. In Figure 5.11 the HR and HRV obtained from the ECG signal of one ASD subject during the phase of familiarization with FACE is reported.

The frequency-domain analysis allows the power spectrum density for each subject and each phase of interaction with FACE to be computed. In Figure 5.12 the spectrum obtained for the same subject and the same phase as in Figure 5.11 is reported. The re-

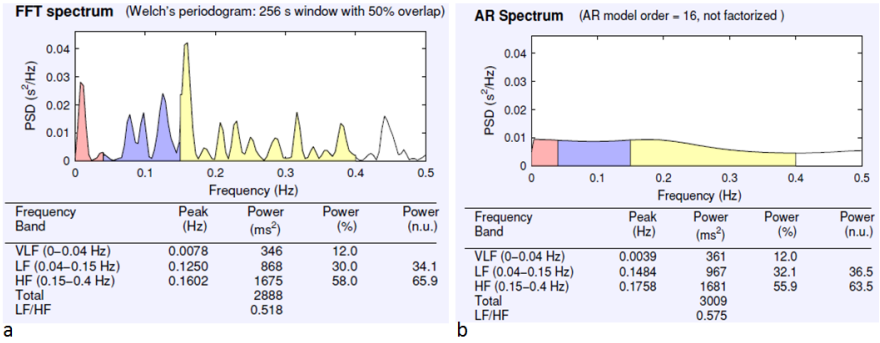

Figure 5.12: *Power spectrum density of one ASD subjects during the phase of familiarization with FACE obtained with the FFT method (a) and with the AR method (b). In each spectrum the lobes refererring to the different frequency components are shown: the pink lobe corresponds to the VLF component, the cyan lobe to the LF component and the yellow one to the HF component. In the tables under the spectra the values of the computed parameters are reported.*

sults for both spectra are displayed in tables below the corresponding spectrum axes.

The t-test was performed on the indices extracted with time and frequency domain analysis. The mean values of the parameters were computed for each group and compared. The mean values were represented by means of histograms where the values for each phase are reported.
The t-test showed a statistically significant differences in the time-domain parameters RRmean (Figure 5.13) (p=0.007) and HRmean (Figure 5.14) (p=0.004). In particular the RRmean values were increased in ASDs and so the HRmean values were reduced.

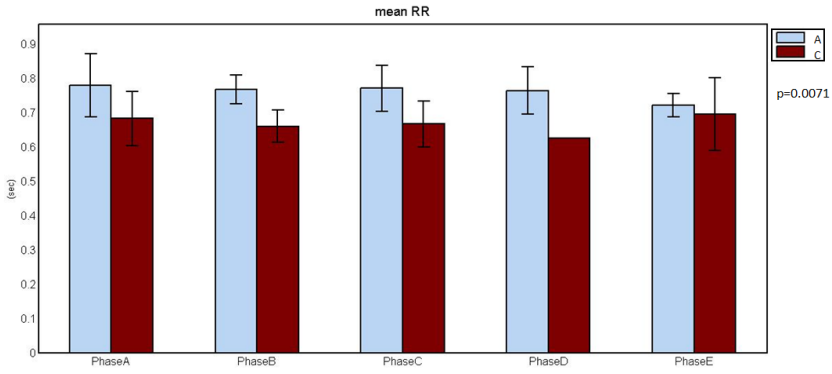

Figure 5.13: *Histogram of the HRmean values for ASD subjects (cyan) and controls (red) for each phase of the interaction with FACE.*

The t-test on HRV showed no statistically significant results (p=0.1).

Results of the frequency-domain parameters statistical analysis are reported only for the AR method as it has higher resolution with respect to the FFT method.

The statistical analysis of frequency-domain parameters revealed differences close to significance in VLF (Figure 5.15) (p=0.07) and LF (Figure 5.16) (p=0.07). In both cases values were increased in ASD subjects with respect to controls.

No significant differences were found in HF (p=0.4). However it was interesting to notice that in the histogram in Figure 5.17 the highest HF value, that means the highest parasympathetic activity, corresponded to the phase of conversation with FACE.

The comparison between the values of LF/HF of the two groups was not statistically significant (p=0.1), but the histogram in Figure 5.18 shows a trend of higher LF values in ASD subjects as the ratio is for every phase much higher than one.

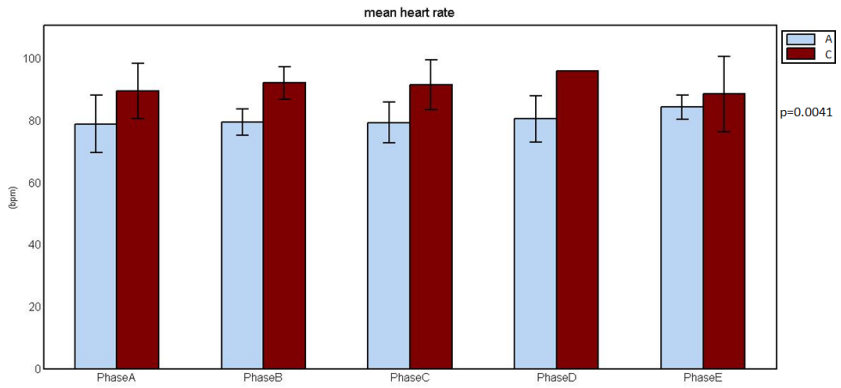

Figure 5.14: *Histogram of the HRmean values for ASD subjects (cyan) and controls (red) for each phase of the interaction with FACE.*

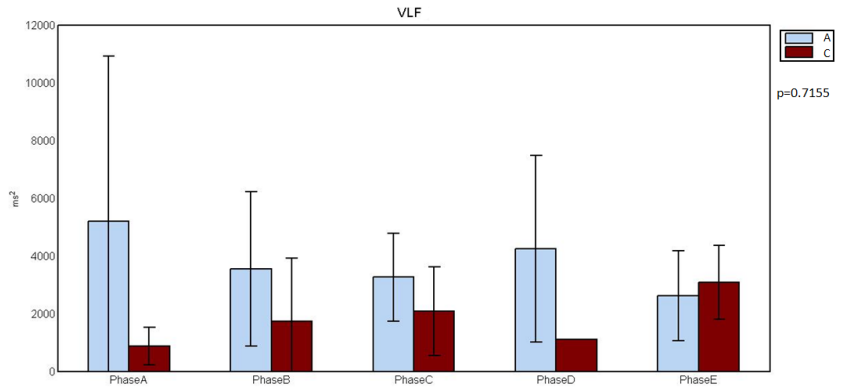

Figure 5.15: *Histogram of the VLF values for ASD subjects (cyan) and controls (red) for each phase of the interaction with FACE.*

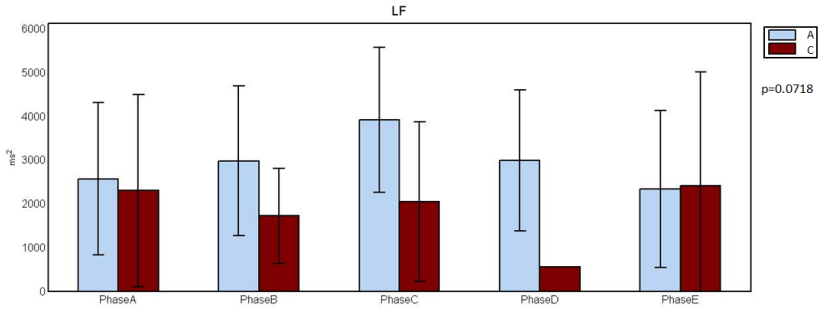

Figure 5.16: *Histogram of the LF values for ASD subjects (cyan) and controls (red) for each phase of the interaction with FACE.*

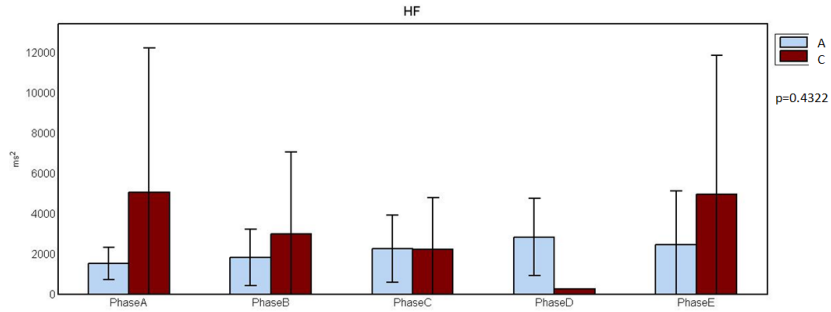

Figure 5.17: *Histogram of the HF values for ASD subjects (cyan) and controls (red) for each phase of the interaction with FACE.*

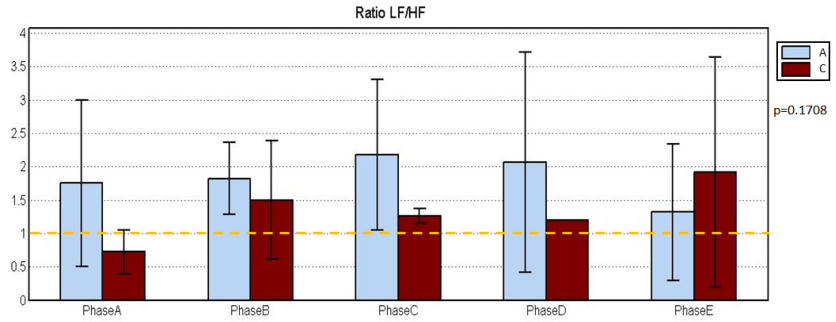

Figure 5.18: *Histogram of the LF/HF values for ASD subjects (cyan) and controls (red) for each phase of the interaction with FACE. The dotted yellow line correspond to LF/HF=1.*

5.6 Discussion and conclusions

In this chapter the platform FACE-T was described and preliminary results obtained by the application of this tool in the interaction with ASD subjects and controls, were reported. The FACE-T platform is made up of the android FACE, and a therapeutic setup comprising sensorized shirt, video cameras and eye tracking hat.
The interactive FACE-T scenario provides a novel semi-naturalistic tool that is able to engage in emotive exchange with subjects with ASD. This could be conveniently used to support cognitive behavioral therapy in order to enhance comprehension and expression of imitation, shared attention, and facial mimicry in people with ASDs. A series of trials on subjects affected by ASDs and controls were carried out, assessing both spontaneous behavior of the participants and their reactions to therapist presses in correlation with the time course of the physiological and behavioral data, as well as the focusing of at-

tention towards FACE's eye movements and the spontaneous ability to imitate gesture and expressions of the android. Overall, subjects demonstrated a score decrease in the areas of social communication, implying a marked improvement in these areas after interacting with FACE.

Moreover ECG signals acquired during the interaction with FACE of both ASD subjects and controls were analyzed. The ECG signal was synchronized to the recording during the sessions so that it was possible to correlate particular phenomena revealed by the signal analysis to specific phases of the session.

A dedicated tool for the extraction and analysis of parameters characterizing ECG was created and applied to the analysis of the signals acquired during the trials. Time-domain and frequency-domain analyses were performed and a statistical analysis was used to compare results obtained for the two groups. HR and HRV were computed and plotted for each subject and each phase, in addiction the minimum, maximum and mean RR interval were calculated. The Kubios tool was then used to obtain power density spectra and to compute the different frequency components.

The temporal analysis of ECG signals revealed a significant increase of RR mean interval and so a decrease in HR mean in ASDs with respect to controls. In the literature the heart rate in autistic children is reported increased with respect to controls [314, 315]. The result found in this study, that is a decrease in heart rate in ASDs children with respect to controls, could be partially due to the effect of age; in fact heart rate is lower in teen-ager than in younger children and the mean age of the ASD group in this study is higher than the mean age of the control group. The heart rate in controls

could be increased also because they are more stressed by the presence of FACE. The heart rate is indeed influenced by the emotional condition and increases with agitation [314].
The frequency analysis showed almost significant differences in VLF and in LF. In both cases values were increased in ASDs with respect to controls. As mentioned in section 5.2.5.3 LF is related mainly to sympathetic activity while VLF is linked to humoral factors. This results means that the sympathetic activity and humoral factors are increased in ASD subjects.
Moreover, although not statistically significant, HF was found decreased in ASDs with respect to controls. As HF is linked to parasympathetic activity it means that this function is reduced in ASD. This result was confirmed by LF/HF which was increased in ASDs.
The result of reduced in parasympathetic activity associated with increased sympathetic tone in autistic children is in agreement with other studies in which cardiac activity in autism was analyzed [314].
An interesting observation was that the higher value of HF, that is the higher parasympathetic activity, was found in the phase of conversation with FACE, Phase D.
This result could mean that the conversation with the android "relaxed" the autistic subject more than the other phases of the sessions where the interaction with the therapist is requested. The increased parasympathetic activity could be also linked to the fact that in this phase children perform a mental task and this kind of activity seems to activate the parasymapthetic system [316].
It is important to underline that the these results are preliminary because the number of subjects submitted to the sessions of interaction with FACE was very low and the two groups were not well-matched

by age. The significance of the results obtained could be improved increasing the number of subjects and mathing the groups of ASDs and controls by age.
The tool developed in this work could be used to analyze signals acquired in the future experimental trials.

Conclusions

The aim of this thesis was the development of novel tools and methodologies for the study of Autism Spectrum Disorders (ASDs).
ASDs are a complex, heterogeneous and still largely unknown group of disorders so that novel instruments for the multimodal analysis of its different aspects are necessary. In the past few years several bioengineering approaches have been adopted for the study of neurological or neuropsychiatric disorders, like ASDs. In this work some of these approaches were selected and applied developing novel and optimized methodologies to improve our knowledge and understanding with respect to the current state of the art.
Researchers agree on the fact that ASDs are a set of genetic disorders characterized by several abnormalities in brain structure and functionality. These abnormalities can be found at global or local levels.
At a microscale level deficits in neuronal morphology and connectivity have been found in a lot of brain areas. The study of ASDs at a local level is very important for obtaining an early diagnosis.
In this work neural growth was followed and quantified to demonstrate how neurodevelopmental alterations in cerebellar circuitry

confer vulnerability to autism, an area of investigation which is still largely unexplored. A non-invasive methodology that allowed the evolution of cerebellar neurons to be followed in-vitro was set up and a software for the extraction of metrical and topological features, called NEMO, was developed. An effective approach based on 3-way PCA was applied for the statistical analysis of dynamic data. The application of these tools to the analysis of Purkinje cells and slices extracted from wild-type mice and animal models of autism revealed that they are powerful tools for the automatic and dynamic characterization of morphology and topology and for the discrimination of neurons cultured in different environments or extracted from different groups of animals.

These studies for the first time allowed a quantification of microstructural properties in ASDs during the evolution of neurons.

Recently, a novel imaging methodology called DTI, allows acquisition of information on the microstructure also in-vivo, in the human brain. In this thesis the DTI technique was used to evaluate microstuctural abnormalities of white matter in ASDs with respect to controls. The target of the analysis were very young children with ASDs in which there is a very little knowledge about white matter properties and integrity due to the very few studies present in the literature.

An optimized methodology for the analysis of diffusion tensor imaging data was set up consisting in a diffusion tensor analysis for the individualization of compromised areas and a tractographic analysis on the tracts that were found particularly altered. The DTI study focused on echolalia which is, to my knowledge, for the first time considered in a DTI study in ASDs. The DTI analysis was also sen-

sitive enough in discriminating between subgroups of subjects with ASDs revealing alteration in the measurements and indices characterizing the tracts analyzed.
To have a complete characterization of ASDs it is important to acquire both structural data of brain and functional properties as well as psychological and physiological parameters of subjects.
In order to establish a link between brain structure and function, an fRMI analysis was therefore performed. In particular face processing, a function always altered in ASDs, was investigated. A novel fMRI task consisting in the presentation not only of human faces, as in the studies already performed by other researchers, but also robotic and android faces was developed. Specific areas of the brain were found hypoactivated in people with ASDs with respect to controls, moreover it was found that while controls respond more to human faces, ASDs are more sensitive to android faces. This is an important result that encourage the use of robotic tools as instruments for ASDs therapy.
In order to characterize behavior and physiology of ASD children an experimental laboratory was set up where physiological signals (ECG, body temperature; etc.) and behavioral performances were recorded during a session where the children were interacting with an android robot called FACE. The integrated sensing, monitoring, processing and emotionally responsive android-based therapeutic platform is termed FACE-T. The FACE-T platform can be used to devise and validate an evaluation and treatment protocol, to individualize physiological, electrophysiological, psychophysiological and behavioral factors related to social reciprocity, to characterize gaze behavior and imitation in socio-emotional interactions and to en-

hance imitation, shared attention and facial mimicry in ASDs. In this work, the platform was used to correlate behavioral with cardiac signals acquired using a sensing T-shirt.
The results obtained showed an improvement of social performance in ASD children and an involvement of these subjects in the interaction with FACE as underlined by ECG data acquired during the session.
In conclusion the quantitative analysis of microstructure both in-vitro and in-vivo have lead to increase of knowledge about autistic brain connectivity, providing objective ways to identify and characterize morphology, topology and connectivity of neurons and white matter.
Thanks to the novel DTI techniques that are currently under development, the worlds of in-vitro observation and of in-vivo imaging are getting closer allowing a verification of characteristics measured in-vitro such as axon diameter and cellular density, through the direct observation of the human brain.
Hopefully, these kind of analyses and results will also enable early identification of ASDs and lead to new cures geared towards rewiring of neural circuitry before establishment of permanent networks.
A further important aspect of this work is the characterization of the functionality of the brain and the acquisition of physiological and behavioral parameters using non-invasive instruments that allow an objective characterization of behavior and physiology. These studies are aimed at yielding new knowledge on endophenotypes and brain-behavior relationships. All the measurements acquired can in fact be correlated with structural abnormalities of the brain in order to understand the anatomical bases of particular deficits in brain

activation, in social interaction problems and in physiological alterations. This kind of characterization opens new opportunities in the field of personalized autism research and treatment. On the basis of all the measures acquired and analyzed, the medic can decide which treatment is the most suitable for each specific child and tailored the therapy consequently.

Bibliography

[1] E. Courchesne. Abnormal early brain development in autism. *Mol Psychiatry*, 7 Suppl 2:S21–S23, 2002.

[2] Eric Courchesne, Ruth Carper, and Natacha Akshoomoff. Evidence of brain overgrowth in the first year of life in autism. *JAMA*, 290(3):337–344, Jul 2003.

[3] G. Allen. Cerebellar contributions to autism spectrum disorders. *Clinical Neuroscience Research*, 6(3-4):195–207, 2006.

[4] Marco Catani, Derek K Jones, Eileen Daly, Nitzia Embiricos, Quinton Deeley, Luca Pugliese, Sarah Curran, Dene Robertson, and Declan G M Murphy. Altered cerebellar feedback projections in asperger syndrome. *Neuroimage*, 41(4):1184–1191, Jul 2008.

[5] Dafna Ben Bashat, Vered Kronfeld-Duenias, Ditza A Zachor, Perla M Ekstein, Talma Hendler, Ricardo Tarrasch, Ariela Even, Yonata Levy, and Liat Ben Sira. Accelerated maturation of white matter in young children with autism: a high b value dwi study. *Neuroimage*, 37(1):40–47, Aug 2007.

[6] Matthew K Belmonte, Greg Allen, Andrea Beckel-Mitchener, Lisa M Boulanger, Ruth A Carper, and Sara J Webb. Autism and abnormal development of brain connectivity. *J Neurosci*, 24(42):9228–9231, Oct 2004.

[7] D.W. Austin, J.M. Abbott, and C. Carbis. The use of virtual reality hypnosis with two cases of autism spectrum disorder: a feasibility study. *Contemporary Hypnosis*, 25(2):102–109, 2008.

[8] C. Plaisant, A. Druin, C. Lathan, K. Dakhane, K. Edwards, and J. Vice. A storytelling robot for pediatric rehabilitation. In *Proceedings of ASSETS 2000, Washington DC*, 2000.

[9] F. Michaud, A. Duquette, and I. Nadeau. Characteristics of mobile robotic toys for children with pervasive developmental disorders. In *Proc. IEEE Int Systems, Man and Cybernetics Conf*, volume 3, pages 2938–2943, 2003.

[10] Aude Billard, Ben Robins, Jacqueline Nadel, and Kerstin Dautenhahn. Building robota, a mini-humanoid robot for the rehabilitation of children with autism. *Assist Technol*, 19(1):37–49, 2007.

[11] H. Kozima. *Socially Intelligent Agent*, chapter Infanoid: A babybot that explores the social environment, pages 157–164. Kluwer Academic Publishers, 2002.

[12] R. Picard and J. Scheirer. The galvactivator: A glove that senses and communicates skin conductivity. In *Proceedings*

from the 9th International Conference on Human-Computer Interaction (pp. 91-101), 2001.

[13] J. Healey, Picard R.W., and F. Dabek. A new affect-perceiving interface and its application to personalized music selection. In *Proceedings of the 1998 Workshop on Perceptual User Interfaces, San Francisco, CA*, 1998.

[14] Y. Qi and R.W. Picard. Context-sensitive bayesian classifiers and application to mouse pressure pattern classification. In *Proceedings of the International Conference on Pattern Recognition (ICPR)*, 2002.

[15] J. Scheirer, R. Fernandez, and R.W. Picard. Expression glasses: A wearable device for facial expression recognition. In *Proceedings of the CHI ?99 extended abstracts on Human factors in computing systems (pp. 262-263)*, 1999.

[16] A. Klin, W. Jones, R. Schultz, F. Volkmar, and D. Cohen. Visual fixation patterns during viewing of naturalistic social situations as predictors of social competence in individuals with autism. *Arch Gen Psychiatry*, 59:809–816, 2002.

[17] Roy V Sillitoe and Alexandra L Joyner. Morphology, molecular codes, and circuitry produce the three-dimensional complexity of the cerebellum. *Annu Rev Cell Dev Biol*, 23:549–577, 2007.

[18] Christian Beaulieu. The basis of anisotropic water diffusion in the nervous system - a technical review. *NMR Biomed*, 15(7-8):435–455, 2002.

[19] E. Stejskal and J. Tanner. Spin diffusion measurements: spin echoes in the presence of a time-dependent field gradient. *Journal of Chemical Physics*, 42:288–292, 1965.

[20] Stephen W Porges. The polyvagal theory: phylogenetic contributions to social behavior. *Physiol Behav*, 79(3):503–513, Aug 2003.

[21] R. Paradiso, G. Loriga, N. Taccini, A. Gemignani, and B Ghelarducci. Wealthy:a wearable healthcare system: new frontier on e-textile. *International Journal of Information and Communication Technology*, 4:105–113, 2005.

[22] J. Malmivuo and r. Plonsey. *Bioelectromagnetism: Principles and Applications of Bioelectric and Biomagnetic Fields.* Oxford University Press, 1995.

[23] Nouchine Hadjikhani, Robert M Joseph, Josh Snyder, and Helen Tager-Flusberg. Abnormal activation of the social brain during face perception in autism. *Hum Brain Mapp*, 28(5):441–449, May 2007.

[24] Peter J Basser and Derek K Jones. Diffusion-tensor mri: theory, experimental design and data analysis - a technical review. *NMR Biomed*, 15(7-8):456–467, 2002.

[25] Naama Barnea-Goraly, Hower Kwon, Vinod Menon, Stephan Eliez, Linda Lotspeich, and Allan L Reiss. White matter structure in autism: preliminary evidence from diffusion tensor imaging. *Biol Psychiatry*, 55(3):323–326, Feb 2004.

[26] Jee Eun Lee, Erin D Bigler, Andrew L Alexander, Mariana Lazar, Molly B DuBray, Moo K Chung, Michael Johnson, Jubel Morgan, Judith N Miller, William M McMahon, Jeffrey Lu, Eun-Kee Jeong, and Janet E Lainhart. Diffusion tensor imaging of white matter in the superior temporal gyrus and temporal stem in autism. *Neurosci Lett*, 424(2):127–132, Sep 2007.

[27] Eric Courchesne and Karen Pierce. Why the frontal cortex in autism might be talking only to itself: local over-connectivity but long-distance disconnection. *Curr Opin Neurobiol*, 15(2):225–230, Apr 2005.

[28] S.E. Bryson and Fombonne E Rogers SJ. Autism spectrum disorders: early detection, intervention, education and psychopharmacological management. *Can J Psychiatry*, 48:506–516, 2003.

[29] K. Pierce, K. S. Glad, and L. Schreibman. Social perception in children with autism: an attentional deficit? *J Autism Dev Disord*, 27(3):265–282, Jun 1997.

[30] E.R. Kandel, Schwartz J.H., and T.M. Jessel. *Principles of Neural Science*. 2000.

[31] Vladislav Volman, Itay Baruchi, and Eshel Ben-Jacob. Manifestation of function-follow-form in cultured neuronal networks. *Phys Biol*, 2(2):98–110, Jun 2005.

[32] I. Baruchi and E. Ben-Jacob. Functional holography of recorded neuronal networks activity. *Neuroinformatics*, 2(3):333–352, 2004.

[33] Ronen Segev, Itay Baruchi, Eyal Hulata, and Eshel Ben-Jacob. Hidden neuronal correlations in cultured networks. *Phys Rev Lett*, 92(11):118102, Mar 2004.

[34] Orit Shefi, Ido Golding, Ronen Segev, Eshel Ben-Jacob, and Amir Ayali. Morphological characterization of in vitro neuronal networks. *Phys Rev E Stat Nonlin Soft Matter Phys*, 66(2 Pt 1):021905, Aug 2002.

[35] G.A. Silva and B. Culp. High throughput alghoritms for mapping the topology of neural and glial networks. *Proceedings of the 2nd International IEEE EMBS Conference of Neural Engineering*, pages 344 – 347, 2005.

[36] L. Billeci, G. Pioggia, F. Vaglini, and A. Ahluwalia. Assessment and comparison of neural morphology through metrical feature extraction and analysis in neuron and neuron-glia cultures. *J Biol Phys*, 35(4):447–464, Oct 2009.

[37] L. Billeci, G. Pioggia, F. Vaglini, and A. Ahluwalia. Automated extraction and classification of dynamic metrical features of morphological development in dissociated purkinje neurons. *J Neurosci Methods*, 185(2):315–324, Jan 2010.

[38] J. D. Lewis and J. L. Elman. Growthrelated neural reorganization and the autism phenotype: a test of the hypothesis

that altered brain growth leads to altered connectivity. *Developmental Science*, 11:135–155, 2008.

[39] Robert T Schultz, David J Grelotti, Ami Klin, Jamie Kleinman, Christiaan Van der Gaag, Ren Marois, and Pawel Skudlarski. The role of the fusiform face area in social cognition: implications for the pathobiology of autism. *Philos Trans R Soc Lond B Biol Sci*, 358(1430):415–427, Feb 2003.

[40] B. Luna, N. J. Minshew, K. E. Garver, N. A. Lazar, K. R. Thulborn, W. F. Eddy, and J. A. Sweeney. Neocortical system abnormalities in autism: an fmri study of spatial working memory. *Neurology*, 59(6):834–840, Sep 2002.

[41] M. Lungarella, G. Metta, R. Pfeifer, and G Sandini. Developmental robotics: a survey. *Connection Science*, 15(4):51–190, 2003.

[42] D. Mazzei, L. Billeci, A. Armato, N. Lazzeri, A. Cisternino, G. Pioggia, Igliozzi R., F. Muratori, A. Ahluwalia, and D. De Rossi. The face of autism. *Proceeding of 19th IEEE International Symposium on Robot and Human Interactive Communication*, pages 844–849, Viareggio, Italy, 2010.

[43] Craig J Newschaffer, Lisa A Croen, Julie Daniels, Ellen Giarelli, Judith K Grether, Susan E Levy, David S Mandell, Lisa A Miller, Jennifer Pinto-Martin, Judy Reaven, Ann M Reynolds, Catherine E Rice, Diana Schendel, and Gayle C Windham. The epidemiology of autism spectrum disorders. *Annu Rev Public Health*, 28:235–258, 2007.

[44] Eric Fombonne. Epidemiology of pervasive developmental disorders. *Pediatr Res*, 65(6):591–598, Jun 2009.

[45] Scott M Myers, Chris Plauch Johnson, and American Academy of Pediatrics Council on Children With Disabilities. Management of children with autism spectrum disorders. *Pediatrics*, 120(5):1162–1182, Nov 2007.

[46] U. Frith. *Autism: explaining the enigma*. 2003.

[47] Isabelle Rapin and Roberto F Tuchman. Autism: definition, neurobiology, screening, diagnosis. *Pediatr Clin North Am*, 55(5):1129–46, viii, Oct 2008.

[48] S. Baron-Cohen, H. Tager-Flusberg, and D. J. Cohen. *Understanding other minds: Perspectives from autism and developmental cognitive neuroscience*. Oxford: Oxford University Press, 2000.

[49] J. W. Bodfish, F. J. Symons, D. E. Parker, and M. H. Lewis. Varieties of repetitive behavior in autism: comparisons to mental retardation. *J Autism Dev Disord*, 30(3):237–243, Jun 2000.

[50] John R Hughes. A review of recent reports on autism: 1000 studies published in 2007. *Epilepsy Behav*, 13(3):425–437, Oct 2008.

[51] C. Gillberg. Chromosomal disorders and autism. *J Autism Dev Disord*, 28(5):415–425, Oct 1998.

[52] F. Happ. *Autism: an introduction to psychological theory*. London: UCL Press, 1994.

[53] Susan E Levy, David S Mandell, and Robert T Schultz. Autism. *Lancet*, 374(9701):1627–1638, Nov 2009.

[54] Catalina Betancur, Takeshi Sakurai, and Joseph D Buxbaum. The emerging role of synaptic cell-adhesion pathways in the pathogenesis of autism spectrum disorders. *Trends Neurosci*, 32(7):402–412, Jul 2009.

[55] Christopher A Walsh, Eric M Morrow, and John L R Rubenstein. Autism and brain development. *Cell*, 135(3):396–400, Oct 2008.

[56] Tara L Arndt, Christopher J Stodgell, and Patricia M Rodier. The teratology of autism. *Int J Dev Neurosci*, 23(2-3):189–199, 2005.

[57] P. Michel. The use of technology in the study, diagnosis and treatment of. *Final term paper for CSC350: Autism and Associated Development Disorders.*, 2004.

[58] G. Baird, H. Cass, and V. Slonims. Diagnosis of autism. *BMJ*, pages 327–488, 2003.

[59] J.S. (Ed) Handleman and S (Ed) Harris. *Preschool Education Programs for Children with Autism ., eds. (2nd ed). , TX: Pro-Ed. 2000.* PRO-ED, 8700 Shoal Creek Blvd., Austin, TX 78757-6897, 2000.

[60] C. (Ed.) Lord and J.P. (Ed.) McGee. *Educating Children with Autism.* National Academy Press, 2001, National Research

Council, Division of Behavioral and Social Sciences and Education. Washington DC.

[61] Jennifer Harrison Elder. The gluten-free, casein-free diet in autism: an overview with clinical implications. *Nutr Clin Pract*, 23(6):583–588, 2008.

[62] George T Capone, Parag Goyal, Marco Grados, Brandon Smith, and Heather Kammann. Risperidone use in children with down syndrome, severe intellectual disability, and comorbid autistic spectrum disorders: a naturalistic study. *J Dev Behav Pediatr*, 29(2):106–116, Apr 2008.

[63] F. R. (Ed.) Volkmar. *Autism and pervasive developmental disorders*. Cambridge, UK: Cambridge University Press, 1998.

[64] K.B. Nelson, Grether J.K., L.A. Croen, M. Dambrosia, J, F Dickens, B, L.L. Jelliffe, R.L. Hansen, and T.M. Phillips. Neuropeptides and neurotrophins in neonatal blood of children with autism or mental retardation. *Ann Neurol*, 49(5):597–606, 2001.

[65] M. A. Junaid and R. K. Pullarkat. Proteomic approach for the elucidation of biological defects in autism. *J Autism Dev Disord*, 31(6):557–560, Dec 2001.

[66] S. L. Baader, S. Sanlioglu, A. S. Berrebi, J. Parker-Thornburg, and J. Oberdick. Ectopic overexpression of engrailed-2 in cerebellar purkinje cells causes restricted cell loss and retarded external germinal layer development at lobule junctions. *J Neurosci*, 18(5):1763–1773, Mar 1998.

[67] R. Benayed, N. Gharani, I. Rossman, V. Mancuso, G. Lazar, S. Kamdar, S. E. Bruse, S. Tischfield, B. J. Smith, E. Zimmerman, R. A.and DiciccoBloom, L. M. Brzustowicz, and J. H. Millonig. Support for the homeobox transcription factor gene engrailed 2 as an autism spectrum disorder susceptibility locus. *Am J Hum Genet*, 77:851–868, 2005.

[68] K. J. Millen, W. Wurst, K. Herrup, and A. L. Joyner. Abnormal embryonic cerebellar development and patterning of postnatal foliation in two mouse engrailed-2 mutants. *Development*, 120(3):695–706, Mar 1994.

[69] I.T. Rossman, S. Kamdar, J. Millonig, and E. DiCicco-Bloom. Extracellular growth factors interact with engrailed 2 (en2) an autism-associated gene, to control cerebellar development. *Soc Neurosci Abstr*, 31:596.2, 2005.

[70] M.A. Cheh, J.H. Millonig, L.M. Rosellie, X. Mingf, E. Jacobsene, S. Kamdar, and G.C. Wagnera. En2 knockout mice display neurobehavioral and neurochemical alterations relevant to autism spectrum disorder. *Brain Res*, 1116(1):166–176, 2006.

[71] B. Kuemerle, H. Zanjani, A. Joyner, and K. Herrup. Pattern deformities and cell loss in engrailed-2 mutant mice suggest two separate patterning events during cerebellar development. *J Neurosci*, 17(20):7881–7889, Oct 1997.

[72] E. Costa, J. Davis, D. R. Grayson, A. Guidotti, G. D. Pappas, and C. Pesold. Dendritic spine hypoplasticity and downregula-

tion of reelin and gabaergic tone in schizophrenia vulnerability. *Neurobiol Dis*, 8(5):723–742, Oct 2001.

[73] Fadel Tissir and Andr M Goffinet. Reelin and brain development. *Nat Rev Neurosci*, 4(6):496–505, Jun 2003.

[74] Antonio M Persico and Thomas Bourgeron. Searching for ways out of the autism maze: genetic, epigenetic and environmental clues. *Trends Neurosci*, 29(7):349–358, Jul 2006.

[75] S. Hossein Fatemi, Amy R Halt, George Realmuto, Julie Earle, David A Kist, Paul Thuras, and Amelia Merz. Purkinje cell size is reduced in cerebellum of patients with autism. *Cell Mol Neurobiol*, 22(2):171–175, Apr 2002.

[76] U. De Silva, G. D'Arcangelo, and V.V. Braden. The human reelin gene: isolation, sequencing, and mapping on chromosome 7. *Genome Res*, 7:157–164, 1997.

[77] V. S. Caviness and P. Rakic. Mechanisms of cortical development: a view from mutations in mice. *Annu Rev Neurosci*, 1:297–326, 1978.

[78] A. M. Goffinet. Determinants of nerve cell patterns during development: a review. *Eur J Morphol*, 28(2-4):149–168, 1990.

[79] Maria Cristina Marrone, Silvia Marinelli, Filippo Biamonte, Flavio Keller, Carmelo Alessio Sgobio, Martine Ammassari-Teule, Giorgio Bernardi, and Nicola B Mercuri. Altered

cortico-striatal synaptic plasticity and related behavioural impairments in reeler mice. *Eur J Neurosci*, 24(7):2061–2070, Oct 2006.

[80] W. S. Liu, C. Pesold, M. A. Rodriguez, G. Carboni, J. Auta, P. Lacor, J. Larson, B. G. Condie, A. Guidotti, and E. Costa. Down-regulation of dendritic spine and glutamic acid decarboxylase 67 expressions in the reelin haploinsufficient heterozygous reeler mouse. *Proc Natl Acad Sci U S A*, 98(6):3477–3482, Mar 2001.

[81] Walter L Salinger, Pamela Ladrow, and Catherine Wheeler. Behavioral phenotype of the reeler mutant mouse: effects of reln gene dosage and social isolation. *Behav Neurosci*, 117(6):1257–1275, Dec 2003.

[82] P. Tueting, E. Costa, Y. Dwivedi, A. Guidotti, F. Impagnatiello, R. Manev, and C. Pesold. The phenotypic characteristics of heterozygous reeler mouse. *Neuroreport*, 10(6):1329–1334, Apr 1999.

[83] Giovanni Laviola, Walter Adriani, Chiara Gaudino, Ramona Marino, and Flavio Keller. Paradoxical effects of prenatal acetylcholinesterase blockade on neuro-behavioral development and drug-induced stereotypies in reeler mutant mice. *Psychopharmacology (Berl)*, 187(3):331–344, Aug 2006.

[84] Elisa Ognibene, Walter Adriani, Simone Macr, and Giovanni Laviola. Neurobehavioural disorders in the infant reeler mouse model: interaction of genetic vulnerability and consequences

of maternal separation. *Behav Brain Res*, 177(1):142–149, Feb 2007.

[85] Kristen S L Lam, Michael G Aman, and L. Eugene Arnold. Neurochemical correlates of autistic disorder: a review of the literature. *Res Dev Disabil*, 27(3):254–289, 2006.

[86] P. A. McBride, G. M. Anderson, M. E. Hertzig, M. E. Snow, S. M. Thompson, V. D. Khait, T. Shapiro, and D. J. Cohen. Effects of diagnosis, race, and puberty on platelet serotonin levels in autism and mental retardation. *J Am Acad Child Adolesc Psychiatry*, 37(7):767–776, Jul 1998.

[87] G. M. Anderson, D. X. Freedman, D. J. Cohen, F. R. Volkmar, E. L. Hoder, P. McPhedran, R. B. Minderaa, C. R. Hansen, and J. G. Young. Whole blood serotonin in autistic and normal subjects. *J Child Psychol Psychiatry*, 28(6):885–900, Nov 1987.

[88] E. H. Cook, B. L. Leventhal, and D. X. Freedman. Free serotonin in plasma: autistic children and their first-degree relatives. *Biol Psychiatry*, 24(4):488–491, Aug 1988.

[89] S. Chiu, J.A. Wegelin, J. Blank, M. Jenkins, J. Day, D. Hessl, F. Tassone, and R. Hagerman. Early acceleration of head circumference in children with fragile x syndrome and autism. *J Dev Behav Pediatr*, 28(1):31–5, 2007.

[90] E. Courchesne, C. M. Karns, H. R. Davis, R. Ziccardi, R. A. Carper, Z. D. Tigue, H. J. Chisum, P. Moses, K. Pierce, C. Lord, A. J. Lincoln, S. Pizzo, L. Schreibman, R. H. Haas,

N. A. Akshoomoff, and R. Y. Courchesne. Unusual brain growth patterns in early life in patients with autistic disorder: an mri study. *Neurology*, 57(2):245–254, Jul 2001.

[91] Margaret L Bauman and Thomas L Kemper. Neuroanatomic observations of the brain in autism: a review and future directions. *Int J Dev Neurosci*, 23(2-3):183–187, 2005.

[92] E. H. Aylward, Q. Li, N. A. Honeycutt, A. C. Warren, M. B. Pulsifer, P. E. Barta, M. D. Chan, P. D. Smith, M. Jerram, and G. D. Pearlson. Mri volumes of the hippocampus and amygdala in adults with down's syndrome with and without dementia. *Am J Psychiatry*, 156(4):564–568, Apr 1999.

[93] S. R. Dager, L. Wang, S. D. Friedman, D. W. Shaw, J. N. Constantino, A. A. Artru, G. Dawson, and J. G. Csernansky. Shape mapping of the hippocampus in young children with autism spectrum disorder. *AJNR Am J Neuroradiol*, 28(4):672–677, Apr 2007.

[94] M. M. Haznedar, M. S. Buchsbaum, M. Metzger, A. Solimando, J. Spiegel-Cohen, and E. Hollander. Anterior cingulate gyrus volume and glucose metabolism in autistic disorder. *Am J Psychiatry*, 154(8):1047–1050, Aug 1997.

[95] Manuel F Casanova, Imke A J van Kooten, Andrew E Switala, Herman van Engeland, Helmut Heinsen, Harry W M Steinbusch, Patrick R Hof, Juan Trippe, Janet Stone, and Christoph Schmitz. Minicolumnar abnormalities in autism. *Acta Neuropathol*, 112(3):287–303, Sep 2006.

[96] Eric Courchesne, Elizabeth Redcay, John T Morgan, and Daniel P Kennedy. Autism at the beginning: microstructural and growth abnormalities underlying the cognitive and behavioral phenotype of autism. *Dev Psychopathol*, 17(3):577–597, 2005.

[97] P. J. Basser and C. Pierpaoli. Microstructural and physiological features of tissues elucidated by quantitative-diffusion-tensor mri. *J Magn Reson B*, 111(3):209–219, Jun 1996.

[98] Andrew L Alexander, Jee Eun Lee, Mariana Lazar, Rebecca Boudos, Molly B DuBray, Terrence R Oakes, Judith N Miller, Jeffrey Lu, Eun-Kee Jeong, William M McMahon, Erin D Bigler, and Janet E Lainhart. Diffusion tensor imaging of the corpus callosum in autism. *Neuroimage*, 34(1):61–73, Jan 2007.

[99] Timothy A Keller, Rajesh K Kana, and Marcel Adam Just. A developmental study of the structural integrity of white matter in autism. *Neuroreport*, 18(1):23–27, Jan 2007.

[100] Senthil K Sundaram, Ajay Kumar, Malek I Makki, Michael E Behen, Harry T Chugani, and Diane C Chugani. Diffusion tensor imaging of frontal lobe in autism spectrum disorder. *Cereb Cortex*, 18(11):2659–2665, Nov 2008.

[101] Luca Pugliese, Marco Catani, Stephanie Ameis, Flavio Dell'Acqua, Michel Thiebaut de Schotten, Clodagh Murphy, Dene Robertson, Quinton Deeley, Eileen Daly, and Declan G M Murphy. The anatomy of extended limbic pathways in asperger

syndrome: a preliminary diffusion tensor imaging tractography study. *Neuroimage*, 47(2):427–434, Aug 2009.

[102] David Rudrauf, Olivier David, Jean-Philippe Lachaux, Christopher K Kovach, Jacques Martinerie, Bernard Renault, and Antonio Damasio. Rapid interactions between the ventral visual stream and emotion-related structures rely on a two-pathway architecture. *J Neurosci*, 28(11):2793–2803, Mar 2008.

[103] Cibu Thomas, Kate Humphreys, Kwan-Jin Jung, Nancy Minshew, and Marlene Behrmann. The anatomy of the callosal and visual-association pathways in high-functioning autism: A dti tractography study. *Cortex*, Aug 2010.

[104] Marlene Behrmann, Galia Avidan, Grace Lee Leonard, Rutie Kimchi, Beatriz Luna, Kate Humphreys, and Nancy Minshew. Configural processing in autism and its relationship to face processing. *Neuropsychologia*, 44(1):110–129, 2006.

[105] Armando Bertone, Laurent Mottron, Patricia Jelenic, and Jocelyn Faubert. Enhanced and diminished visuo-spatial information processing in autism depends on stimulus complexity. *Brain*, 128(Pt 10):2430–2441, Oct 2005.

[106] Kate Humphreys, Uri Hasson, Galia Avidan, Nancy Minshew, and Marlene Behrmann. Cortical patterns of category-selective activation for faces, places and objects in adults with autism. *Autism Res*, 1(1):52–63, Feb 2008.

[107] Philip S Lee, Jennifer Foss-Feig, Joshua G Henderson, Lauren E Kenworthy, Lisa Gilotty, William D Gaillard, and Chandan J Vaidya. Atypical neural substrates of embedded figures task performance in children with autism spectrum disorder. *Neuroimage*, 38(1):184–193, Oct 2007.

[108] C. Lord, E.H. Cook, and Amaral D.G. Leventhal, B.L. Autism spectrum disorders. *Neuron*, 28:355–363, 2000.

[109] Emanuel DiCicco-Bloom, Catherine Lord, Lonnie Zwaigenbaum, Eric Courchesne, Stephen R Dager, Christoph Schmitz, Robert T Schultz, Jacqueline Crawley, and Larry J Young. The developmental neurobiology of autism spectrum disorder. *J Neurosci*, 26(26):6897–6906, Jun 2006.

[110] A.K. Pelphrey, J.P. Morris, and G. McCarthy. Neural basis of eye gaze processing deficits in autism. *Brain*, 128:10381048, 2005.

[111] S. Baron-Cohen, H. A. Ring, S. Wheelwright, E. T. Bullmore, M. J. Brammer, A. Simmons, and S. C. Williams. Social intelligence in the normal and autistic brain: an fmri study. *Eur J Neurosci*, 11(6):1891–1898, Jun 1999.

[112] H. Critchley, E. Daly, M. Phillips, M. Brammer, E. Bullmore, S. Williams, T. Van Amelsvoort, D. Robertson, A. David, and D. Murphy. Explicit and implicit neural mechanisms for processing of social information from facial expressions: a functional magnetic resonance imaging study. *Hum Brain Mapp*, 9(2):93–105, Feb 2000.

[113] Robert T Schultz. Developmental deficits in social perception in autism: the role of the amygdala and fusiform face area. *Int J Dev Neurosci*, 23(2-3):125–141, 2005.

[114] K. Pierce, R. A. Mller, J. Ambrose, G. Allen, and E. Courchesne. Face processing occurs outside the fusiform 'face area' in autism: evidence from functional mri. *Brain*, 124(Pt 10):2059–2073, Oct 2001.

[115] *"Written by Susan Stokes under a contract with CESA 7 and funded by a discretionary grant from the Wisconsin Department of Public Instruction."*.

[116] L. C. Bryan and D. L. Gast. Teaching on-task and on-schedule behaviors to high-functioning children with autism via picture activity schedules. *J Autism Dev Disord*, 30(6):553–567, Dec 2000.

[117] A. Bondy and L. Frost. The picture exchange communication system. *Behav Modif*, 25(5):725–744, Oct 2001.

[118] V. Bernard-Opitz, N. Sriram, and S. Nakhoda-Sapuan. Enhancing social problem solving in children with autism and normal children through computer-assisted instruction. *J Autism Dev Disord*, 31(4):377–384, Aug 2001.

[119] G. E. Lancioni. Using pictorial representations as communication means with low-functioning children. *J Autism Dev Disord*, 13(1):87–105, Mar 1983.

[120] M. M. Schepis, D. H. Reid, M. M. Behrmann, and K. A. Sutton. Increasing communicative interactions of young children with autism using a voice output communication aid and naturalistic teaching. *J Appl Behav Anal*, 31(4):561–578, 1998.

[121] *Attainment Company P.O. Box 930160 Verona, WI 5359 (Source for VoicePod).*

[122] D. Moore, McGrath P., and J. Thorpe. Computer-aided learning for people with autism?a framework for research and development. *Innovations in Education and Training International*, 37(3):218–228, 2000.

[123] C. MacArthur. New tools for writing: Assistive technology for students with writing difficulties. *Topics in Language Disorders*, 20(4):85–100, 2000.

[124] S. Baron-Cohen and T. Tead. *Mind reading: the interactive guide to emotion.* Autism Research Centre, Cambridge., 2003.

[125] Ralf W Schlosser and Doreen M Blischak. Effects of speech and print feedback on spelling by children with autism. *J Speech Lang Hear Res*, 47(4):848–862, Aug 2004.

[126] D. Strickland. Virtual reality for the treatment of autism. *Stud Health Technol Inform*, 44:81–86, 1997.

[127] D. Strickland, L. M. Marcus, G. B. Mesibov, and K. Hogan. Brief report: two case studies using virtual reality as a learning tool for autistic children. *J Autism Dev Disord*, 26(6):651–659, Dec 1996.

[128] J. Scholtz. Theory and evaluation of human robot interactions. In *Proceeding of Hawaii Internartional Conference on System Science*, 2003.

[129] J. Han, J. Lee, and Y. Cho. Evolutionary role model and basic emotions of service robots originated from computers. In *IEEE International Workshop on Robots and Human Interactive Communication*, 2005.

[130] K. Dautenhahn. Robots as social actors: Aurora and the case of autism. In *Proceedings of the International Cognitive Technology Conference (pp. 359-374)*, 1999.

[131] K. Dautenhahn and Clarkson PJ Langdon PJ Robinson P (eds) P Billard, A. . In: Keates S. Games children with autism can play with robota, a humanoid robotic doll. In *Proceedings of the 1st Cambridge workshop on Universal Access and Assistive Technology [CWUAAT]. Universal Access and Assistive Technology. Springer, London (pp 179-190)*, 2002.

[132] Kerstin Dautenhahn. Just child's play? - applications of robot assisted play in autism therapy. In *Proc. IEEE 10th Int. Conf. Rehabilitation Robotics ICORR 2007*, page 20, 2007.

[133] K. Dautenhahn and I. Werry. The aurora project: Using mobile robots in autism therapy. *Learning Technology, online newsletter, publication of IEEE Computer Society Learning Technology Task Force (LTTF)*, 3(1), 2001.

[134] H. Kozima and C. Nakagawa. A robot in a playroom with preschool children: Longitudinal field practice. In *The 16th*

IEEE International Symposium on Robot and Human interactive Communication, RO-MAN, 2007.

[135] Rana el Kaliouby, Rosalind Picard, and Simon Baron-Cohen. Affective computing and autism. *Ann N Y Acad Sci*, 1093:228–248, Dec 2006.

[136] J.E. LeDoux. *The Emotional Brain.* New York: Simon & Schuster, 1996.

[137] R. el Kaliouby and P. Robinson. The emotional hearing aid: An assistive tool for autism. In *Proceedings of the 10th International Conference on Human-Computer Interaction (HCII): Universal Access in HCI (volume 4, pp. 68-72)*, 2003.

[138] R. el Kaliouby and P. Robinson. Real-time inference of complex mental states from facial expressions and head gestures. In *In the IEEE International Workshop on Real Time Computer Vision for Human Computer Interaction at CVPR*, 2004.

[139] R. el Kaliouby and P. Robinson. Mind-reading machines: Automated inference of cognitive mental states from video. In *Proceedings of IEEE Conference on Systems, Man and Cybernetics, The Hague, Netherlands.*, 2004.

[140] R. el Kaliouby and P. Robinson. Therapeutical versus prosthetic assistive technologies: the case of autism. 2007.

[141] K.A. Pelphrey, N. Sasson, J.S. Reznick, G. Paul, B. Goldman, and J. Piven. Visual scanning of faces in autism. *J Autism Dev Disord*, 32:249–261, 2002.

[142] K.M. Dalton, B.M. Nacewicz, T. Johnstone, H.S. Schaefer, M.A. Gernsbacher, H.H. Goldsmith, A.L. Alexander, and R.J. Davidson. Gaze fixation and the neural circuitry of face processing in autism. *Nat Neurosci*, 8(4):519–26, 2005.

[143] Natacha Akshoomoff, Catherine Lord, Alan J Lincoln, Rachel Y Courchesne, Ruth A Carper, Jeanne Townsend, and Eric Courchesne. Outcome classification of preschool children with autism spectrum disorders using mri brain measures. *J Am Acad Child Adolesc Psychiatry*, 43(3):349–357, Mar 2004.

[144] Bruce E McKay and Ray W Turner. Physiological and morphological development of the rat cerebellar purkinje cell. *J Physiol*, 567(Pt 3):829–850, Sep 2005.

[145] T. Hollingworth and M. Berry. Network analysis of dendritic fields of pyramidal cells in neocortex and purkinje cells in the cerebellum of the rat. *Philos Trans R Soc Lond B Biol Sci*, 270(906):227–264, May 1975.

[146] M. E. Dunn, K. Schilling, and E. Mugnaini. Development and fine structure of murine purkinje cells in dissociated cerebellar cultures: dendritic differentiation, synaptic maturation, and formation of cell-class specific features. *Anat Embryol (Berl)*, 197(1):31–50, Jan 1998.

[147] Makoto Mori and Toshiya Matsushima. Post-hatch development of dendritic arborization in cerebellar purkinje neurons of quail chicks: a morphometric study. *Neurosci Lett*, 329(1):73–76, Aug 2002.

[148] Josef P Kapfhammer. Cellular and molecular control of dendritic growth and development of cerebellar purkinje cells. *Prog Histochem Cytochem*, 39(3):131–182, 2004.

[149] Cristopher M Niell and Stephen J Smith. Live optical imaging of nervous system development. *Annu Rev Physiol*, 66:771–798, 2004.

[150] Harry B M Uylings and Jaap van Pelt. Measures for quantifying dendritic arborizations. *Network*, 13(3):397–414, Aug 2002.

[151] P. Blinder, I. Baruchi, Volman, Levine V., D. H., Baranes, and E. Ben-Jacob. Functional topology classification of biological computing networks. *Nat. Comput*, 4:339–361, 2005.

[152] Y. Arai, Y. Momose-Sato, K. Sato, and K. Kamino. Optical mapping of neural network activity in chick spinal cord at an intermediate stage of embryonic development. *J Neurophysiol*, 81(4):1889–1902, Apr 1999.

[153] P. G. Haydon. Glia: listening and talking to the synapse. *Nat Rev Neurosci*, 2(3):185–193, Mar 2001.

[154] A. Araque, G. Carmignoto, and P. G. Haydon. Dynamic signaling between astrocytes and neurons. *Annu Rev Physiol*, 63:795–813, 2001.

[155] A. Volterra and P.G Magistretti, P.J.and Haydon. *The Tripartite Synapse Glia in Synaptic Transmission.* Oxford University Press, New York, 2002.

[156] Erik M Ullian, Karen S Christopherson, and Ben A Barres. Role for glia in synaptogenesis. *Glia*, 47(3):209–216, Aug 2004.

[157] Jing ming Zhang, Hui kun Wang, Chang quan Ye, Wooping Ge, Yiren Chen, Zheng lin Jiang, Chien ping Wu, Mu ming Poo, and Shumin Duan. Atp released by astrocytes mediates glutamatergic activity-dependent heterosynaptic suppression. *Neuron*, 40(5):971–982, Dec 2003.

[158] P. Liesi, D. Dahl, and A. Vaheri. Laminin is produced by early rat astrocytes in primary culture. *J Cell Biol*, 96(3):920–924, Mar 1983.

[159] H. H. Althaus and C. Richter-Landsberg. Glial cells as targets and producers of neurotrophins. *Int Rev Cytol*, 197:203–277, 2000.

[160] C. M. Mller, A. C. Akhavan, and M. Bette. Possible role of s-100 in glia-neuronal signalling involved in activity-dependent plasticity in the developing mammalian cortex. *J Chem Neuroanat*, 6(4):215–227, 1993.

[161] R. Donato. S100: a multigenic family of calcium-modulated proteins of the ef-hand type with intracellular and extracellular functional roles. *Int J Biochem Cell Biol*, 33(7):637–668, Jul 2001.

[162] O. Blondel, C. Collin, W. J. McCarran, S. Zhu, R. Zamostiano, I. Gozes, D. E. Brenneman, and R. D. McKay. A glia-derived signal regulating neuronal differentiation. *J Neurosci*, 20(21):8012–8020, Nov 2000.

[163] F. J. Seil. Interactions between cerebellar purkinje cells and their associated astrocytes. *Histol Histopathol*, 16(3):955–968, Jul 2001.

[164] S. Yuasa, K. Kawamura, R. Kuwano, and K. Ono. Neuron-glia interrelations during migration of purkinje cells in the mouse embryonic cerebellum. *Int J Dev Neurosci*, 14(4):429–438, Jul 1996.

[165] Diana L Vargas, Caterina Nascimbene, Chitra Krishnan, Andrew W Zimmerman, and Carlos A Pardo. Neuroglial activation and neuroinflammation in the brain of patients with autism. *Ann Neurol*, 57(1):67–81, Jan 2005.

[166] Janet Kinnear Kern. Purkinje cell vulnerability and autism: a possible etiological connection. *Brain Dev*, 25(6):377–382, Sep 2003.

[167] N. Otsu. A threshold selection method from gray-level histograms. *IEEE Trans. Sys., Man., Cyber*, 9:6266, 1979.

[168] L. Billeci. Analisi della connettivit e della dinamica di crescita di cellule di purkinje tramite imaging in-vitro ed algoritmi computazionali. Master's thesis, University of Pisa, 2007.

[169] Orit Shefi, Sharon Golebowicz, Eshel Ben-Jacob, and Amir Ayali. A two-phase growth strategy in cultured neuronal networks as reflected by the distribution of neurite branching angles. *J Neurobiol*, 62(3):361–368, Feb 2005.

[170] D. A. Sholl. Dendritic organization in the neurons of the visual and motor cortices of the cat. *J Anat*, 87(4):387–406, Oct 1953.

[171] Nebojsa T Milosević and Dusan Ristanović. The sholl analysis of neuronal cell images: semi-log or log-log method? *J Theor Biol*, 245(1):130–140, Mar 2007.

[172] T. Takeda, A. Ishikawa, K. Ohtomo, Y. Kobayashi, and T. Matsuoka. Fractal dimension of dendritic tree of cerebellar purkinje cell during onto- and phylogenetic development. *Neurosci Res*, 13(1):19–31, Feb 1992.

[173] Alves S.G., Martin M.L., Fernandes P.A., and Pittella J.E.H. Fractal patterns for dendrites and axon terminals. *Physica A*, 232:5160, 1996.

[174] H. F. Jelinek and E. Fernandez. Neurons and fractals: how reliable and useful are calculations of fractal dimensions? *J Neurosci Methods*, 81(1-2):9–18, Jun 1998.

[175] F. Caserta, W. D. Eldred, E. Fernandez, R. E. Hausman, L. R. Stanford, S. V. Bulderev, S. Schwarzer, and H. E. Stanley. Determination of fractal dimension of physiologically characterized neurons in two and three dimensions. *J Neurosci Methods*, 56(2):133–144, Feb 1995.

[176] B.B. Mandelbrot. *The Fractal Geometry of Nature*. 2004.

[177] P. Rakic. Neuron-glia relationship during granule cell migration in developing cerebellar cortex. a golgi and electronmicro-

scopic study in macacus rhesus. *J Comp Neurol*, 141(3):283–312, Mar 1971.

[178] Jerzy Wegiel, Izabela Kuchna, Krzysztof Nowicki, Humi Imaki, Jarek Wegiel, Elaine Marchi, Shuang Yong Ma, Abha Chauhan, Ved Chauhan, Teresa Wierzba Bobrowicz, Mony de Leon, Leslie A Saint Louis, Ira L Cohen, Eric London, W. Ted Brown, and Thomas Wisniewski. The neuropathology of autism: defects of neurogenesis and neuronal migration, and dysplastic changes. *Acta Neuropathol*, 119(6):755–770, Jun 2010.

[179] R. Leardi, C. Armanino, S. Lanteri, and L. Alberotanza. Three-mode principal component analysis of monitoring data from venice lagoon. *J Chemometrics*, 14:187–95, 2000.

[180] H.A.L. Kiers and I.T. Van Mechelen. Three-way component analysis: principles and illustrative application. *Psychol Methods*, 6:84–110, 2001.

[181] X. Zhang, S. L. Baader, F. Bian, W. Mller, and J. Oberdick. High level purkinje cell specific expression of green fluorescent protein in transgenic mice. *Histochem Cell Biol*, 115(6):455–464, Jun 2001.

[182] D. T. Nordquist, C. A. Kozak, and H. T. Orr. cdna cloning and characterization of three genes uniquely expressed in cerebellum by purkinje neurons. *J Neurosci*, 8(12):4780–4789, Dec 1988.

[183] J. Oberdick, F. Levinthal, and C. Levinthal. A purkinje cell differentiation marker shows a partial dna sequence homology to the cellular sis/pdgf2 gene. *Neuron*, 1(5):367–376, Jul 1988.

[184] J. Oberdick, R. J. Smeyne, J. R. Mann, S. Zackson, and J. I. Morgan. A promoter that drives transgene expression in cerebellar purkinje and retinal bipolar neurons. *Science*, 248(4952):223–226, Apr 1990.

[185] Laura Lossi, Silvia Alasia, Chiara Salio, and Adalberto Merighi. Cell death and proliferation in acute slices and organotypic cultures of mammalian cns. *Prog Neurobiol*, 88(4):221–245, Aug 2009.

[186] S. Furuya, A. Makino, and Y. Hirabayashi. An improved method for culturing cerebellar purkinje cells with differentiated dendrites under a mixed monolayer setting. *Brain Res Brain Res Protoc*, 3(2):192–198, Nov 1998.

[187] T. Tabata, S. Sawadaa, K. Arakia, Y. Bonoa, S. Furuya, and M. Kano. A reliable method for culture of dissociated mouse cerebellar cells enriched for purkinje neurons. *J. Neurosci. Methods*, 104:4553, 2000.

[188] M.J. McAuliffe, F.M. Lalonde, D. McGarry, W. Gandler, K. Csaky, and B.L. Trus. Medical image processing, analysis & visualization in clinical research. In *IEEE Symposium on Computer-Based Medical Systems (CBMS), pp. 381386*, 2001.

[189] M.D. Abramoff, P.J. Magelhaes, and S.J. Ram. Image processing with imagej. *Biophotonics International*, 11(7):3642, 2004.

[190] J. Cohen and G.P. Wilkin. *Neural Cell Culture. A Practical Approach.* Oxford University Press, Oxford, 1995.

[191] J. Panico and P. Sterling. Retinal neurons and vessels are not fractal but space-filling. *J Comp Neurol*, 361(3):479–490, Oct 1995.

[192] E. Fernndez, G. Guiloff, H. Kolb, D. Ammermller, D. Zhang, and W. Eldred. Fractal dimension as a useful parameter for morphological classification of retinal neurons. *Invest. Ophthalmol. Vis. Sci.*, 33:940, 1992.

[193] Edward L White. Reflections on the specificity of synaptic connections. *Brain Res Rev*, 55(2):422–429, Oct 2007.

[194] Kerry M Brown, Todd A Gillette, and Giorgio A Ascoli. Quantifying neuronal size: summing up trees and splitting the branch difference. *Semin Cell Dev Biol*, 19(6):485–493, Dec 2008.

[195] J. van Pelt, A. van Ooyen, and H. B. Uylings. The need for integrating neuronal morphology databases and computational environments in exploring neuronal structure and function. *Anat Embryol (Berl)*, 204(4):255–265, Oct 2001.

[196] Yo Otsu, Volker Bormuth, Jerome Wong, Benjamin Mathieu, Guillaume P Dugu, Anne Feltz, and Stphane Dieudonn. Op-

tical monitoring of neuronal activity at high frame rate with a digital random-access multiphoton (ramp) microscope. *J Neurosci Methods*, 173(2):259–270, Aug 2008.

[197] Thomas Knpfel, Javier Dez-Garca, and Walther Akemann. Optical probing of neuronal circuit dynamics: genetically encoded versus classical fluorescent sensors. *Trends Neurosci*, 29(3):160–166, Mar 2006.

[198] K.P. Lillis, A. Eng, J.A. White, and J. Mertz. Two-photon imaging of spatially extended neuronal network dynamics with high temporal resolution. *J Neurosci Methods*, 172:17884, 2008.

[199] W.T. Wong and R.O. Wong. Rapid dendritic movements during synapse formation and rearrangement. *Curr Opin Neurobiol*, 10:11824, 2000.

[200] T. Hollingworth and M. Berry. Network analysis of dendritic fields of pyramidal cells in neocortex and purkinje cells in the cerebellum of the rat. *Philos Trans R Soc Lond B Biol Sci*, 270(906):227–264, May 1975.

[201] M. E. Dunn, K. Schilling, and E. Mugnaini. Development and fine structure of murine purkinje cells in dissociated cerebellar cultures: dendritic differentiation, synaptic maturation, and formation of cell-class specific features. *Anat Embryol (Berl)*, 197(1):31–50, Jan 1998.

[202] Laurens W J Bosman, Jana Hartmann, Jaroslaw J Barski, Alexandra Lepier, Michael Noll-Hussong, Louis F Reichardt,

and Arthur Konnerth. Requirement of trkb for synapse elimination in developing cerebellar purkinje cells. *Brain Cell Biol*, 35(1):87–101, Feb 2006.

[203] M. Tanaka, Y. Yanagawa, K. Obata, and T. Marunouchi. Dendritic morphogenesis of cerebellar purkinje cells through extension and retraction revealed by long-term tracking of living cells in vitro. *Neuroscience*, 141(2):663–674, Aug 2006.

[204] S. Gianola and F. Rossi. Evolution of the purkinje cell response to injury and regenerative potential during postnatal development of the rat cerebellum. *J Comp Neurol*, 430(1):101–117, Jan 2001.

[205] K. Schrenk, J. P. Kapfhammer, and F. Metzger. Altered dendritic development of cerebellar purkinje cells in slice cultures from protein kinase cgamma-deficient mice. *Neuroscience*, 110(4):675–689, 2002.

[206] Kerry M Brown, Duncan E Donohue, Giampaolo D'Alessandro, and Giorgio A Ascoli. A cross-platform freeware tool for digital reconstruction of neuronal arborizations from image stacks. *Neuroinformatics*, 3(4):343–360, 2005.

[207] H. Morais, C. Ramos, E. Forgcs, T. Cserhti, J. Oliviera, and T. Ills. Three-dimensional principal component analysis employed for the study of the b-glucosidase production of lentinus edodes strains. *Chemometr Intell Lab Syst*, 57:57–64, 2001.

[208] Emilio Marengo, Riccardo Leardi, Elisa Robotti, Pier Giorgio Righetti, Francesca Antonucci, and Daniela Cecconi. Application of three-way principal component analysis to the evaluation of two-dimensional maps in proteomics. *J Proteome Res*, 2(4):351–360, 2003.

[209] Alberto Pasamontes and Santiago Garcia-Vallve. Use of a multi-way method to analyze the amino acid composition of a conserved group of orthologous proteins in prokaryotes. *BMC Bioinformatics*, 7:257, 2006.

[210] B. Marchetti. Cross-talk signals in the cns: role of neurotrophic and hormonal factors, adhesion molecules and intercellular signaling agents in luteinizing hormone-releasing hormone (lhrh)-astroglial interactive network. *Front Biosci*, 2:d88–125, Mar 1997.

[211] Sheila S Rosenberg, Eve E Kelland, Eleonora Tokar, Asia R De la Torre, and Jonah R Chan. The geometric and spatial constraints of the microenvironment induce oligodendrocyte differentiation. *Proc Natl Acad Sci U S A*, 105(38):14662–14667, Sep 2008.

[212] A. Einstein. *Investigations on the Theory of the Brownian Movement*. Dover Pubns, 1965.

[213] A. Fick. On liquid diffusion. *Philos. Mag. J. Sci.*, 10:31–39, 1855.

[214] D. Le Bihan, J. F. Mangin, C. Poupon, C. A. Clark, S. Pappata, N. Molko, and H. Chabriat. Diffusion tensor imaging:

concepts and applications. *J Magn Reson Imaging*, 13(4):534–546, Apr 2001.

[215] P. J. Basser, J. Mattiello, and D. LeBihan. Mr diffusion tensor spectroscopy and imaging. *Biophys J*, 66(1):259–267, Jan 1994.

[216] Pabitra N Sen and Peter J Basser. A model for diffusion in white matter in the brain. *Biophys J*, 89(5):2927–2938, Nov 2005.

[217] C. Pierpaoli, P. Jezzard, P. J. Basser, A. Barnett, and G. Di Chiro. Diffusion tensor mr imaging of the human brain. *Radiology*, 201(3):637–648, Dec 1996.

[218] D. Le Bihan. Molecular diffusion nuclear magnetic resonance imaging. *Magn Reson Q*, 7(1):1–30, Jan 1991.

[219] E. O. Stejskal and J. E. Tanner. Spin diffusion measurements: Spin echoes in the presence of a time-dependent field gradient. *Journal of Chemical Physics*, 42 (1):288–292, 1965.

[220] N. G. Papadakis, C. D. Murrills, L. D. Hall, C. L. Huang, and T. Adrian Carpenter. Minimal gradient encoding for robust estimation of diffusion anisotropy. *Magn Reson Imaging*, 18(6):671–679, Jul 2000.

[221] K. M. Hasan, D. L. Parker, and A. L. Alexander. Comparison of gradient encoding schemes for diffusion-tensor mri. *J Magn Reson Imaging*, 13(5):769–780, May 2001.

[222] Andrew L Alexander, Jee Eun Lee, Mariana Lazar, and Aaron S Field. Diffusion tensor imaging of the brain. *Neurotherapeutics*, 4(3):316–329, Jul 2007.

[223] Pajevic and Pierpaoli. Color schemes to represent the orientation of anisotropic tissues from diffusion tensor data: application to white matter fiber tract mapping in the human brain. *Magn Reson Med*, 43(6):921, Jun 2000.

[224] P. J. Basser, S. Pajevic, C. Pierpaoli, J. Duda, and A. Aldroubi. In vivo fiber tractography using dt-mri data. *Magn Reson Med*, 44(4):625–632, Oct 2000.

[225] S. Mori, B. J. Crain, V. P. Chacko, and P. C. van Zijl. Three-dimensional tracking of axonal projections in the brain by magnetic resonance imaging. *Ann Neurol*, 45(2):265–269, Feb 1999.

[226] T. Delmarcelle and L. Hesselink. Visualization of second order tensor fields and matrix data. In *In Proceedings of IEEE Visualization 92 (pp 316-323)*, 1992.

[227] David S Tuch, Timothy G Reese, Mette R Wiegell, Nikos Makris, John W Belliveau, and Van J Wedeen. High angular resolution diffusion imaging reveals intravoxel white matter fiber heterogeneity. *Magn Reson Med*, 48(4):577–582, Oct 2002.

[228] David S Tuch. Q-ball imaging. *Magn Reson Med*, 52(6):1358–1372, Dec 2004.

[229] Bejoy Thomas, Maria Eyssen, Ronald Peeters, Guy Molenaers, Paul Van Hecke, Paul De Cock, and Stefan Sunaert. Quantitative diffusion tensor imaging in cerebral palsy due to periventricular white matter injury. *Brain*, 128(Pt 11):2562–2577, Nov 2005.

[230] B. M. Prizant and J. F. Duchan. The functions of immediate echolalia in autistic children. *J Speech Hear Disord*, 46(3):241–249, Aug 1981.

[231] P. J. Rydell and B. M. Prizant. *Teaching children with autism: Strategies to enhance communication and socialization.*, chapter Assessment and intervantion strategies for children who use echolalia. New York: Delmar, 1995.

[232] D. Scelfo. Misure di diffusione in mri: realizzazione di un modello sperimentale per la validazione di tecniche di ricostruzione tramite algoritmi di fiber tracking. Master's thesis, Universit di Pisa, 2008/2009.

[233] Stephen M Smith, Mark Jenkinson, Mark W Woolrich, Christian F Beckmann, Timothy E J Behrens, Heidi Johansen-Berg, Peter R Bannister, Marilena De Luca, Ivana Drobnjak, David E Flitney, Rami K Niazy, James Saunders, John Vickers, Yongyue Zhang, Nicola De Stefano, J. Michael Brady, and Paul M Matthews. Advances in functional and structural mr image analysis and implementation as fsl. *Neuroimage*, 23 Suppl 1:S208–S219, 2004.

[234] T. E J Behrens, M. W. Woolrich, M. Jenkinson, H. Johansen-Berg, R. G. Nunes, S. Clare, P. M. Matthews, J. M. Brady, and S. M. Smith. Characterization and propagation of uncertainty in diffusion-weighted mr imaging. *Magn Reson Med*, 50(5):1077–1088, Nov 2003.

[235] Stephen M Smith. Fast robust automated brain extraction. *Hum Brain Mapp*, 17(3):143–155, Nov 2002.

[236] Marco Catani and Michel Thiebaut de Schotten. A diffusion tensor imaging tractography atlas for virtual in vivo dissections. *Cortex*, 44(8):1105–1132, Sep 2008.

[237] Marco Catani, Matthew P G Allin, Masud Husain, Luca Pugliese, Marsel M Mesulam, Robin M Murray, and Derek K Jones. Symmetries in human brain language pathways correlate with verbal recall. *Proc Natl Acad Sci U S A*, 104(43):17163–17168, Oct 2007.

[238] D Le Bihan and E. Breton. Imagerie de diffusion in vivo par resonance magnetique nucleaire. *Cr Acad Sci*, 301:11091112, 1985.

[239] Denis Le Bihan. Looking into the functional architecture of the brain with diffusion mri. *Nat Rev Neurosci*, 4(6):469–480, Jun 2003.

[240] Stephen M Smith, Mark Jenkinson, Heidi Johansen-Berg, Daniel Rueckert, Thomas E Nichols, Clare E Mackay, Kate E Watkins, Olga Ciccarelli, M. Zaheer Cader, Paul M Matthews,

and Timothy E J Behrens. Tract-based spatial statistics: voxelwise analysis of multi-subject diffusion data. *Neuroimage*, 31(4):1487–1505, Jul 2006.

[241] D. Rueckert, L. I. Sonoda, C. Hayes, D. L. Hill, M. O. Leach, and D. J. Hawkes. Nonrigid registration using free-form deformations: application to breast mr images. *IEEE Trans Med Imaging*, 18(8):712–721, Aug 1999.

[242] Thomas E Nichols and Andrew P Holmes. Nonparametric permutation tests for functional neuroimaging: a primer with examples. *Hum Brain Mapp*, 15(1):1–25, Jan 2002.

[243] L. Kanner. Autistic disturbances of affective contact. *Acta Paedopsychiatr*, 35(4):100–136, 1968.

[244] P. J. Rydell and B. M. Prizant. *Teaching children with autism: Strategies to enhance communication and socialization.*, chapter Assessment and intervention strategies for children who use echolalia. New York: Delmar, 1995.

[245] M. Rutter. Concepts of autism: a review of research. *J Child Psychol Psychiatry*, 9(1):1–25, Oct 1968.

[246] A. L. Schuler. Echolalia: issues and clinical applications. *J Speech Hear Disord*, 44(4):411–434, Nov 1979.

[247] W. H. Fay. On the basis of autistic echolalia. *Journal of Communication Disorders*, 2:38–47, 1969.

[248] K. DeHirish. Differential diagnosis beetwin aphasic and schizophrenic language in children. *Journal of Speech and Hearing Disorders*, 32:3–10, 1967.

[249] B. M. Prizant. Language acquisition and communicative behavior in autism: toward an understanding of the "whole" of it. *J Speech Hear Disord*, 48(3):296–307, Aug 1983.

[250] B. M. Prizant and P. J. Rydell. Analysis of functions of delayed echolalia in autistic children. *J Speech Hear Res*, 27(2):183–192, Jun 1984.

[251] W. H. Fay and A. L. Schuler. *Emerging language in autistic children.* University Park Press (Baltimore), 1980.

[252] D. Cantwell, L. Baker, and M. Rutter. A comparative study of infantile autism and specific developmental receptive language disorder–iv. analysis of syntax and language function. *J Child Psychol Psychiatry*, 19(4):351–362, Oct 1978.

[253] N. Geschwind, F.A. Quadfasel, and J.M. Segarra. Isolation of speech area. *Neuropsychologia*, 6:327–340, 1968.

[254] J. Cambier, D. Elghozi, M. Khoury, and A. Strube. Echolalic repetition and severe comprehension disorders. left hemisphere deactivation syndrome? *Rev Neurol*, 136(10):689–98, 1980.

[255] A. B. Rubens. Aphasia with infarction in the territory of the anterior cerebral artery. *Cortex*, 11(3):239–250, Sep 1975.

[256] K. Hadano, H. Nakamura, and T. Hamanaka. Effortful echolalia. *Cortex*, 34(1):67–82, Feb 1998.

[257] S. Jonas. The thalamus and aphasia, including transcortical aphasia: a review. *J Commun Disord*, 15(1):31–41, Jan 1982.

[258] D. McFarling, L. J. Rothi, and K. M. Heilman. Transcortical aphasia from ischaemic infarcts of the thalamus: a report of two cases. *J Neurol Neurosurg Psychiatry*, 45(2):107–112, Feb 1982.

[259] Yang-Je Cho, Sang-Don Han, Sook Keun Song, Byung In Lee, and Kyoung Heo. Palilalia, echolalia, and echopraxia-palipraxia as ictal manifestations in a patient with left frontal lobe epilepsy. *Epilepsia*, 50(6):1616–1619, Jun 2009.

[260] Marco Catani, Derek K Jones, and Dominic H ffytche. Perisylvian language networks of the human brain. *Ann Neurol*, 57(1):8–16, Jan 2005.

[261] Marco Catani and Dominic H ffytche. The rises and falls of disconnection syndromes. *Brain*, 128(Pt 10):2224–2239, Oct 2005.

[262] Y. Assaf, R. Z. Freidlin, G.K. Rohde, and P.J. Basser. New modeling and experimental framework to characterize hindered and restricted water diffusion in brain white matter. *Magnetic Resonance in Medicine*, 52:965978, 2004.

[263] B. Horwitz, K. J. Friston, and J. G. Taylor. Neural modeling and functional brain imaging: an overview. *Neural Netw*, 13(8-9):829–846, 2000.

[264] R. S. Menon. Imaging function in the working brain with fmri. *Curr Opin Neurobiol*, 11(5):630–636, Oct 2001.

[265] David J Heeger and David Ress. What does fmri tell us about neuronal activity? *Nat Rev Neurosci*, 3(2):142–151, Feb 2002.

[266] S. Ogawa, D. W. Tank, R. Menon, J. M. Ellermann, S. G. Kim, H. Merkle, and K. Ugurbil. Intrinsic signal changes accompanying sensory stimulation: functional brain mapping with magnetic resonance imaging. *Proc Natl Acad Sci U S A*, 89(13):5951–5955, Jul 1992.

[267] S. Ogawa, T. M. Lee, A. R. Kay, and D. W. Tank. Brain magnetic resonance imaging with contrast dependent on blood oxygenation. *Proc Natl Acad Sci U S A*, 87(24):9868–9872, Dec 1990.

[268] S. Ogawa, T. M. Lee, A. S. Nayak, and P. Glynn. Oxygenation-sensitive contrast in magnetic resonance image of rodent brain at high magnetic fields. *Magn Reson Med*, 14(1):68–78, Apr 1990.

[269] Kmil Ugurbil, Louis Toth, and Dae Shik Kim. How accurate is magnetic resonance imaging of brain function? *Trends Neurosci*, 26(2):108–114, Feb 2003.

[270] P. T. Fox, M. E. Raichle, M. A. Mintun, and C. Dence. Nonoxidative glucose consumption during focal physiologic neural activity. *Science*, 241(4864):462–464, Jul 1988.

[271] G. K. Aguirre and M. D'Esposito. *Functional MRI*, chapter Experimental design for brain fMRI, pages 369–380. Heidelberg: Springer-Verlag Berlin, 2000.

[272] K.J. Friston, P. Jezzard, and R. Turner. The analysis of functional mri time-series. *Hum Brain Mapp*, 1:153171, 1994.

[273] K.J. Friston, A.P. Holmes, K.J. Worsley, J.P. Poline, C.D. Frith, and R.S.J. Frackowiak. Statistical parametric maps in functional imaging: a general linear approach. *Hum Brain Mapp*, 2:189210, 1995.

[274] K.N. Kirby. *Advanced data analysis with SYSTAT*. Van Nostrand Reinhold, New York, 1993.

[275] Marcel Adam Just, Vladimir L Cherkassky, Timothy A Keller, and Nancy J Minshew. Cortical activation and synchronization during sentence comprehension in high-functioning autism: evidence of underconnectivity. *Brain*, 127(Pt 8):1811–1821, Aug 2004.

[276] Hideya Koshino, Patricia A Carpenter, Nancy J Minshew, Vladimir L Cherkassky, Timothy A Keller, and Marcel Adam Just. Functional connectivity in an fmri working memory task in high-functioning autism. *Neuroimage*, 24(3):810–821, Feb 2005.

[277] Marcel Adam Just, Vladimir L Cherkassky, Timothy A Keller, Rajesh K Kana, and Nancy J Minshew. Functional and anatomical cortical underconnectivity in autism: evidence

from an fmri study of an executive function task and corpus callosum morphometry. *Cereb Cortex*, 17(4):951–961, Apr 2007.

[278] Rajesh K Kana, Timothy A Keller, Vladimir L Cherkassky, Nancy J Minshew, and Marcel Adam Just. Sentence comprehension in autism: thinking in pictures with decreased functional connectivity. *Brain*, 129(Pt 9):2484–2493, Sep 2006.

[279] Daniel P Kennedy and Eric Courchesne. The intrinsic functional organization of the brain is altered in autism. *Neuroimage*, 39(4):1877–1885, Feb 2008.

[280] Vladimir L Cherkassky, Rajesh K Kana, Timothy A Keller, and Marcel Adam Just. Functional connectivity in a baseline resting-state network in autism. *Neuroreport*, 17(16):1687–1690, Nov 2006.

[281] Natalia M Kleinhans, Todd Richards, Lindsey Sterling, Keith C Stegbauer, Roderick Mahurin, L. Clark Johnson, Jessica Greenson, Geraldine Dawson, and Elizabeth Aylward. Abnormal functional connectivity in autism spectrum disorders during face processing. *Brain*, 131(Pt 4):1000–1012, Apr 2008.

[282] Sandra Maestro, Filippo Muratori, Maria Cristina Cavallaro, Francesca Pei, Daniel Stern, Bernard Golse, and Francisco Palacio-Espasa. Attentional skills during the first 6 months of age in autism spectrum disorder. *J Am Acad Child Adolesc Psychiatry*, 41(10):1239–1245, Oct 2002.

[283] G. Dawson, A. N. Meltzoff, J. Osterling, J. Rinaldi, and E. Brown. Children with autism fail to orient to naturally occurring social stimuli. *J Autism Dev Disord*, 28(6):479–485, Dec 1998.

[284] Justin H G Williams. Self-other relations in social development and autism: multiple roles for mirror neurons and other brain bases. *Autism Res*, 1(2):73–90, Apr 2008.

[285] Blythe A Corbett, Vanessa Carmean, Susan Ravizza, Carter Wendelken, Melissa L Henry, Cameron Carter, and Susan M Rivera. A functional and structural study of emotion and face processing in children with autism. *Psychiatry Res*, 173(3):196–205, Sep 2009.

[286] Karen Pierce and Elizabeth Redcay. Fusiform function in children with an autism spectrum disorder is a matter of "who". *Biol Psychiatry*, 64(7):552–560, Oct 2008.

[287] David J Grelotti, Ami J Klin, Isabel Gauthier, Pawel Skudlarski, Donald J Cohen, John C Gore, Fred R Volkmar, and Robert T Schultz. fmri activation of the fusiform gyrus and amygdala to cartoon characters but not to faces in a boy with autism. *Neuropsychologia*, 43(3):373–385, 2005.

[288] Kerstin Dautenhahn. Socially intelligent robots: dimensions of human-robot interaction. *Philos Trans R Soc Lond B Biol Sci*, 362(1480):679–704, Apr 2007.

[289] Andrea C Pierno, Morena Mari, Dean Lusher, and Umberto Castiello. Robotic movement elicits visuomotor priming in children with autism. *Neuropsychologia*, 46(2):448–454, Jan 2008.

[290] C. Lord, M. Rutter, and A. Le Couteur. Autism diagnostic interview-revised: a revised version of a diagnostic interview for caregivers of individuals with possible pervasive developmental disorders. *J Autism Dev Disord*, 24(5):659–685, Oct 1994.

[291] C. Lord, S. Risi, L. Lambrecht, E. H. Cook, B. L. Leventhal, P. C. DiLavore, A. Pickles, and M. Rutter. The autism diagnostic observation schedule-generic: a standard measure of social and communication deficits associated with the spectrum of autism. *J Autism Dev Disord*, 30(3):205–223, Jun 2000.

[292] D Wechsler. *Wechsler Intelligence Scale for ChildrenRevised.* New York: The Psychological Corporation, 1974.

[293] J. Talairach and P. Tournoux. *Co-planar Stereotaxic Atlas of the Human Brain.* Thieme Medical, New York, 1988.

[294] G. M. Boynton, S. A. Engel, G. H. Glover, and D. J. Heeger. Linear systems analysis of functional magnetic resonance imaging in human v1. *J Neurosci*, 16(13):4207–4221, Jul 1996.

[295] G. Pioggia, A. Ahluwalia, F. Carpi, A. Marchetti, M. Ferro, W. Rocchia, and D. De Rossi. Face: Facial automaton for conveying emotions. *Appl. Bionics Biomech.*, 1:91–100, 2004.

[296] G. Pioggia, R. Igliozzi, M. Ferro, A. Ahluwalia, F. Muratori, and D. De Rossi. An android for enhancing social skills and emotion recognition in people with autism. 13(4):507–515, 2005.

[297] G. Pioggia, R. Igliozzi, M.L. Sica, M. Ferro, F. Muratori, A. Ahluwalia, and D. De Rossi. Exploring emotional and imitational android-based interactions in autistic spectrum disorders. *J. Cybertherapy and Rehabilitation*, 1 (1):49–61, 2008.

[298] N. Mavridis and D. Hanson. The ibnsina center: An augmented reality theater with intelligent robotic and virtual characters. In *Proc. 18th IEEE Int. Symp. Robot and Human Interactive Communication RO-MAN 2009*, pages 681–686, 2009.

[299] T. Wu, N.J. Butko, P. Ruvulo, M.S Bartlett, and Movellan J.R. Learning to make facial expressions. In *IEEE 8TH INTERNATIONAL CONFERENCE ON DEVELOPMENT AND LEARNING*, 2009.

[300] C. Eppner, J. Sturm, M. Bennewitz, C. Stachniss, and W. Burgard. Imitation learning with generalized task descriptions. In *Proc. IEEE Int. Conf. Robotics and Automation ICRA '09*, pages 3968–3974, 2009.

[301] G.R. Bradski. Computer vision face tracking for use in a perceptual user interface. *Intel Technology Journal*, 2 (2):12–21, 1998.

[302] A. Cisternino, D. Colombo, G. Ennas, and D. Picciaia. Robotics4.net: software body for controlling robots. *IEE Proceedings -Software*, 152(5):215–222, 2005.

[303] E.S. Maini, G. Pioggia, A. Armato, Dispositivo e procedimento per la misurazione del punto di mira visiva di un soggetto TO2008A000862. Italy. 2008.

[304] Christa J Anderson, John Colombo, and D. Jill Shaddy. Visual scanning and pupillary responses in young children with autism spectrum disorder. *J Clin Exp Neuropsychol*, 28(7):1238–1256, Oct 2006.

[305] Leslie L Speer, Anne E Cook, William M McMahon, and Elaine Clark. Face processing in children with autism: effects of stimulus contents and type. *Autism*, 11(3):265–277, May 2007.

[306] Kim M Dalton, Laura Holsen, Leonard Abbeduto, and Richard J Davidson. Brain function and gaze fixation during facial-emotion processing in fragile x and autism. *Autism Res*, 1(4):231–239, Aug 2008.

[307] A. Tyrrell and G. Greenwood. Fundamentals of evolutionary computation. In *Introduction to Evolvable Hardware:A Practical Guide for Designing Self-Adaptive Systems*, pages 1–15. IEEE, 2006.

[308] A. Armato. Hatcam: a wearable gaze tracking device for ecological investigation of social interaction in autistic spectrum disorders. In *Torino GNB Conference*, 2010.

[309] N. Ramanauskas, G. Daunys, and D. Dervinis. Computers helping people with special needs. In *Investigation of Calibration Techniques in Video Based Eye Tracking System.*, 2008.

[310] G. G. Berntson, J. T. Bigger, D. L. Eckberg, P. Grossman, P. G. Kaufmann, M. Malik, H. N. Nagaraja, S. W. Porges, J. P. Saul, P. H. Stone, and M. W. van der Molen. Heart rate variability: origins, methods, and interpretive caveats. *Psychophysiology*, 34(6):623–648, Nov 1997.

[311] N. Montano, T. G. Ruscone, A. Porta, F. Lombardi, M. Pagani, and A. Malliani. Power spectrum analysis of heart rate variability to assess the changes in sympathovagal balance during graded orthostatic tilt. *Circulation*, 90(4):1826–1831, Oct 1994.

[312] D. B. Percival and A. T. Walden. *Wavelet Methods for Time Series Analysis*. Cambridge University Press, 2000.

[313] S.L. Marple. *Digital Spectral Analysis*. Prentice-Hall International, 1987.

[314] Xue Ming, Peter O O Julu, Michael Brimacombe, Susan Connor, and Mary L Daniels. Reduced cardiac parasympathetic activity in children with autism. *Brain Dev*, 27(7):509–516, Oct 2005.

[315] Elgiz Bal, Emily Harden, Damon Lamb, Amy Vaughan Van Hecke, John W Denver, and Stephen W Porges. Emotion

recognition in children with autism spectrum disorders: relations to eye gaze and autonomic state. *J Autism Dev Disord*, 40(3):358–370, Mar 2010.

[316] Motomi Toichi and Yoko Kamio. Paradoxical autonomic response to mental tasks in autism. *J Autism Dev Disord*, 33(4):417–426, Aug 2003.